DEVELOPING LIQUID CHROMATOGRAPHY-MASS SPECTROMETRY STRATEGIES FOR INVESTIGATING ENERGY METABOLISM WITH APPLICATION TO ISOCITRATE DEHYDROGENASE MUTATIONS IN CANCER

KHALID MOHAMMAD AL-QAHTANI

CHEMISTRY RESEARCH LABORATORY
DEPARTMENT OF ORGANIC CHEMISTRY
HERTFORD COLLEGE

TRINITY TERM 2015

A THESIS SUBMITTED TO THE BOARD OF THE FACULTY OF PHYSICAL SCIENCES AT THE UNIVERSITY OF OXFORD IN PARTIAL FULFILMENT OF THE REQUIREMENTS FOR THE DEGREE OF DOCTOR OF PHILOSOPHY

Abstract

DEVELOPMENT AND APPLICATION OF METHODS FOR QUALITATIVE AND QUANTITATIVE ANALYSIS OF TCA CYCLE METABOLITES USING LIQUID CHROMATOGRAPHY COUPLED TO MASS SPECTROMETRY

Isocitrate dehydrogenases (IDHs) act in the tricarboxylic acid (TCA) cycle to catalyse the conversion of isocitrate to 2-oxoglutarate (2-OG) with concomitant production of NADH and/or NADPH. In humans, mutations causing IDH1 and IDH2 substitutions have been found during DNA sequencing of human glioblastomas. Some cancer-associated IDH mutations promote the reduction of 2-OG to give *D*-2-hydroxyglutarate (*D*-2-HG) a chiral, polar dicarboxylic acid.

Investigations on the underlying links between 2-HG and cancer require sensitive methods for monitoring IDH1 and IDH2 activities. The reported LC/MS methods for the analysis of TCA cycle metabolites are limited in term of their accuracy and ability to identity isomers. Methods for the direct measurement of levels of TCA cycle and associated metabolites using mass spectrometry-based metabolomics are desired. However, for the reported methods, the limits of detection are often prohibitive; they are normally suited for the investigation of known metabolites rather than for the discovery of new compounds. With some exceptions, the existing methods have not been extensively validated, e.g. with respect to limits of detection and quantification as well as precision. The main aim of the research presented in this thesis was to develop methods for TCA cycle metabolite analysis in cells and to apply these methods to investigations on variant IDH enzymes.

A range of LC-MS approaches were investigated including: (1) C18 reversed phase chromatography of non-derivatised TCA cycle metabolites, (2) ion paring chromatography, and (3) mixed mode chromatography with either MS, or isotope ratio mass spectrometry detection, gas chromatography of TBDMS derivatised TCA cycle metabolites. Analysis of the elution patterns for these separation techniques enabled estimation of the retention parameters of TCA cycle metabolites and investigations on their metabolism. The most sensitive approach developed employed mixed mode chromatography coupled to isotope ratio mass spectrometry, which was optimised for the analysis of TCA cycle metabolites. This was shown to have a limit of detection two orders of magnitude lower (4μM) than more conventional mass

spectrometry techniques. Using ^{13}C-[4C]-Aspartate labelling in cell culture, a quantification protocol was developed which employed a non-labelled internal standard and selectively labelled cell culture. The method was shown to be suitable for both very accurate quantification at low concentration levels and metabolic studies.

The analytical methods developed for TCA cycle metabolites analysis were successfully applied to the analysis of 2-OG and *D*-2-HG metabolism. The stereochemistry of 2-HG in the cell pellets as well as of the citrate/isocitrate isomers was investigated. IDH1^{R132H} was shown to catalyse reduction of 2-OG resulting in *D*-2-HG. TCA cycle analysis was used in order to investigate 2-OG and 2-HG metabolism related to IDH1^{R132H}. Using the method developed for the analysis of non-derivatised TCA cycle intermediates, the screening of potential substrates of IDH1^{R132H} was carried out. The isotope ratio mass spectrometry protocol was applied to the study of IDH1^{R132H} in cell culture; levels of D-2-HG were quantified.

The analytical methods described complement the established metabolomics techniques. The methods developed enable the investigation into the regio- and stereo- chemistry of TCA cycle and associated metabolites and are powerful tools for investigating cancer cell metabolism.

Thesis Title:

DEVELOPMENT AND APPLICATION OF METHODS FOR QUALITATIVE AND QUANTITATIVE ANALYSIS OF TCA CYCLE METABOLITES USING LIQUID CHROMATOGRAPHY COUPLED TO MASS SPECTROMETRY

Submitted for the degree of Doctor of Philosophy in Chemical Biology by:

Khalid Mohammad AL-Qahtani

Hertford College, University of Oxford

Trinity Term 2015

Acknowledgements

First thanks must be to Allah the all mighty then to King Faisal Specialist Hospital and Research Centre for generous funding to accomplish my D.Phil. research. Many thanks goes to Hertford College, Oxford and to the Graduate scholarship for their provision of additional financial support.

Many thanks goes to the Executive Director of the Research Center, Dr. Sultan AL- Sedairy; the Deputy Executive Director of the Research Center, Dr. Fatwan Al-Mohana; the Chairman of the Genetics Department, Dr.Brian Meyer; and to the Director & Senior Scientist of the NLNS Lab, Dr. Ali AL-Odaib.

To my supervisors:

I am indebted to my two supervisors, Prof. James McCullagh and Prof. Christopher Schofield for their advice and support throughout the project. Their willingness to work at the interface between different scientific disciplines has been inspiring and has enabled me to gain exposure to a wide range of techniques that has made for an altogether more interesting project. I would like to thank James for sharing his technical and scientific expertise with me and for demonstrating a truly critical analytical approach to the chemistry problems. I would like to thank Chris for letting me into the realm of biochemistry research and providing a word of advice and encouragement. The support and friendship of members of the McCullagh group, past and present, has made my D.Phil. particularly enjoyable. Special mentions must

go to Dr. James Wickens, Dr. Nikita Loik, Dr Shweta Chavan, Lingzhi Gong and Colin Sparrow for sharing their profound knowledge and providing endless support with the very nuts and bolts of the chromatography and mass spectrometry. Without them, my scientific journey would be stopped at the first red light when an instrument flashed. I would also like to extend my thanks to all members of the Schofield group, past and present. In particular, Dr Refaat Hamed, Dr Emily Flashman, Rok Sekirnik, Hannah Tarhonskaya, who, apart from being great researchers, were always good friends.

I would like to thank Prof. Timothy D.W. Claridge for introducing me to NMR.

My project has been highly collaborative and I am extremely grateful to all those who I have been worked with over the past 4 years; Dr Chiara Bardella and Prof. Ian Tomlinson (Wellcome Trust Centre for Human Genetics, University of Oxford); Dr Sarah Larkin and Dr Olaf Ansorge (Department of Neuropathology, John Radcliffe Hospital, University of Oxford) Dr Angela Russell and Dr. Jonathan Williams (Chemistry Research Laboratory, University of Oxford).

Special thanks to Dr. Jonathan Williams (Chemistry Research Laboratory, University of Oxford) for give my the copyright authorisation form his thesis Titled “Isoenzyme Specific PFK-2/FBPase-2 Inhibition as an Anti-cancer Strategy” and Dr.Hui-Kuo Shu (Department of Radiation Oncology, The Emory Clinic, Atlanta,US) for give me the copyright authorisation to use his book chapter “The Role of Isocitrate Dehydrogenase Mutations in Glioma Brain Tumors” from the book entitled Molecular Targets of CNS Tumors edited by Miklos Garami.

To my family: My whole hearted thanks and gratefulness go to my parents who stood by me with their kind and valuable words of encouragement and advice, and last but not least a warm thanks goes to my wife Ibtisam, my daughter Deema and son Basil for their assistance and for their support during the last four years and for being understanding even when I showed the gloomiest side of myself.

Thank you all and May God bless you all…

Abbreviations

%CV	-	Coefficient of variation
2-HG	-	2-Hydroxyglutarate
2-OG	-	2-Oxoglutarate
ACN	-	Acetonitrile
ACT	-	cis-Acontate
Asp	-	Aspartate
CA	-	Isocitrate
DHAP	-	Dihydroxyacetone phosphate
ESI	-	Electrospray ionization
F-1,6-BP	-	Fructose-1,6-bisphosphate
F-1,6-BPase	-	Fructose-1,6-bisphosphatase
F-2,6-BP	-	Fructose-2,6-bisphosphate
F-6-P	-	Fructose-6- phosphate
F-6-P	-	Fructose-6-phosphate
FH	-	Fumarate hydratase
Fum	-	Fumarate
G-6-P	-	Glucose-6-phosphate
G-6-P	-	Glucose-6-phosphate
GC-MS	-	Gas chromatography-mass spectrometry
Gln	-	Glutamate
Glu	-	Glutamine
H	-	Hypoxia (0.1% O2)
HEK 293T	-	Human embryonic kidney cell line
HIF	-	Hypoxia inducible factor
HPLC	-	High performance liquid chromatography
I.S.	-	Internal standard
ICA	-	Isocitrate
IDH1	-	Isocitrate dehydrogenase1
IDH2	-	Isocitrate dehydrogenase2
IDH3	-	Isocitrate dehydrogenase3
IP	-	Ion pairing
IPLC	-	Ion pairing liquid chromatography
IR	-	Isotope ratio
IRMS	-	Isotope ratio mass spectrometry
L-malH	-	L-Malate dehydrogenase
LC	-	liquid chromatography
LoD	-	limit of detection
LoQ	-	limit of quantification
m/z	-	Atomic mass units per charge
Mal	-	Malate
Mel	-	Maleate
MeOH	-	Methanol
min	-	Minutes
MRI	-	Magnetic resonance imaging

MRS	-	Magnetic resonance spectroscopy
MS	-	Mass spectrometry
MW	-	Molecular weight
N	-	Normoxia
NAD+	-	Nicotinamide adenine dinucleotide
NADH	-	Nicotinamide adenine dinucleotide (reduced)
NADP+	-	Nicotinamide adenine dinucleotide phosphate
NADPH	-	Nicotinamide adenine dinucleotide phosphate (reduced)
NMR	-	Nuclear Magnetic Resonance spectroscopy
OAA	-	Oxaloactate
PCA	-	Perchloric acid
PFK-1	-	6-Phosphofructo-1-kinase
PFK-15	-	1-(4-Pyridinyl)-3-(2-quinolinyl)-2-propen-1-one
PFK-2/FBPase-2	-	6-Phosphofructo-2-kinase/fructose-2,6-bisphosphatase
PFKFB1-4	-	6-Phosphofructo-2-kinase/fructose-2,6-bisphosphatase isoenzymes 1-4
PFKFB4s	-	6-Phosphofructo-2-kinase/fructose-2,6-bisphosphatase-4 splice variant
PFKL	-	6-Phosphofructo-1-kinase (liver-type)
PFKM	-	6-Phosphofructo-1-kinase (muscle-type)
PFKP	-	6-Phosphofructo-1-kinase (platelet-type)
PFP	-	Pentafluorophenyl
PHD	-	Prolyl hydroxylase
PPP	-	Pentose phosphate pathway
R-6-P	-	Ribulose-5-phosphate
SA	-	Succinate
SDH	-	Succinate dehydrogenase
shRNA	-	Small hairpin ribonucleic acid
si3	-	siPFKFB3-1 and siPFKFB3-2
si3/4	-	siPFKFB3-1, siPFKFB3-2, siPFKFB4-1 and siPFKFB4-2
si4	-	siPFKFB4-1 and siPFKFB4-2
SIM	-	Selected ion monitoring
SIR	-	Selected ion recording
TCA cycle	-	Tricarboxylic acid cycle
TIC	-	Total ion count
UPLC	-	Ultra performance liquid chromatography
V	-	Volt
µM	-	Micromolar

TABLE OF CONTENTS

LIST OF FIGURES

LIST OF TABLES

NOTE: SOME OF THE WORK AND DESCRIPTIONS IN THIS THESIS HAVE BEEN REPORTED IN THE ACADEMIC LITERATURE:

Elena et al., (2013). "Investigations on the Oxygen Dependence of a 2-Oxoglutarate Histone Demethylase." Biochem J. 449(2):491-6.

Khalid et al.,(2015). "The broad spectrum 2-oxoglutarate oxygenase inhibitor N-oxalylglycine is present in rhubarb and spinach leaves." Phytochemistry. 117:456-61.

Emir et al., "Noninvasive Quantification of 2-Hydroxyglutarate in Human Gliomas with IDH1 and IDH2 Mutations." Cancer Res.**76**(1):43-9.

Chapter 1: INTRODUCTION AND AIMS

1.1. Hallmarks of Cancer

The lifetime risk of developing cancer now stands at 40% for males and 37% for females in the UK; cancer is a leading cause of death worldwide (Sasieni, Shelton et al., 2011). Ageing populations, unhealthy diets, the prevalence of smoking, and other poor lifestyle choices, all mean that the number of people suffering with cancer is projected to continue increasing worldwide; this trend will serve to further exacerbate the social and economic burden of cancer.

Despite extensive research, patients remain heavily reliant on the surgical excision of tumours and non-selective chemo- and radio-therapies, which have limited efficacy and numerous side-effects, as a result of normal tissue damage. Identifying targetable features that distinguish cancer cells from normal cells is a major challenge, which is further compounded by the heterogenic nature of tumours (Yap, Gerlinger et al., 2012). At any one time, a tumour may consist of several colonies of cancer cells with different mutations, all striving to out-compete one other (Gerlinger, Rowan et al., 2012; Gerlinger, Verduzco et al., 2012; Swanton 2012). Even if chemotherapy destroys the bulk of the tumour, those resistant sub-populations that may remain have the ability to spawn new tumours.

Treatment and diagnosis further are complicated by the apparent common existence of tumour-initiating cells (TICs), otherwise known as cancer stem cells (Frame and Maitland 2011). These cells may be broadly defined as cells having the capacity to give rise to new tumours and are thought to be the driving force behind many cancers, through their capacity for self-renewal and generation of the heterogeneous cell lineages that comprise a tumour (Frank, Schatton et al., 2010; Frameand and Maitland 2011).

In general, mutations in two types of genes are linked to the onset of cancer development; i.e. proto-oncogenes and tumour suppressor genes. Mutations in proto-oncogenes, which usually have a critical role in regulating cell growth, produce oncogenes with a dominant gain of function. For example, Ras proteins mediate signaling pathways intimately involved in cell growth, such as promoting an increase in DNA, protein and lipid synthesis, in response to growth factors. Mutation in the Ras proto-oncogene leads to continued proliferative signaling, which is linked to de-regulated cell growth and transformation (Downward 2003).

Neoplastic disease is enormously complex. Hanahan and Weinberg (Hanahan and Weinberg 2000) consolidated the plethora of scientific literature into a single conceptual framework and originally proposed that there were six biological capabilities that all cancer cells acquire during the process of carcinogenesis. These were (1) self-sufficiency in growth signals, (2) insensitivity to growth-inhibitory signals, (3) evasion of apoptosis, (4) limitless replicative potential, (5) sustained angiogenesis and (6) tissue invasion and metastasis (Figure 1-1).

The Hallmarks of Cancer

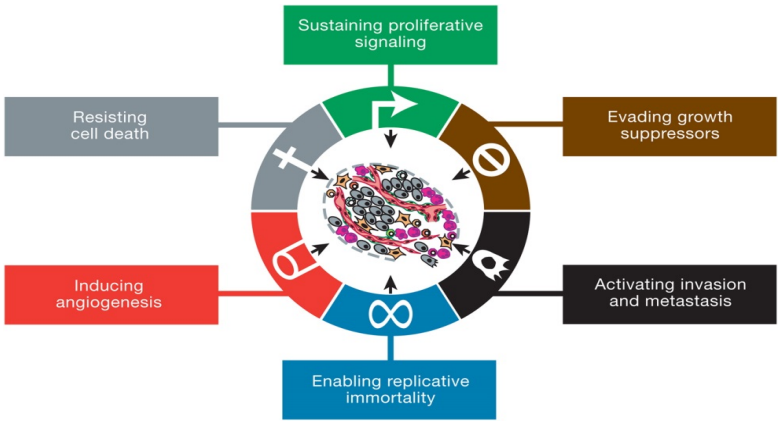

Figure 1-1: The hallmarks of cancer. Figures reproduced from (Hanahan and Weinberg 2011) with kind permission of the publishers (license number 3151300078227).

These were later refined to include two emerging hallmarks; evading immune destruction, and reprogramming of energy metabolism, to support the capacity of the cancer cell to relentlessly divide and proliferate (Figure 1-2) (Hanahan and Weinberg 2011). These hallmarks are underpinned by two "enabling characteristics"; tumour-promoting inflammation and genomic instability. The latter promotes the genetic mutations necessary for acquisition of each of the hallmarks (Figure 1-2). It follows that the most effective therapeutic strategies will likely be those that specifically target one or more of the hallmarks of cancer, or the enabling characteristics.

Emerging Hallmarks and Enabling Characteristics

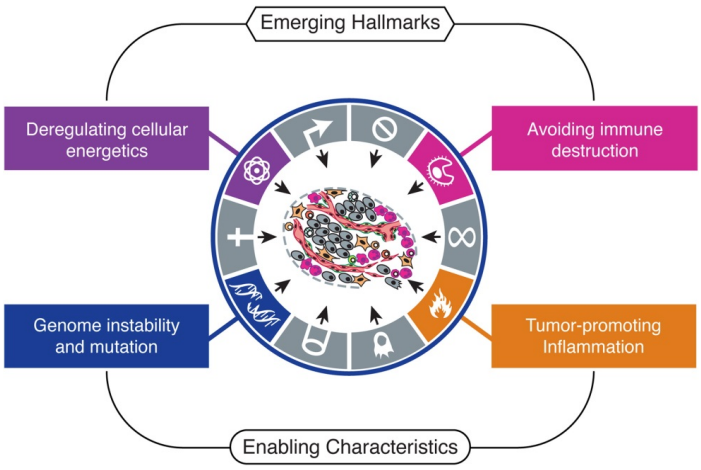

Figure 1-2: Emerging hallmarks and enabling characteristics. Figures reproduced from (Hanahan and Weinberg 2011) with kind permission of the publishers (license number 3151300078227).

These guiding concepts must always be considered against the backdrop of tumour heterogeneity and the tumour micro-environment. In particular, it is important to keep in mind that a solid tumour is a complex tissue consisting of multiple cell types, in addition to stromal cells recruited from normal tissues (Hanahan and Weinberg 2011). It has become increasingly apparent that the interactions between tumour cells and the stromal component can have a fundamental role in tumour progression and chemo-resistance. Much of the in vitro and in vivo work conducted to date has not taken this

into account (Udagawa and Wood 2010).

1.2. Towards Tergeted Chemotherapy for Cancer

The development of modern chemotherapies began with the identification of the 'nitrogen mustards', which are derivatives of former World War One chemical weapons that were found to successfully treat patients with Hodgkin's lymphoma and lymphosarcoma (Gilman and Philips 1946; Goodman, Wintrobe et al., 1946). The 'nitrogen mustards' function via the formation of highly electrophilic intermediates, which act as non-specific alkylating agents, binding DNA and causing inter-strand cross-linking, thereby preventing replication (Mattes, Hartley et al., 1986). In the 1940s, Sydney Farber observed that folate accelerated the progression of patients with acute lymphoblastic leukemia (ALL) (Farber, Cutler et al., 1947; Chabner and Roberts, 2005). This led to arguably the first example of rational drug design, where the folate analogue Aminopterin was tested in a clinical trial and found to induce temporary remission in some patients with ALL (Farber and Diamond 1948). Other therapeutic agents include the anti-metabolites, such as 5-fluorouracil, which inhibits nucleotide synthesis, and the taxanes and vinca alkaloids, which both act to inhibit cell division (Lewis 2006; Morrison 2010). However, whilst many are relatively effective, they generally suffer from a lack of specificity, targeting all highly proliferative cells. This includes cells in normal tissue, leading to toxicity, i.e. a low therapeutic index. The use of these agents therefore depends on exploiting a narrow therapeutic window, maximising efficacy and minimising toxicity in non-target tissue (Masui, Gini et al., 2013).

In recent years there has been a paradigm shift in cancer treatment from such traditional chemotherapies to more specific "targeted therapies", which are selective

for a specific molecular target with a crucial role in promoting tumour growth and advancement (Sawyers 2004; Thompson 2009). For example, selective estrogen receptor modulators (SERMs) such as tamoxifen, have been used to treat patients with invasive estrogen receptor positive breast cancer, as well as reducing occurrence when used preventatively in women with elevated risk of the disease (Jordan 2007; Cuzick, Sestak et al., 2013).

The first major success of rational drug design targeting a specific molecular aberration in cancer cells came with the identification of Imatinib (Gleevec®) (Druker, Tamura et al., 1996; Druker, Sawyers et al., 2001). Imatinib is an ATP-competitive inhibitor of the Breakpoint cluster region–Abelson (BCR-ABL) tyrosine kinase fusion protein, which is responsible for driving cellular proliferation in Philadelphia chromosome-positive chronic myelogenous leukemia (CML) cells (Oda, Heaney et al., 1994). Through furthering understanding of such underlying molecular changes in cancer, the oncology community is making a sustained effort to identify new suitable molecular targets that represent the root cause of cancer. The corresponding anti-neoplastic agents developed are anticipated to be more efficacious and less toxic than their chemotherapeutic predecessors (Sawyers 2004; Thompson 2009). Nevertheless, intrinsic or acquired resistance to such molecularly targeted therapies will likely require most to be employed in combination with other therapeutic agents. However, most patients, including those highly responsive to the initial therapy, experience relapse within a year (Dummer and Flaherty 2012). This is due to a variety of resistance mechanisms, including those that mediate reactivation of the MAPK pathway or up-regulation of alternative signaling pathways, such as the phosphoinositide 3-kinase (PI3K)/Akt pathway (Giroux 2013; Sullivan and Flaherty 2013). It will be important to increase understanding of mechanisms of resistance to

such targeted therapies in order to develop more effective combination treatments in the future.

1.3. Tumour Hypoxia in Cancer

Hypoxia is a common and distinguishing characteristic of many solid tumours, which is defined as a reduction in the normal oxygen tension in cells (Harris 2002). The development of new blood vessels is deregulated in tumours, leading to a structurally and functionally abnormal microvasculature, culminating in poor, irregular tumour blood flow (Harris 2002; Jain 2005). This, coupled with the rapid, uncontrolled proliferation of cancer cells, causes them to outgrow their blood, and therefore their oxygen, supply (Jain 2005). Intra-tumoural oxygen concentration is thus highly heterogeneous and in a constant state of flux, and as the oxygen diffusion limit is around 150 µm (Helmlinger, Yuan et al., 1997), the majority of tumours exceeding 1-3mm are found to contain hypoxic and necrotic regions (Dewhirst 1998; Shannon, Bouchier-Hayes et al., 2003) (Figure 1-3).

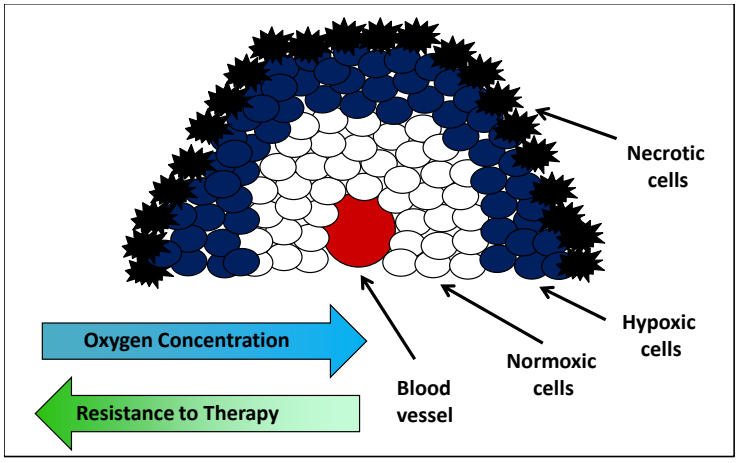

Figure 1-3: Simplified depiction of hypoxic and necrotic regions of tumour tissue with respect to the blood vessel.

Hypoxia is associated with poor prognosis as it can promote tumour progression through increased angiogenesis (Kuwai, Kitadai et al., 2003), invasiveness, metastasis (Brizel, Scully et al., 1996; Subarsky and Hill 2003) and genetic instability (Reynolds, Rockwell et al., 1996). Hypoxia is also related to the up-regulation of genes encoding proteins involved in drug resistance, such as P-gp (permeability glycoprotein) (Wartenberg, Ling et al., 2003), which actively pumps many drugs out of the cell (Brown and William 2004). Hypoxia is intimately linked with changes in cancer cell metabolism (Bertout, Patel et al., 2008) and is also known to promote a more aggressive phenotype. For example, it selects for a more apoptosis-resistant clonal population that lacks functional p53, a key tumour-suppressor transcription factor (Graeber, Osmanian et al., 1996). Hypoxic cells have been shown to have a three-fold greater resistance to radiation damage than normoxic cells, because it is the presence of oxygen in cells that enables "fixing" of radiation damage, through production of DNA-damaging oxygen free radicals (Gray, Conger et al., 1953; Overgaard and Horsman 1996). Furthermore, the "leaky", irregular vasculature and high interstitial pressures, coupled with large diffusion distances, mean delivery of cytotoxic agents to hypoxic areas of a tumour can be extremely inefficient (Brown and Giaccia 1998; Harris 2002; Wouters, Pauwels et al., 2007). In addition, the low oxygen, low nutrient environment reduces proliferation, leading to the presence of viable, non-cycling cells that are insensitive to those drugs targeting highly proliferative cells. The combination of these factors often promotes resistance to multiple structurally and functionally unrelated chemotherapeutic agents (multi-drug resistance) (Krishna and Mayer 2000).

1.4. The Hypoxia-Inducible Factors Pathway

The hypoxia-inducible factors (HIFs) are a family of transcription factors that play a central role in both sensing and responding to changes in oxygen concentration, through inducing the expression of genes that mediate the physiologic response to hypoxia (Semenza 2007). Hypoxia regulated genes are linked with processes such as regulation of angiogenesis, e.g. vascular endothelial growth factor (VEGF), energy metabolism, e.g. lactate dehydrogenase-A (LDH-A) and pyruvate kinase-2 (PKM-2), cellular differentiation, apoptosis and tumour metastasis, among others (Williams, Telfer et al., 2005; Patiar and Harris 2006; Semenza 2007). Such pathways are integral to cancer pathogenesis.

HIF is a α, β-heterodimer, consisting of the oxygen-sensitive HIF-α subunit and the constitutively expressed aryl hydrocarbon receptor nuclear translocator subunit (ARNT, also termed HIF-1β). Both subunits are members of the basic Helix-Loop-Helix PER-ARNT-SIM (bHLH-PAS) family of transcription factors (Wang, Jiang et al., 1995). Three isoforms of HIF-α are known to exist in mammals: HIF-1α, HIF-2α and HIF-3α, each having distinct biological properties and tissue distributions.

Hypoxia-inducible factor-1 (HIF-1) was first identified as a transcriptional regulator of the human erythropoietin gene (Semenza and Wang, 1992; Wang, Jiang et al., 1995). The steady-state abundance of the HIF-1α subunit is dependent on oxygen concentration. Under normoxic conditions, HIF-1α protein undergoes rapid degradation ($t1/2 < 5$ minutes) (Huang, Arany et al., 1996), controlled by an oxygen-dependent degradation (ODD) domain (Huang, Gu et al., 1998).

The Prolyl-Hydroxylase Domain (PHD)-containing enzymes are ferrous iron and 2-oxoglutarate-dependent oxygenases. PHDs are able to post-translationally modify HIF-1α and HIF-2α, through hydroxylation on at least one of two proline residues (Pro-402 and Pro-564) within the ODD domain (Ivan, Kondo et al., 2001; Jaakkola,

Mole et al., 2001 and Yu, White et al., 2001). The von Hippel-Lindau tumour suppressor protein (pVHL), which is the recognition component of an E3 ubiquitin ligase complex (Iwai, Yamanaka et al., 1999), is then able to bind to the hydroxylated HIF-1α, and mediates degradation of HIF-1α via the ubiquitin/proteasome pathway (Figure 1-4) (Maxwell, Wiesener et al., 1999 and Cockman, Masson et al., 2000). The PHDs require oxygen as a stoichiometric co-substrate

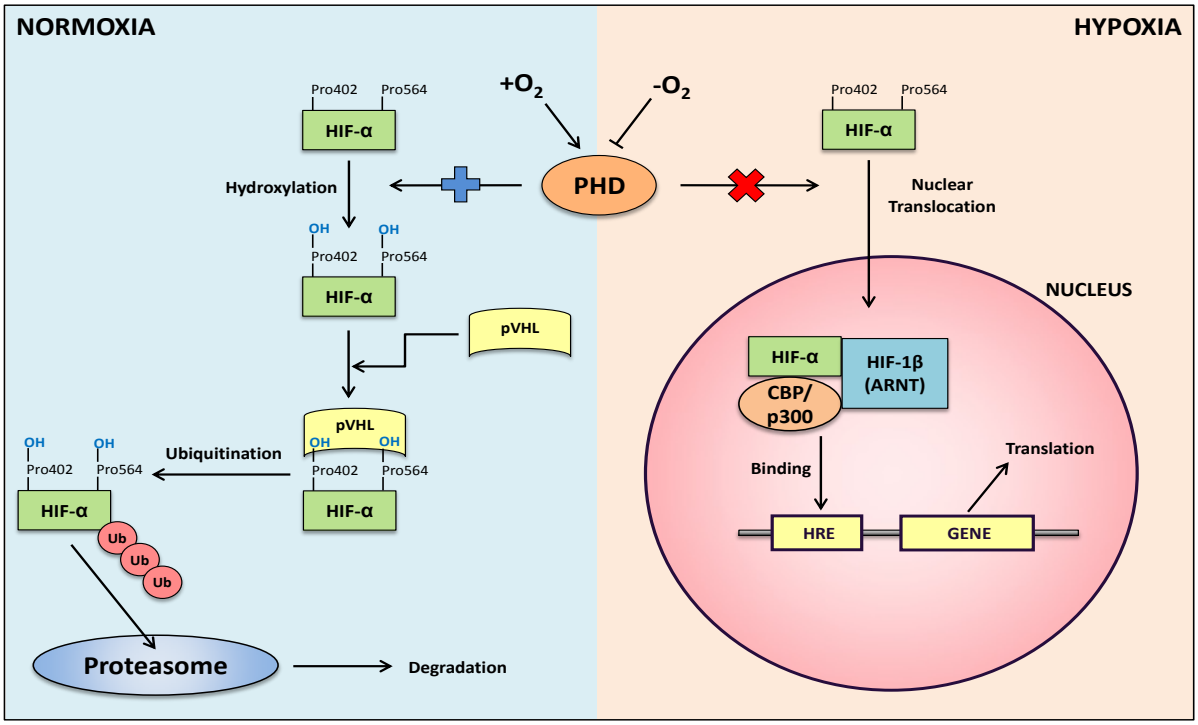

Figure 1-4: The hypoxia inducible factor (HIF) pathway under normoxic and hypoxic conditions. HIF-α is degraded under normoxic conditions via the ubiquitin/proteasome pathway. Under hypoxic conditions, HIF-α translocates to the nucleus, binds HIF-1β and mediates transcription of numerous hypoxia response genes through binding to hypoxia response elements (HREs) in their promoter regions. pVHL (von Hippel-Lindau tumour suppressor protein); Pro (proline); Ub (ubiquitin); PHD (prolyl-hydroxylase domain containing enzymes); ARNT (aryl nuclear hydrocarbon receptor nuclear translocator subunit); CBP (CREB-binding protein).

HIF-2α was the second Hypoxia-Inducible Factor to be discovered (Ema, Taya et al., 1997), and is structurally similar to HIF-1α, sharing approximately 48% overall amino acid sequence similarity. As with HIF-1α, HIF-2α able to bind ARNT and is regulated by pVHL.

HIF-3α was first identified by Gu and colleagues (Gu, Moran et al., 1998), and shares high amino acid sequence homology with both HIF-1α and HIF-2α. However, HIF-3α has been proposed to lack structures necessary for transactivation (increased gene expression), which are found to be present in the C-terminal domains of HIF-1α and HIF-2α (Hara, Hamada et al., 2001). In common with the other HIF subunits, HIF-3α is able to dimerise with ARNT, and bind HREs but has not been extensively studied to date (Ke and Costa 2006).

1.5. Cancer Metabolisms and the Warburg-Effect

Metabolic reprogramming is inextricably linked to each of the hallmarks of cancer (Ward and Thompson 2012). Whilst being traditionally viewed as a secondary effect in response to damaged mitochondria, or reduced ATP levels, many now consider altered metabolism to be an independent hallmark of cancer in its own right (Kroemer and Pouyssegur 2008; Hanahan and Weinberg 2011; Ward and Thompson 2012). Altered metabolism is a common feature of cancer cells; malignancy is proposed to be dependent on changes in metabolic pathways involved in glycolysis, glutaminolysis and biosynthesis of fatty acids, amino acids and nucleic acids (Ward and Thompson 2012).

A metabolic change observed almost universally in primary and metastatic cancers is a marked increase in glucose consumption, coupled with the up-regulation of glycolysis, which is the conversion of glucose to pyruvate. Many cancer cells sustain the up-regulation of glucose consumption, even in the presence of oxygen, a

phenomenon first identified by Otto Warburg, now referred to as the 'Warburg effect' (Warburg 1956) (Figure 1-5). Glycolysis uses the oxidative potential of 2 NAD+ molecules to yield 2 pyruvate and 2 ATP molecules per molecule of glucose. In normal cells, the pyruvate is then channeled to the mitochondria, where it is oxidised via the tricarboxylic acid (TCA) cycle. This generates NADH, which fuels oxidative phosphorylation (OXPHOS) and produces a maximum 38 ATP molecules per original molecule of glucose (Figure 1-5).

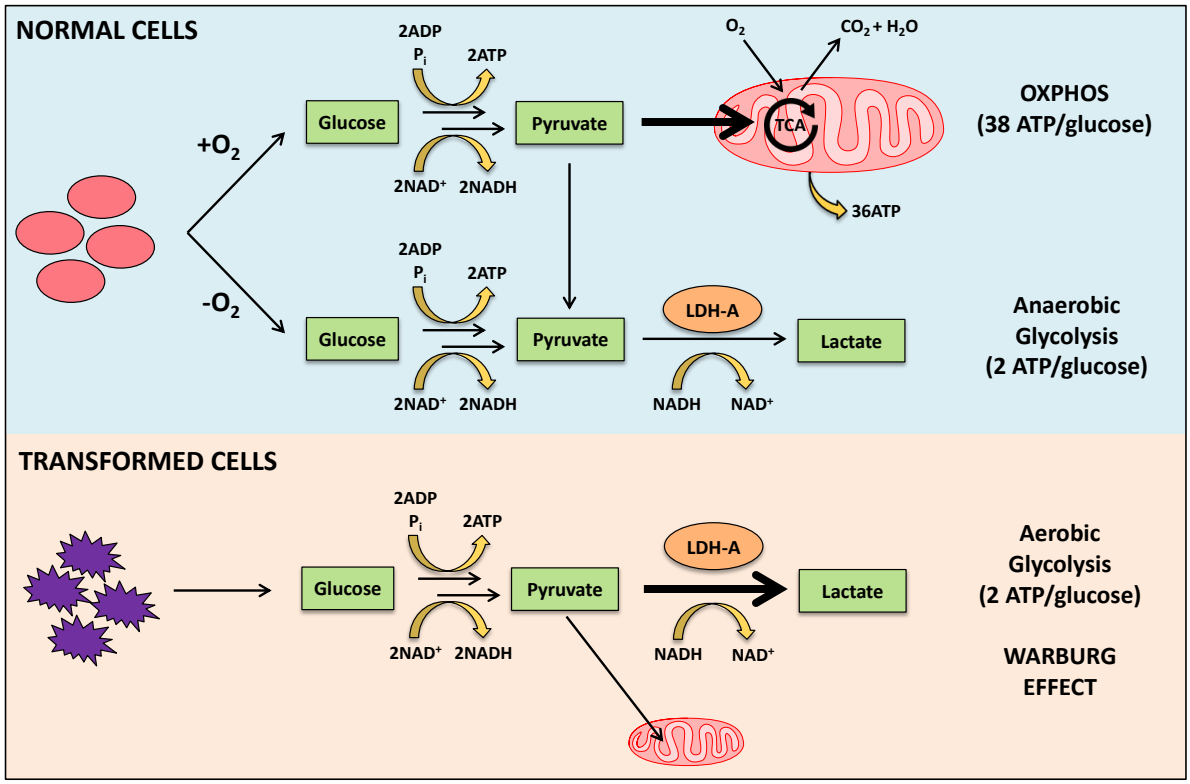

Figure 1-5: The Warburg effect. Glucose flux through glycolysis is increased under both normoxic and hypoxic conditions in transformed cells, whereas normal cells channel pyruvate to the mitochondria for full oxidative phosphorylation. ATP (adenosine triphosphate); ADP (adenosine diphosphate); LDH-A (lactate dehydrogenase A); NADH (nicotinamide adenine dinucleotide (reduced)); NAD^+ (nicotinamide adenine dinucleotide); TCA (tricarboxylic acid cycle).

It is somewhat counterintuitive then, that cancer cells would by-pass OXPHOS and switch to a form of metabolism that is over an order of magnitude less efficient in terms of ATP production. Nevertheless, numerous studies have correlated increased aerobic glycolysis with more aggressive tumour phenotypes and poor patient prognosis. Evolutionary theory dictates that glycolysis must therefore confer a significant proliferative advantage on the cancer cells (Gillies and Gatenby, 2007).

1.5.1. Why do Cancer have High Aerobic Glycolysis?

Warburg originally proposed that increased aerobic glycolysis could be a direct result of dysfunctional mitochondria in cancer cells. However, many cancer cells have now been shown to have fully functional mitochondria and active TCA cycles (Weinhouse 1976; Zu and Guppy 2004). A widely held view was that cyclical, periodic exposure to hypoxia would select for those cells able to constitutively up-regulate glycolysis, as they would better survive the periods of hypoxia (Gatenby and Gillies 2004). This theory warrants merit, yet would only partly explain the switch to aerobic glycolysis, as some cancer cells are able to utilise glycolytic metabolism before hypoxic exposure.

Whilst aerobic glycolysis produces ATP less efficiently than OXPHOS, it produces ATP approximately 100 times faster, suggesting this energetic trade-off may be utilised in cancer cells to maximal benefit (Bartrons and Caro, 2007). Accordingly, much literature has reinforced the perception that the primary purpose of increased glucose uptake by cancer cells is to facilitate an increase in ATP production through glycolysis (Pelicano, Martin et al., 2006; Gillies and Gatenby, 2007). However, studies have now shown that most cancer cells produce the majority of their ATP oxidatively, with only a relatively minor fraction of their ATP deriving from aerobic

glycolysis (Guppy, Leedman et al., 2002; Zu and Guppy 2004; Stubbs and Griffiths 2010). ATP is no longer considered to be a limiting factor for cancer cell survival and proliferation (Vander Heiden, Cantley et al., 2009; Lunt and Vander Heiden 2011). In fact, it is actually the rate of consumption of ATP that may be the limiting factor, due to the inhibitory effects ATP can exert on key glycolytic enzymes, such as 6-phosphofructo-1-kinase (PFK-1) (Scholnick, Lang et al., 1973; Israelsen and Vander Heiden 2010). Researchers have therefore been forced to look beyond cellular energetics to understand the Warburg effect and two theories currently prevail (Kroemer and Pouyssegur 2008); these are related to biomass generation and an increase in extracellular acidity.

1.5.2. Biomass Generation

A new theory relating to Warburg effect is the role that increased glucose consumption plays in the production of the biosynthetic precursors required for growth and proliferation (anabolic synthesis). This is linked to increased production of intermediates such as acetyl-CoA and NADPH for fatty acid production and ribose-5-phosphate (via the Pentose Phosphate Pathway (PPP)), which is required for nucleic acid production. The synthesis of these intermediates and other glycolytic intermediates used to produce non-essential amino acids, clearly imparts a proliferative advantage on the cancer cell (Vander Heiden, Cantley et al., 2009; Lunt and Vander Heiden 2011).

Furthermore, the by-product NADPH from the PPP has important anti-oxidant functions, acting as a co-factor in glutathione synthesis, which protects the cell from the effects of reactive oxygen species (ROS) (Vander Heiden, Cantley et al., 2009). Although this does in part explain the Warburg Effect, a large proportion of glucose metabolised by the cell is still exported as lactate or alanine (some studies suggest up

to 90% (DeBerardinis, Mancuso et al., 2007)), which is highly carbon-inefficient. It has been speculated that this apparent inefficiency is outweighed by the ability to rapidly up-regulate biomass production when required (Lunt and Vander Heiden 2011).

1.5.3. Acidic Extracellular and Cancer

A second theory, which stems from the observation that cancer, cells lower the pH of their extracellular space, at least substantially through the generation of lactic acid (from glycolysis) and carbonic acid (from oxidative phosphorylation). The normal physiological pH is 7.4, whereas the average extracellular pH of the tumour environment is often found to be in the range 6.2-6.7 (Paradise, Lauffenburger et al., 2011). In lowering the extracellular pH, cancer cells create a microenvironment selectively more toxic to normal tissue by promoting apoptosis in cells with functional p53 (Williams, Collard et al., 1999), as well as driving evolution of a more acid-resistant tumour phenotype (Bhujwalla, Artemov et al., 2002). This is known to facilitate tumour progression (Smallbone, Gavaghan et al., 2005), invasion via degradation of the extracellular matrix (Swietach, Vaughan-Jones et al., 2007), metastasis (Rofstad, Mathiesen et al., 2006) and suppression of the anti-cancer immune response (Fischer, Hoffmann et al., 2007).

1.5.4. Reprogramming and Regulation of Cancer Cell Metabolism

Metabolic regulation is extremely complex and can be controlled at multiple levels, including by expression of different splice isoforms of metabolic enzymes, e.g. pyruvate kinase M-2 (PKM-2) over pyruvate kinase M-1 (PKM-1), amplification or post-translational modification of metabolic enzymes, e.g. 6-phosphofructo-1-kinase (PFK-1). Furthermore, oncogenic mutations can occur in the enzymes themselves, e.g. isocitrate dehydrogenase-1 (IDH-1) and isocitrate dehydrogenase-2 (IDH-2) (Mardis, Ding et al., 2009). All of these factors are proposed to be important drivers

of altered metabolism (Ward and Thompson 2012). HIF-1 is also able to regulate metabolism through increasing the expression of numerous glycolytic enzymes, such as PFK-1 and LDH-A. Furthermore, HIF-1 also induces pyruvate dehydrogenase kinase-1 (PDK-1), which deactivates pyruvate dehydrogenase (PDH), thus restricting entry of pyruvate to the TCA cycle and therefore also suppressing OXPHOS (Kim, Tchernyshyov et al., 2006) (Figure 1-6).

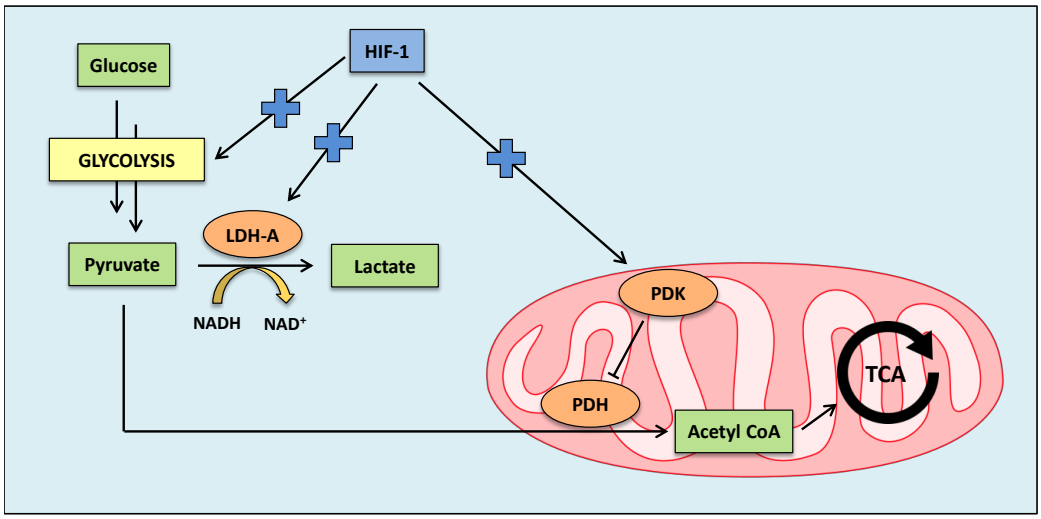

Figure 1-6: The role of hypoxia inducible factor 1 (HIF-1) in promoting glycolysis and restricting entry of pyruvate to the mitochondria. HIF-1 promotes up-regulation of glycolysis through increasing expression of glycolytic enzymes and lactate dehydrogenase A (LDH-A), and also restricts the entry of pyruvate into the tricarboxylic acid (TCA) cycle through pyruvate dehydrogenase kinase (PDK)-mediated down-regulation of pyruvate dehydrogenase (PDH) activity.

Aside from HIF, there are several upstream regulators of metabolic pathways. Of particular interest is the PI3K/Akt pathway, which has emerged as likely the most important and frequently activated in cancer (Robey and Hay 2009). Phosphoinositide 3-kinase (PI3K) signaling mediates activation of Protein Kinase B (Akt) via production of the phospholipid phosphatidylinositol (3,4,5)-triphosphate (PIP3). The activation of Akt and its downstream targets promotes cell survival, growth and proliferation, and is known to increase glucose uptake and glycolysis (Vivanco and Sawyers 2002; Elstrom, Bauer et al., 2004). Akt is therefore considered to be

intimately involved in the Warburg effect (Robey and Hay 2009). Mammalian target of rapamycin complex-1 (mTORC1), downstream of PI3K/Akt, is central to enhancing protein synthesis, de novo lipogenesis and promoting mitochondrial biogenesis (Cunningham, Rodgers et al., 2007). Myc is also known to be important in regulating mitochondrial biogenesis, glycolysis and glutaminolysis (Li, Wang et al., 2005; Kaadige, Elgort et al., 2010).

The tumour suppressor function of p53 now appears to be closely linked to its ability to regulate metabolism, in addition its widely accepted function in controlling cell cycle arrest, apoptosis and senescence (Li, Kon et al., 2012). Indeed, loss of wild-type p53 can promote glycolysis and anabolic synthesis in cancer cells (Matoba, Kang et al., 2006). An understanding of these regulators is important, but many function through protein-protein interactions, making therapeutic targeting difficult, hence the focus on inhibiting the downstream metabolic enzyme targets of these regulators (Vander Heiden 2011).

1.5.5. Targeting Cancer Tumour Metabolism

The search for drug-able metabolic targets for cancer is compounded by a number of factors. The first is an issue of selectivity akin to the limitations of chemotherapy. Many of the features of metabolic reprogramming found in cancer cells, such as aerobic glycolysis (Wang, Marquardt et al., 1976), are also shared by normal proliferative tissue. This renders many targets unsuitable due to associated side effects. The second is an issue of plasticity; cancer cells, like normal cells are often able to make use of multiple alternative biosynthetic routes to regenerate a depleted metabolite, as well as exchanging some metabolites between cells (Schulze and Harris 2012). A successful therapeutic strategy must therefore invoke a detailed understanding of such compensatory pathways. The third is an extension of tumour

heterogeneity; cancer cells within the same tumour with differing genetic mutations, or in response to differences in the microenvironment, may employ alternative metabolic reprogramming to promote their survival and proliferation (Vander Heiden 2011; Gerlinger, Rowan et al., 2012). This may necessitate the use of combination therapies to target different metabolic changes and complementary pathways.

Targeting tumour metabolism is attractive because all cancer cells likely rely on metabolic alterations to support their survival (Vander Heiden 2011). To date, only a small number of agents targeting metabolic pathways have been tested as potential cancer therapeutics (Vander Heiden 2011). A major challenge is to identify and exploit those metabolic differences that do exist between normal cells and cancer cells (Tennant, Duran et al., 2010). Targeting tumour-specific isoforms, or harnessing the high dependency of cancer cells on their altered metabolic pathways by suppressing, but not eliminating pathway activity, may permit selective targeting (Tennant, Duran et al., 2010). Indeed, cancer cells are thought to be more susceptible to perturbations in the activity of these pathways (Schulze and Harris 2012).

Numerous opportunities exist to target metabolic enzymes for cancer therapy, including inhibition of enzymes involved in nucleotide biosynthesis, amino acid and protein synthesis, lipid synthesis, glycolysis and TCA cycle/mitochondrial metabolism, which have been extensively reviewed elsewhere (Tennant, Duran et al., 2010; Vander Heiden 2011). Selection of suitable metabolic targets for the development of small molecule inhibitors requires a detailed understanding of the expression patterns and regulation of metabolic enzymes.

In considering potential metabolic targets, the near universal up-regulation of aerobic glycolysis in transformed cells and presence of hypoxia in most tumour microenvironments, is proposed to make glycolysis apart as a particularly attractive

target (Pelicano, Martin et al., 2006). Specifically targeting glycolysis in cancer cells with inhibitors may thus be expected to have broad therapeutic benefit. There are numerous strategies for targeting glycolysis, including via inhibition of glucose transporters (GLUTs), hexokinase (HK), pyruvate kinase M-2 (PKM-2) and lactate dehydrogenase A (LDH-A), which are all key proteins involved in this pathway (Pelicano, Martin et al., 2006; Porporato, Dhup et al., 2011).

A number of agents targeting metabolic pathways are now in clinical trials, which are discussed in several literature reviews (Porporato, Dhup et al., 2011; Vander Heiden 2011; Schulze and Harris 2012). For example, dichloroacetate (DCA) activates PDH, by inhibiting PDK-1, which increases delivery of pyruvate to the mitochondria, thereby shifting the balance from glycolysis to mitochondrial respiration (Michelakis, Webster et al., 2008). The DCA-mediated increase in mitochondrial respiration has been found in numerous studies to increase ROS levels and induce apoptosis, whilst suppressing proliferation of cancer cells (Saed, Fletcher et al., 2011; Sanchez, McGee et al., 2013).

The glucose analogue 2-deoxyglucose (2-DG) is transported into cells by the glucose transporters (GLUTs), where it is phosphorylated by hexokinase (HK) to 2-deoxyglucose-6-phosphate. This intermediate then becomes trapped in the cell, itself inhibiting both HK and glucose-6-phosphate isomerase activity, and therefore glycolytic flux (Wick, Drury et al., 1957). Nevertheless, 2-DG has shown a lack of efficacy as a single agent in the clinic, but has demonstrated promise as a combination therapy. For example, 2-DG has been found to sensitise osteosarcoma and non-small cell lung cancers to adriamycin and paclitaxel in pre-clinical mouse models (Maschek, Savaraj et al., 2004). Much interest has also focussed on the anti-diabetic drug metformin. Observational studies have found metformin to provide a significant

survival benefit in cancer patients with diabetes (Currie, Poole et al., 2012; Garrett, Hassabo et al., 2012). Metformin is thought to activate AMP-activated kinase (AMPK), which induces the up-regulation of cellular processes that increase ATP production, such as glycolysis and fatty acid β-oxidation, and down-regulates ATP-consuming processes (Buzzai, Jones et al., 2007; Dowling, Goodwin et al., 2011; Schulze and Harris 2012). However, the underlying molecular mechanisms that translate Metformin into the cancer-preventative effect of metformin remain poorly understood. The potential of metformin as a cancer treatment is currently being investigated in a series of clinical studies involving patients without diabetes (Pierotti, Berrino et al., 2013).

1.6. Normal Function of Isocitrate Dehydrogenases

1.6.1. Isocitrate Dehydrogenase Enzymatic Activity

IDH is an enzyme whose activity is to oxidatively decarboxylate isocitrate producing 2-OG and CO_2 (Haselbeck & McAlister-Henn, 1993). A schematic of the IDH reaction with all the family members is shown (Figure 1-7). During this process, NAD^+ or $NADP^+$ is reduced to NADH or NADPH, respectively, depending on the isoform that is catalysing this reaction. The IDH1 and IDH2 isoforms are $NADP^+$ dependent and function as homodimers (Bailey & Colman, 1985; Kelly & Plaut, 1981). The IDH isoform are structurally related sharing approximately 70% sequence identity (Xu et al., 2004). IDH1 is most highly expressed in liver and IDH2 is most lightly expressed in muscle (Haselbeck et al., 1992; Jennings et al., 1994). However, both isoforms show moderate expression within a variety of other tissues including the brain (Jennings et al., 1994). IDH1 and IDH2 enzymes are thought to play roles in the metabolism of glucose, fatty acids, and glutamine, and to contribute to the maintenance of normal cellular redox status. The IDH3 isoform is NAD^+ dependent,

functions as a heterotetramer consisting of 2 α, 1 β and 1 γ subunits (Ramachandran & Colman, 1980), and is structurally unrelated to IDH1 and IDH2 (Nichols et al., 1993; Nichols et al., 1995). IDH3 is the classical TCA cycle enzyme and plays an integral role in cellular energy metabolism, IDH3 is found predominantly in the mitochondria (Haselbeck & McAlister-Henn, 1993). IDH2 also localises to the mitochondria and has a mitochondrial signal peptide at its N-terminus (Nekrutenko et al., 1998). In contrast, IDH1 is localised mainly in the cytoplasm but has a type 1 peroxisomal targeting sequence permitting localisation in peroxisomes (Henke et al., 1998; Nekrutenko et al., 1998). The reactions catalysed by IDH1/2 are reversible while the similar reaction catalysed by IDH3 is apparently irreversible (Figure 1-7). Because only IDH1 and IDH2 mutations have been shown to be important in malignancies, I will not be addressing IDH3 further.

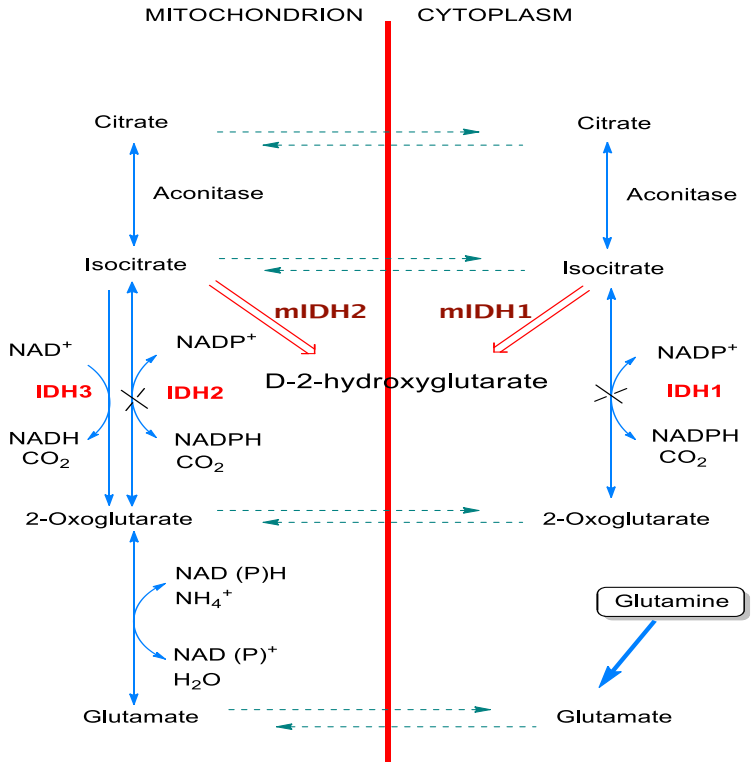

Figure 1-7: The role of the IDH family of enzymes in the tricarboxylic acid cycle and related transformations. Were Isocitrate Dehydrogenase 1/2 mutation (mIDH1/mIDH2) shown to be important in malignancies by increased in D-2-hydroxyglutarate levels.

1.6.2. Normal Function of Isocitrate Dehydrogenase in cells Metabolism

Both IDH1 and IDH2 play key roles in various cellular metabolic functions. IDH1 and IDH2 are involved in the oxidation of polyunsaturated fatty acids within peroxisomes (IDH1) and mitochondria (IDH2) by using the NADPH generated by their IDH activity (Minard & McAlister-Henn, 1999; van Roermund et al., 1998). In the brian, IDH1 is regulated by sterol regulatory element-binding proteins and also generates NADPH for peroxisomal lipogenesis (Shechter et al., 2003). In pancreatic islet cells, IDH1 has an important role in cellular glucose sensing as evidenced by impairment of glucose-stimulated insulin secretion after knockdown of IDH1 expression (Ronnebaum et al., 2006). Consistent with these functions, IDH1 transgenic mice display fatty livers, hyperlipidemia, obesity and higher glucose sensitivity on glucose tolerance testing consistent with enhanced insulin secretion (Koh et al., 2004). Finally, IDH2 has a possibly roles in the TCA cycle as evidenced by the lack of pathology in most normal tissues of certain retinitis pigmentosa patients with a homozygous IDH3 subunit defect (Hartong et al., 2008). The reverse IDH reaction (producing isocitrate and $NADP^+$ from 2-OG and NADPH) by IDH2 has been proposed as a way of limiting flux through the TCA cycle and dissipating the proton electrochemical gradient across the inner mitochondrial membrane with heat generation (Sazanov & Jackson, 1994). The various metabolic functions that have been defined to date show the central role that IDH1 and IDH2 play at the crossroads of lipid synthesis and carbohydrate utilization.

1.6.3. The role of Isocitrate Dehydrogenase and Response to Oxidative Stress

IDH1 and IDH2 likely also play a part in the oxidative stress response and helps limit damage from such insults. Consistent with this proposed, Mailloux et al., found that oxidative stress enhances 2-OG and NADPH production by IDH1 and IDH2 with a concomitant decrease in IDH3, 2-OG dehydrogenase, and succinate dehydrogenase activities decreasing utilization of the TCA cycle (Mailloux et al., 2007). NADPH produced by IDH1 and IDH2 also may be used by glutathione reductase for converting the oxidized form of glutathione disulfide (GSSG) to the reduced form glutathione (GSH) that can neutralize free radicals and reactive oxygen species (Jo et al., 2001; Kehrer & Lund, 1994; Lee et al., 2002). While the pentose phosphate pathway is the major source of NADPH required for regeneration of GSH, IDH1 and IDH2 also may contribute to the NADPH pool (Winkler et al., 1986). Lee et al. proposed a series of NIH3T3 derivatives that expressed varying levels of IDH1 and found that the ratio of GSH: GSSG was directly correlated with IDH1 expression level consistent with a role of this enzyme in the regeneration of GSH (Lee et al., 2002). Reduced expression of both IDH1 and IDH2 results in higher levels of reactive oxygen species and greater oxidative damage in response to an oxidative insult (Jo et al., 2001; Lee et al., 2002). In fact, numerous reports have now demonstrated that overexpression of IDH1 and IDH2 can protect cells against a variety of insults that produce oxidative stress (Jo et al., 2002; Kim et al., 2007; Lee et al., 2004; Shin et al., 2004). Based on the wealth of evidence demonstrating a role in the response of IDH1/2 to oxidative damage, the $NADP^+$-dependent IDHs clearly have significant functions beyond energy metabolism and biosynthetic processes.

1.7. Isocitrate Dehydrogenase 1 Mutations

1.7.1. Discovery of IDH 1 Mutations in Glioblastomas Multiforme

Glioblastoma multiforme GBMs are highly aggressive brain tumors classified by the World Health Organization (WHO) grading system as grade IV astrocytomas (Louis et al., 2007). While outcomes for patients diagnosed GBMs have gradually improved with better surgical/radiation therapy techniques and temozolomide chemotherapy, median survival still remain only slightly longer than one year (Stupp et al., 2005). With recent genomic technology advances, projects were initiated to perform detailed genomic analysis of various malignancies including GBMs; this effort quickly bore fruit with the discovery that IDH1 is frequently mutated in GBMs (Parsons et al., 2008). They performed an initial screen a consisting of comprehensive analysis of 20,661 protein-coding genes in 22 GBM samples. This yielded 21 mutated genes that were further analysed in a follow up screen on 83 additional GBMs. In addition to finding expected mutations at several genes known to be important in GBMs, the IDH1 gene was surprisingly found to be altered in 11% of analyzed GBMs. Most striking, mutations were invariably at a highly conserved arginine at position 132 (R132) found in the isocitrate binding site and was mutated to either histidine (R132H) (10 of 12) or serine (R132S) (remaining 2). This unexpected finding implicated IDH1 in the development and/or maintenance of glial neoplasms.

Follow up studies confirmed the presence of IDH mutations in GBMs (Balss et al., 2008; Hartmann et al., 2009; Sanson et al., 2009; Watanabe et al., 2009; Yan et al., 2009) (Table 1-1). GBMs are classified as primary or secondary depending on whether they arise spontaneously or from malignant transformation of a low-grade glioma. Interestingly, the frequency of IDH1 mutations was significantly higher in secondary (82%) than primary (6%) GBMs. Thus, the incidence of IDH mutations in an undifferentiated cohort of GBMs would depend on the distribution of primary and

secondary tumors in that group. Of note, initial studies suggest that pediatric GBMs only rarely harbor IDH mutations (Antonelli et al., 2010; Balss et al., 2008; Paugh et al., 2010; Yan et al., 2009). However, a recent paper suggests that pediatric malignant glioma patients ≥14 years of age appear to harbor IDH mutations at a substantial rate (7 of 20) (Pollack et al., 2011). This result suggests that high-grade gliomas in younger pediatric patients may be a different entity that those presenting in late adolescence with the older pediatric patients likely having a tumor that may be more similar to such tumors that present in young adulthood (eg. 20-40 years of age).

WHO Grade	Tumor type	Balss/Hartmann[1]	Yan[2]	Watanabe[3]	Sanson[4]	Total (percent)
IV	1° GBM	7/99	6/123	3/59	11/183	27/464 (5.8%)
	2° GBM	7/8	11/13	28/34	10/13	5668 (82.4%)
III	AA	148/228	38/52	21/27	9/18	216/325 (66.5%)
	AOA	128/177	7/7	10/14	34/35	179/252 (71.0%)
	AO	130/174	34/36	6/8	24/49	194/267 (72.7%)
II	A	167/227	27/30	60/68	10/12	264/337 (78.3%)
	OA	63/76	3/3	16/17	26/34	108/130 (83.1%)
	O	111/128	43/51	31/39	41/54	226/272 (83/1%)
I	Pilocytic Astrocytoma	1/41	0/21	3/31	NT	4/93 (4.3%)
I-III	Ependymoma	0/31	0/30	0/24	NT	0/85 (0%)

[1] Combined results of Balss and Hartmann studies due to duplication of some cases (Balss et al., 2008; Hartmann et al., 2009), [2] (Yan et al., 2009), [3] (Watanabe et al., 2009), [4] (Sanson et al., 2009). Abbreviations: WHO, World Health Organization; GBM, glioblastoma multiforme; AA, anaplastic astrocytoma; AOA, anaplastic oligoastrocytoma; AO, anaplastic oligodendroglioma; A, astrocytoma; OA, oligoastrocytoma; O, oligodendroglioma; NT, not tested.

Table 1-1: **Frequency of Isocitrate Dehydrogenase mutations in various glial brain tumors.**

Since secondary GBMs have a high incidence of IDH mutations, such mutations were postulated to be present in low-grade gliomas as well. As predicted, pooled results found IDH mutations in 65% to 80% of grade 2/3 astrocytomas (Table 1-1) (Balss et al., 2008; Hartmann et al., 2009; Sanson et al., 2009; Watanabe et al., 2009; Yan et al., 2009). Grade 2/3 oligodendrogliomas and oligoastrocytomas also had a high incidence of IDH1 mutations in the 70-85% range. Finally, pilocytic astrocytomas only rarely harbor IDH1 mutations (<5%) while no IDH1 mutations were found in ependymomas of any grade (Balss et al., 2008; Watanabe et al., 2009; Yan et al., 2009).

Although IDH1 and IDH2 reside largely in different subcellular compartments, they have the same enzymatic activity, utilize $NADP^+$, and are believed to provide some redundant function(s) in the cell. Yan et al. also sequenced IDH2 in addition to IDH1 in their series of brain tumors and found that IDH2 was, in fact, mutated at a low frequency on arginine at position 172 (R172), the analogous residue to R132 of IDH1 (Yan et al., 2009). Based on pooled results from multiple studies examining glioma brain tumors, when IDH is mutated, IDH1 is affected 96% of the time and IDH2 is affected in only 4% of cases (Table 1-2) (Hartmann et al., 2009; Sonoda et al., 2009; Yan et al., 2009). In addition, mutation on one IDH isoform was always mutually exclusive for mutation on the other isoform.

Type	Balss[1]	Ya[2]	Hartman[3]	Sanson[4]	Sonoda[5]	Total (percent)
IDH1	221	161	716	155	39	1292
R132H	205	142	664	138	39	1188 (92.0%)
R132C	8	7	29	5	--	49 (3.8%)
R132L	1	7	2	2	--	12(0.9%)
R132S	4	4	11	3	--	22 (1.7%)
R132G	2	1	10	7	--	20 (1.5%)
R132V	1	--	--	--	--	1 (0.1%)
IDH2	NT	9	31	NT	1	41
R172K	NT	4	20	NT	1	25 (61.0%)
R172M	NT	3	6	NT	--	9 (22.0%)
R172G	NT	2	--	NT	--	2 (4.9%)
R172W	NT	--	5	NT	--	5 (12.2%)

[1] (Balss et al., 2008), [2] (Yan et al., 2009), [3] (Hartmann et al., 2009), [4] (Sanson et al., 2009), [5] (Sonoda et al., 2009). Abbreviations: IDH, isocitrate dehydrogenase; NT, not tested.

Table 1-2: **Type and frequency of Isocitrate Dehydrogenase 1/2 (IDH1/IDH2) mutations in gliomas.**

1.7.2. Isocitrate Dehydrogenase Mutations in other Malignancies

After discovery of the specific $IDH1^{R132}$ and $IDH2^{R172}$ mutations in gliomas, there was significant interest in determining whether these mutations were also present in other malignancies. Despite screening of a large number of tumor specimens, very few non-glioma, solid malignancies were found to contain these mutations. One study found 2 in 75 (2.7%) prostate cancers with $IDH1^{R132}$ mutations while a second study found a metastatic melanoma with an $IDH1^{R132}$ mutant (Bleeker et al., 2009; Kang et al., 2009; Lopez et al., 2010). Kang et al. also found an $IDH1^{R132}$ mutation in 1 in 60 cases of B-cell acute lymphoblastic leukemia (Kang et al., 2009). Mutations at both $IDH1^{R132}$ and $IDH2^{R172}$ have now been shown to be present in acute myelogenous leukemias (AMLs). Mardis et al. were the first to report that 16 of 188 (8.5%) primary, cytogenetically normal AMLs had a mutation at R132 in IDH1 (Mardis et al., 2009). Likewise, Ward et al. found in their cohort that 6 in 60 (10%) karyotypically normal AMLs had the expected $IDH1^{R132}$ mutation (Ward et al., 2010). They also found that these AMLs were actually more likely to harbor mutations in $IDH2^{R172}$, with the previously defined R172K mutation observed in 5 cases together

with a new mutation altering arginine at position 140 to glutamine (R140Q) in IDH2. These specific mutations all resulted in elevated levels of 2-hydroxyglutarate (2-HG), a marker of mutant $IDH1^{R132}$ and $IDH2^{R172}$ activity. Marcucci et al., reported similar results in a Cancer and Leukemia Group B study where, out of 358 cases of cytogenetically normal AMLs, 47 had IDH1 mutations at R132, 13 had IDH2 mutations at R172 and 56 had IDH2 mutations at R140 (Marcucci et al., 2010). Based on these studies, it appears that ~30% of cytogenetically normal AMLs harbor mutations in IDH1/2. In addition, whereas the great majority of IDH mutations found in gliomas involve IDH1, IDH mutations in AML are more evenly distributed between IDH1 and IDH2 with a slight favoring of the latter. Unlike the case where IDH1 and IDH2 mutations were always mutually exclusive, rare instances of AMLs with both mutations present have been reported (Paschka et al., 2010).

1.8. Functional consequence of isocitrate dehydrogenase mutations

1.8.1. Isocitrate Dehydrogenase Mutants When lose Normal Enzymatic Activity

Based on modeling studies, the side chain of $IDH1^{R132}$ can form three hydrogen bonds with the α– and β–carboxyl groups of isocitrate while other residues within the binding site forms no more than two such bonds (Zhao et al., 2009). Thus, replacement of R132 is likely to impair interactions between isocitrate and this site. In fact, this residue in IDH1 has been previously mutated to glutamic acid (R132E) and resulted in almost complete abrogation of enzymatic activity (Jennings et al., 1997). Zhao and co-workers show that the activity of the R132H, R132C and R132S mutants dropped to less than 20% of the wild type IDH1 enzyme with a corresponding increase in the Km for isocitrate by 60 to 94-fold (Zhao et al., 2009). Porcine IDH2 have also been mutated at the site comparable to R172 in human IDH2 (R133Q) and

found to have decreased activity and increased Km for isocitrate (Soundar et al., 2000). All of the mutations found in $IDH1^{R132}$ and in $IDH2^{R172}$ have now been tested and the normal enzymatic activity is impaired in each case (Ichimura et al., 2009; Zhao et al., 2009).

1.8.2. Possible Dominant Negative Activity of Isocitrate Dehydrogenase 1 Mutant

The observation that $IDH1^{R132}$ mutations are specific, suggested the possibility of an activating mutation. This hypothesis appeared to be incorrect with the discovery that $IDH1^{R132}$ and $IDH2^{R172}$ mutations resulted in loss of enzymatic activity (see chapter 3) (Yan et al., 2009; Zhao et al., 2009). However, since homozygous deletions or other inactivating mutations of IDH1 and IDH2 had not been reported, the $IDH1^{R132}$ mutations (and the $IDH2^{R172}$ mutations) were clearly acting in a more complex fashion. These observations showed that $IDH1^{R132}$ mutants could act in a dominant negative inhibititory manner (Zhao et al., 2009). To investigate, His-tagged $IDH1^{wild-type}$ and a FLAG-tagged $IDH1^{R132H}$ variants were purified, mixed and subjected to affinity purification using nickel resin and anti-FLAG beads to obtain preparations of wild-type homodimer, R132H homodimers and wild-type: R132H heterodimers. The R132H homodimer was found to have no activity while the wild-type : R132 heterodimer had 4% of the wild-type homodimer activity. While this result partially explained how mutant $IDH1^{R132H}$ can act as a tumor suppressor in the absence of deletion of its second allele, this model was still not completely satisfying. In this model, mutant $IDH1^{R132H}$ needs to be in large excess (although amplification/overexpression has never been shown) or the wild-type mutant $IDH1^{R132H}$ interactions need to be favored over wild-type interactions (although such differential affinity has also never been demonstrated). In addition, the cellular metabolite profiles of cells engineered either to express the $IDH1^{R132H}$ variant or to

suppress expression of $IDH1^{wild\text{-}type}$ have been assessed and showed very little similarity, again consistent with the putative dominant negative function of mutant $IDH1^{R132H}$ having little if any role in vivo (Reitman et al., 2011). Finally, Jin others found that the various IDH1 and IDH2 variants did not associate with, or inhibit, the activity of the corresponding native IDH enzyme (Jin et al., 2011).

1.8.3. Isocitrate Dehydrogenase Mutations Results In A Neomorphic Enzyme Activity

Based on the results described in the previous section, it was considered that activating mutations in $IDH1^{R132}$ or $IDH2^{R172}$ might better fit the available observations. This hypothesis was finally proven with the report that 2-HG accumulates in glioma cells that express the $IDH1^{R132H}$ mutant (Dang et al., 2009). In particular, the (*D*)-enantiomer of 2-HG (*D*-2-hydroxyglutarate, *D*-2-HG) was detected with no difference in (*L*)-enantiomer (*L*-2-hydroxyglutarate, *L*-2-HG) levels found in mutant IDH1-expressing cells when compared with normal IDH1. Like previous investigators, Dang and co-workers found that the $IDH1^{R132H}$ mutant apparently inhibited the ability to oxidatively decarboxylate isocitrate to form 2-OG (Dang et al., 2010; Yan et al., 2009; Zhao et al., 2009). However, they showed that this mutant now gained a new activity, namely, the NADPH-dependent reduction of 2-OG to *D*-2-HG (Figure 1-8) (Dang et al., 2010). Importantly, co-expression of $IDH1^{wild\text{-}type}$ and the $IDH1^{R132H}$ mutant did not reduce this new enzymatic activity but actually appear to enhance it. This has led to the suggestion that heterodimers can more efficiently produce *D*-2-HG due to higher local concentrations of 2-OG and NADPH produced by the wild-type partner. The structures of $IDH1^{wild\text{-}type}$ and the $IDH1^{R132H}$ mutant have been compared (Dang et al., 2009; Xu et al., 2004).

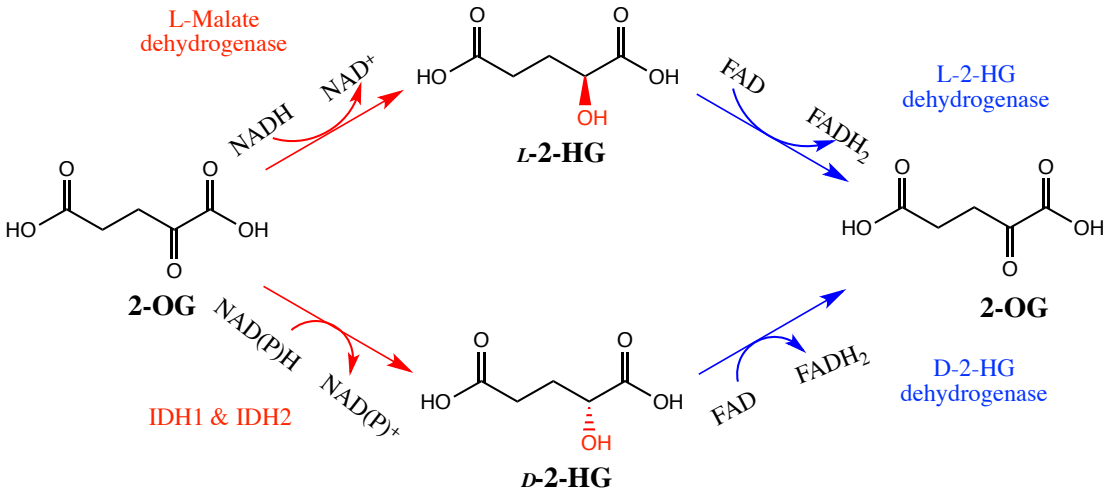

Figure 1-8: 2-hydroxyglutarate (2-HG) enantiomer formation. L-2-HG and D-2-HG formation via NAD(P)H-dependent reduction of 2-oxoglutarate (2-OG) by side reactions of L-malate dehydrogenase and variants of isocitrate dehydrogenase 1/2 (IDH1/ IDH2), respectively. they showed that this mutant now gained a new activity, namely, the NADPH-dependent reduction of 2-oxoglutarate (2-OG) to *D*-2-Hydroxyglutrarte (D-2-HG).

Ward et al. performed a comparative analysis of the $IDH2^{R172K}$ variant found in AMLs and gliomas (Ward et al., 2010). Similar to the finding of Dang et al., this $IDH2^{R172K}$ mutant also displayed 2-OG dependent NADPH consumption and accumulation of 2-HG within expressing cells and surrounding media (Dang et al., 2010; Ward et al., 2010). Interestingly, they also found that knockdown of both wild-type IDH1 and IDH2 with siRNA dramatically decreased the proliferative capacity of a cancer cell line (Ward et al., 2010). These findings provide another explanation for why the corresponding normal IDH allele is not deleted and actually appears to always be present with the mutant IDH allele. Finally, this study investigated a new IDH mutant $IDH2^{R140Q}$ that also resulted in accumulation of 2-HG in cytogenetically normal AMLs. $IDH2^{R140}$ is also a highly conserved residue and structural modeling puts it immediately adjacent to $IDH2^{R172}$ in the isocitrate-binding site, which helps explain acquisition of this neomorphic enzymatic activity in $IDH2^{R140}$ mutants. To date, R140 mutations in IDH2 have not been identified in gliomas. Based on previous discussions, IDH1 mutations at R132 and IDH2 mutations at R140 and R172 gain

similar new enzymatic function. However, differences must still exist between these mutations due to the observed disparity in distribution of IDH1 and IDH2 mutations in gliomas (ratio of ~9:1) and AMLs (ratio of ~2:3). One factor in this difference may lie in their respective subcellular locations. IDH1 is primarily cytosolic and peroxisomal where NADPH is more limiting, while IDH2 is mitochondrial where NADPH is more readily available (because it can be easily interchanged with NADH produced by IDH3 through the action of H^+-transhydrogenase) (Sazanov & Jackson, 1994). Despite this, both mutant IDH1 and IDH2 can produce 2-HG, which can readily pass throughout the cell and even be secreted, and no definite functional differences between the two mutants enzyme have been demonstrated.

1.9. The Effect Of Mutant Isocitrate Dehydrogenase On Normal Cellular Functions

1.9.1. The Effect Of Mutant Isocitrate Dehydrogenase On Cellular Metabolism

Mutant IDHs are clearly selected for in gliomas and AMLs. While $IDH1^{wild\text{-}type}$ and $IDH2^{wild\text{-}type}$ have well-defined roles in metabolism, it remains unclear in what way expression of mutant IDHs will alter these various processes. One consequence of mutant IDH expression is decreased NADPH levels, which can potentially affect cellular biosynthetic processes such as lipogenesis. Similarly, depletion of cytosolic NADPH may be sensed in the cell as a low nutrient status leading to a response marked by increasing cellular nutrient consumption (eg. increase glucose transporters, increase throughput in the pentose phosphate pathway, etc.). These responses may provide malignant cells expressing mutant IDHs with a selective growth advantage. Reitman et al. have now profiled >200 metabolites in human oligodendroglioma cells engineered to express mutant $IDH1^{R132H}$ and $IDH2^{R172K}$ (Reitman et al., 2011). One striking finding from this study was that the profiles of mutant IDH-expressing cells were very similar to those of corresponding cells treated with 2-HG, a cell permeable

precursor of 2-HG. Their observations implicate this $IDH1^{R132H}$ and $IDH2^{172K}$ product as a key component of the cellular changes seen in mutant IDH-expressing cells. The main changes found on this study include increases in 1) free amino acids, 2) increases in lipid precursors such as glycerol-phosphates and 3) glycerophosphocholine, 4) depletion of TCA cycle intermediaries and 5) depletion of N-acetylated amino acids such as N-acetyl-aspartate and N- acetyl-aspartyl-glutamate, two of the most abundant small-molecule in brain.

1.9.2. Mutant Isocitrate Dehydrogenase Is Associated With A Hypermethylation Phenotype In Gliomas

Association of IDH1 mutations with the proneural GBM subtype was a key finding from the assessment of GBMs in The Cancer Genome Atlas (TCGA) as based mainly on expression profiling (Verhaak et al., 2010). This project provided a host of genetic and epigenetic information about GBMs; the investigators also looked for other factors that may associate with mutant $IDH1^{R132}$. This work culminated in finding a glioma-CpG island methylator phenotype (G-CIMP) that defined a subgroup of GBMs that was tightly associated with $IDH1^{R132}$ mutations (Noushmehr et al., 2010). Patients with proneural GBMs have been previously shown to have a better prognosis (Phillips et al., 2006; Verhaak et al., 2010). This study replicated that finding but found that G-CIMP positivity was an even stronger predictor of better outcomes (Noushmehr et al., 2010). The association between mutant $IDH1^{R132}$ and G-CIMP positivity also held in grade II and III gliomas and G-CIMP positivity still predicted for survival in the lower grade tumors. These results have now been replicated in an independent set of gliomas with the presence of IDH mutations correlating more strongly with hypermethylation than TP53 mutation or lack of EGFR alterations (Christensen et al., 2011). Hypermethylation of the O-6-methylguanine-DNA-methyltransferase (MGMT) promoter is highly associated with better outcomes in

patients with GBM (Hegi et al., 2005; Stupp et al., 2009). Given its prognostic value, MGMT methylation testing has become relatively standard in the pathologic workup of GBMs. Although MGMT was not among the 50 most differentially hypermethylated genes on the TCGA study (Noushmehr et al., 2010), MGMT hypermethylation is correlated with $IDH1^{R132}$ mutations in gliomas (Christensen et al., 2011; Laffaire et al., 2010; Sanson et al., 2009).

1.9.3. Mutant Isocitrate Dehydrogenase Is Associated With Hypermethylation In AMLs

Previously, AMLs without known genetic or molecular features were found to be classifiable into five distinct clusters with particular epigenetic signatures (Figueroa et al., 2010b). Similar to the association of IDH1 mutation and G-CIMP, IDH1/2 mutations were also associated with certain DNA methylation patterns in AML (Figueroa et al., 2010a). AMLs with IDH mutations fell primarily in two epigenetically-defined clusters that tended toward increased DNA methylation, was reminiscent of G-CIMP (Figueroa et al., 2010a; Noushmehr et al., 2010). Hypermethylation was associated with decreased expression of the relevant gene in the majority of cases. Unlike GBMs where >90% of IDH mutations were on IDH1, mutations in AMLs are more equally distributed permitting comparisons in the type of methylation phenotypes that arise. Giving more support for IDH mutants having a causative role in increasing DNA methylation, engineered overexpression of mutant IDH1 or IDH2 both leads to increased 5-methylcytosine levels (Figueroa et al., 2010a).

1.10. 2-Hydroxyglutaric acid

2-Hydroxyglutarate is a five-carbon dicarboxylic acid with a hydroxyl group at its alpha (C-2) position. There are therefore two possible enantiomers of 2HG: *D*-2-HG [otherwise known as *R*-2HG] and *L*-2-HG [otherwise known as *S*-2-HG]. The 2-HG metabolite occurs naturally in animals (Gregersen et al., 1977 and Rasmussen et al., 1990), plants (Araújo et al., 2010 and Engqvist et al., 2011), yeast (Albers et al., 1998 and Coote and Kirsop, 1974), bacteria (Kopchick and Hartline, 1979, Wegener et al., 1968 and Zhao and Winkler, 1996) and humans (Dang et al., 2010; Nyhan et al., 1995 and Rashed et al., 2000).

Two three dimensional (3D) structures of 2-HG exist (Figure 1-9), *D*-2-HG and *L*-2-HG, which represent "non-superimposable" mirror images (Figure 1-9). Whereas enantiomers share identical chemical and physical properties (melting point, mass, solubility and pKa), their differing 3D-structures result in considerable differences in enzymatic and molecular properties.

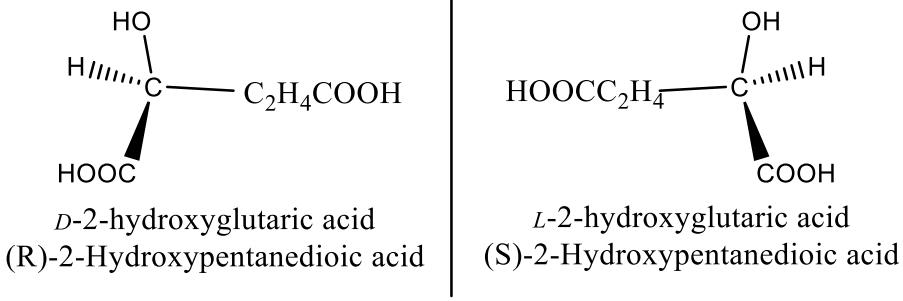

Figure 1-9: Two three dimensional (3D) structures of *D*- and *L*-2-hydroxyglutaric acid structures (D-2-HG and L-2HG enantiomers; systemic IUPAC names are given).

D-2-HG and *L*-2-HG are proposed to be unwanted byproducts of cellular metabolism; their intracellular levels in normal cells are maintained at <0.1 mM (Struys et al., 2004). 2-HG is prevented from accumulating in cells by the actions of two enzymes *D*-2-HG and *L*-2-HG dehydrogenase (2-HGDH) that convert *D*-2-HG and *L*-2-HG, 'back' to 2-OG (Struys et al., 2004). There is currently no known physiological role for either enantiomer in normal metabolism.

1.10.1. Disorders That Result In Accumulations Of 2-Hydroxyglutarate

Gregersen and co-workers were the first to identify enantiomeric *L*- and *D*-2-HG as normal constituents of human urine (Gregersen et al., 1977). Three years later, two related novel inborn errors of metabolism were simultaneously reported in the Journal of Inherited Metabolic Disease. Chalmers and co-workers identified a patient with *D*-2-hydroxyglutaric aciduria (*D*-2-HGA) (Chalmers et al., 1980). Duran and co-workers described a case of *L*-2-hydroxyglutaric aciduria (*L*-2-HGA) (Duran et al., 1980). There were landmark publications that identified the metabolic 'hallmarks' *L*- and *D*-2-HG in these disorders. Muntau et al., (2000) described a third biochemical variant of 2-hydroxyglutaric aciduria (2-HGA); they reported three patients with elevated urinary *L*- and *D*-2-HG, denoted by these authors as "combined *L*, *D*-2hydroxyglutaric aciduria" (*L*, *D*-2-HGA).

A major milestone, in research on these disorders came with the discovery of 2-HG dehydrogenase: D2HGDH encodes for a *D*-2-hydroxyglutarate dehydrogenase (*D*-2-HGDH) (Achouri et al., 2004) and L2HGDH encodes for a *L*-2-hydroxyglutarate dehydrogenase (L-2-HGDH) (Rzem et al., 2004; Topcu et al., 2004). In many patients with elevated *D*-2-HGA, and the majority of patients with elevated *L*-2-HGA, genetic characterization revealed pathogenic mutations in these genes (Struys et al., 2005b; Steenweg., 2010). Nonetheless, in one-half of *D*-2-HGA patients no mutations in

D2HGDH were detected (Kranendijk et al., 2010). Subsequently, (Kranendijk et al., 2010) gain-of-function mutations in isocitrate dehydrogenase 2 (IDH2) were described, which proved causative for the *D*-2-HG accumulation in previously unclassified *D*-2-HGA patients. In summary, the preceding decade has provided tremendous advances in our understanding of the inborn 2-HG acidurias, which provide a solid foundation from which to develop novel and effective treatment strategies.

1.10.2. Mutant IDH-Derived D-2-hydroxyglutarate Is An Oncometabolite

IDH mutants exclusively (as far as is known) produce the *D*-enantiomer of 2-HG, and the levels of *D*-2-HG in IDH mutant tumors can be extremely elevated, ranging from 1 mM to as high as 30 mM (Dang et al., 2009; Gross et al., 2010; Choi et al., 2012). These high levels of *D*-2-HG appear to be a consequence of a significant imbalance between *D*-2-HG production and metabolism in tumor cells. $IDH1^{R132H}$ has an estimated catalytic rate (k_{cat}) of 1.0×10^{3} sec^{-1} (Dang et al., 2009), whereas recombinant D2HGDH has an estimated k_{cat} of 0.8 sec^{-1} (Engqvist et al., 2011). It is therefore possible that the activity of the mutant IDH overwhelms the capacity of D2HGDH to oxidize the excess *D*-2-HG back to 2-OG. This model is supported by the observation that in patients with type I *D*-2-HGA, an inborn neurometabolic disorder caused by germline mutations in D2HGDH, levels of *D*-2-HG are elevated but to a much lesser extent than is observed in IDH^{R132H} mutant tumors (Wickenhagen et al., 2009). Type II D2HGA, which is caused by germline $IDH2^{R140Q}$ and $IDH2^{R140G}$ mutations, is associated with higher levels of *D*-2-HG and a more severe clinical course (Kranendijk et al., 2010). Interestingly, D2HGA is not associated with an increased incidence of cancer. It is important to note, however, that many patients with severe D2HGA die in infancy and early childhood, and it is therefore difficult to

make definitive conclusions about an association between high levels of *D*-2-HG and long-term susceptibility to cancer.

High intracellular concentrations of *D*-2-HG are sufficient to mediate the in vitro transforming effects of mutant IDH. Treatment of TF-1 leukemia cells with concentrations of a cell-permeable form of *D*-2-HG that achieve tumor-relevant intracellular levels is able to recapitulate the effects of mutant IDH expression (Losman et al., 2013); treatment of cells with cell-permeable *D*-2-HG is able to inhibit the differentiation of murine 3T3-L1 fibroblasts and immortalized murine myeloid progenitor cells (Lu et al., 2012; Losman et al., 2013). Furthermore, tumor cells that harbor IDH mutations and produce high levels of *D*-2-HG appear to require continuous *D*-2-HG to remain transformed. Withdrawal of *D*-2-HG from TF-1 leukemia cells transformed by cell-permeable *D*-2-HG reverses their growth factor independence and restores their ability to differentiate (Losman et al., 2013); inhibition of mutant IDH1 expression in glioma cell lines that harbor naturally occurring IDH1 R132H mutations impairs in vitro colony formation and in vivo tumor engraftment by the cells (Rohle et al., 2013).

Finally, highly potent and specific inhibitors of mutant IDH have been developed that are able to reverse the transformation of TF-1 cells expressing $IDH1^{R132H}$ and $IDH2^{R140Q}$ (Popovici-Muller et al., 2012; Losman et al., 2013; Wang et al., 2013). These inhibitors also induce the differentiation of primary IDH mutant human leukemia cells in vitro and recapitulate the effects of suppression of $IDH1^{R132H}$ expression in IDH mutant glioma cell lines in vitro and in vivo (Rohle et al., 2013; Wang et al., 2013). Taken together, these findings suggest that the transforming activity of mutant IDH is mediated by *D*-2-HG and that *D*-2-HG is necessary to maintain the transformed phenotype of tumor cells that harbor IDH mutations.

1.10.3. IDH1 and IDH2 mutants differ in D-2-hydroxyglutarate production

The different IDH1 and IDH2 mutants ($IDH1^{R132}$, $IDH2^{R140}$, $IDH2^{R172}$ and their variants) possess varying enzymatic properties. The most common IDH1 and IDH2 mutants in AML (IDH1R132H and IDH2R140Q, respectively) are weak *D*-2-HG producers, as compared with same variants in glioma. For example, the most common IDH1 mutant in CS ($IDH1^{R132C}$) produces relatively high levels of *D*-2-HG (Ward et al., 2010, Jin et al., 2011 and Ward et al., 2013). The only IDH2 mutant that is found in the inherited metabolic disease *D*-2-HG aciduria is the weakest identified *D*-2-HG-producing $IDH2^{R140Q}$ mutant. It has been proposed that only the lower *D*-2-HG levels that result from such mutations are compatible with embryogenesis; IDH1 and IDH2 germline mutations leading to higher *D*-2HG levels may be embryonically lethal (Ward et al., 2013). It is hypothesized that in oncogenesis, the intracellular *D*-2HG concentration that gives the largest growth advantage varies depending on the tumor's cell type of origin. This could explain why each type of cancer has a specific IDH1/2 mutation. In addition, an IDH1/2 mutation and the subsequent high *D*-2-HG levels may affect which specific type of cancer is being formed (Horbinski et al., 2013).

It is likely that a spectrum of variants/activities cause a spectrum of *D*-2-HG accumulation levels (Ward et al., 2013, Pusch et al., 2014, Ward et al., 2012). Thus, optimal *D*-2-HG concentrations alone do not satisfactorily explain why $IDH1^{R132H}$ mutations are much more prevalent than $IDH2^{R172K}$ mutations in glioma. Another reason may be that in hypoxia, IDH1 and IDH2 can operate in reverse using glutaminolysis to produce citrate, which can subsequently be used for fatty acid production. In vitro studies have shown that different cell lines use either IDH1 or

IDH2 or both for these reversed reactions. SF188 glioblastoma cells use IDH2 to catalyze reductive carboxylations (Wise et al., 2011), A549 lung carcinoma, HCT116 colon carcinoma, MF10A mammary epithelial and MDA-MB-231 mammary carcinoma cells use IDH1 (Metallo et al., 2012, Grassian et al., 2014) and 143B osteosarcoma cells can use both IDH1 and IDH2 (Mullen et al., 2012). The reason why some cells prefer IDH1 or IDH2 over the other for reductive carboxylation is unknown at this moment.

Mutations can inactivate the capacity of IDH1 and IDH2 to carry out their forward and reverse reactions (Leonardi et al., 2012). Thus, IDH2 mutations may hinder glioblastoma citrate production, which is essential for cellular proliferation. Although both IDH1 and IDH2 mutations promote oncogenesis, only IDH1 mutations may retain the glioblastoma cells' ability to synthesize critical macromolecules from glutaminolysis. This model captures a selective pressure for IDH1 mutations over IDH2 mutations in glioblastoma. Because of the balanced frequencies of IDH1 and IDH2 mutations in AML, it is speculated that leukemic cells may be able to use both IDH1 and IDH2 for reductive carboxylation.

1.10.4. Metabolic consequence of 2-hydroxyglutarate accumulation

The direct treatment of cells with *D*-2-HG results in a metabolite profile, that was similar to that observed with mutant IDH1 and IDH2-expressing cells (Reitman et al., 2011). Of the 204 assessed metabolites, from 107 to 130 were altered either up or down in the R132H-expressing or 2-HG-treated cells. Of these, 64 metabolites changes were shared between these cells. This number was much greater than the metabolites changes seen when comparing the R132H-expressing and the IDH1 knockdown cells where only 28 metabolites were altered similarly. Likewise, mutant $IDH2^{R172K}$ gave a profile similar to the $IDH1^{R132H}$ mutant. While these results suggest

that *D*-2-HG is mediating some of the downstream effects of mutant IDH1 and IDH2, significant differences still exist, highlighting 2-HG-independent effects of the mutant IDHs. One potential difference between these cells is that mutant IDH1 expression leads to glutamate depletion due to its conversion to 2-OG and 2-HG while simply treating cells with 2-HG will not deplete glutamate. Some of the observed differences are consistent with this explanation as decreases in glutamate and several metabolites that are directly or indirectly derived from glutamate including glutathiones, N-acetylglutamate, N-acetyl-aspartyl-glutamate, 2-OG, malate and fumarate are seen uniquely in mutant IDH1-expressing cells (Reitman et al., 2011). However, this explanation does not account for all the differences seen and mutant IDH expression is still likely to be causing some changes in the metabolite profile that is 2-HG independent. These exact changes remain to be defined. The overall implication of these metabolite shifts on glioma-genesis is currently still largely unknown. However, there is an increasing recognition that changes in metabolism can have effects on tumorigenesis (for review, see (Vander Heiden et al., 2009)) and further research will likely begin to unravel the answers to these questions in the near future.

1.10.5. What can 2-hydroxyglutarate Cellular metabolism inhibit?

A possible breakthrough in elucidating the function of 2-HG came with the discovery that it can inhibit the function of the Tet methylcytosine dioxygenase (TET) (Xu et al., 2011). Members of the TET family catalyze the conversion of 5-methylcytosine to 5-hydroxymethylcytosine (5-OH-MeC) in a reaction requiring 2-OG, iron and oxygen (Tahiliani et al., 2009). While the physiological significance of 5-OH-MeC has not been fully defined, it is proposed to be an intermediate in the pathway that demethylates 5-methylcytosine. Thus, TET activity will result in decreased DNA methylation with potential widespread changes in gene expression. The first clue that

2-HG may be interacting with TET was the discovery that TET2 loss-of-function mutations seen in AML was mutually exclusive with IDH1/2 mutations (Of 375 cases, 57 were IDH mutants, 28 were TET2 mutants, 0 were both IDH and TET2 mutants) (Figueroa et al., 2010a). This result suggests that IDH1/2 mutations and TET2 mutations have overlapping roles in AML pathogenesis. Forced expression of TET2 also resulted in increased 5-OH-MeC levels and this could be blocked by co-transfection with mutant but not wild type IDH1. Xu and co-workers have shown that 2-HG can act as a competitive inhibitor of multiple 2-OG-dependent dioxygenases including the TET family of 5-methylcytosine hydroxylases, histone demethylases and even prolyl hydroxylases (Xu et al., 2011). Using an in vitro enzymatic assay, *D*-2-HG could inhibit the activity of TET1 and TET2 reducing 5-OH-MeC in a dose-dependent fashion. Interestingly, *L*-2-HG, which is not produced by mutant IDH, was actually even more effective at inhibiting the TET enzymes than the *D*-enantiomer (Xu et al., 2011). This result may partially explain why malignant brain tumors were associated with the *L*-2-HGA but not the *D*-2-HGA genetic disorder.

A number of other 2OG-dependent enzymes might be inhibited by *D*-2HG in IDH mutant tumors. Three types of collagen hydroxylases—the Leprecan family of prolyl-3-hydroxylases, the P4HA family of prolyl-4-hydroxylases, and the PLOD family of lysyl-5-hydroxylases— all require 2-OG for activity, and P4HA1 has been found to be inhibited by *D*-2-HG in vitro (Koivunen et al., 2012). The collagen prolyl-hydroxylases mediate the hydroxylation of proline residues required for formation of the collagen triple helix (Gorres and Raines 2010), and the collagen lysyl-hydroxylases mediate the hydroxylation of lysine residues required for collagen cross-linking into stable fibrils (Bank et al., 1999). Interestingly, collagen maturation has been found to be impaired in the brain-specific $IDH1^{R132H}$ knock-in mice, suggesting

that these enzymes are targets of inhibition by mutant IDH in vivo (Sasaki et al., 2012a). Although a role for these enzymes in cancer has not been established, the observation that expression of collagen prolyl-3-hydroxylases and prolyl-4-hydroxylases is down- regulated in many B-cell lymphomas suggests that these enzymes function as tumor suppressors in some tissues (Teodoro et al., 2006; Hatzimichael et al., 2012). Other potential 2OG-dependent targets of *D*-2-HG include FIH1 (factor inhibiting hypoxia-inducible factor1), an asparaginyl hydroxylase that regulates the tran- scriptional activity of HIF (Mahon et al., 2001); the ABH family of DNA demethylases that are involved in DNA damage repair (Lee et al., 2005); and the RNA demethylase FTO (fat mass and obesity-associated), which is believed to be important for the regulation of cellular metabolism (Jia et al., 2008; Berulava et al., 2013).

1.11. 6-Phosphofructo-2-kinase/fructose-2,6-bisphosphatase (PFG-2/FBP ase-2)

PFK-2/FBPase-2 is a homodimeric, bifunctional enzyme. It catalyses the ATP-mediated phosphorylation of Fructose-6-phosphate (F-6-P) to Fructose 2,6-bisphosphate (F-2,6-BP) at its N-terminal kinase domain, whilst catalysing the degradation of F-2,6-BP to F-6-P and P_i at its C-terminal phosphatase domain. There are four isoenzymes, designated 6-phosphofructo-2-kinase/fructose-2,6-biphosphatas 1-4 **(**PFKFB1-4) and numerous cells and tissue types exhibit simultaneous expression of multiple isoenzymes, suggesting they may have distinct roles in regulating intracellular F-2,6-BP concentration (Calvo, Bartrons et al. 2006; Telang, Yalcin et al. 2006; Bartrons and Caro 2007). The PFK-2/FBPase-2 isoenzymes are thought to tightly control flux through the glycolytic and PPP pathways, maintaining a balance between the ATP, biosynthetic and antioxidant requirements of the cell (Herrero-Mendez, Almeida et al. 2009).

Originally identified in bovine brain (Ventura, Ambrosio et al., 1995) and human placenta (Sakai, Kato et al., 1996), at least six splice variants of PFKFB3 are now known to exist, which vary in the length of their C-termini. The two principle variants are inducible PFK-2 (iPFK-2) and ubiquitous (uPFK-2 or PFKFB3-ACG), also denoted UBI2K4 and UBI2K5, respectively. The remaining four variants were identified in human brain and are denoted UBI2K1-3 and UBI2K6 (Kessler and Eschrich 2001). PFKFB3 mRNA is constitutively expressed in proliferating tissue (Hamilton, Callaghan et al., 1997; Goren, Manzano et al., 2000), and can be induced by stress stimuli (Novellasdemunt, Bultot et al., 2013), insulin (Riera, Manzano et al., 2002) and progestins (Hamilton, Callaghan et al., 1997; Novellasdemunt, Obach et al., 2012).

PFKFB3 is over-expressed in a wide range of transformed cells (Hirata, Kato et al., 1998) and human cancers, including breast, colon (Minchenko, Ochiai et al., 2005), lung (Minchenko, Ogura et al., 2005), gastric (Bobarykina, Minchenko et al., 2006), glioblastoma (Kessler, Bleichert et al., 2008), ovarian and prostate (Atsumi, Chesney et al., 2002). Studies have also shown PFKFB3 is required for tumour cell growth in vitro and in vivo (Chesney, Mitchell et al., 1999) and that expression of PFKFB3 is selectively required to mediate the increase in glycolytic flux that results from introduction of oncogenic ras to cells (Telang, Yalcin et al., 2006).

PFKFB3 has been observed to have the highest basal kinase: bisphosphatase (K: B) activity ratio of the four isoenzymes (740:1) (Sakakibara, Kato et al., 1997). A PFKFB3 crystal structure has revealed a structural rationale for this unusually high kinase activity (Kim, Manes et al., 2006). The N-terminus was found to bind to the FBPase-2 domain in the C-terminal region, leading to a local change in structure that enhances binding of the FBPase-2 catalytic site to the fructose-6-phosphate product,

thereby slowing its release (the rate determining step), reducing turnover and lowering the FBPase-2 catalytic activity (Kim, Manes et al., 2006). A key catalytic Arg residue, present in the FBPase-2 domains of the other three isoenzymes, is replaced with a Ser residue, further reducing catalytic activity. Furthermore, a more rigid confirmation of the N-terminal kinase domain likely leads to higher affinity substrate (fructose-6-phosphate and ATP) binding, compared to other isoforms, promoting enhanced kinase activity (Kim, Manes et al., 2006).

Studies by Telang and colleagues have suggested that despite the co-expression of several isoenzymes, it is the relatively high kinase activity of PFKFB3 that determines the intracellular concentration of F-2,6-BP (Telang, Yalcin et al., 2006). This would suggest it is a critical activator of glycolysis, being largely responsible for malignant F-2,6-BP production (Atsumi, Chesney et al., 2002).

PFKFB3 mRNA trascription has been shown to be induced under hypoxic conditions in a range of cancer cell lines, including those derived from glioblastoma (Obach, Navarro-Sabate et al., 2004), colon (Atsumi, Chesney et al., 2002), gastric and pancreatic cancers (Bobarykina, Minchenko et al., 2006). The hypoxic response was shown, at least in part, to be mediated by HIF-1α binding to a HRE in the 5'-promoter region of PFKFB3 (Obach, Navarro-Sabate et al., 2004). A study of organs explanted from mice exposed to hypoxia showed that whilst all four PFK-2/FBPase-2 isoenzymes were induced, it was PFKFB3 mRNA that showed the highest induction (Minchenko, Opentanova et al., 2003).

PFKFB3 mRNA differs from the other isoforms by the presence of multiple copies of the AUUUA instability motif in its 3-untranslated region, which confers instability and enhanced translational activity (Chen and Shyu 1995; Chesney, Mitchell et al., 1999). PFKFB3 has a phosphorylation site at Ser-461, which is phosphorylated by

AMPK, leading to activation of its kinase activity (Marsin, Bouzin et al., 2002). The same residue is also a target for phosphorylation by Protein Kinase A (PKA) and PKC (Okamura and Sakakibara 1998). This is consistent with highly phosphorylated PFKFB3 observed in many human cancers (Bando, Atsumi et al., 2005). AMPK is known to activate PFKFB3 in this manner in response to prolonged exposure to low pH (Mendoza, Pocceschi et al., 2012), or hypoxia (Marsin, Bouzin et al., 2002).

Deregulation of PFKFB3 degradation may be important in transformation and tumour progression. Indeed, mutations in APC subunits have been reported in colon (Wang, Moyret-Lalle et al., 2003) and breast cancer (Park, Choi et al., 2005). Furthermore, the tumour suppressor phosphatase and tensin homolog (PTEN), which promotes APC/C-Cdh1 activity, is also frequently mutated or deleted in cancer cells (Garcia-Cao, Song et al., 2012).

1.12. PFKFB4

Human PFKFB4 was first identified as a gene encoding a testis-specific PFK-2/FBPase-2 isoenzyme, T-PFK-2, which shares high amino acid sequence homology with the other human PFK-2/FBPase-2 isoenzymes (66-72%) (Manzano, Perez et al., 1999). Splice variant PFKFB4s were later identified (Minchenko, Ogura et al., 2005), and found to be co-expressed with the main isoform in DB-1 melanoma cells. PFKFB4s has a conserved PFK-2 catalytic domain, whilst the FBPase-2 is subject to modifications, which may confer different kinetic and/or regulatory properties, suggesting a potential role for different variants in tissue-specific regulation of glycolysis (Minchenko, Ogura et al., 2005; Ros and Schulze 2013).

Elevated PFKFB4 expression has been reported in human breast, colon (Minchenko, Opentanova et al., 2005), lung (Minchenko, Ogura et al., 2005) and gastric cancers (Bobarykina, Minchenko et al., 2006). PFKFB4 mRNA expression in the malignant

tissue was generally found to exceed that of PFKFB3 mRNA, and was found to be particularly high in breast tumours (Minchenko, Ochiai et al., 2005; Bobarykina, Minchenko et al., 2006).

However, it is only recently that elevated PFKFB4 expression levels have been linked with clinical outcome; one group showed positive correlation with reduced survival in primary glioblastoma patients (Goidts, Bageritz et al., 2012). Furthermore, PFKFB4 expression correlates positively with bladder cancer tumour recurrence and progression, suggesting it could be used as a prognostic marker for disease management (Yun, Jo et al., 2011).

Minchenko and colleagues (Minchenko, Opentanova et al., 2003) reported the first evidence for hypoxic induction of both splice variants of PFKFB4 in vivo, when they examined testis from mice exposed to 6 hours reduced oxygen concentration (7.5% oxygen). The same group observed induction of PFKFB4 mRNA expression in a wide range of cell lines under hypoxic conditions, and after exposure to a series of hypoxia-mimics, including dimethyloxalylglycine (DMOG), a specific inhibitor of HIF hydroxylase enzymes (Minchenko, Opentanova et al., 2004; Minchenko, Opentanova et al., 2005). This suggested hypoxic regulation was mediated by HIF proteins, which the group confirmed through the use of a dominant-negative HIF-1α construct in transient transfection experiments with HeLa cells, which prevented induction of PFKFB4 by DMOG (Minchenko, Opentanova et al., 2004). However, this final experiment has not been extended to other cell lines and the regulation of PFKFB4 expression by HIF-2α cannot currently be ruled out. Although no post-translational modifications of PFKFB4 have yet been reported, a recent study suggested that the heme oxygenase enzyme (HO-2) might have a role in regulating PFKFB4. Expression

of the two enzymes was found to be co-ordinated, suggesting they both play a role in maintaining glucose homeostasis (Li, Takeda et al., 2012).

PFKFB4 lacks the key serine Ser-32 phosphorylation site, critical for down-regulation of PFKFB1 activity, so was hypothesised to have a high K: B activity, and therefore to play a significant role in promoting glycolytic flux (Okar, Manzano et al., 2001; Minchenko, Opentanova et al., 2004; Minchenko, Ochiai et al., 2005 and Caro 2007). A number of studies have supported this (Sakata, Abe et al., 1991; Goidts, Bageritz et al., 2012; Gomez, Manzano et al., 2012), although PFKFB4 from human testis was found to have more balanced activity (K:B = 0.9, (Okar, Manzano et al., 2001)).

1.13. Mass spectrometry in metabolomics

The study of metabolism is becoming increasingly important in understanding the effects of gene mutations associated with different types of cancer. Metabolites supply not only the building blocks for all classes of biological molecules, including DNA, RNA, and proteins, but also regulate their expression and activities. The field of metabolomics, i.e. the global measurement of metabolites in a system, has seen significant growth in the post-genomic era coincident with advances in analytical instrumentation, data processing, and chemometric tools designed to facilitate efficient and accurate large-scale metabolite quantification (Fiehn, O. 2002). Since the Nicholson Group at Imperial College London and the Fiehn group at The Max-Planck Institute of Molecular Plant Physiology in Germany coined the terms “metabonomics” and "metabolomics" in 1999 and 2002, respectively (Nicholson et al.,1999; Fiehn, O. 2002). The number of publications indexed by these terms (now generally considered interchangeable) has grown exponentially to ~1600 PubMed indexed citations in 2014 (Figure 1-10) (Robertson, 2005; John et al., 2007). Accordingly, metabolomics has become a vital tool in biomedical research as practiced independently to study

metabolite interaction or in combination with genomic, transcriptomic, and/or proteomic data to study biological systems in a holistic manner (e.g. systems biology). Approaches for the analysis of metabolites in biological systems can be classified broadly as directed (targeted) or undirected (untargeted). This distinction is dependent upon whether the methodology implemented is designed to identify and quantify a number of specific metabolites (directed) or to measure a larger set of metabolites restricted only by the sensitivity and applicability of the analytical platform(s) and data processing employed (undirected). Both approaches are employed in this thesis.

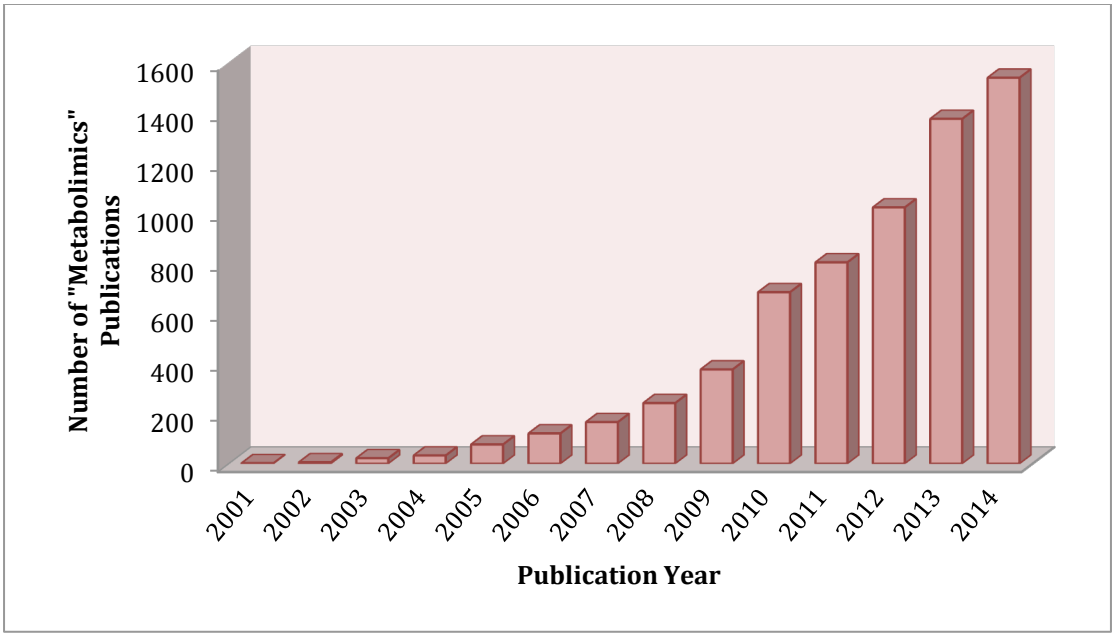

Figure 1-10: Number of publications returned with "metabolomics" keyword search of NCBI-pubmed. The number of publications indexed by these metabolomics has grown exponentially to ~1600 PubMed indexed citations in 2014.

These two approaches have found growing applications in a range of biological investigations including areas such as biomarker studies, study of disease states (particularly metabolic oncology) pharmacological toxicity, biomarkers of disease, functional genomics, and nutrigenomics (obertson 2005; Mamas et al., 2011; Saghatelian et al., 2004; Gibney et al., 2005). Metabolomic platforms usually

comprise a separation system (often chromatography) coupled to a detector, which is usually mass spectrometry or NMR. Increasingly sophisticated data analysis and bioinformatics are being used to interpret and organize the increasingly large amounts of data that are collected using these platforms (Mamas et al., 2011). Sample types commonly investigated include human tissues, cultured eukaryotic and prokaryotic cells, plasma, urine, and cerebral spinal fluid. Accordingly, the efficient extraction of metabolites from these various samples through customized sample preparation procedures is a critical parameter in accurate metabolomics analysis. Complementary preparation techniques and analysis platforms are therefore necessary to approach accurate metabolite measurements.

Targeted metabolomics and the quantification of small numbers of metabolites (< ~20) in biological samples have been well studied for decades. Initial studies used chemical or enzymatic assays to convert a metabolite of interest into a detectable product. These approaches do not require advanced analytical equipment and are therefore still used in many research laboratories today. ^{1}H-NMR has found limited use for the absolute quantification of metabolites in cell and tissue samples due to the inherent sensitivity and specificity limitations. However, NMR has enabled the reported quantification of up to 87 metabolites in urine and 48 in whole blood (Wishart et al., 2001; Begley et al., 2009; Monton et al., 2007). Metabolomics based techniques such as Ultra-high Performance Liquid Chromatography coupled to Mass Spectrometry (UHPLC/MS) have been used for metabolite quantification and identification but suffer from limited sensitivity and selectivity to distinguish between critical isomers and enantiomers. Larger sets of specified metabolites (as many as 205) have been quantified in bio-fluids and cellular extracts, using separation based approaches coupled with mass spectrometry detection CE-MS (Wei et al., 2010), GC-

MS (Lu et al., 2010), and LC-MS (Huang et al., 2007; Buscher et al., 2009) as discussed below.

Untargeted metabolomics aims to measure, as comprehensively as possible, all the ion features in a given sample. While the chemical identity of each unique feature or signal measured in an analysis may ultimately be of interest, an undirected experiment does not aim to identify a compound, rather it seeks to look for statistical differences between samples which received different treatments. From peak area and positional differences it is inferred that differences in metabolite, concentrations are present between groups of samples. Studies that terminate at feature identification fall under the category of metabolite profiling and can be useful in areas such as biomarker identification. Alternatively, these features can be further interrogated and structurally identified in a targeted fashion. Hence, untargeted experiments are often referred to as hypothesis generating.

Due to the inherent limitations of the various separation and ionisation techniques mentioned, several groups have proposed to use parallel approaches (e.g. GC/MS and LC/MS) to increase coverage of the metabolomics (Yang et al., 2010; Reaves et al., 2011). GC and LC methods are commonly used in parallel as GC generally offers superior analysis of metabolite classes such as fatty and amino acids, whereas LC is superior for high and small molecular weight and multiply charged metabolite classes such as nucleotides and acetyl-CoA carboxylic acids. Dual (two separation mode) UPLC methods have been used, including hydrophilic interaction liquid chromatography (HILIC) for amines and ion pairing chromatography for carboxylic acids and sugar phosphates (Dunn et al., 2006). Combined HILIC and reverse phase approaches have also been reported (Pierce et al., 2008). Multi-dimensional

separations have also been applied to metabolomic analysis to improve sensitivity and peak capacity. The application of GC x GC has been reported for the metabolomic analysis of microbes and plasma (Edwards et al., 2007; Yang et al., 2009; Yang et al., 2010). The focus of much of the GC x GC research efforts has been on methodology to improve chemometrics since the 3D data sets generated by the technique are particularly difficult to process (Fairchild et al., 2010). Finally, LC x LC methods have been applied in a limited number of studies of microbes and found to give substantial coverage for of metabolites (Vincent et al., 2000; Peuhkurinen et al., 1983).

1.14. The aims of the research described in this thesis

The research described in this thesis concerns method development followed by application for the investigation of IDH mutations discovered in brain tumours in 2008 and in particular the effects of these mutations on cellular metabolism. When this thesis began in 2011, it was known that these mutations led to increased production of 2-HG but it remained unclear to what extent this had a significant effect on central energy metabolism and beyond. It was decided to investigate the impact of IDH mutations on metabolism and whether 2-HG could be used as a useful biomarker for gliomas. To pursue these goals a number of specific aims were identified:

1. The development and application of LC/MS and GC/MS methods for targeted and untargeted metabolomics focusing specifically on central energy metabolism (Chapter 2). It was clear from the literature that there was no existing methods that were ideal for the specific application outlined and none could be found which accommodated both comprehensive coverage of the metabolites of interest and was able to do so with relatively small amounts of sample which were anticipated. Derivatisation is normally essential for

GC/MS analysis for example but then when sample amounts are limited this can become prohibitory. Another challenge was working with the small, highly polar compounds found in central energy metabolism. These have always challenged chromatographic approaches to achieve acceptable retention and resolution, whilst maintaining MS compatible eluents. The challenge of the first part of the research was therefore to develop a range of methods, which would provide information complimentary to that of standard metabolomics to enable (1) the identification of metabolites especially relative to 2-HG and TCA cycle metabolism, (2) methods for the identification of enantiomers especially *D*-2-HG and *L*-2-HG, and (3) methods for the absolute quantification of low abundance of TCA cycle metabolites in cells and tissues. The works described in Chapter 2 focused on the development of these methods which are then applied in the applications described in later chapters.

2. The second main aim was to identify whether metabolic changes in central energy metabolism were associated with the presence of IDH mutations (Chapter 3). Although it was known that 2-HG levels increased significantly it was not clear at that time to what extent other central energy metabolism intermediates were affected. This involved the application of methods developed in chapter 2 to both wild-type and mutant forms of the brain tumour cell lines as well as the analysis of resected tumour tissue from patients with IDH positive gliomas. The aim was to investigate the metabolomes of mutant and non-mutant cells to discover differences, which may downstream be exploitable as drug targets or other therapeutic targets.
3. The third aim of the project was to investigate 2-HG as a biomarker for gliomas and work with groups interested in using magnetic resonance

spectroscopy to detect and quantify 2-HG in vivo from brain tissue and, as part of this, to compare 2-HG measurements by MRS with quantification by mass spectrometry (Chapter 4).

4. A fourth aim was to investigate whether the 2-OG oxygenase inhibitor N-oxalylglycine (NOG) is present naturally (Chapter 5). Ferrous iron and 2-oxoglutarate (2-OG) dependent oxygenases are enzymes presently of intense biomedicinal interest because for their roles in hypoxic signaling and epigenetic regulation. N-Oxalyl amino acids may play a natural role in regulating gene expression by inhibiting 2OG dependent oxygenases. This is important because TCA-cycle intermediate inhibition of 2OG depdendent oxygenases has attracted major interest with respect TCA cycle mutations in brain tumours and elsewhere. We focused specifically of NOG in the first instance because these compounds appeared to us to be good natural product candidates.
5. Finally, PFKFB3/4 are overexpressed in human cancers, as regulated by HIF-α levels, these are both required for the survival and growth of multiple cancer types and they regulate the balancing of glucose carbon at a branching point between glycolysis and the pentose phosphate pathway (Chapter 6). The aim was to examine the effect of PFKFB3 and PFKFB4 on cancer cellular metabolism in the glycolytic and pentose phosphate pathways when PFKFB3 and PFKFB 4 are knocked down using siRNA in normoxic and hypoxic conditions. The aim of these experiments was to investigate both the identification and quantification of key intermediates in both pathways and to compare normoxia and hypoxia in a cancer cell line.

Chapter 2: DEVELOPMENT OF THREE LC/MS METHODS FOR THE ANALYSIS OF TCA CYCLE METABOLISM IN CANCER CELLS AND TISSUES

2.1. Introduction

In 1971, the application of ion-moderated partition chromatography for organic acid analysis enabled the separation of non-isomeric TCA cycle intermediates (Yang et al., 2009; Reaves et al., 2011; Yang et al., 2010) and this became the method of choice for determining organic acids in biological samples (Dunn et al., 2006; Pierce et al., 2008; Edwards et al., 2007). These methods were not however compatible with mass spectrometry.

Soga et al., 2003, developed a method for simultaneous determination of TCA cycle metabolites based on capillary electrophoresis (CE) coupled to electrospray ionization mass spectrometry for separation of TCA cycle and glycolysis metabolites. The CE method, however suffered from poor sensitivity and retention time drift (Comte et al., 1997). Bylund and co-workers developed a selective ion exclusion LC-MS/MS method for analysis of TCA cycle metabolites in natural water with sensitivity to 5 μM LoD using Suplcogel C610-H Reverse-Phase (RP) column (300mm × 7.8mm, 9 μm) (Bylund et al., 2007). In 2007, Luo group reported a powerful LC-MS/MS method using TBA as volatile ion pairing (IP) reagent, this method was developed for the identification of intracellular metabolites involved in glycolysis and the TCA cycle in extracts from E.coli and mammalian cells using Synergi Hydro-RP-C18 column (150mm × 2.1mm I.D., 4 μm) (Luo et al., 2007). IP reagents work well but can often lead to severe contamination and prove detrimental to subsequent mass spectrometry.

In 2010, Yang et al. reported an LC-MS/MS approach involving comparison between HILIC with RP chromatography for the separation of ‘metabolic pairs’ includes

isomer (citrate/isocitrate) using a Luna NH_2 column (250mm × 2mm, 5 μm). There followed a method by Birkler et al., 2010, for resolving TCA cycle isomers found in micro-dialysates using RP LC-MS/MS using an Acquity HSS C18 column (100 × 2.1 i.d., 1.7 μm). As particle sizes have reduced over the years this allowed significant improvement in resolution and sensitivity at higher flow rates, which has made analysis more efficient and reduced analysis times (Luo et al., 2007; Yang et al., 2010 and Birkler et al., 2010).

Accurate and sensitive quantitation is usually difficult to achieve because of the complex matrices associated with biological samples. Kubota, described a method employing chemical derivatisation with 4-N,N-dimethylaminosulfonyl-7-piperazino-2,1,3-benzoxadiazole as a preanalytical derivatizing reagent for the LC-fluorescence determination of seven carboxylates relating to the TCA cycle intermediates followed by introduced N-methyl-2-phenylethanamine as a reagent for the selective derivatisation of several keto-, di-, and tri-carboxylic compounds of the TCA cycle for LC/positive-ion ESI-MS (Kubota et al., 2005). However, this method cannot be used for analysis of the TCA cycle metabolites due to the low sensitivity for the derivatives of TCA intermediate in positive-ion MS. Hence, examined the use of (3-nitrophenylhydrazine) 3-NPH as an efficient preanalytical derivatising reagent for the simultaneous determination of ten TCA cycle Intermediates found in heart tissue by negative-ion mode LC-MS/MS (Han et al., 2013).

It can be seen from the literature that a choice of methods utilising chromatography coupled to mass spectrometry, covering both metabolite profiling and comprehensive metabolomics analysis, are available however when closely examined very few of these are appropriate for focusing on central energy metabolism in cells and tissues.

The main reasons include: 1) a lack of specificity in complex biological matrices. 2) Complex and/or time consuming sample preparation including derivatisation for Gas Chromatography–Mass Spectrometry (GC/MS) and some LC/MS methods often making analysis of larger numbers of samples prohibitive. 3) Lack of compatibility with mass spectrometry. 4) Lack of a comprehensive coverage for metabolites of interest, particularly for the various isomeric components involved. One of the specific challenges regarding comprehensive analysis was the fact that the TCA cycle contains a number of metabolically important structural and enantiomeric isomers. These include the *D*- and *L*-forms of 2-hydroxyglutarate of direct interest in this development.

In this chapter three new chromatographic methods are developed for the separation of TCA cycle intermediates and associated metabolites aimed at solving the drawbacks outlined above. This led to three basic chromatographic techniques: (1) Ion pairing (IP) chromatography-using tributylamine (TBA), (2) chiral phase chromatography (CC) with ion pairing (IP) chromatography, and (3) GC/MS.

2.2. Method 1: Developing ion pair –reversed phase (IP/RP) chromatography for the separation of TCA cycle intermediates.

2.2.1. Method background

Liquid chromatography triple quadrupole mass spectrometer (LC/MS) was used for method development in negative ion mode. In order to optimize cone voltage and collision energies 11 metabolites were directly injected individually (100μM, 5μL/min). A suitable capillary voltage was found to be 2.50 ± 0.30 kV; and a cone voltage of 13.0 ± 0.1 V (n=3).

In the following method development experiments, a mixture of standard TCA cycle compounds was used (in 50:50 MeCN/H2O containing 1 mM of each the metabolites). Composition of this standard mixture is given in Table 2-1.

Metabolite	Abbrev.	Neutral formula	Theoretical mass	SIR mass	Retention time (min)	RSD %
fumarate	FUM	C4H4O4	116.0037	114	10.54	1.7
succinate	SUC	C4H6O4	118.0193	116	8.56	1.5
aspartate	ASP	C6H7NO4	133.0302	132	6.13	4.2
malate	MAL	C4H6O5	134.0143	133	9.79	1.3
glutamine	Gln	C5H10N2O3	146.0619	145	3.24	3.6
glutamate	Glu	C5H9NO4	147.0459	146	5.65	1.6
2-oxoglutarate	2-OG	C5H6O5	146.1102	145	9.72	1
2-hydroxyglutarate	2-HG	C5H8O5	148.1100	147	8.91	0.7
cis-aconitate	ACT	C6H6O6	174.0092	173	10.58	2.3
isocitrate	ICA	C6H8O7	192.0197	191	9.33	2.6
citrate	CA	C6H8O7	192.0197	191	9.55	2.0

Table 2-1: Tricarboxylic acid cycle (TCA) metabolites abbreviations, retention time, Selected Ion Recording (SIR) mass and quantitative reproducibility of Relative Standard Deviation (RSD%) for 11 metabolites used for method development were show RSD% <5.

2.2.2. Ion pairing reagents

Ion pair chromatography has been widely used for the separation of ionic compounds which cannot be adequately retained or separated using conventional reverse phase high-performance liquid chromatography (RP–HPLC) techniques. The retention mechanism in ion pair chromatography is based on the interactions formed between the ionic solutes and ion pairing reagent molecules adsorbed on the stationary phase (Figure 2-1) (Hung and Taylor 1981). Numerous studies have evaluated parameters, which affect ion pair reagent adsorption behaviors (Bartha and Vigh 1983; Bartha et al., 1984 and Barth et al., 1984). These studies have shown that the extent of the adsorption on the stationary phase is a function of the ion pairing reagent

concentration in the mobile phase, its hydrophobicity, and the concentration of the organic solvent present. In addition, eluent pH and ionic strength were shown to play important roles in ion pairing reagent adsorption (Figure 2-2) (Knox and Hartwick 1981 and Kolb et al., 1993). The most commonly used IP reagents are either alkyl sulfonates or tetra alkyl ammonium salts that are typically nonvolatile (Kolb et al., 1993). However, care must be taken when using IP agents in combination with LC/MS due to the possibility of ion suppression, contamination of the MS source, and adduct formation, which will have significant consequences for the robustness of the method (Barth et al., 1984 and Melin et al., 1979).

As developed by Dr. Gordon Schill in 1973, IP chromatography relies upon the addition of ionic compounds to the mobile phase to promote the formation of ion pairs with charged analytes (Eksborg and Schill. 1973). These reagents are comprised of an alkyl chain with an ionisable terminus (Figure 2-1). When used with common hydrophobic stationary phases in reversed-phase mode, ion pairing reagents can be used to selectively increase the retention of charged analytes (Figure 2-2).

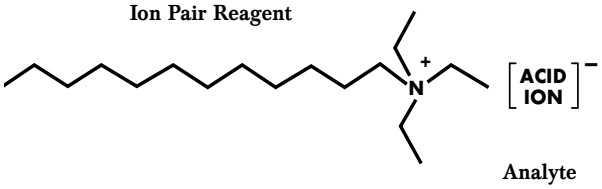

Figure 2-1: Quaternary Amine of ion pair reagent with analyte. These ion pair reagents are comprised of an alkyl chain with an ionisable terminus. The retention mechanism in ion pair chromatography is based on the interactions formed between the ionic solutes and ion pairing reagent molecules adsorbed on the stationary phase.

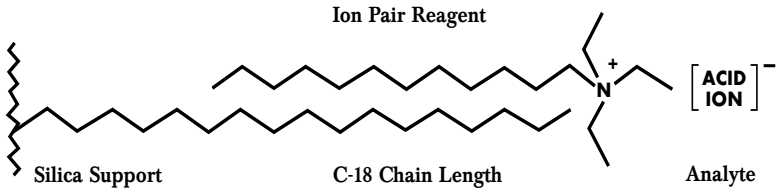

Figure 2-2: Quaternary Amine ion pairing with C-18 stationary support. When used ion pairing with common hydrophobic stationary phases in reversed-phase mode, ion pairing reagents can be used to selectively increase the retention of charged analytes.

Three different volatile alkyl-amines triethylamine (TEA), tributylamine (TBA), and trihexylamine (THA), with diverse alkyl chains were investigated as suitable IP reagents as part of the method development. Their specific elution capabilities can be seen in Figure 2-3. 5 mM of aqueous TEA, TBA, and THA, adjusted to pH 6.8 with 5 mM CH_3CO_2H, was used as phase A. At pH 6.8 the acidic groups of the TCA metabolites, and the amine groups of the alkyl-amines, is charged assisting the formation of IP interactions. The results show a systematic increase in analyte retention (TEA < TBA< THA), which correlates with the increase in hydrophobicity of alkyl chain length (data not shown). It was found that the amines with shorter alkyl chains than TEA provided insufficient resolution for a number TCA cycle intermediates, especially for the separation of isomers such as isocitrate/citrate and fumarate/maleate. The long alkyl chains in THA led to unnecessarily long retention times resulting in poor peak shape and lower sensitivity (data not shown). Among the IP agents investigated, TBA provided the best compromise between elution time, resolution and sensitivity, and was used for stationary phases evaluations and application in cell studies.

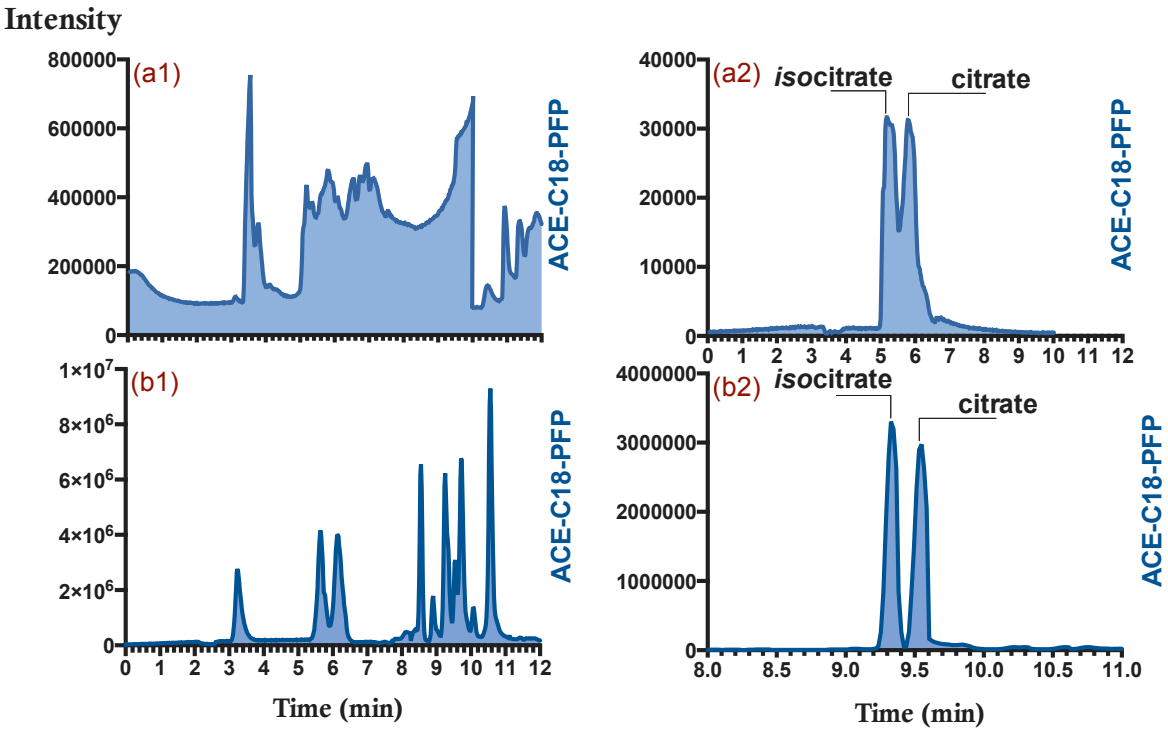

Figure 2-3: Single Reaction Monitoring (SRM) chromatograms show the difference in sensitivity and resolution for 11 Tricarboxylic acid cycle (TCA cycle) intermediates comparing reverse phase separation with and without tributylamine (TBA) in the mobile phase, (a1) reverse phase (RP) only and (b1) reverse phase- ion pairing stationary phase. A comparison of the effect of the tributylamine (TBA) on the resolution of structural isomers citrate and isocitrate can be seen by comparing (a2) reverse phase and (b2) reverse phase- ion pairing. Abscissa: retention time in minutes; ordinate: intensity of ion count. Were reverse phase- ion pairing show more resolving of isomers citrate and isocitrate.

TBA was chosen as the IP reagent as it afforded optimum retention for all TCA metabolites and in particular separation between TCA cycle isomers (Figure 2-3 (b2)). In addition, the somewhat more stable operating conditions of the RP-IP approach, including the less acidic pH (6.85 vs 2.4) than RP methods and higher temperature than RP-IP, made it particularly practical for the evaluation of biological extracts and thermally labile metabolites.

Finally, b2 in Figure 2-3 shows the intensity of the citrate and isocitrate peaks from the RP-IP method are 100 times higher than the RP method, which demonstrates that the use of the IP reagent enhances metabolite sensitivity for TCA cycle analysis.

2.2.3. Stationary phase development

The IP separation developed above used a standard C18 reversed phased column, which provided adequate resolution for TCA cycle intermediates. The next step was to investigate alternative stationary phases to try and improve both resolution and sensitivity further. Three different columns, providing functionality for enhancing polar retention, were investigated. These were a Kinetex-PFP, an HSST3 and an ACE-PFP. The standard mixture of TCA cycle intermediates was used for evaluating these stationary phases. Four chromatographic parameters were evaluated: Column temperature, mobile phase composition, and chromatographic gradient and flow rate. Chromatographic gradients were investigated starting from the simple gradient developed for the ion pairing evaluations above (Time (min): MPA (%)): 0:100, 8:65, 9:100, 15:100). The percentage of mobile phase A at the end of the gradient was varied between 80% and 20%. It was found that for each of the columns investigated the optimum % MP-A varied within the range 65% - 40% with this parameter having greatest effect on the sensitivity of the analysis, resolution stayed fairly constant for each column. Flow rate usually has an optimal value for a given set of chromatographic conditions most significantly affected by the column dimensions and particle size, which differed for each column (see methods and materials chapter for further details). The optimised flow rates can be found in Table 2-2. For column temperature four different temperatures were investigated. 25^{o}C, 30^{o}C, 35^{o}C, and 40^{o}C (the latter being the max recommended for ACE-PFP, different temperature were found to be optimal for the three different columns investigated. These can be found in Table 2-2. Finally the percentage of formic acid in mobile phase B was also varied between 1% and 3%. This had a relatively small but significant effect on resolution and was optimised for each column, values for which can be found in Table

2-2. Figure 2-4 shows the chromatographic differences between the 3 columns, using the optimised conditions, for the analysis of the 11 TCA cycle intermediates in the standard mixture used for method development. Optimised separation conditions for each column investigated are summarised in Table 2-2.

Method	Column	MPA	MPB	Flow rate (mL/min)	Time (min): MPB (%)	T (°C)
RP-IP	HSST3	H_2O, 10mM TBA, 15mM AcOH	ACN,0.3%FA	0.1	0:0%,4:40%,6:60%, 10:0%, 15:0%	40
	Kinetex-C18-PFP		ACN,0.2%FA	0.1	0:10%,4:50%,7:10%, 15:10%	25
	ACE-C18-PFP		ACN,0.2%FA	0.18	0:0%,8:35%,9:0%, 15:0%	25

Table 2-2: Individual chromatographic parameters for each of the three developed separation methods, optimised for maximal separation and signal of the compounds listed in table 2-1. (MPA) Mobile Phase A, (MPB) Mobile Phase B, (ACN) Acetonitrile, (TBA) Tributylamine, (AcOH) Acetic acid, (FA) Formic Acid.

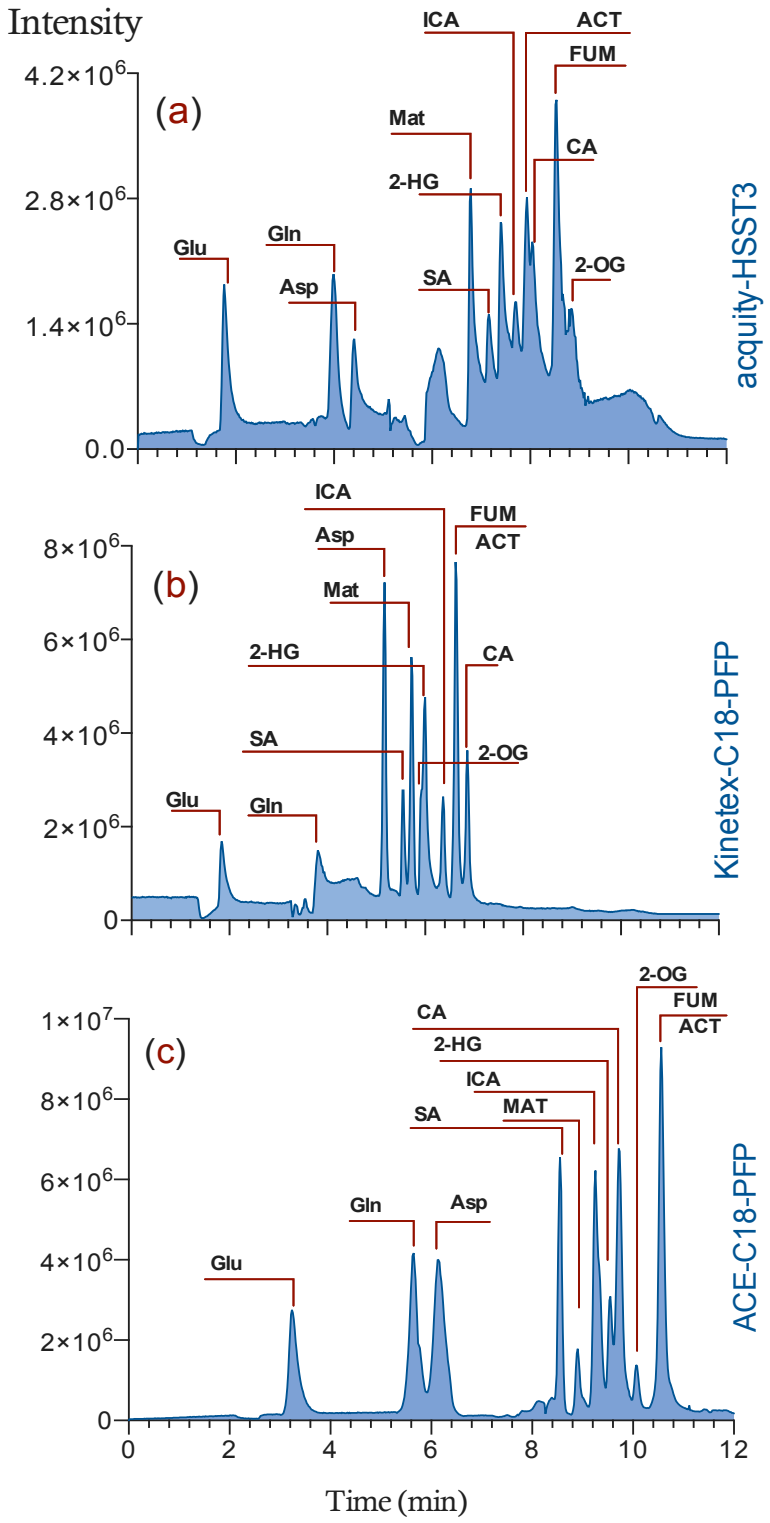

Figure 2-4: Combined Selected Reaction Monitoring (SRM) chromatograms for a standard mixture of 10 metabolites analysed with three different stationary phases (columns) and optimised conditions: (a) UPLC-C18; (b) UPLC-C18-PFP; (c) HPLC-C18-PFP. X-axis: retention time in minutes; y-axis; ion count. Metabolites (Glu) glutamine, (Gln) glutamate, (Asp) aspartate, (SA) succinate, (Mat) malate, (isocit) isocitrate, (2-HG) 2-hydroxyglutate, (2-OG) 2-oxoglutarate, (cit) citrate, (fum) fumarate. HPLC-C18-PFP column provide the maximum ion counts and return metabolites.

All three stationary phase columns showed retention of TCA cycle metabolites but the HSST3 column showed some tailing as well as the lowest ion intensity. The Kinetex-PFP column provided increased resolution and peak-shape with a higher ion intensity (almost 2 fold compared to the HSST3 stationary phase), it also provided the shortest run time. However, the ACE-PFP column provided even greater peak intensity (between 1 and 2x that of the Kinetex column) and enhanced resolution. The limits of separation for the HSST3 and Kinetex columns using citrate and 2-OG were shown to be >25uM (see Figure 2-5 for comparison) whereas the ACE-PFP column was well below this level making it potentially more suitable for cellular studies where some intermediates would likely be at low concentrations.

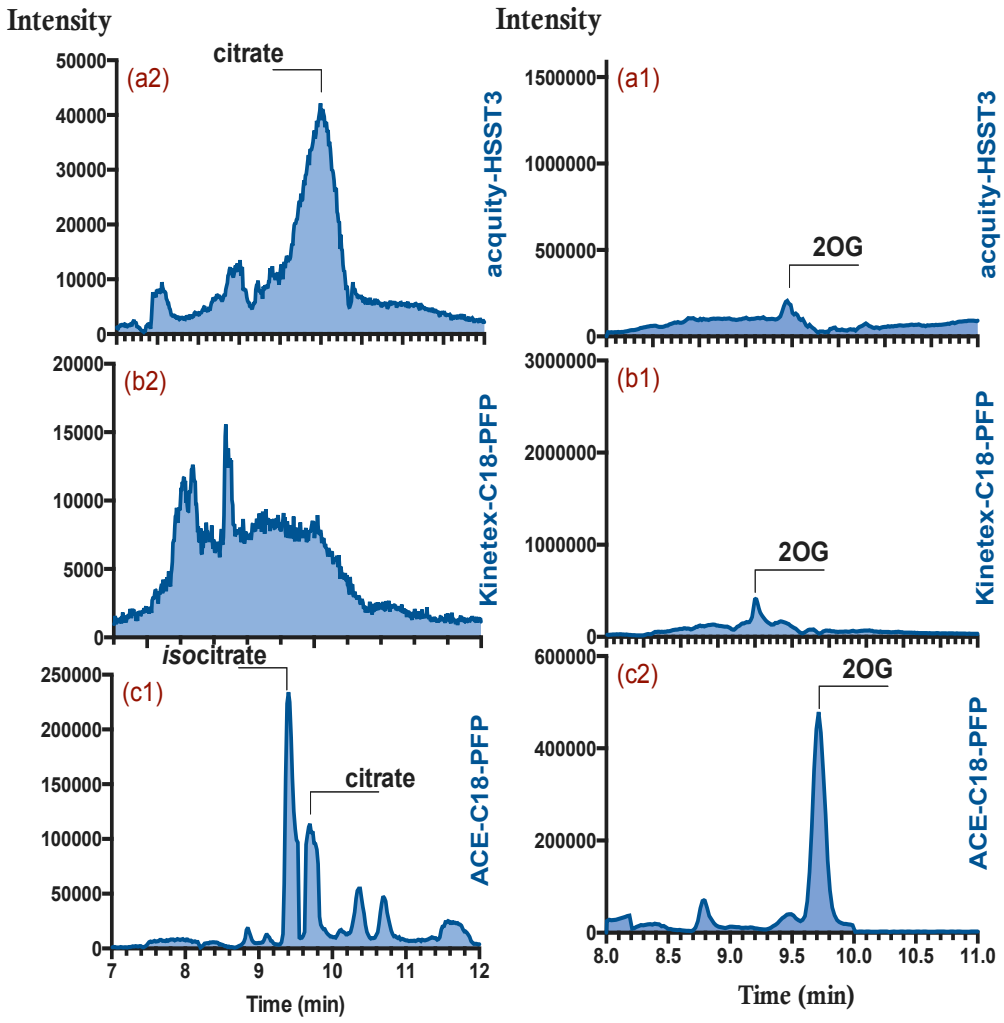

Figure 2-5: Combined extracted ions for citrate and isocitrate (m/z 191) isomers shown in (a2), (b2) and (c1); and for 2-oxoglutarate (m/z 145) shown in (a1), (b1) and (c2) chromatograms for a standard mixture of 11 metabolites (25 µM) under different optimised chromatographic conditions: (a) acquity-C18; (b) kinetex-C18-PFP; (c) ACE-C18-PFP. X-axis: retention time in minutes; y-axis; ion count. HPLC-C18-PFP column provide the lowest Limit of Quantitation (LoD) compered with other columns (acquity-C18 and kinetex-C18-PFP).

Figure 2-6, shows the ability of the three columns to separate the structural isomers of fumarate, maleate, isocitrate, and citrate, which generally prove difficult to resolve. For isomeric forms, it is clear that the ACE-PFP column provides necessary superior resolution. It is possible that the additional selectivity is in part provided by stronger dipole–dipole interactions between the negative fluorine on the stationary phase and the positively charged amine group of the ion pairing agent, leading to a stronger ion

pair, and hence achieving overall higher resolution, using the ACE-PFP column compared to the other two columns.

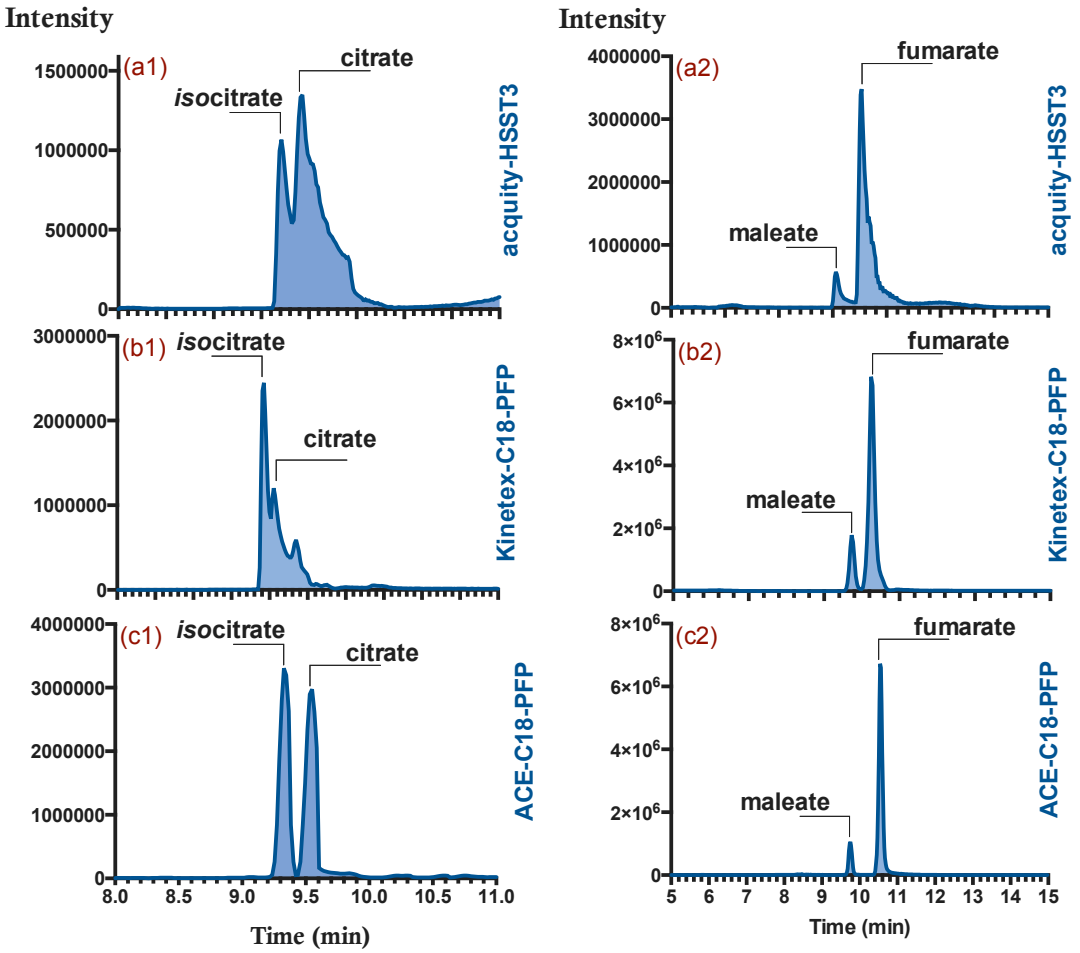

Figure 2-6: Combined extracted ions for citrate and isocitrate of (m/z 191) isomer show in (a1), (b1) and (c1); and for fumarate and maleate (m/z 115) isomers showed in (a2), (b2) and (c2) chromatograms for a standard mixture of 11 metabolites (1000 µM) under different optimised chromatographic conditions: (a) acquity-C18; (b) kinetex-C18-PFP; (c) ACE-C18-PFP. X-axis: retention time in minutes; y-axis; ion count. HPLC-C18-PFP column provide the maximum ion counts, return and must separation of isomers metabolites when compered with other columns (acquity-C18 and kinetex-C18-PFP).

An optimized IP-RP method using an ACE-PFP stationary phase for the separation of TCA cycle intermediates was developed and the chromatogram results can be seen in Figure 2-7. Higher proportions of TBA in mobile phase A with elution using ACN in mobile phase B improved peak shapes and sensitivity using the ACE-PFP column.

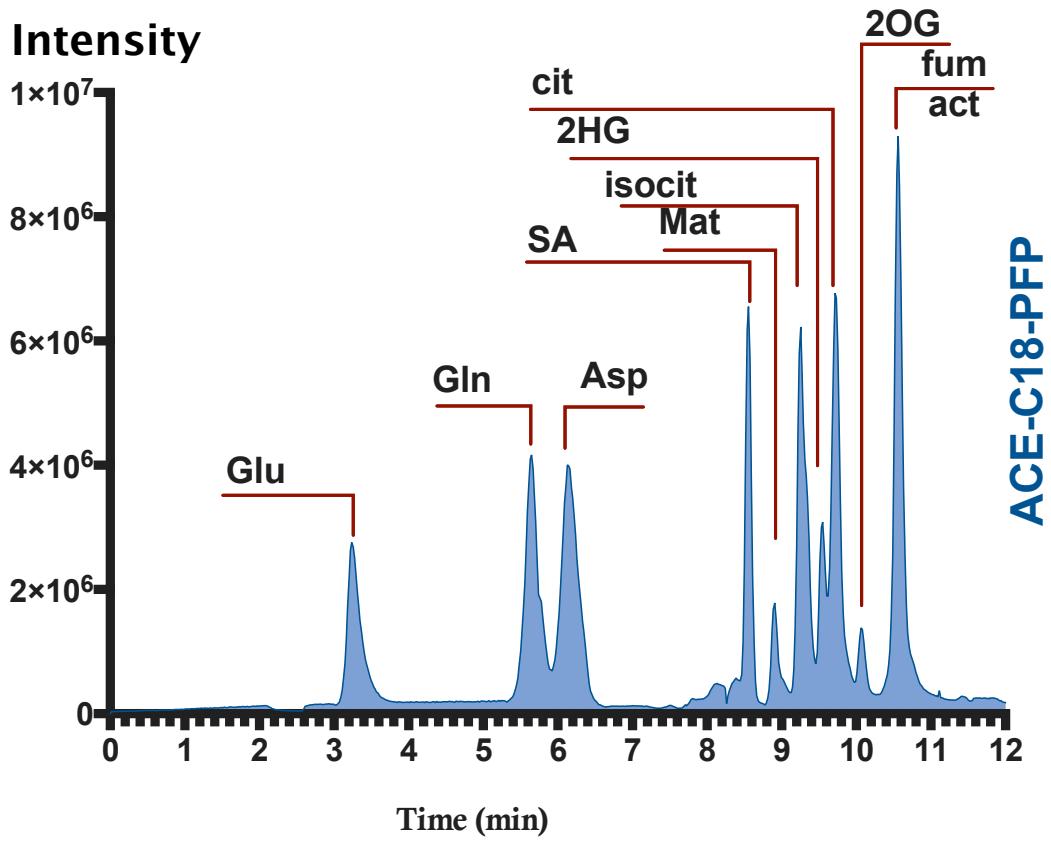

Figure 2-7: Final optimised condition for the non-derivatised 11 standard of Tricarboxylic acid cycle separated on ACE-PFP using Tributylamine as an ion pairing reagent. Metabolites (Glu) glutamine, (Gln) glutamate, (Asp) aspartate, (SA) succinate, (Mat) malate, (isocit) isocitrate, (2-HG) 2-hydroxyglutate, (2-OG) 2-oxoglutarate, (cit) citrate, (fum) fumarate.

2.2.4. Method Validation

2.2.4.1. Precision

The precision of method can be expressed as the percentage coefficient of variation (%CV) of the replicate measurements and it is calculated using the following formula:

(%CV)= (Standard deviation (SD)/ mean) x 100

The precision was determined by spiking 2-HG into 20µl of LN18 cell pellets extracted at two different concentrations, 50 and 500 µM, to assess intra and inter-day variation and repeatability.

The intra-day variation was determined by carrying out the procedure for four aliquots at the two concentration levels on the same day (the results are listed in Table 2-3).

2-HG added	2-HG peak area	Conc. (µM)		
50 µM	23	61.23	Mean	56.54
	21	56.54	SD	2.58
	19	51.85	%CV	11.74
	25	65.91		
500 µM	195	464.41	Mean	479.26
	201	478.48	SD	7.53
	208	494.89	%CV	3.69
	212	504.26		

Table 2-3: the intra-day precision of 2-hydroxyglutarte carried out for 4 control aliquots of concentration (50 and 500 µM) in the same day. Standard deviation (SD), coefficient of variation (%CV).

The inter-day values were established by analysing additional batches at these three concentrations once a day for three days. For calculation purposes, the mean slope and intercept for these 3 different days were used in these calculations (see Table 2-4).

2-HG added	Day	2-HG peak area	Conc. (µM)		
50 µM	1	19	51.85	Mean	56.54
	2	23	61.23	SD	2.00
	3	21	56.54	%CV	12.70
500 µM	1	196	466.76	Mean	478.48
	2	201	478.48	SD	5.00
	3	206	490.20	%CV	2.49

Table 2-4: the inter-day precision carried on three different days of concentration (50 and 500 µM). (SD) Standard deviation, (%CV) coefficient of variation.

For comparison, method precision, using the standard mixture at three concentration levels, can be found in Table 2-5. The standard mixture was injected five times and the relative standard deviations (RSD) are better than 9% for the 50 µM standard and 4% for the 250 µM and 500 µM standards (Table 2-5).

Metabolite	Repeatability		
	500 µM	250 µM	50 µM
FUM	6.21	3.98	0.91
SUC	5.01	3.30	1.00
ASP	8.3	2.15	0.49
MAL	7.1	3.25	1.28
Glu	6.6	1.41	0.56
Gln	6.00	2.51	1.87
2OG	7.5	1.88	1.94
2HG	2.75	1.93	0.56
ACT	3.33	1.64	1.25
ICA	5.11	2.30	1.76
CA	4.42	1.97	1.10

Table 2-5: The Relative standard deviation of three different concentration levels added of standards (n = 5), by the established LC/MS method (2 µL injection). Metabolites (Glu) glutamine, (Gln) glutamate, (Asp) aspartate, (SA) succinate, (Mat) malate, (isocit) isocitrate, (2-HG) 2-hydroxyglutate, (2-OG) 2-oxoglutarate, (cit) citrate, (fum) fumarate.

2.2.4.2. Recovery and accuracy

For accuracy and recovery determination, the same-pooled control cell samples were divided into three portions; each was spiked with 2-HG at two different concentrations (50 and 500 µM). Three aliquots at each concentration were taken through the procedure, and the concentration of 2-HG was calculated to determine the accuracy of the method. Accuracy will be determined by calculating the mean recovery of the measured concentration as a percentage of the nominal concentration after subtracting the endogenous 2-HG concentration. The following formula was used:

$$\textbf{(Mean found/ added concentration) } \times 100$$

The recoveries ranged from 96.40 % to 97.60 %, with the coefficient of variation (CV %) ranging from 0.87 % to 5.87%. See Table 2-6 below:

2-HG Conc. Added (µM)	Recovery **			Accuracy (%)
	Mean (µM)	SD	CV (%)	
50 µM	48.2	2.83	5.87	96.40
500 µM	488	4.24	0.87	97.60

**** After subtracting endogenous 2-hydroxyglutaric acid markers, n = 2.**

Table 2-6: Summary of the Recovery and accuracy of 2-hydroxyglutaric acid determination in LN18-Cell line. (SD) Standard deviation, (%CV) coefficient of variation.

2.2.4.3. Linearity, Limit of Detection (LOD) and Limit of quantification (LOQ)

Known concentrations of standard TCA cycle intermediates were analysed using the ACE-PFP optimised method and concentration vs peak area values were plotted. The linearity was measured by calculation of R2 values. The relevant values can be found in Table 2-7. In general, the calibration graphs showed excellent linearity, mainly over three orders of magnitude with correlation coefficients (R2) higher than 0.998 equivalent to other published methods. The LoD and the LoQ were calculated according to DIN 32645 (Kolb et al., 1993) were determined the limits of detection at a signal to noise ratio of 3:1 and limits of quantification at 10:1. As shown in Table 2-7, the LoDs vary from 1 to 5 µM and the LoQs are from 5 µM to 10 µM. On the whole, the LoD and LoQ values acquired with the new LC/MS methods are 1 or 2 orders of magnitude lower than the values described by other related articles (Kolb et al., 1993). With such low LoDs and LoQs, determination of these metabolites by injection of standard, without any previous enrichment step is readily achieved.

Metabolite	Retention time (min)	Linearity		LoD (µM)	LoQ (µM)
		Range	R^2		
FUM	**10.85**	5 µM-1 mM	0.9995	1	5
SUC	**8.66**	5 µM-1 mM	0.9995	1	5
ASP	**6.23**	10 µM -1 mM	0.9992	3	8
MAL	**8.92**	10µM- 1 mM	0.9993	3	8
Glu	**3.22**	10 µM -1 mM	0.9994	5	10
Gln	**5.81**	10 µM -1 mM	0.9994	3	10
2-OG	**10.21**	10 µM -1 mM	0.9991	5	12
2-HG	**9.34**	5 µM -1 mM	0.9999	1	5
ACT	**10.97**	5 µM -1 mM	0.9993	5	8
ICA	**9.41**	10 µM -1 mM	0.9990	5	10
CA	**9.83**	5 µM -1 mM	0.9993	3	5

Table 2-7: Linearity of calibration, and limits of detection and quantification, determined by the established LC/MS method (2 µL injection). Metabolites (Glu) glutamine, (Gln) glutamate, (Asp) aspartate, (SA) succinate, (Mat) malate, (isocit) isocitrate, (2-HG) 2-hydroxyglutate, (2-OG) 2-oxoglutarate, (cit) citrate, (fum) fumarate.

2.3. Method 2: Developing chiral chromatography for the separation of stereoisomers associated with the TCA cycle

2.3.1. Method background

Chromatographic methods for the determination of the concentrations of *D*- and *L*-2-HG are very limited in the literature. Some researchers have used the stable isotope dilution (SID) method described by Gibson et al., 1993, in which *D*- and *L*-2-HG are converted into their corresponding di-(*R*)-butyl-O-acetyl derivatives followed by analysis by GC-MS. The method described by Kim et al., 2000, in which the analytes were converted to *O*-trifluoroacetyl-(-)-menthyl derivatives followed by GC analysis, is a second example of the use of a chiral derivatisation reagent to enable diastereomeric separation using conventional GC analysis. In other methods, a chiral GC column connected to MS is used to separate the achiral derivatives of *D*- and *L*-2-HG (Dasneves et al., 1996, Kaunzinger et al., 1996, Muth et al., 2003). In 2000, a LC-MS/MS method was described in which underivatised *D*- and *L*-2-HG were separated on a chiral LC column (Rashed et al., 2000). Struys and co-workers reported that 2-

HG analytes can be derivatised by use of diacetyl-(*L*)-tartaric anhydride (DATAN) to obtain diastereomers, which were separated on an achiral C18 HPLC column and detected by MS/MS using multiple-reaction-monitoring (MRM) (Struys et al., 2004). With the exception of the method of Gibson et al., 1993, Kim et al., 2000, Muth et al., 2003 and Struys et al., 2004, other GC-MS methods have not been extensively validated (e.g. LoD, LoQ and %CV), their applicability has only been shown in patient urine samples containing very large amounts of the corresponding *L*-2-HG. The Gibson et al. method has the disadvantage of being time consuming and, because of the use of the reagent was *R*-(-)-2-butanol, relatively expensive (Gibson et al.,1993).

Therefore, it was decided that a reliable, robust, and simple LC/MS method for the analysis of *L*- and *D*-2-HG enantiomer in cells and tissues should be investigated.

2.3.2. Method development

Macrocyclic antibiotics bonded to stationary phases have shown to be useful for the separation of enantiomers of biological and pharmacological importance by high-performance liquid chromatography (HPLC), thin-layer chromatography (TLC), and capillary electrophoresis (CE) (Rashed et al., 2000). To date, the most useful types of antibiotics for enantioseparations are the ansamycins and the glycopeptides, but the glycopeptide macrocyclic antibiotics, including ristocetin A, may have broader enantiomric selectivity than the ansamycins (Ekborg-Ott et al., 1998). This is likely to be for several reasons: (1) they are amphoteric (i.e., contain acidic and basic ionisable groups), (2) they have the necessary geometry and functionalities that accentuate chiral recognition in solution, and (3) they contain both hydrophilic and hydrophobic moieties and are soluble in water, aqueous buffers, and slightly soluble in several hydro-organic solvents (Ekborg-Ott et al., 1998). Ristocetin A has a mass of 2,066

with an aglycon portion with four joined macrocyclic rings (one twelve-membered, one fourteen-membered, and two sixteen-membered rings) to which several sugars (including arabinose, glucose, mannose, and rhamnose) are covalently attached: this includes 38 stereogenic centers, seven aromatic rings, six amide link ages, 21 hydroxyl groups, two primary amine groups, and one methyl ester (Ekborg-Ott et al., 1998). These various functional groups are useful for chiral recognition through hydrophobic interactions, π-π-interactions, charge-charge (electrostatic) interactions, hydrogen bonding, dipolar interactions, and steric interactions (Ekborg-Ott et al., 1998).

Because ristocetin A is a multimodal chiral stationary phase (CSP), ranges of chromatography modes were investigated including normal-phase, polar-organic andreversed-phase using Chirobiotic columns (R, T and V). Performance was evaluated by measuring the efficiency and selectivity of separation using 2-HG enantiomers and the amino acids Glu, Gln and Asp. By using triple-quadrupole MS detection, the product ion spectrum of 2-HG was acquired in negative-ion mode using a capillary voltage of 3.0 kV, a cone voltage of 20 V, collision energy of 10eV, and a gas pressure of 2.5×10^{-3} bars. The $[M-1]^-$ ion for standard 2-HG at 147 was monitored in SIR mode.

2.3.3. Results of enantiomer IP/RP-LC chromatography method

The parameters for MS detection of 2-HG were the same as previously developed for the RP-IP chromatography developed above. Two factors complicate of the chiral LC analysis of underivatised 2-HG in biological samples: the lack of a chromatography to allow for UV detection and the complexity of the cell or tissue matrix, which contains a large number of acids even after selective acidic extraction. Therefore, I resorted to a more specific approach—enantiomer RP-IP chromatography. Physiologically, 2-HG

circulates in the blood, is accumulated in tissue, cells and urine as carboxylate anions, and thus is suited for electrospray analysis in the negative ion mode.

A standard solution of a mixture of the *D*- and *L*-2-HG was injected directly into the mass spectrometer without a column at flow of 0.8 mL/min. Attempts at chiral LC/MS separation of 2-HG were carried out using three chiral columns ristocetin A (Chirobiotic R), teicoplanin (Chirobiotic T) and vancomycin (Chirobiotic V) in the reversed-phase mode using a tributylamine-acetate buffer at pH 7.0 with either methanol or acetonitrile as organic solvent. It became apparent that neither the Chirobiotic T nor Chirobiotic V provided suitable separation potential. The teicoplanin column gave <30% separation and the peaks were very broad (>2 min) with considerable tailing that was independent of the concentration of organic modifier, while the vancomycin column gave no indication of any separation, again independent of the organic modifier. The Chirobiotic R gave <50% of 2-HG peaks separation using MeOH, which was unsatisfactory. It was found that the Chirobiotic R with MeCN provided satisfactory separation at a flow rate of 0.5 mL/min. As the MS conditions were optimised at 0.8 mL/min and the system was intolerant this high flow rate, a split was employed where only a fraction of the effluent (1/8) was directed to the mass spectrometer. The separation of the *D*- and *L*-2-HG standard using 2.5 % ACN at a flow of 0.8 mL/min was achieved *L*-form eluted at about 10.10 min, while the *D*-form eluted at about 11.70 min with >90 % peak separation and used for further experiments see Figure 2-8. Decreasing the flow rate did not further improve the separation.

The effect of pH and organic modifiers was studied next; different percentages of ACN (2.5, 5, 10,20 and 50 %) were used in parallel with different percentages of formic acid (FA) (0, 0.01, 0.02, 0.05, 0.1%) with the same MS conditions (Figure 2-

8). A remarkable change in selectivity was observed for the 2-HG enantiomers with different percentages of formic acid and acetonitrile. Figure 2-8 illustrates the separation of several carboxylic acids at pH 4.95 and 6.8; it shows that at pH 4.95 most of the organic acids were better resolved this is likely because carboxylic acids are only partially ionised at pH 6.8 and almost fully ionised at pH 4.95. Obviously, this pH dependent dissociation resulted in significant variation in selectivity for organic acids see Figure (2-9).

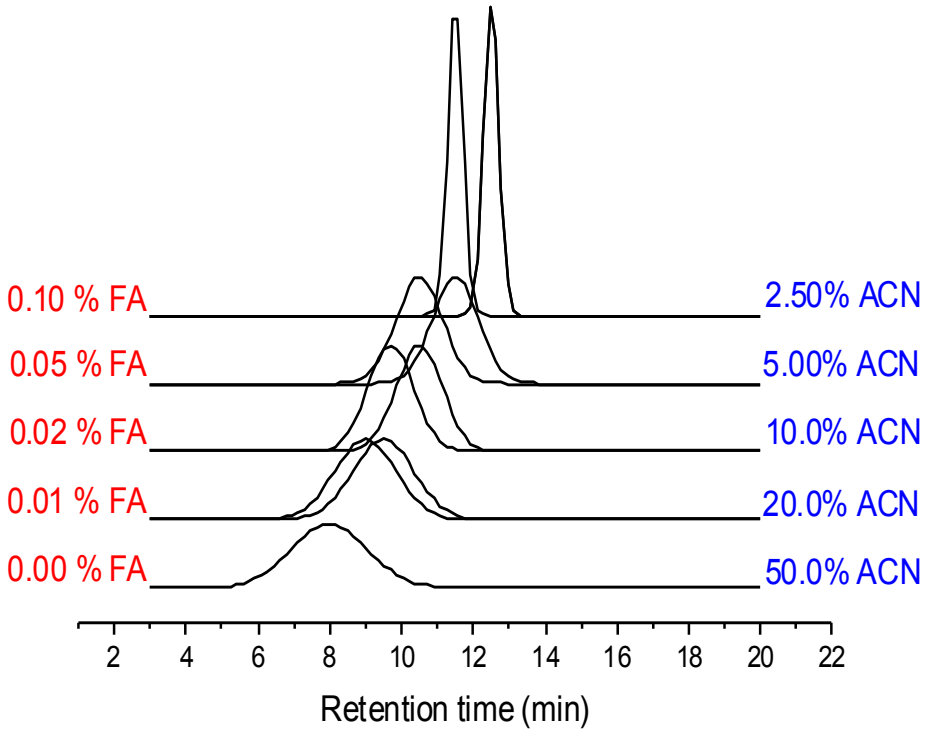

Figure 2-8: Ion count for (m/z) 147 of 2-hydroxyglutarate separation chromatography, for different percentages of acetonitrile (ACN) and formic acid (FA). It shows that at pH 4.95 most of the enantiomer acids were better resolved this is likely because carboxylic acids are only partially ionised at pH 6.8 and almost fully ionised at 0.10% formic acid (FA) pH 4.95.

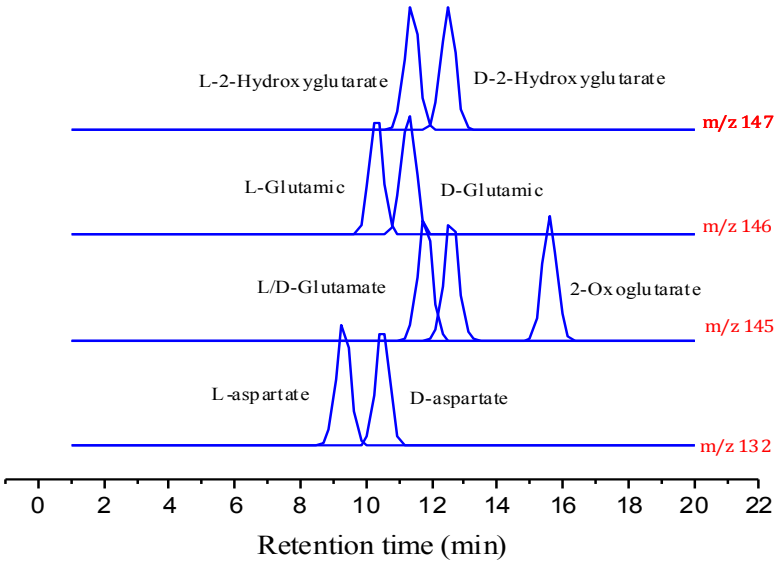

Figure 2-9: Shows selected ion counts for separation of different enantiomers associated with the Tricarboxylic acid cycle. This pH dependent dissociation resulted in significant variation in selectivity for enantiomer organic acids.

The development of this method made use of the rapidly evolving column technologies for chiral separation using macrocyclic glycopeptides antibiotics bonded to silica gel through a spacer of optimum length, which yields stable ether linkages that are non-hydrolytic. As for detection, the method employed ESI-Quadrupole MS as a specific and sensitive detector. The method is simple, direct, rapid, and offers a high degree of selectivity and specificity .The LC-RP-IP enantiomerically selective method described above was used for the analysis of samples from cancer cells and patient tissues diagnosed with glioblastoma described in Chapter 3.

2.3.4. Method validation

2.3.4.1. Resolution

The separation factor (α) measures this efficiency. A value of 1.5 or greater between 2 analyst peaks will ensure that the analyte is 'baseline' separated sufficiently such that

peak area or the height of each peak may be accurately measured. For chiral separation, an important aspect of efficiency is the ability to resolve one peak from another. Resolution can be calculated for the separation of two peaks in terms of their average peak width at the base ($t_R^2 > t_R^1$). In the case of two adjacent peaks, it may be assumed that the peak width at the base wb1 ≈ wb2. Thus, the width of the second peak may be substituted for the average value.

The separation results for the *D*- and *L*-2-HG were strongly dependent on the pH of the mobile phase. Use of pH ≅4.6 enabled baseline separation with a total LC runtime of 14 min. The elution order was determined by use of enantiomerically pure standards: *L*-2-HG eluted at 10.10 min, and *D*-2-HG eluted at 12.60 min. The separation factor (α) was ≅1.3, as calculated by:

$$\alpha = t_R^2 / t_R^1$$

The resolution of the two peaks (R_s) was calculated by the equation:

$$R_s = 2 \times \Delta t/(wb_1 + wb_2)$$

Where Δt represents the time difference between the apexes of the two peaks; wb1 represents the peak width at baseline of the *L*-2-HG peak; and wb2 represents the peak width at baseline of *D*-2-HG peak. The Rs was ≅ 2, indicating baseline separation.

2.3.4.2. LoD and LoQ

Calibration curves were created using *D*- and *L*-enantiomers. They were show to be linear over the range of 5–1000 μM for *L*- and *D*-2-HG (over two orders of magnitude). In both cases, the coefficient of linear regression (R^2) was >0.995 for both calibration curves (Figure 2-10). The LoD and the LoQ were calculated according to DIN 32645 (Kolb et al., 1993). Limits of detection were determined at a signal to noise ratio of 3:1 and limits of quantification at 10:1. These measurements provided a LoD of 5 μM and an LoQs of 10 μM. With such low LoDs and LoQs,

determination of these metabolites by direct injection of cell extract samples without any previous enrichment step was achieved. To check the method repeatability, three concentration levels of a standard mixture were injected (n=5) and the relative standard deviations (RSD) are better than 8 % for 50 µM standard and 4 % for the 250 µM and 3.5 % for 500 µM standards.

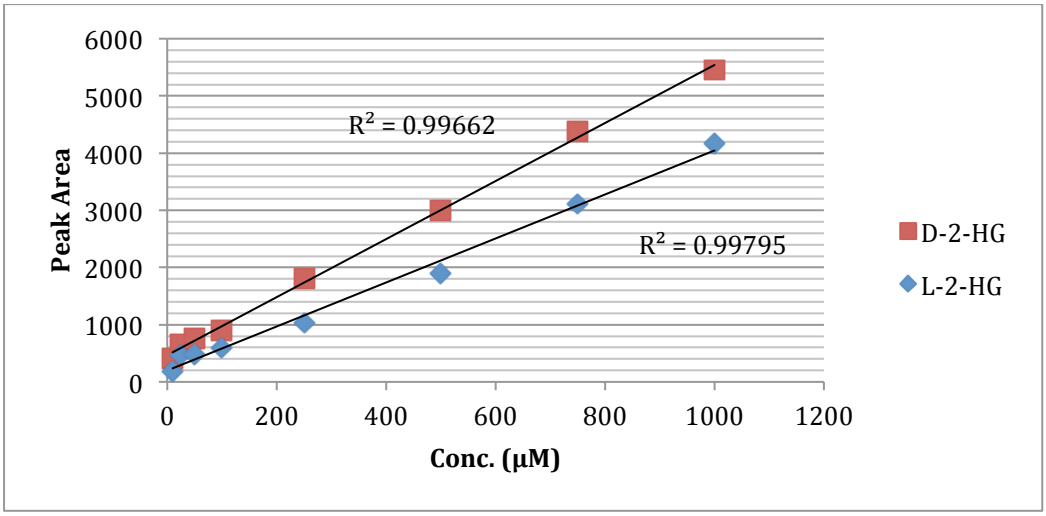

Figure 2-10: Calibration curve constructed from the triplicate Liquid chromatography–mass spectrometry (LC/MS) analysis of *L*- and *D*-2-hydroxyglutarate (D-2-HG and L-2-HG). The calibration curve was used to determine the absolute amount of both enantiomers in LN18 cells. The straight line provided an R2 value of >0.995 over the range 10-1000 µM.

2.4. Method 3: Developing of gas chromatography for the analysis of TCA cycle intermediates

2.4.1. Method background

GC-MS in full scan mode is used for non-targeted metabolic profiling and the discovery of novel compounds and metabolites (Farre et al., 2007). GC-MS has limitations in the analysis of polar compounds due to their low volatility therefore compounds for analysis must first be derivatised to increase volatility and stability. Before analysis by GC-MS, derivatisaing agents such as a silylating reagent are used to derivatise amine, and thiol groups. There are two main classes of silylating reagents: those producing trimethylsilyl (TMS) derivatives, and those producing *tert*-

butyldimethylsilyl (TBDMS) derivatives. TMS derivatives can be produced by a wide variety of reagents, including *N*,*O*-bis-(trimethylsilyl) trifluoroacetamide (BSTFA) and *N*-methyl-*N*-(trimethylsilyl)-trifluoroacetamide (MSTFA). TBDMS derivatives are prepared by the reaction with *N*-methyl-*N*-(*tert*- butyldimethylsilyl) trifluoroacetamide (MTBSTFA) (Ghassempour et al., 2004 and Rosenqvi et al., 1972). Often higher reproducibility and resolution can be achieved by GC-MS when compared to LC-MS. One of the main advantages of LC-MS over the classical GC-MS procedures is the reduced complexity in sample preparation by elimination of derivatisation steps before the chromatographic separation.

2.4.2. Development of a GC/MS method for the analysis of TCA cycle intermediates

Quantitative analysis, especially of oxaloacetate (OAA), isocitrate (ICA) and 2-OG were difficult using all the LC/MS methods developed because: (1) These metabolites (OAA, ICA and 2-OG) are present at low concentration in the biological samples, (2) OAA is unstable after extraction, it needs to be stabilised or derivatised very quickly (Bajad et al., 2006), (3) The isomers of citrate need to be separated, (4) 2-OG and OAA are thermally unstable, as they are liable to decarboxylation and need to be derivatised at the lowest possible temperature. Further, methoxyamine reacts with ketones (e.g. 2-OG, OAA and isocitrate) to form an oxime derivative as showed in (Trygg et al., 2005 and Wagner et al., 2010).

The GC temperature program started at 120 °C followed by a 10 °C/min ramp to 300 °C. Bake-out was set at 320 °C for 10 min. The injector and interface of the MS were held at 285 °C. The helium carrier flow rate was held constant at 1.5 mL/min (or a

flow rate such that the TBDMS derivative of to d_4-succinate has a retention time of 13.4 min). When operated in full scan mode, the scan range was 50–700 Da.

A method for assaying the concentration profiles of TCA metabolites was developed using cell extracts.

Metabolite	Fragments	Retention time (min)	selected ion monitoring interval (sec)
fumarate	287,329	13.2	
succinate	289,331	13.5	
malate	419,287	16.75	
oxaloacetate	417,333	18.25	
aspartate	418,	17.20	
glutamine	432,	19.55	±0.05
glutamate	432,	18.04	
2-oxolglutarate	431	18.05	
cis-aconitate	459,501	19.15	
isocitrate	459,431,403	21.18	
citrate	459,431,403	21.05	

Table 2-8: Gas Chromatography Mass Spectrometry fragment ions monitored for quantitating Tertbutyldimethylsilyl (TBDMS) of Tricarboxylic acid cycle metabolites.

2.4.3. GC/MS TBDMS of TCA-cycle metabolites

A mixture of derivatives was investigated for our target metabolites, MTBSTFA and TBDMS to form silylated derivatives (see Figure 2-11 for silylated TCA metabolites standard analyzed by GC/MS). The analysis TBDMS derivatives of these metabolites/intermediates were performed on tissue extracts and cell media preparations in analysis performed in later chapters.

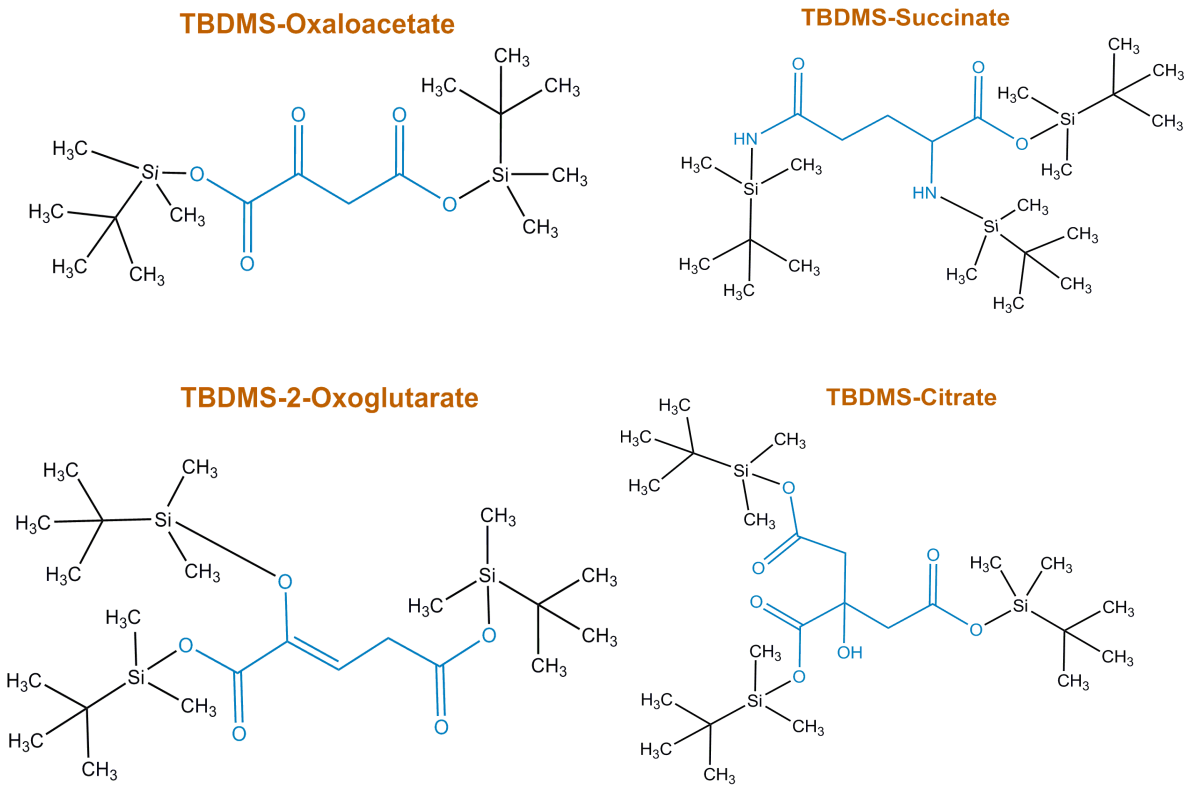

Figure 2-11: Tricarboxylic acid cycle standard derivatives analysed by Gas Chromatography Mass Spectrometry, The derivatisation was performed using *N*-methyl-*N*-(*tert*-butyldimethylsilyl) trifluoroacetamide (MTBSTFA) reagent for 55min at 60 °C. The blue part corresponds to the atoms belonging to the Tricarboxylic acid cycle metabolites.

In order to investigate further derivatisation steps, the concentrations (250 µM) of the TCA metabolites were optimised after added (spiked) to cell culture media pool (100 µL) and extraction. An internal standard (I.S) d_4-succinate was added to eliminate the effect on precision of signal fluctuations due to variations in matrix effects. 80% aqueous methanol has been widely used for, protein precipitation by virtue of the high reproducibility and efficiency.

A methoximation step was tested (Trygg et al., 2005; Wagner et al., 2010 and Kloos et al., 2012). Methoximation, was found to be unnecessary for the required analysis Figure 2-12 shows that a decrease of methoxyamine concentrations in the pretreatment of (2-OG; 250 µM) improved the formation of TBDMS-2-OG (Kombu et al., 2011; Paavilainen and Korpela 1993 and Yang et al., 2006).

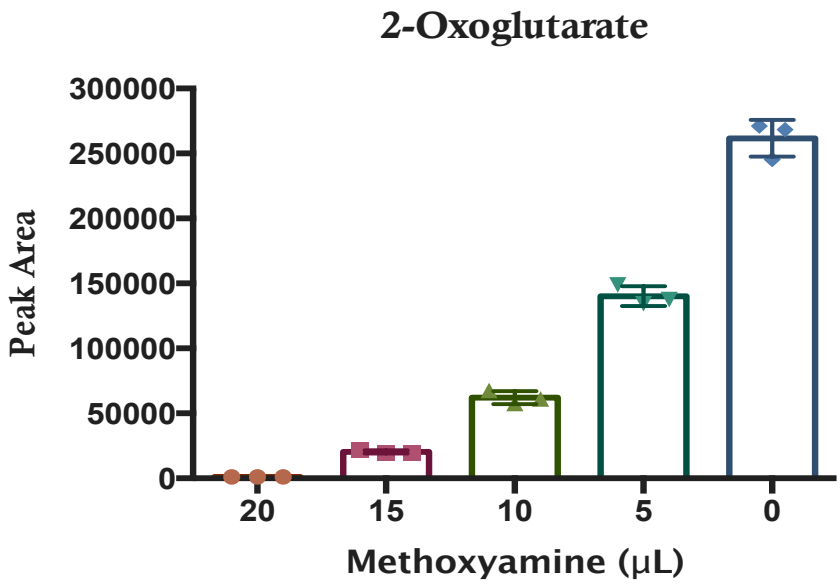

Figure 2-12: 2-Oxoglutarate (25 µM) magnetic peak area response when different volume of methoxyamine (20 mg/L) in pyridine used for 55min at 60 °C. Methoximation, was found to be unnecessary for the required analysis.

Therefore, any future residues from evaporation of samples was directly reconstituted by use of 9 µL of pyridine (the optimum medium for derivatisation with MTBSTFA + 1% TBDMCS) (Yang et al., 2006 and Kombu et al., 2011). The difficulty at complete dissolution of the residue made it necessary to added 1µL of formic acid to 90 µL of the derivatisation mixture.

In order to investigate further, several aliquots of the TCA standards (SA, CA, Gln and OAA) were prepared as mentioned previously. The standards were derivatised and maintained at different temperatures (from 25 to 80 °C) for different times (from 5 to 70 min) to establish the optimum operational conditions for derivatisation of the target metabolites at 250 µM. The best results were obtained at 55 °C for 60 min. Figure 2-13 and 2-14 shows the effects of temperature and silylation derivatisation reaction time on the efficiency of the reaction for four representative metabolites. The results show the optimum temperature for selected metabolites was < 60 °C with a derivatisation time > 50 min.

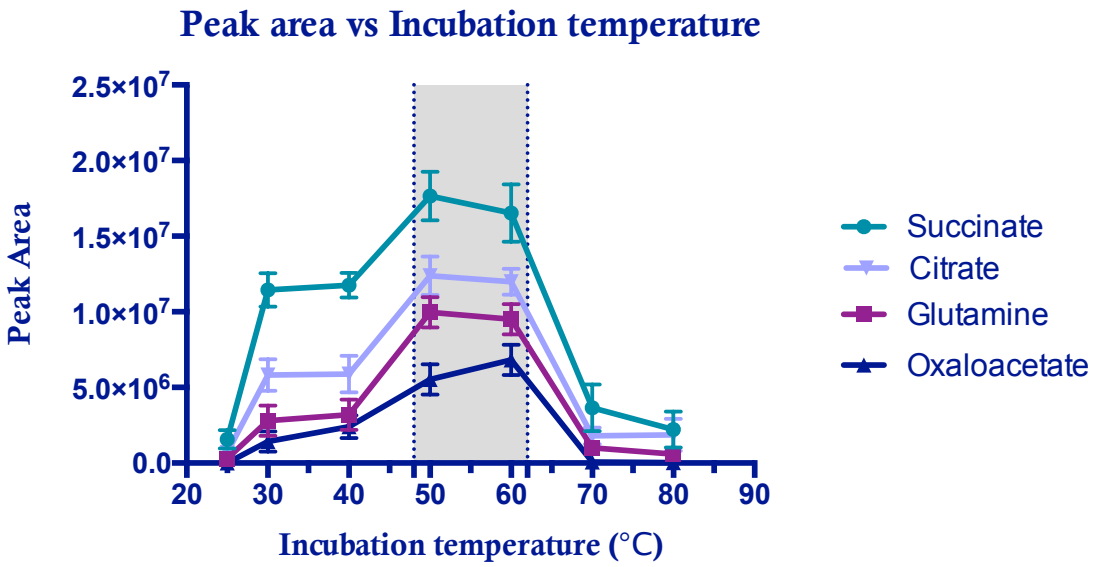

Figure 2-13: Optimum formation rates of tricarboxylic acid cycle standards measured by using *N*-methyl-*N*-(*tert*- butyldimethylsilyl) trifluoroacetamide (MTBSTFA) reagent for Gas chromatography-mass spectrometry (GC-MS) analysis. The results show the optimum temperature for selected metabolites was between (48-63°C).

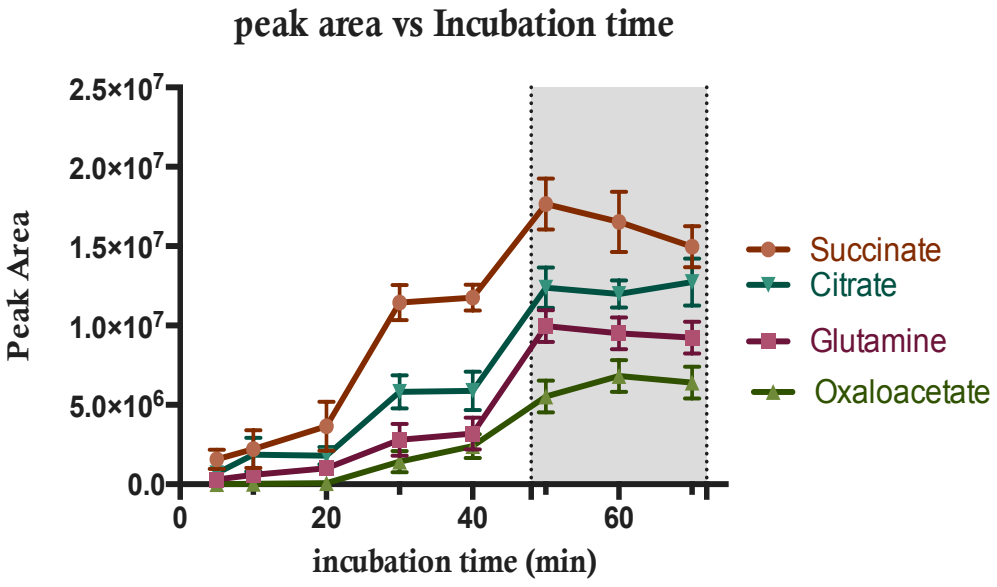

Figure 2-14: Optimum formation temperatures of tricarboxylic acid cycle standard measured by using *N*-methyl-*N*-(*tert*- butyldimethylsilyl) trifluoroacetamide (MTBSTFA) reagent for Gas chromatography-mass spectrometry (GC-MS) analysis. The results show the optimum derivatisation time between 50-70 min.

Figure 2-15 shows the selected ion chromatograms for the authentic standards and extracts of cell culture medium (control). Peaks for all targeted metabolites are well-resolved including citrate and isocitrate.

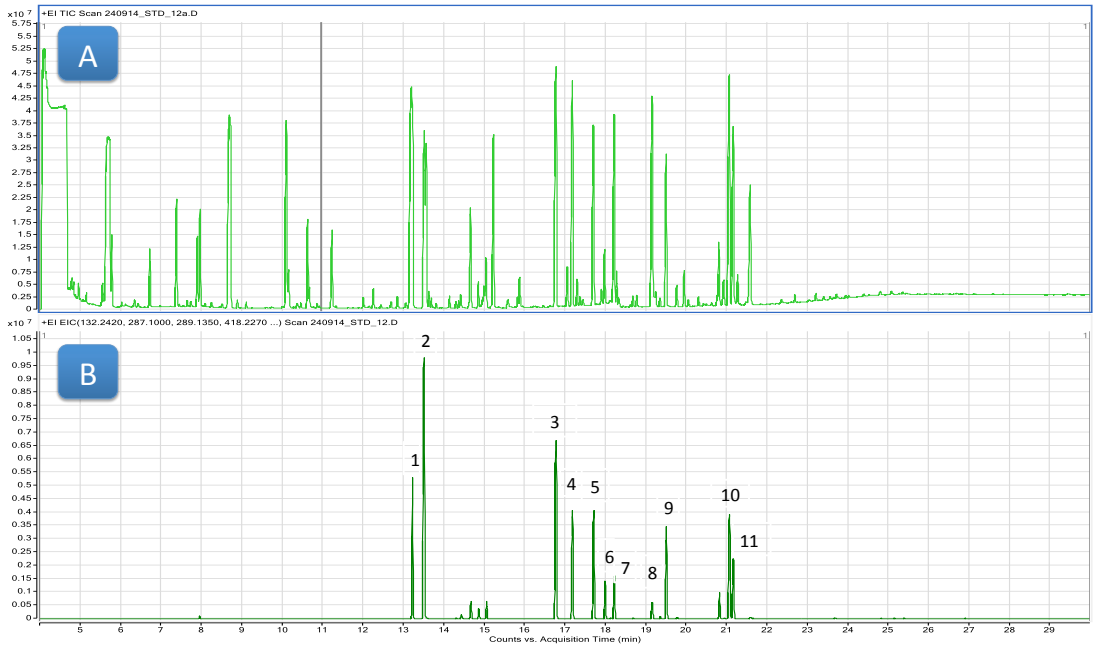

Figure 2-15: A) **Total ion chromatogram of a Tricarboxylic acid cycle standard (500 µM),** B) **Extracted ion chromatogram of a Tricarboxylic acid cycle standard (500 µM), 1 Fumarate, 2 succinate and it d_4-succinate, 3 Malate, 4 Aspartate, 5 Glutamic, 6 2-oxoglutarate, 7 oxaloacetate, 8 Cis-aconatate, 9 Glutamate, 10 Citrate, 11 isocitrate.**

2.4.4. Method validation

The mass spectra of the TBDMS-derivatised compounds formed in the EI source led to fragment ions predicted from their chemical structure (Kombu et al., 2011 and Trygg et al., 2005). The quantification of all target metabolites, including the internal standard, are shown in Table 2-9, which also includes the chromatographic retention times.

Metabolites	R^2	LoD (nM)	Linear dynamic range (µM)	
			LoQ	Maximum limit
FUM	0.9993	500	0.750	500
SUC	0.9992	500	0.750	500
ASP	0.9997	750	1	750
MAL	0.9991	500	0.750	500
OAA	0.9990	820	1	750
Glu	0.9992	850	1.5	750
Gln	0.9996	850	1	750
2-OG	0.9993	850	1	750
2-HG	0.9997	500	0.750	500
ACT	0.9995	750	1	500
ICA	0.9991	600	0.900	500
CA	0.9998	550	0.750	500

Table 2-9: Limits of detection (LoD) and quantitation (LoQ) for each target metabolite and linear dynamic range of the calibration curve. The straight line provided an R2 value of >0.9990 over the range 500-1000 nM. Metabolites (Glu) glutamine, (Gln) glutamate, (Asp) aspartate, (SA) succinate, (Mat) malate, (isocit) isocitrate, (2-HG) 2-hydroxyglutate, (2-OG) 2-oxoglutarate, (cit) citrate, (fum) fumarate.

The calibration equations were established by using the metabolite/internal standard peak-area ratio as a function of the concentration of each metabolite in order to circumvent matrix effects. The linear dynamic range for the metabolites is shown in Table 2-9.

2.4.4.1. LoD and LoQ

A limit of detection and quantification was estimated by diluting an aqueous solution of the target metabolite. The LoD and the LoQ were calculated according to DIN 32645 (Kolb et al., 1993). Values of LoD and LoQ for each metabolite, expressed as concentration in the culture medium, are shown in Table 2-10. Sensitivity values reported with this method were better than those described in recently published methods, which presented minimum LoD values of 750 nM and 500 nM for 2-OG and citrate, respectively (Soga et al., 2002), while in other cases LoDs from 12 to 10 µM have been reported (Lu et al., 2003 and Koubaa et al., 2013).

2.4.4.2. Precision

The precision of the method was calculated by injecting different aliquots of the same sample three times a day for 3 days. The results obtained for each compound in terms of intra-day and inter-days precisions, expressed as percent of relative standard deviation (RSD), are shown in Table 2-10. The values were acceptable for the analysis of biological samples. As an example, Soga et al., 2002, reported intra- day variability twice or six times higher than that provided by our method. The accuracy of the method was calculated by comparative analysis of two aliquots of the culture medium pool, one of which was spiked with a known quantity of target analytes (250 μM). The obtained results, shown in Table 2-10, support high recovery values for all the TCA metabolites.

Metabolites	Intra-day precision	Inter-day precision	Accuracy
FUM	4.9	5.5	102.7
SUC	5.3	8.4	100.8
ASP	7.1	9.0	99.8
MAL	4.5	6.6	100.1
OAA	11.2	14.3	101.5
Glu	8.1	10.2	100.0
Gln	7.4	10.0	98.5
2OG	7.7	13.5	97.8
2HG	4.1	6.8	101.1
ACT	3.2	7.0	109.4
ICA	8.4	13.3	96.3
CA	8.9	12.5	99.2

Table 2-10: Precision study expressed as percent of relative standard deviation (% RSD) and accuracy. The accuracy of the method was calculated by comparative analysis of two aliquots of the culture medium pool, one of which was spiked with a known quantity of target analytes (250 μM). The precision and accuracy values were acceptable for the analysis of biological samples. Metabolites (Glu) glutamine, (Gln) glutamate, (Asp) aspartate, (SA) succinate, (Mat) malate, (isocit) isocitrate, (2-HG) 2-hydroxyglutate, (2-OG) 2-oxoglutarate, (cit) citrate, (fum) fumarate.

2.5. Comparison of LC and GC methods

Table 2-11 provides an overview of the performance differences between the two investigated chromatography methods for analysis of all TCA cycle intermediates (IP-RP LC/MS and GC/MS). The total run time for the 11 TCA cycle standards and resolution of the closely eluted pairs citrate-isocitrate and fumarate-maleate were used to assess the performance of the chromatographic systems. Chromatographic peak widths and chromatographic resolutions were also determined.

Comparison Parameter	LC-MS	GC-MS
Total Run Time (min)	15	35
Peak Width	0.2	0.2
Chromatographic Resolution	≥1.55	≥ 2.21
Flow Rate (mL/min)	0.18	0.1
Injection Volume (µL)	2	1
$R_{cit/isocit}$	1.59	2.44
$R_{fum/mel}$	1.87	2.31

Table 2-11: Comparison of the two investigated chromatography methods. TBDMCS-derivatised tricarboxylic acid cycle metabolites using Gas Chromatography Mass Spectrometry as a tool for the separation and analysis of structural isomers of tricarboxylic acid cycle interesting more then Liquid chromatography–mass spectrometry.

Comparisons between the GC/MC and LC/MS methods are listed below:

1. TBDMCS-derivatised TCA metabolites using GC/MS chromatography as a tool for the separation and analysis of structural isomers of TCA interesting more then LC/MS (Table 2-11), Because the GC/MS method showed more sensitivity (lower LoD and LoQ) (Table 2-9) then the LC/MS (Table 2-7).
2. GC-MS chromatography shows less matrix effects than LC/MS, probably because any residue after the extraction can be crystallised or precipitated at the derivatisation step.

3. LC-MS chromatography has the advantage that it does not require derivatisation, so the removal of these pre-analytical steps reduces the time needed for sample processing from a few hours to a few minutes.
4. The LC/MS sample-processing mode has the advantage compared to GC/MS full-scan, that it reduces the amount of time devoted to each ion.

2.6. Conclusions

In conclusion, the development and validations of three robust methods for identification and quantification of TCA cycle and associated metabolites was achieved.

Chapter 3: MEASURING TCA CYCLE METABOLISM IN GLIOBLASTOMA CELLS

3.1. Introduction And Aims

This chapter describes work focusing on identifying whether changes to central metabolism, in particular the TCA cycle, take place as a result of the presence of each of the IDH mutant forms found in glioma cells. The chromatographic methods developed in Chapter 2 were used for the analysis of metabolites extracted from LN18 glioma cell line with over expression of the IDH1 gene mutations (R132H and R132C) and IDH2 gene mutations (R172K and R172M). These are compared with analysis of IDH1 and IDH2 wild-type cells.

The work in this chapter was carried out in collaboration with Dr. Chiara Bardella and Professor Ian Tomlinson's research group at the Wellcome Trust Centre for Molecular Genetics, University of Oxford and Nick de Pennington (Neurosurgery – ORH) (Clinical Neurology in Nuffield Oxford Hospitals – University of Oxford). Chiara performed all cell culture experiments expect where, Nick cultured $IDH1^{WT}$ and $IDH1^{R132H}$ cells for the AGI-5198 experiments. The author performed all cell extractions, samples analysis and data processing and interpretations.

3.2. Investigating TCA Cycle Metabolism In The Presence Of IDH Mutations

To investigate the impact of IDH mutations on cellular metabolism, TCA cycle metabolite levels were measured and compared between wild-type (IDH1 and IDH2) LN18 cells and those from the same cell line over-expressing ($IDH1^{R132H/C}$) and ($IDH2^{R172K/M}$). For each LN18 cell type, cells were cultured under the same conditions and harvested when confluent obtaining approximately 4 million cells per sample type. The cell numbers for each experiment were recorded and metabolites were extracted using ice-cold 80% methanol (see Chapter 8 for details). Initially

untargeted metabolite analysis was conducted using direct infusion of IDH^{WT} and $IDH1^{R132H}$ cell extracts using a LC/MS Waters Quattro Micro triple quadrupole MS system in full scan mode. Around 280 ion features were identified within the mass range m/z 100-350 from each sample and the peak areas for each were graphed using a binary plot for the purposes of data comparison. Figure 3-1 shows the results, which clearly demonstrate that significant differences in concentration are apparent between the wild-type and mutant cells for two ions in particular; one shows a smaller peak area and the other a larger peak area in the mutant compared to the wild-type cell samples. These correspond to differences in the concentration of the metabolites represented by these ions. This result suggests that there are two compounds present in cells expressing mutant $IDH1^{R132H}$ which are at quite different concentration from those found in $IDH1^{WT}$ cells from the same cell line. It also notable that generally as the mass increases there is a gradual increase in the variability in peak area between the two cell types. This is not significant in the context of the results of the experiments described here and is likely to represent a general decrease in measurement accuracy as ions increase in mass. The direct infusion analyses described were made with the MS providing nominal mass accuracy and so it was not possible to provide a definitive accurate mass determination of the chemical formula. The m/z values of 147 and 145 correspond to the masses of 2-HG and 2-OG, respectively.

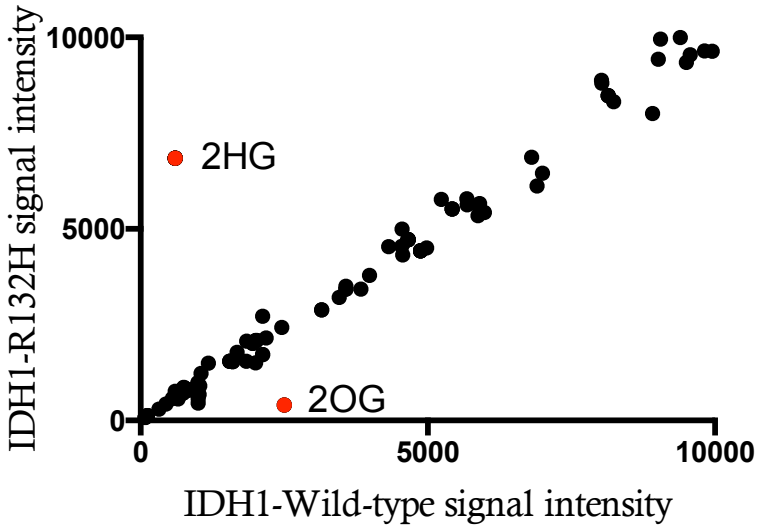

Figure 3-1: Metabolite profiles from cells expressing isocitrate dehydrogenase R132H/wild-type ($IDH1^{R132H}$ and $IDH1^{WT}$) as detected by direct infusion-MS scanning for species between 100–350 m/z ($M\text{-}H^-$). These data show a linear relationship, implying the concentration of most metabolites is similar in both samples except for nominal masses representing 2-hydroxyglutarate (2-HG) and 2-oxoglutarate (2-OG) which suggests higher and lower concentrations in the mutant sample respectively.

In order to investigate the results further and confirm the identity of the two outlying components, the same samples were analysed by LC/MS employing the isomer-RP-IR-MS method developed for TCA cycle analysis in Chapter 2 (method 1). All analyses are a combination of at least three independent biological experiments and three replicate measurements of each experiment. This resulted in a retention time for both 2-HG and 2-OG respectively which were used to confirm the identity of the peaks, which gave different peaks areas in mutant and wild-type cells. The data is shown in Figure 3-2 and shows that the two outliers are identified as 2-OG and 2-HG. In summary the untargeted metabolite analyses revealed that markedly altered levels of two ions were present in cells with over expression of $IDH1^{R132H}$ and their identity was confirmed by subsequent targeted LC/MS analysis of the samples.

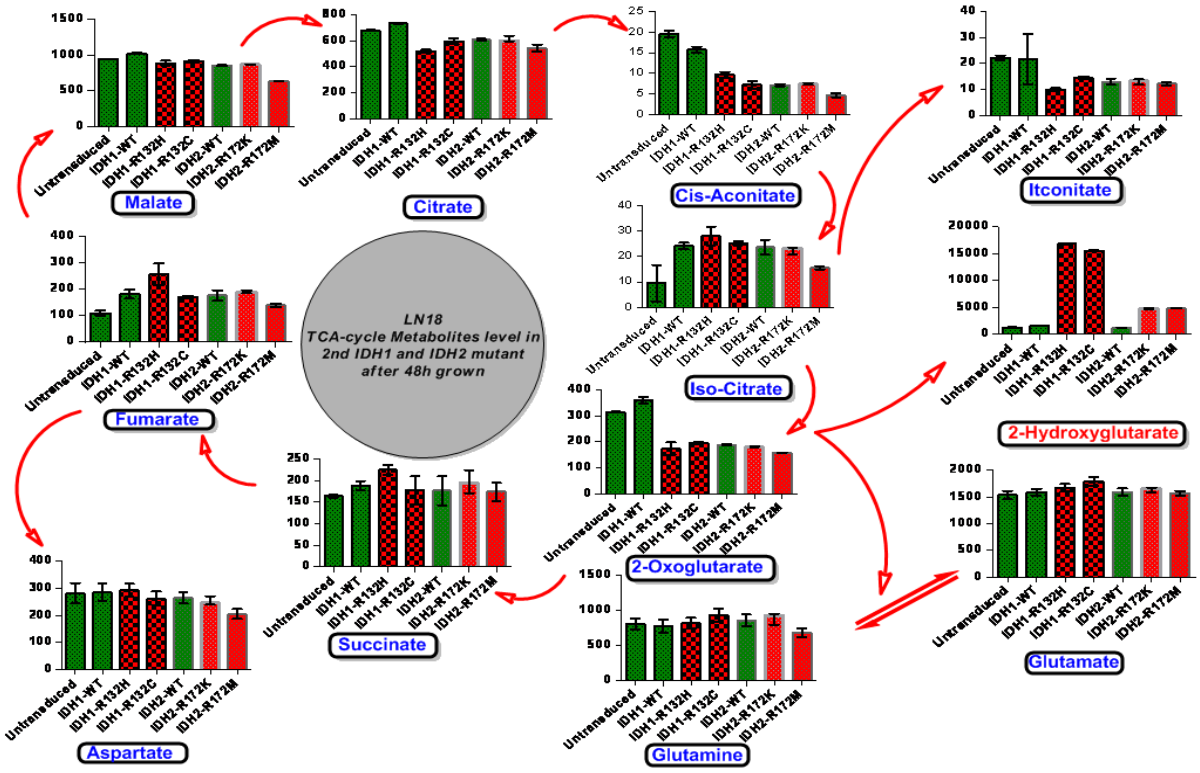

Figure 3-2: Schematic showing the concentrations of Tricarboxylic acid cycle intermediates measured by quantitative LC/MS mapped onto the conventional view of Tricarboxylic acid cycle metabolism. IDH1$^{R132H/C}$ and IDH2$^{R172K/M}$ cells contain increased concentrations of 2-hydroxyglutarate, the changes in the abundance of metabolites in response to different concentrations with mutant red column (n=4) and IDH1/2^{WT} green column (n=3). Error bars depict one standard deviation (s.d.) from the mean of three injections from three biological repeat cell culture analyses. Were y-axis represent the metabolite concentration (µM).

The data in Figure 3-2 show that the presence of R132H/C and R172K/M mutations in the cell line correlated directly with a significant increase in the concentration of 2-HG compared with the wild-type and a lower level of 2-OG (Figure 3-2); see Appendix A1 for raw data. These results do not demonstrate a direct link between 2-OG depletion and 2-HG accumulation but the facts that these two metabolites are chemically and metabolically close in the TCA cycle supports this possibility. The results reveal that the average 2-OG level from four samples harbouring various IDH1/2 mutations was less than the average 2-OG level observed in four samples that

are wild-type for IDH1/2. This difference in 2-OG is statistically significant (Figure 3-3) shows a graph of these raw data.

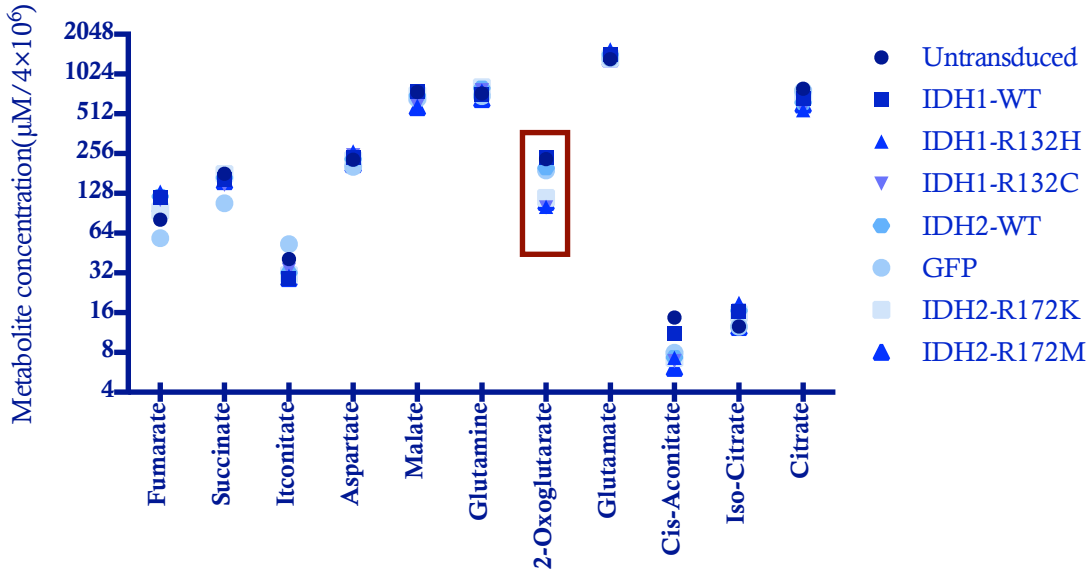

Figure 3-3: LN18 glioma cells containing R132 and R172 mutations in isocitrate dehydrogenase 1/2 (IDH1 /IDH2) contain increased concentrations of 2-hydroxyglutarate metabolites concentrations from the mean of three independent experiments (n=3). Cell samples extraction by 80% Methanol in water, wild-type (n=12) or carrying an R132 mutant (n=6) and R172 mutant (n=6), metabolites extracted for LC–MS analysis. Each symbol represents the amount of the listed metabolite found in each cell sample. There were no statistically significant differences in malate, fumarate, succinate, isocitrate, glutamine, or glutamate levels between the wild type and R132 and R172 mutant IDH1 and IDH2 cells, except 2-oxoglutarate where it showed low levels in mutant compared to wild-type [see the red box].

Of additional interest was the fact that 2-HG was also found at higher concentration in the cell culture media in the $IDH1^{R132H}$ compared to the $IDH1^{WT}$ cells (data shown in Figure 3-4). This suggested that not only was 2-HG being produced at higher levels by mutant cells but it was also able to exit from those cells into the surrounding matrix.

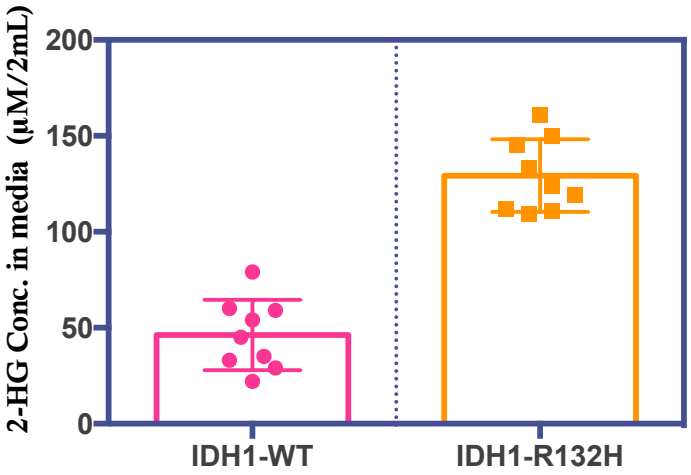

Figure 3-4: LN18 glioma cells containing R132 mutations in isocitrate dehydrogenase 1 contain increased concentrations of 2-Hydroxyglutarate in culture media from the mean of three independent experiments (n=9).

Similarly, to the analysis of 2-HG in IDH1$^{R132H/C}$ and IDH2$^{R172K/M}$ cell lines after 24 and 48h of culture, there were no significant differences in concentration observed for TCA cycle intermediates between IDH1/2^{WT} and cells with mutations IDH1$^{R132H/C}$ and IDH2$^{R172K/M}$, other than for 2-OG and 2-HG.

Increased 2-HG levels were found in all cells that contained IDH1 and IDH2 mutations when compared to wild-type (Figure 3-4). IDH1 and IDH2 mutant cells after 48h of culture showed a 3-fold increase in concentration for 2-HG when compared with the same experiment after only 24h (Figure 3-5). This increase in 2-HG in R132 and R172 mutant cells was statistically significant (< ±3SD).

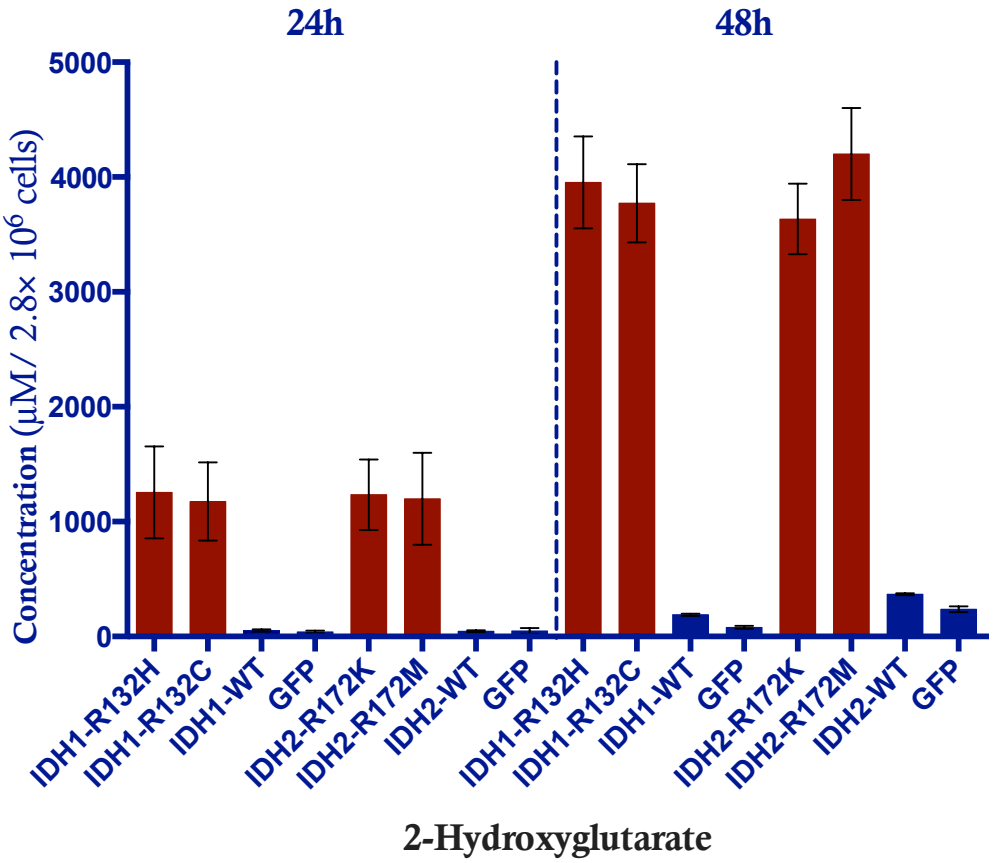

Figure 3-5: 2-Hydroxyglutarate concentrations in LN18 gliomas cells containing R132 and R172 mutations in isocitrate dehydrogenase 1/2 (IDH1/IDH2) contain increased concentrations of 2-Hydroxyglutarate after 24h and 48h of incubation. Metabolites from cells overespressing either wild type (n=4) or R132 IDH1 mutants (n=2) or IDH2 R172 mutant s (n=2), were extracted by using 80% Methanol in water and analysed using Liquid chromatography–mass spectrometry. Each symbol represents the amount of the 2HG metabolite found in extracted pellets.

In summary, the data shows that the presence of specific IDH1/2 mutations correlates with higher levels of 2-HG and lower levels of 2-OG in both IDH1/2 mutations in LN18 cell lines. I was decided to investigate whether it was the presence of the specific IDH1/2 mutations which leads to the changes in 2-OG and 2-HG concentrations observed, or rather the result of reduced wild-type IDH1/2 activity.

3.3. IDH Knockdown In IDH1/2 And 3 Wild-Type Ln18 Cells

IDH1/2 and three wild-type LN18 cells were cultured containing an shRNA sequence target against the wild-type IDH codon to initiate knockdown of IDH1, IDH2, and IDH3 protein expression. These cells were cultured, harvested, extracted and analysed in the same way as previous experiments. Figure 3-6 shows normalised concentrations of the TCA cycle intermediates measured from the knockdown LN18-IDHs cells. No statistically significant accumulation or decrease of 2-OG in any shRNA-IDHs was detectable compared to the scramble cells (Figure 3-6).

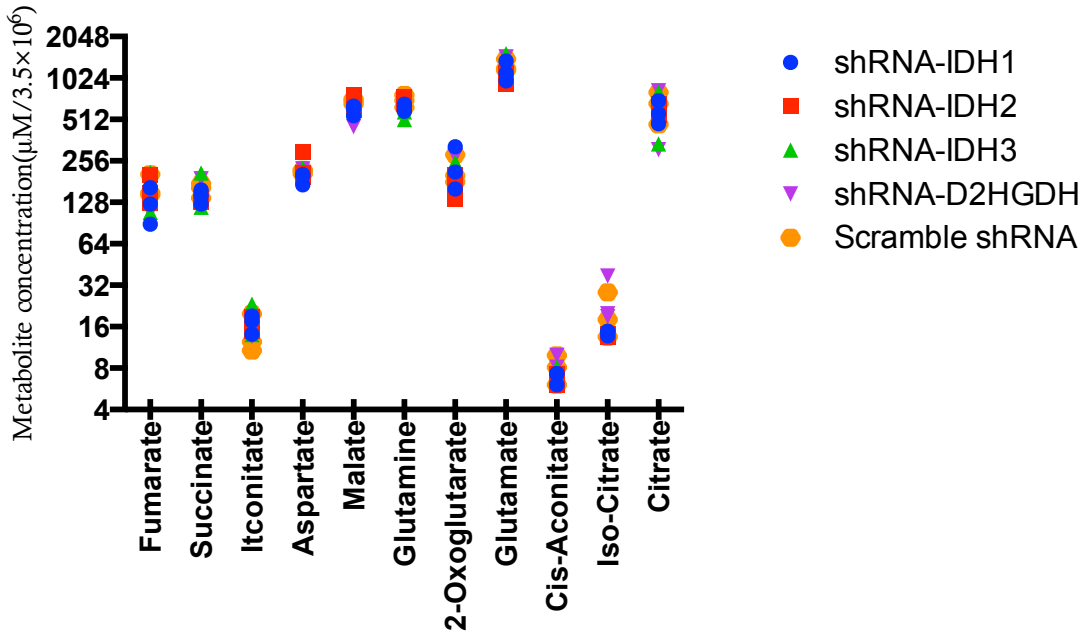

Figure 3-6: Tricarboxylic acid cycle metabolite concentrations for LN18 cell containing knockdown wild-type Isocitrate dehydrogenase 1, 2 and 3, metabolites concentrations from the mean of three independent experiments (n=3). Cell sample extractions by 80% Methanol in water, Isocitrate dehydrogenase isoform (n=9) and control (n=6), metabolites extracted for LC–MS analysis. Each symbol represents the amount of the listed metabolite found in each cell sample. There were no statistically significant differences in all Tricarboxylic acid cycle and associated metabolites.

These results suggested a change of function associated with the mutated IDH enzyme found in the glioma cell lines and primary tissues samples (as opposed to a loss of function). They help to explain the depletion of 2-OG and significant increase in 2-HG levels observed. Similar increases in 2-HG have also been reported by other researchers during the course of these studies and increasing evidence suggests a change of function to be characteristic of IDH1/2 mutations in gliomas (Stancheva et al., 2014). The depletion in 2-OG we observed and this result was also found in another study where it was concluded that a reduction in IDH1 activity produces a reduction in 2-OG levels (Zhao et al., 2009).

3.4. Analysis Of 2-HG Chiral Forms In Cell And Tissue Samples

2-HG has two enantiomeric forms (*D* and *L*), and it is well known that some enzymatic processes can recognise one form from the other and are only act in association with one isomeric form. Considering the evidence found for a change of function it was decided to investigate the 'enantiomeric selectivity' of the IDH1/2^{WT} and mutant IDH1/2 enzymatic reactions.

To determine the chirality of the (*L*/*D*)-2-HG produced; the chiral chromatographic method developed in chapter 2 was used. Analysis of the same LN18 IDH1^{R132} and IDH1^{WT}cell extracts was made using this method (the same samples used for TCA cycle metabolite analysis in Figure 2-9).

50µL of mobile phase A was added to each freeze dried sample, vortexed, and filtered through a 0.45 mm membrane filter. The filtrate was injected (2µL) via an auto sampler. After analysis, the samples were independently spiked with purified standards of the 2-HG enantiomers in order to confirm the identity of the resolved peaks. The results are shown in Figure 3-7. Spiking of the biological samples

demonstrated the retention times observed for the two enantiomers and provided a discriminatory parameter, as the m/z values were identical. *L*-2-HG eluted slightly earlier than *D*-2-HG. The two enantiomers were baseline resolved enabling both identification and relative quantification by comparison of the integrated chromatographic peak areas.

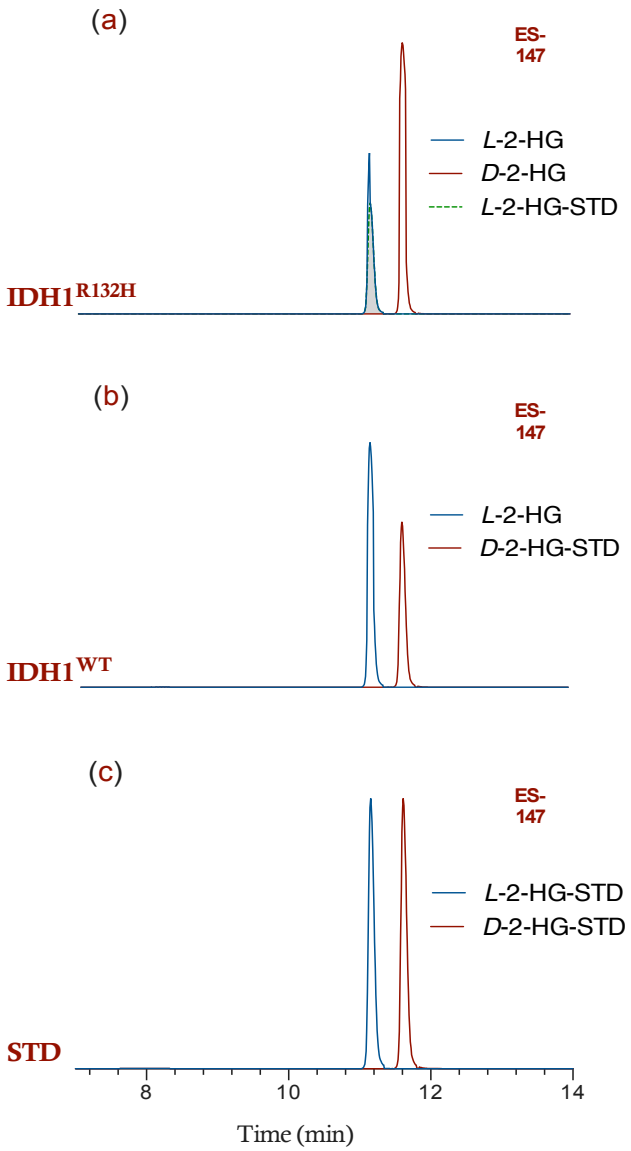

Figure 3-7: Three chromatography for determination of configuration for the Chiral (*L*/*D*)-2-Hydroxyglutarate in Isocitrate dehydrogenase R132H ($IDH1^{R132H}$) (a); were spiked with *L*-2-Hydroxyglutarate standards (STD) and $IDH1^{WT}$ (b); spiked with with *D*-2-Hydroxyglutarate. Peak identification of the two configurations of (*L*/*D*)-2-Hydroxyglutarate was established by analysing commercially available standards of (*L*/*D*)-2-Hydroxyglutarate (c) using chromatographic conditions.

This method was used to measure the absolute concentrations of the *L*- and *D*-forms of 2-HG in mutant IDH1^{R132H} and IDH1^{WT} extracts from cultured cells using a standard calibration curve (shown in Chapter two). The results showed a 4000-fold increase in the concentration of the *D*-enantiomer of 2-HG in the mutant compared to the wild-type with little change in the *L*-form. Figure 3-8 shows the concentration calculated from the peak areas of the *D*-2-HG form in IDH1^{R132} compared with the chromatography signal under the limit of detection in IDH1^{WT}; whereas the concentration as determined by integration of the chromatographic peak area of *L*-2-HG showed similar (2-4 fold change) concentrations for both IDH1^{R132H} and IDH1^{WT} see (Figure 3-8). For comparison, Dang and co-workers (2009) showed an increase of total 2-HG concentration of around 100 fold in IDH1^{R132H} compared to IDH1^{WT}.

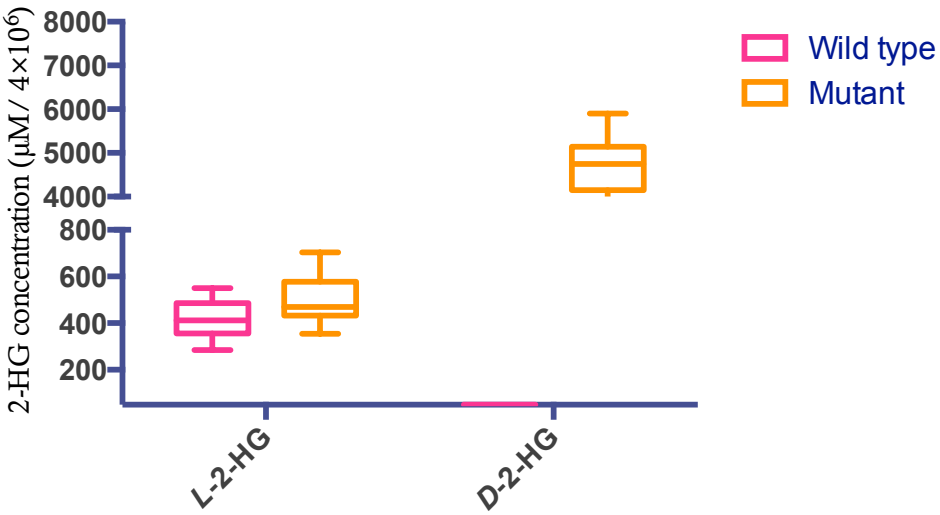

Figure 3-8: Configuration of (*L*/*D*)-2-Hydroxyglutarate (L-2-HG/D-2-HG) development in Isocitrate dehydrogenase mutant or wild-type LN18 cells. As it is shown, these Isocitrate dehydrogenase mutant cells contain increased concentrations of *D*-2-Hydroxyglutarate after 48h of incubation. Cellular metabolites from cells over expressing wild type (n=4), Isocitrate dehydrogenase-1 R132 (n=2) or Isocitrate dehydrogenase-2 R172 mutants (n=2), have been extracted by using 80% Methanol in water, and analysed for enantiomers using RP-IP LC–MS. Each symbol represents the amount of the (*L*/*D*)-2-Hydroxyglutarate metabolite found in each cell sample from the mean of three independent experiments (n=3). The results showed a 4000-fold increase in the concentration of the *D*-enantiomer of 2-HG in the mutant compared to the wild-type with little change in the *L*-form.

In addition, the levels of 2-HG enantiomers were measured in cells where either IDH1 or IDH2 or IDH3 genes expression was deleted. To investigate whether loss of IDH isoforms led to changes in cellular levels of *D*-2-HG, we used shRNA interference to down-regulate the endogenous IDH isoforms. Chiral analysis of 2-HG revealed no statistically significant differences in concentration in either the *L*-form or *D*-form of 2-HG (Figure 3-9).

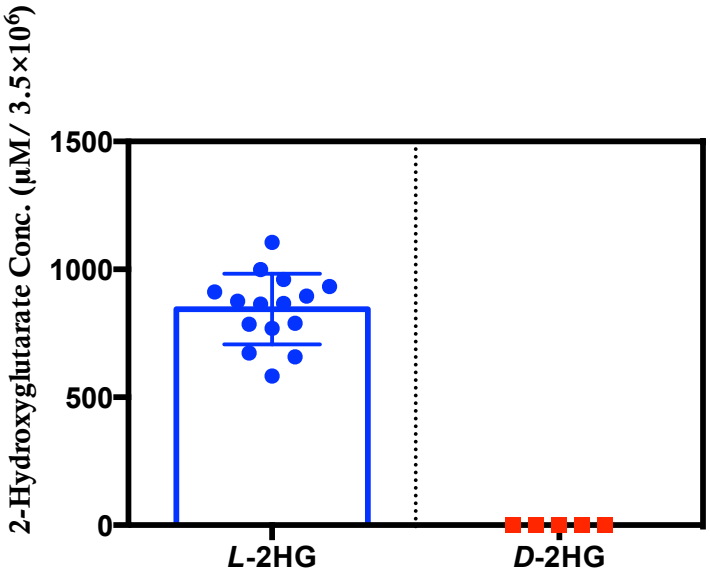

Figure 3-9: Determination of configuration of the chiral (*L*/*D*)-2-Hydroxyglutarate in shRNA Isocitrate dehydrogenase isoforms and control, 2-Hydroxyglutarate concentration from the mean of three independent experiments. The results suggest were that there is no accumulation of *D*-2-Hydroxyglutarate with shRNA as an inhibitor. Error bars represent one standard deviation (s.d.) from the mean of three replicate injections.

These results suggest that not only does the mutation in IDH1/2, found in >70% of grade 2 and 3 gliomas infer a change of function leading to the accumulation of 2-HG, this accumulation is from the *D*-enantiomer exclusively. The mechanism(s) by which mutant $IDH1^{R132H/C}$ and $IDH2^{R172K/M}$ contribute to the accumulation of *D*-2-HG remain unclear however as does the function of *D*-2-HG accumulation. It is also not clear whether 2-HG accumulation facilitates tumourogensis or alternatively whether it is a cellular response mechanism to help inhibit tumourogenic changes or indeed a

benign change of function, which simply leads to 2-HG accumulation, playing no important functional role in cancer cell development.

During the course of the research described in this thesis another research group published a study using biochemical, structural and cellular assays to show that both the *D*- and *L*-forms of 2-HG can act as inhibitors of 2OG-dependent oxygenases (Chowdhury et al., 2011). The inhibitory effects of 2-HG do not however appear to be enantiomerically sensitive. Whether 2-HG accumulation in glioblastomas and leukemia's is actively inhibiting 2-OG-dependent oxygenases, in a strategically important way for tumourgensis, is not yet understood and the question of 2-HG function was therefore one I decided to investigate further.

3.5. Mutant IDH1-R132H Inhibition And Its Effects Of D-2-HG Levels

AGI-5198 is a selective $IDH1^{R132H}$ inhibitor (Rohle et al., 2013), which was shown to reduce the concentration of *D*-2-HG in a dose dependent manner, for the mutant enzyme $IDH1^{R132H}$. The detailed mechanisms by which AGI-5198 inhibitors affect cell cycle regulation and differentiation remain unclear however (Francine et al., 2013) . While reduction in 2-HG production likely results in reversal of metabolic aberrancies, transcriptional pattern changes leading to cell differentiation may be due to epigenetic reprogramming. Epigenetic mechanisms were suggested from histone methylation pattern changes after AGI-5198 treatment (Rohle et al., 2013).

In order to examine the role of mutant $IDH1^{R132H}$ in fully transformed cells with endogenous $IDH1^{R132H}$ mutations the selective inhibitor AGI-5198 (chemical structure shown in Figure 3-10a) for $IDH1^{R132H}$ was introduced in $IDH1^{R132H}$ and $IDH1^{wild\text{-}type}$ LN18 cell cultures. Figure 3-10b presents a graph comparing the presence and absence of the inhibitor on the levels both 2-HG enantiomers. It can be seen that a 2-fold decrease in the *D*-2HG level occurs when the cells are treated with

AGI-5198; (500µM, 24h). In comparison, Rohle and co-worksers showed in 2013 a 3-fold decrease in *D*-2-HG concentration in $IDH1^{R132H}$ cells with the same inhibitor (AGI-5198; 500µM, 48h).

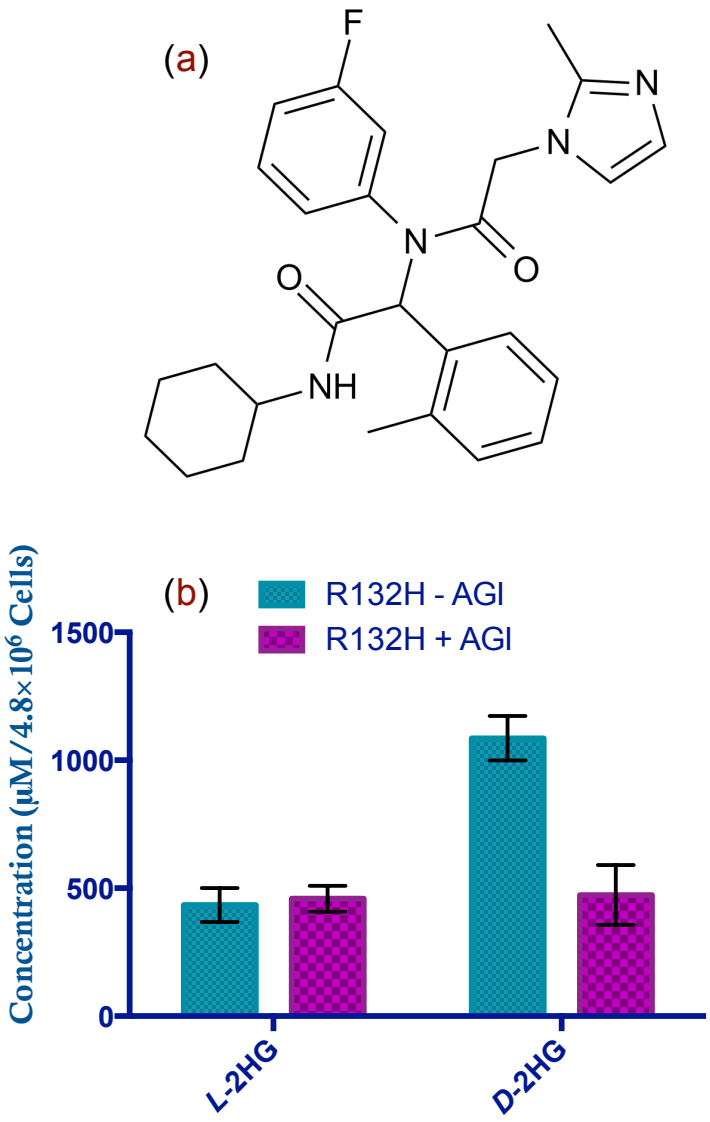

Figure 3-10: An R132H-Isocitrate dehydrogenase-1 inhibitor blocks *D*-2-Hydroxyglutarate production and softagar growth of isocitrate dehydrogenase-1 mutant glioma cells. (a) Chemical structure of AGI-5198. (b) AGI-5198 inhibits *D*-2-Hydroxyglutarate production in R132H-Isocitrate dehydrogenase-1mutant LN18 glioma cells. Cells were treated for 24h with AGI-5198 (500 µM) and *D*-2-Hydroxyglutarate was measured in cell pellets. *D*-2-Hydroxyglutarate concentrations are indicated above each bar (in µM). Error bars depict one standard deviation (s.d.) from the mean of three chromatography peak areas from three injections. It can be seen that a 2-fold decrease in the *D*-2HG level occurs when the cells are treated with AGI-5198; (500µM, 24h).

3.6. GC/MS Analysis Of Mutant And Wild Type IDH1 Ln18 Cells

The GC/MS method developed in chapter 2 (method 3) is a robust method suitable for the identification and quantification of TCA cycle intermediates, amino acids and other polar, small molecules found in cells. In order to investigate quantitative information about oxaloacetate as well as amino acids in these cells it was decided that this method should also be applied to the analysis of LN18 cell metabolite extracts with and without expression of IDH1 mutations $IDH1^{R132H}$ and $IDH1^{WT}$. Ten of the naturally occurring amino acids were found in significantly higher concentrations in the mutant cells compared to the wild-type cells. The degrees of increase were in the range 1.8- to 11.6-fold (Figure 3-11).

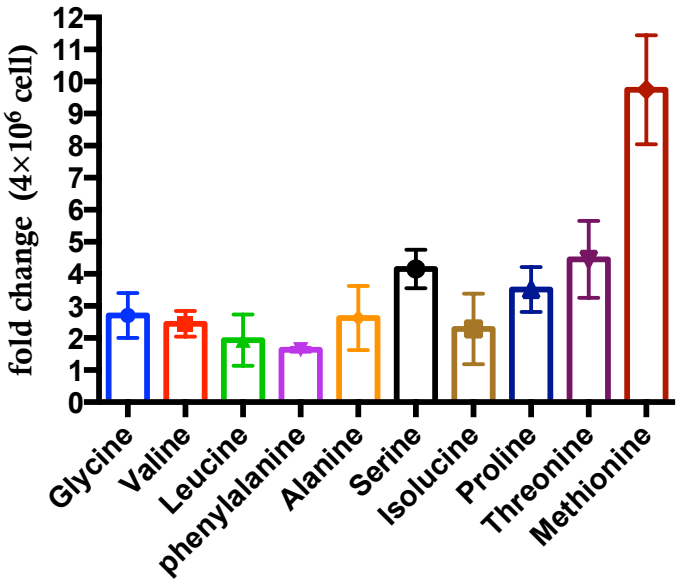

Figure 3-11: Fold change enhancement of R132H metabolite peak area with wild-type Isocitrate dehydrogenase-1, determination of metabolite fold change was established by analysing commercially available standards using Gas Chromatography Mass Spectrometry chromatographic conditions and NIST library. Error bars depict one standard deviation (s.d.) from the mean of three injections from three biological repeat cell culture analyses. Ten of the naturally occurring amino acids were found in significantly higher concentrations in the mutant cells compared to the wild-type cells. The degrees of increase were in the range 1.8- to 11.6-fold.

Other researchers have also found increased levels of amino acids in cancer cells including gliomas (Kranendijk et al., 2010). It is interesting to note however that higher levels are found in LN18 with over expression of $IDH1^{R132H}$ than in $IDH1^{WT}$ LN18 cells which are nevertheless derived from a human grade IV glioblastoma. One of the reasons it was decided to look more closely at the TCA cycle was that changes to the function of the IDH1/2 would seem likely to have some disruptive effect on the normal functioning of the TCA cycle and the very high levels of 2-HG identified, imply that large amounts of carbon are being routed out of the TCA cycle. At least some of the published data indicate that 2-OG is the direct carbon source of 2-HG formation (Dang et al., 2009). The fact that almost all intermediate levels are not changed in mutant cells is surprising but it cannot be ruled out that a significant change in utilisation or even functioning of the TCA cycle in mutant cells occurs with the levels of TCA cycle intermediates being tightly regulated. The levels of intermediates may or may not change as a result of differences in fluxes throughout biosynthetic and bio-catabolic pathways of central metabolism so we may not see these changes reflected in the levels of TCA cycle intermediates. The question of whether changes in biosynthetic pathways are occurring when IDH1/2 mutations are present is pertinent to the biosynthetic origins of 2-HG. To date there has been no definitive study to show how 2-HG is synthesized in IDH1/2 mutant cells and where its carbon atoms come from. Furthermore, whether it is associated with significant changes in biosynthetic pathways of central metabolism. I decided to next pursue answers to these questions.

3.7. Investigating Changes In Biosynthetic Pathways Associated With The Presence Of IDH1 And IDH2 Mutations

It is still unclear how IDH1 mutations affect TCA cycle central carbon metabolism in the heterozygous cellular setting. Therefore, further exploration into how these metabolic pathways differ, and hence how this could be therapeutically exploited, are of interest. An important distinction between IDH1 and IDH2 is their localization in the cytosol/peroxisome and mitochondria, respectively. The distinct locations for the mutant enzymes may significantly influence the metabolic phenotype of tumor cells with IDH1 versus IDH2 mutations.

In order to investigate in more detail the biosynthetic function of the TCA cycle in IDH mutants a series of cell culture experiments were conducted to compare $IDH1^{WT}$ and $IDH1^{R132H}$ LN18 cells in which different TCA cycle intermediates and selected amino acids had been spiked separately into the cell culture media. The aim of the experiments was to probe the effects of increased intermediate load at different positions in the TCA cycle comparing both $IDH1^{WT}$ and $IDH1^{R132H}$ LN18 cells. Differences in the results may provide clues as to how metabolism differs and would inform the design of follow up experiments. A number of independent studies have used this technique to study metabolism (Saguir et al., 2002, Fukunaga et al., 1978 and Grassian et al., 2014). Initial experiments were conducted with organic acids individually spiked into cell culture media, which was used to grow $IDH1^{R132H}$ and $IDH1^{WT}$ LN18 cells (5 mM of the intermediate in 10ml media). The effect on 2-HG levels, was evaluated. Unmodified media (DMEM with L-glutamine, high glucose (4.5g/l) cat. number E15-810, PAA Cell Culture Company) does not normally contain TCA cycle intermediates. The precursor amino acid Gln is present at 18mM and there is no aspartic acid. The levels of TCA cycle intermediates including *D*-2-HG were measured in the cells harvested after 24 hours. Figure 3-12 shows the results of

spiking intermediates into the IDH1^{WT} (a) and IDH1^{R132H} (b) cell lines. The results reveal that for the IDH1^{R132H} cells significantly increased levels of *D*-2-HG were found when 2-OG, Glu, OAA, Asp and Gln were spiked into the IDH1 mutant (Figure 3-12a). This was in contrast with the same experiments using the IDH1^{WT} cells where *D*-2-HG remained below the limit of detection in all experiments (Figure 3-12b). There were no differences in *L*-2-HG levels in either IDH1^{R132H} or IDH1^{WT} cells (Figure 3-12a and b).

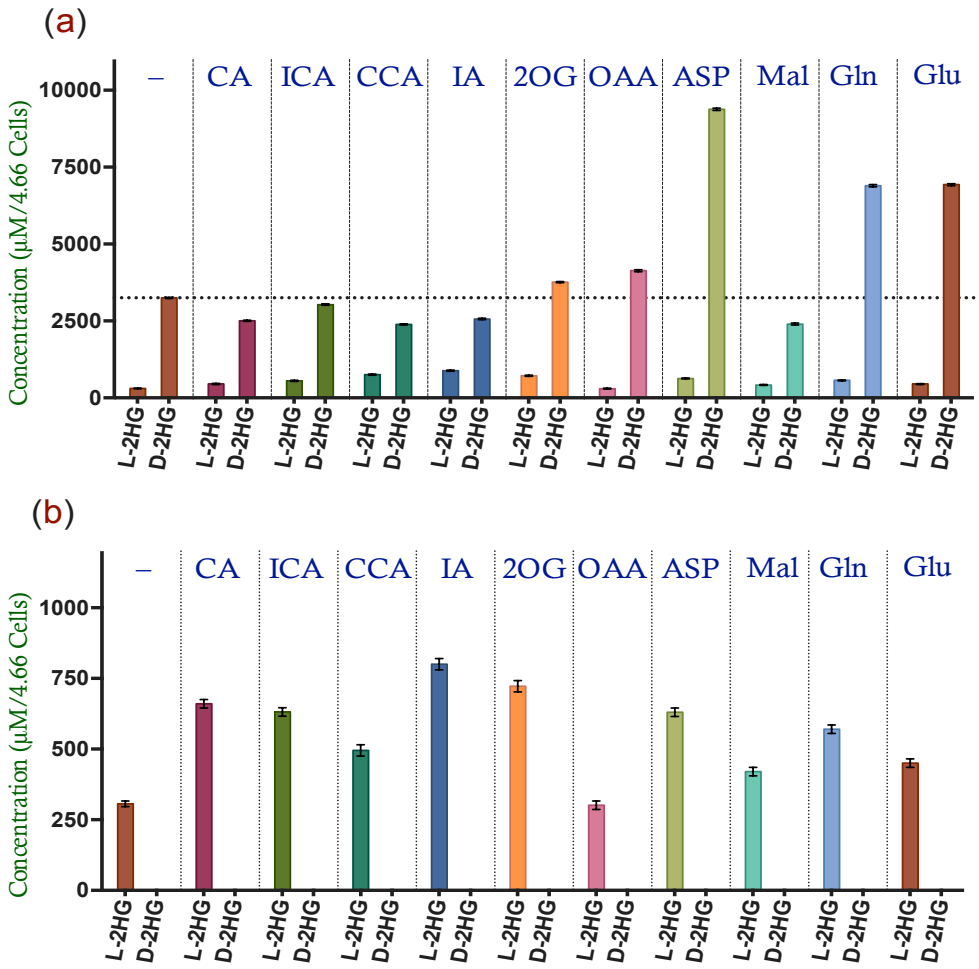

Figure 3-12: The effect of the Tricarboxylic acid cycle metabolites spiked (5mM) in the media of Isocitrate dehydrogenase-1 R132H (IDH1^{R132H})(a) and Isocitrate dehydrogenase-1 wild-type IDH1^{WT} (b) growth on the accumulation of (*L*/*D*)-2-HG. Error bars depict one standard deviation (s.d.) from the mean of three-chromatography peak area from three injections, citrate (CA), isocitrate (ICA), cis-aconate (CCA), itaconatet (IA), 2-oxoglutarate (2-OG), oxaloacetate (OAA), aspartate (ASP), aalate (Mal), glutamine (Gln) and glutamate (Glu). Error bars depict one standard deviation (s.d.) from the mean of triplicate injections.

It was interesting to see that when Glu, Gln and Asp were spiked in to IDH1^{R132H} cells there was a more than 2-fold increase in *D*-2-HG levels. Spiking with Asp showed a 3-fold increase in *D*-2-HG levels Figure 3-12(b). The results from the Asp spiking experiment, suggest a metabolic link between Asp and *D*-2-HG in the metabolism of the mutant specifically which is not explained by the conventional metabolic understanding of TCA cycle function. Spiking with oxaloacetate also showed a significant increase in *D*-2-HG Figure 3-12(b). It is interesting to note the close metabolic association between aspartate and oxaloacetate via de-amination and transamination see Figure 3-13.

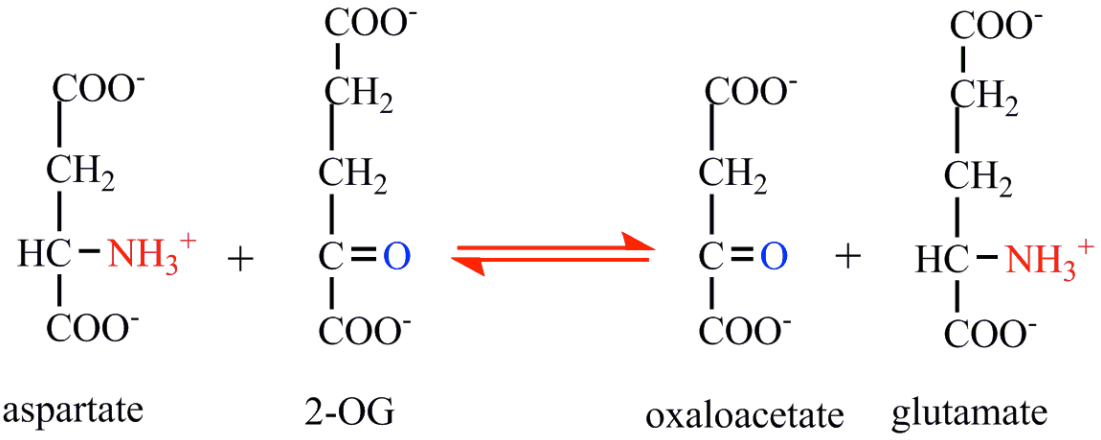

Figure 3-13: Aspartate Transaminase (AST) has multiple names including Aspartate Aminotransferase, Glutamate-Oxaloacetate Transaminase (GOT), and Serum Glutamate-Oxaloacetate Transaminase (SGOT). As a member of the aminotransferase family, AST catalyzes the reversible transfer of the amino group from glutamate to aspartate.

In order to investigate further, cells were spiked separately with *D*- and *L*-aspartic acid, the *D*-aspartic acid used as a control. Aba and co-workers reported increases in intracellular Na^+ which are associated with spiking *D*-aspartic acid which stimulated glucose and lactate oxidation in mouse astrocyte cultures without any changes in TCA cycle metabolism (Aba T at el., 2006).

The effects of this experiment on the concentrations of the enantiomers of 2-HG are shown in Figure 3-14. Spiking with the *L*-form of aspartic acid lead to a 3-fold

increase in the *D*-form of 2-HG in IDH1^{R132H} but not the wild-type cells. Spiking the *D*-form of aspartic acid, however showed no statistical difference in peak areas for *D*-2-HG from the untreated IDH1^{R132H} cells, which is the same as for the non-spiked control. Thus, the changes are specific to *L*-aspartic acid and not due to changes in pH due to addition of acids for example.

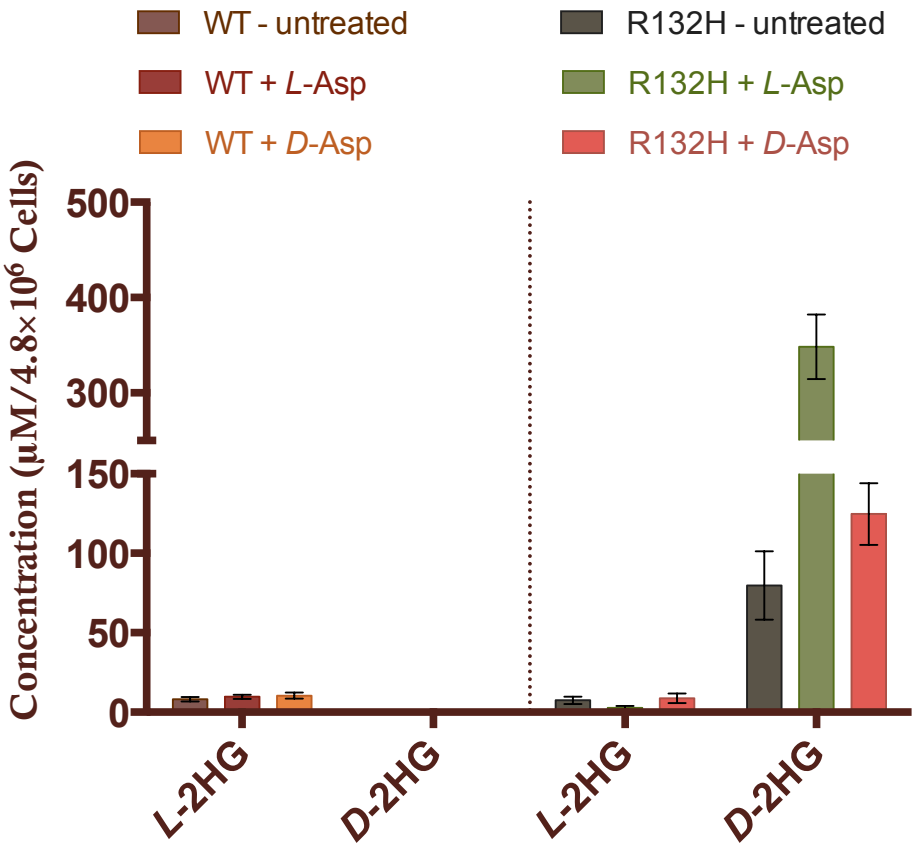

Figure 3-14: This figure shows the effect of the *D*- and *L*-aspartic acid spiked (5mM) in the culture media for Isocitrate dehydrogenase-1 R132H and wild-type (IDH1^{R132H} and IDH^{WT}) cells. Error bars depict one standard deviation of the mean of three-chromatography peak areas from triplicate biological repeats. Spiking with the *L*-form of aspartic acid lead to a 3-fold increase in the *D*-form of 2-HG in IDH1^{R132H} but not the wild-type cells. Spiking the *D*-form of aspartic acid, however showed no statistical difference in peak areas for *D*-2-HG from the untreated IDH1^{R132H} cells, which is the same as for the non-spiked control. Thus, the changes are specific to *L*-aspartic acid and not due to changes in pH due to addition of acids for example.

3.8. Spiking [^{13}C-4]-L-Aspartic Acid Into Mutant And Wild-Type LN18 Cells

Next it was dediced to investigate the association between increased Asp and *D*-2-HG levels further performing a [^{13}C-4]-*L*-aspartic acid metabolic tracer experiment. Both IDH1^{R132H} and IDH1^{WT} cells were grown in multiple flasks using the same media (see materials and method section) which was spiked with ^{13}C-4 aspartic acid (5μM/10mL) for 2,4,8 and 24 hours in different flasks. The consumption and release of aspartic acid was measured; the relative ^{13}C metabolic tracer, as well as the metabolite labelling pattern, was also investigated using time course experiments.

3.8.1. Aspartic Acid Consumption Profiles

To systematically characterize IDH1 cell metabolism, LC/MS was used to create cellular consumption and release (CORE) profiles (figure 3-15a) of [^{13}C-4]-*L*- aspartic acid metabolism (Jain et al., 2012), resulting in a time-averaged CORE profile for [^{13}C-4]-*L*- aspartic acid on a cell culturing pool basis over a period of exponential growth (Figure 3-15b). Using CORE profiling, the amount of [^{13}C-4]-*L*- aspartic acid consumed by the cell from the media and the amount of [^{13}C-4]-*L*-aspartate released back into the media from the cell, can be estimated. This can then be compated between IDH1^{R132H} and IDH1^{WT} (see Figure 3-15c).

As shown in Figure 3-15c, the results of CORE profiles and IDH1^{R132H} cells show that the consumption of [^{13}C-4]-*L*-aspartic acid increases over 24h. However, after 4 and 8 hours there is still a greater proportion of [^{13}C-4]-*L*-aspartic acid in the media compared to the cells. In contrast IDH1^{WT} cells show a geater proportion of [^{13}C-4]-*L*-aspartic acid in the cells at the first two time points (4 and 8 hours) and then a reduction in the proportion in cells after 24 hours.

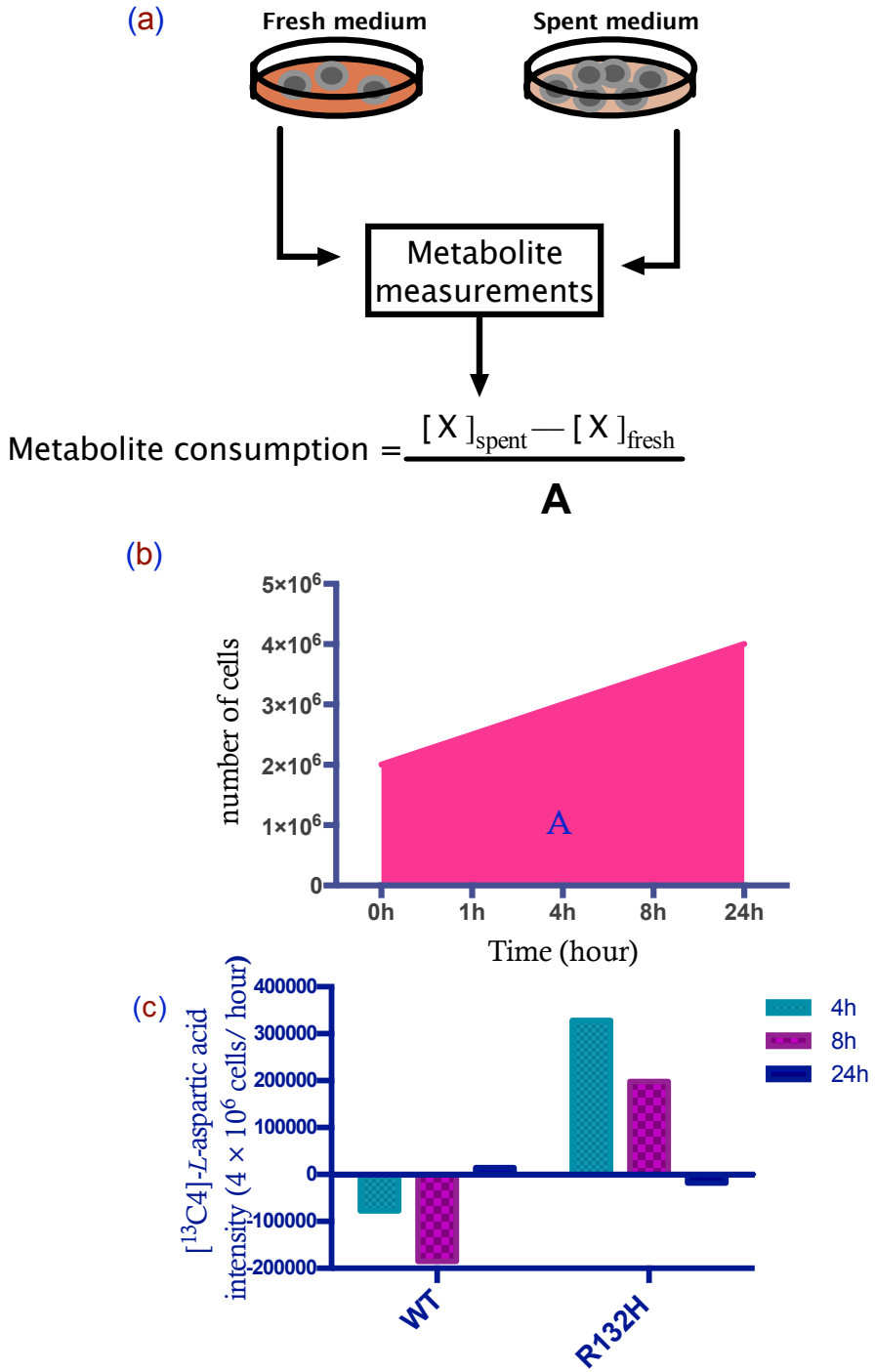

Figure 3-15: For determining metabolite CORE profiles, media samples taken before (fresh) and after (spent) 4 to 24 hour of cell culture are subjected to metabolite profiling by Liquid chromatography–mass spectrometry. For [^{13}C4]-L-aspartic acid X (a), the CORE value is calculated as the difference in signal abundance normalised to the time A under the growth period (b). (c) shown the consumption and release of [^{13}C-4]-*L*-aspartic acid.

3.8.2. [^{13}C]-Aspartic Acid Tracer Profiles

The effects of spiking [^{13}C-4]-*L*-aspartic into culture media on the unlabelled 2-OG and *D*-2-HG content in cells are shown in Figure 3-16. Figure 3-16(a) shows how the realtive concentration of 2-OG changes after 2, 4, 8 and 24 hours of culturing with [^{13}C-4]-*L*-aspartic acid (5mM/10mL). For the IDH1^{R132H} cells it can be seen that after 1,4 and 8 hours there is little difference between the cells growth with [^{13}C-4]-*L*-aspartic acid and without. However, after 24 hours incubation with [^{13}C-4]-*L*-aspartic acid the concentration of 2-OG has increased almost two-fold compared to the levels in cells incubated without [^{13}C-4]-*L*-aspartic acid. It can also be seen that for IDH1^{WT} cells with or whithout [^{13}C-4]-*L*-aspartic acid there is very little difference in 2-OG levels.

Figure 3.16(b) shows the results for measurment of *D*-2-HG, again for 1,4 and 8 hours there is little difference in concentraton between for the IDH1^{R132H} cells with and without [^{13}C-4]-*L*-aspartic acid. However, after 24 hours the concentration of what is more than three-fold increased in the [^{13}C-4]-*L*-aspartic acid spiked cells. The levels of *D*-2-HG are below the limit of detection in IDH1^{WT} cells. Figure 3.16(c) shows the ratio of NAD+ to NADH at the 4 time points. Again, after 24 hours there is a more than fifteen-fold increase in NAD+/NADH ratio in the spiked, compered to non-spiked, IDH1^{R132H} cells. There was no significant change in the NAD+/NADH ratio between 1,4 and 8 hours for spiked and non-spiked IDH1^{WT} cells and after 24 hours an eight-fold increase in NAD+/NADH ratio in the spiked IDH1^{WT}.

The [^{13}C-4]-*L*-aspartic acid spiking experiment provide evidence that aspartic acid is closely linked metabolically with *D*-2-HG production via 2-OG. When 2-OG levels go up a commensurate increase in *D*-2-HG levels is seen which is also correlated with an increase in NAD+, a product of the enzymatic conversion of 2-OG to *D*-2-HG in

the mutant enzyme reaction (there is no production of *D*-2HG from the wild-type enzyme so an increase in NAD+ was not expected from these control experiments).

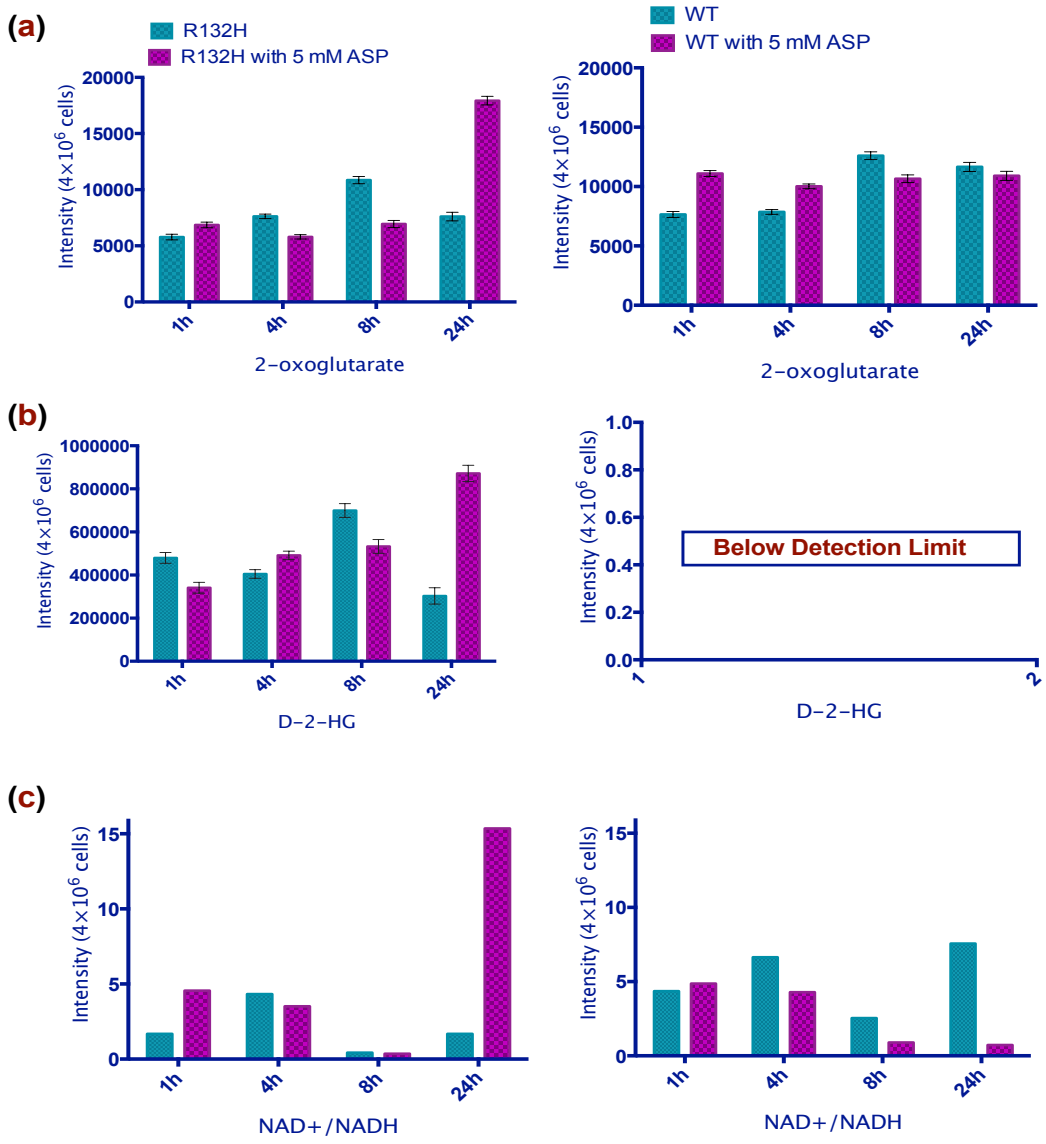

Figure 3-16: The effect of the [^{13}C-4]-*L*-aspartate spiked (5 mM/10 mL) in culture media of Isocitrate dehydrogenase-1 R132H (IDH1^{R132H}) for *D*-2-Hydroxyglutarate, 2-oxoglutarate and the ratio of NAD^{+}/NADH. Error bars depict one mean of three-chromatography peak area from 3-injections of the same sample. (a) shows how the realtive concentration of 2-OG changes after 2, 4, 8 and 24 hours of culturing with [^{13}C-4]-*L*-aspartic acid (5mM/10mL). For the IDH1^{R132H} cells it can be seen that after 1,4 and 8 hours there is little difference between the cells growth with [^{13}C-4]-*L*-aspartic acid and without. (b) shows the results for measurment of *D*-2-HG, again for 1,4 and 8 hours there is little difference in concentraton between for the IDH1^{R132H} cells with and without [^{13}C-4]-*L*-aspartic acid. (c) shows the ratio of NAD+ to NADH at the 4 time points. Again, after 24 hours there is a more than fifteen-fold increase in NAD+/NADH ratio in the spiked, compered to non-spiked, IDH1^{R132H} cells.

The introduction of ^{13}C carbon in the form of [^{13}C-4]-*L*-aspartic acid enabled the identification of compounds that ultimately inherited their carbon atoms from aspartic acid through metabolism. ^{13}C labelled isotopomers of a molecule are readily identified by mass spectrometry due to the single mass unit shift associated with each ^{12}C carbon atom replaced by a ^{13}C carbon atom originating from the tracer. Depending on the number of ^{13}C carbon atoms a molecule inherits, the nominal m/z value can be between m+1 and m+1+n (where m is the mass of the neutral unlabeled molecule and n is the number of carbon atoms in the molecule). Given the complexity of central metabolism it is common to find differing proportions of almost all possible isotopomer forms of a metabolite in cellular experiments although one or two isotopomers often predominate reflecting the major metabolic pathway fluxes for that particular metabolite. Given the apparent close metabolic relationship between aspartic acid and *D*-2-HG from previous experiments, the aim of the tracer experiment was to see to what extent ^{13}C aspartic acid carbon was found in *D*- and *L*-forms of 2-HG and the labelling pattern relationship between closely linked metabolites to try and better understand the biosynthetic pathways linking the two.

LC/MS analysis of TCA cycle intermediates and associated amino acids, in both the IDH1^{WT} and IDH1^{R132H}, provided evidence that a number of metabolites were represented by specific ^{13}C enriched isotopomers. The identity and isotopomer proportions are reported in Figure 3-17 and 3-18. It can be seen that there is very little difference in the isotopomer labelling patterns between the IDH1^{WT} and IDH1^{R132H} cells (see Figure 3-18), except for *D*-2-HG where two ^{13}C enriched isotopomers were detected in the IDH1^{R132H} (see Figure 3-17) and not in the IDH1^{WT} (2-HG below LoD). It can be seen that the TCA cycle intermediates do not show uniform ^{13}C labelling and indeed the majority of intermediates (citrate, cis-aconitate, isocitrate, 2-

OG, succinate, fumarate, glutamine and the *L*-2HG) show no ^{13}C enrichment (see Table 3-1).

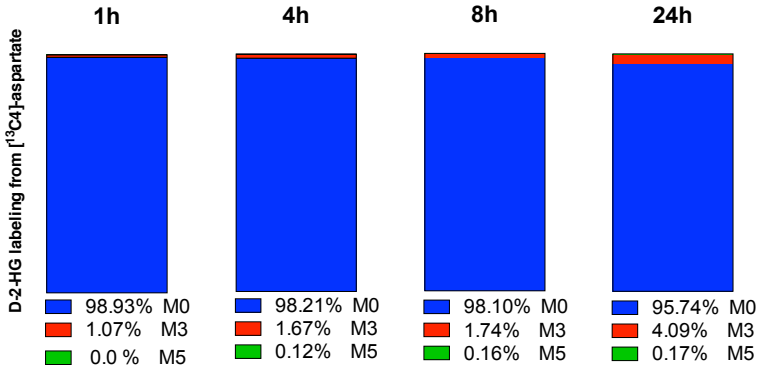

Figure 3-17: *D*-2-Hydroxyglutarate enrichment from [^{13}C4]-*L*-aspartic acid in Isocitrate dehydrogenase-1 R132H IDH1^{R132H} cells cultured for 24 hr. isotopomer labelling patterns for *D*-2-HG where shown two ^{13}C enriched isotopomers were detected in the IDH1^{R132H} and not in the IDH1^{WT} (2-HG below LoD).

Figure 3-18 shows that ^{13}C-labelled malate-M+4 (a) and, aspartate-M+4 (b) increased in cellular concentration between 1 to 8-hours, but then reduced by approximately 50% from 8 to 24 hours (Figure 3-18). NAA was the second most abundant compound in the cell pellet that contained ^{13}C atoms. Four NAA isotopomers were present in the extracted pellet in both IDH1^{R132H} and IDH1^{WT} and MS-signal reached a maximum after a 24-h incubation as shown in Figure 3-18(d).

One of the primary concerns with the tracer experiment was whether the [^{13}C-4]-*L*-aspartic acid would be able to enter the cell from the culture media and subsequently become incorporated into cytoplasmic and mitochondrial metabolism. It can be seen from the experimental results in Figure 3-18(b) that when aspartic acid was measured in the cell extracts [^{13}C-4]-*L*-aspartic acid was found at levels between 4% and 17% demonstrating that a proportion of the tracer had entered the cytoplasm. Given that the [^{13}C-4]-*L*-aspartic acid exposure to the cell was for a relatively short period of time, and the fact that the cells themselves contained free, unlabeled aspartate before

commencement of the tracer experiment, we expected a relatively small amount of labelled aspartate relative to the unlabeled form. However, because 2-HG can be formed via IDH1 in the cytoplasm there is no evidence that the labelled 2-HG carbon has entered the mitochondria although theoretically this is possible via inter-conversion of [^{13}C-4]-*L*-aspartic acid with malate via oxaloacetate.

If the TCA cycle functions as conventionally understood, it expected that labelled *D*-2-HG would receive carbon atoms directly from 2-OG and that they would arrive at 2-OG via inter-conversion from oxaloacetate via citrate, cis-aconitate and isocitrate. The fact that we do not see any ^{13}C carbon incorporate into in citrate, cis-aconitate and isocitrate, in either IDH1^{R132H} or IDH1^{WT} cells, appears surprising. However, given the small amount of [^{13}C-4]-*L*-aspartic acid shown to enter the cells (max was 17%; after 24h) it may be that the amount entering the TCA cycle is too low to provide enriched isotopomers of TCA cycle intermediates within the limits of detection of the LC/MS method. We know from the results that [^{13}C-4]-*L*-aspartic acid interconverts with oxaloacetate to malate but it would appear that the proportion of malate via this route, that then enters the TCA cycle, is low compared to unlabeled malate which is derived from fumarate over the course of the experiments, hence no labelling of the majority of TCA cycle intermediates (see Fig 3-19). The enrichment of 2-HG observed could still come from normal TCA cycle function as it is known that 2-HG accumulates to relatively high levels and can exit mitochondria to the cytoplasm. Whether, the 2-HG carbons originated from aspartic acid carbon atoms via normal TCA cycle function or via an alternative pathway, as indicated initially by the unlabeled spiking experiments, is unfortunately not resolved by these tracer experiments.

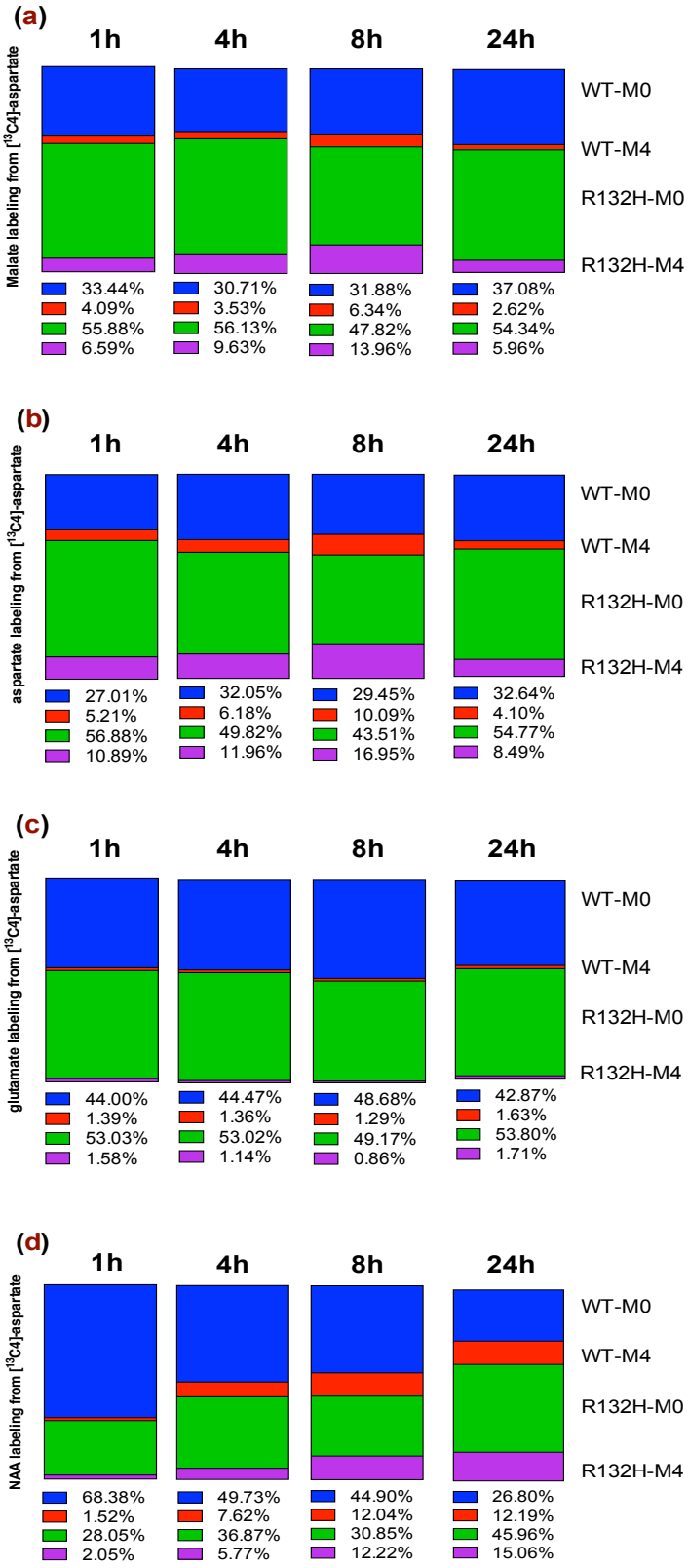

Figure 3-18: The enrichment from [^{13}C4]-*L*-aspartate in Isocitrate dehydrogenase-1 R132H and wildtype (IDH1 R132H and WT) cells cultured for 24 hr. Were show different level of enrichment of C13 from [^{13}C4]-*L*-aspartate.

3.8.3. M+3 and M+5 labelling of *D*-2-HG in mutant cells

If the TCA cycle functioned in these experiments as conventionally expected, fully labelled OAA would be condensed with the unlabelled acetyl group (2x ^{12}C) of acetyl-CoA resulting in citrate comprised of 4x ^{13}C and 2x ^{12}C atoms. This would be followed by dehydration of citrate to cis-aconitate and hydrolysis to isocitrate each with 4x ^{13}C and 2x ^{12}C atoms. In this situation, isocitrate decarboxylation will lead to the loss of a ^{13}C atom to produce 2-OG (3x ^{13}C and 2x ^{12}C). The 2-OG is then converted to *D*-2-HG (3x^{13}C and 2x^{12}C) M+3, see Figure 3-19 and NADH reduced to NAD^+ as showed in figure 3-15(c). The 2-OG (3x-^{13}C and 2x12C) can also be aminated to form glutamate (3x^{13}C and 2x^{12}C).

An alternative pathway could include 4x^{13}C-malate decarboxylating to 3x^{13}C-pyruvate via malate dehydrogenase, followed by conversion (pyruvate dehydrogenase) to give 2x^{13}C-acetyl-CoA by pyruvate decarboxylation, that subsequently combines two (^{13}C) atoms from 4x^{13}C-OAA to form 6x^{13}C-citrate. Following this, cycling round the TCA cycle leads to 5x ^{13}C 2-OG and finally 5x^{13}C 2-HG. These pathways would both account for the M+3 and M+5 isotopomers identified in this study. However, not being clear of the relative contributions of these two pathways, we are not able to compare the isotopomer ratios directly.

Finally, Figure 3-19 shows an atom transition map of the predominant ^{13}C isotope patterns for the TCA cycle using [^{13}C-4]-*L*-aspartic acid labelling of IDH1^{R132H} and IDH1^{WT} cells depicting a model of carbon transfer associated with the conventional TCA cycle.

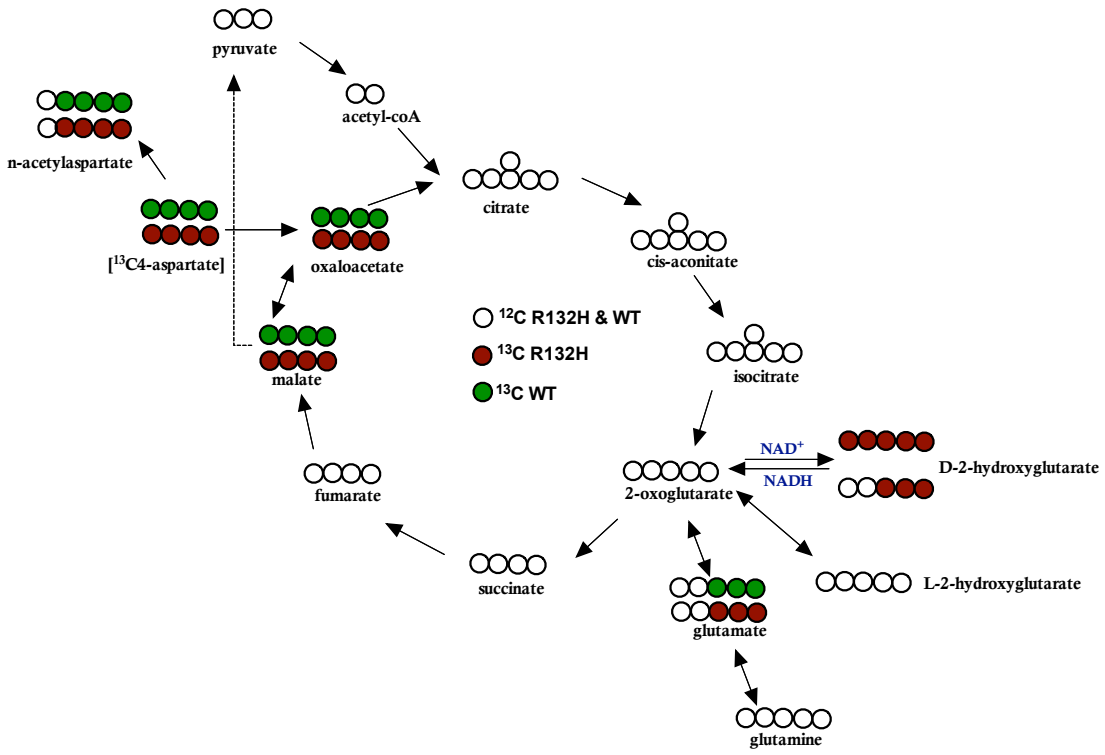

Figure 3-19: Uptake of [^{13}C-4]-*L*-aspartic acid to labelled *D*-2-Hydroxyglutarate in Isocitrate dehydrogenase-1 R132H and wild-type (IDH1^{R132H} and IDH1^{WT}). It can be seen that the TCA cycle intermediates do not show uniform ^{13}C labelling and indeed the majority of intermediates (citrate, cis-aconitate, isocitrate, 2-OG, succinate, fumarate, glutamine and the *L*-2HG) show no ^{13}C enrichment.

Metabolites	IDH1^{R132H}		IDH1^{WT}	
	^{12}C	^{13}C	^{12}C	^{13}C
pyruvate	Yes	No	No	No
n-acetylaspartate	Yes	Yes	Yes	Yes
aspartate	Yes	Yes	Yes	Yes
oxaloacetate	Yes	Yes	Yes	Yes
citrate	Yes	No	No	No
cis-aconitate	Yes	No	No	No
isocitrate	Yes	No	No	No
2-oxoglutarate	Yes	No	No	No
***D*-2-hydroxyglutarate**	Yes	Yes	Yes	Yes
***L*-2-hydroxyglutarate**	Yes	No	No	No
glutamate	Yes	Yes	Yes	Yes
glutamine	Yes	No	No	No
succinate	Yes	No	No	No
fumarate	Yes	No	No	No
malate	Yes	Yes	Yes	Yes

Table 3-1: Table showing the presence of absence of [^{13}C-4]-*L*-aspartic acid derived carbon atoms in Tricarboxylic acid cycle intermediates in the mutant and wild-type cells.

3.9. Discussion

In this chapter, it was show that IDH1-R132H and IDH2-R172K expression in LN18 cells induces a number of changes in the TCA cycle. Cancer cells, expressing R132H IDH1 and R172K IDH2 showed elevated levels of *D*-2-HG compared to wild-type. 2-OG levels were found to be lower in mutant cells compared to wild-type cells. In addition, similar, levels of *L*-2HG were found in both wild-type and cancer cells for IDH1 and IDH2.

shRNA, knockdown of IDH1, IDH2 and IDH3-WT produced few changes that were similar to IDH1-R132H expression. No changes in 2-HG levels were seen. These results indicate that dominant negative inhibition of the functional IDH isoform allele by IDH1-R132H is unlikely to be responsible for the metabolic changes associated with IDH1 mutations, at least in the studies condition.

A commercial inhibitor for IDH1, AGI-5198, given in doses of 500 μM in $IDH1^{R132H}$ cell culture, was able to decrease *D*-2-HG levels by more than 1.5-fold compered to untreated $IDH1^{R132H}$ cell. As may be expected from an engineered cell line that does not exhibit growth dependence on mutant IDH1 or *D*-2-HG, 500 μM of AGI-$IDH1^{R132H}$ had no observable effect on the growth rate of either cell line.

Unlabelled spiking studies showed that addition of Asp led to the greatest increase in *D*-2-HG, showing >3-fold increase in mutant cells, compared to other spiked intermediates. This led to a ^{13}C metabolic flux study using [^{13}C-4]-*L*-aspartic acid in $IDH1^{R132H}$ and $IDH1^{WT}$ LN18 cell. The results showed that carbon from [^{13}C-4]-*L*-aspartic acid carbon are found in D-2-HG as M+3 and M+5 isotopomers. The experiment however did not resolve the exact metabolic pathways involved as it was

unclear whether labelled (M+3 and M+5) *D*-2-HG was produced in the cytosol or inside the mitochondria. Further investigation will be required to resolve this issue.

The combination of methods described here did not resolve the biosynthetic pathways for *D*-2-HG production from aspartic acid but nevertheless provides a robust approach for future experiments which need to ensure a greater proportion of labelled substrate can enter experimental cells.

Chapter 4: ANALYSIS OF 2-HG LEVELS IN GLIOBLASTOMA TISSUES: A COMPARATIVE STUDY USING 3-TESLA MAGNETIC RESONANCE SPECTROSCOPY IN VIVO AND MASS SPECTROMETRY IN VITRO.

This chapter describes work using LC/MS to quantify the levels of 2-HG in brain tissue samples taken from patients during operations to remove tumours. Those samples analysed were subsequently shown to be positive for the 2-HG mutation by histology. Absolute concentrations were compared with a parallel study, conducted in vivo, prior to the tumour being resected, using an experimental in vivo magnetic resonance spectroscopy (MRS) methodology for identification and quantification of 2-HG. Implications for in vivo screening applications to identify and provide relevant clinical measurements in glioma will be discussed.

4.1. Introduction

It has become clear that IDH mutations, which lead to a gain of function in the production of elevated levels of *D*-2HG, occur very early in tumour development (Dang el at. 2009). In Chapter 3 it was reported that increases in 2-HG concentration can be significant in the presence of IDH mutations and that significant levels have been recorded in vivo; for example the 0.1-126 mM range (Pusch el at. 2014). These findings raise the question of whether the elevated levels of 2-HG can act as a reliable biomarker for gliomas and whether Magnetic Resonance Spectroscopy (MRS) could be used to detected and quantify 2-HG non-invasively. If this were successful the ability to detect 2-HG by MRS could provide important diagnostic and prognostic information. Proton MRI measures the chemical shift difference between the proton spectra for water and the proton spectra for the analyte metabolite. 3-T MRS experiments have shown significant advantages for musculoskeletal imaging over proton MRI in, for example, providing high sensitivity and resolution in imaging

ligaments and cartilage as well as meniscal structures of the knee (Craig el at., 2005; Gold el at., 2004; Tanenbaum et al., 2006).

Having successfully developed and tested methodologies for the identification of 2-HG and quantification of its enantiomers in cells, a collaboration with the Department of Neuropathology, John Radcliffe Hospital, Oxford and the Functional MRI of the Brain (FMRIB) led to a pilot study to evaluate 2-HG concentrations in glioma patient tissues and to compare directly 2-HG measurements by mass spectrometry and 3T MRS. The aim was to show whether MRS was capable of making accurate 2-HG identifications and that if a strong correlation could be shown between signal intensity and 2-HG concentration for the two approaches, to lay the foundations for MRS as a potential diagnosis and screening tool. The accuracy of absolute quantification and ability to compare in vivo with in vitro measurements, separated by significant periods of time, provided the need for extensive and careful testing.

The relatively high selectivity of LC–MS does not guarantee the effective elimination of interference from endogenous impurities in the quantification of compounds like 2-HG present in brain tissue extracts. Any quantitative analysis by mass spectrometry, using electrospray ionization (ESI) or atmospheric pressure chemical ionization (APCI), can have a signal response (and hence sensitivity) substantially affected by the occurrence of ion-suppression caused by the presence of compounds in the sample matrix. This phenomenon has been reported on by many authors and it is commonly referred as ‘‘the matrix effect (ME)” (Matuszewsky et al., 2003; Antignac et al., 2005; Taylor et al., 2005 and Niessen et al., 2006). It can be significant and render data collected poor and unreliable for the purposes of quantification; MEs can heavily affect the reproducibility, linearity, and accuracy of the LC/MS method leading to errors in 2-HG quantitation. In order to ensure a sensitive and accurate quantification,

investigation of the process of sample extraction was performed along with evaluation of matrix effects. In addition improvements to the standard method for TCA cycle analysis introduced in Chapter 2 were made to reduce the reliance on ion pairing chromatography, which, although it was very effective at enhancing chromatographic performance, especially for peak shape and resolution, was shown also to supress the analyte ion signals, and hence reduce sensitivity. Here mixed-mode (MM) chromatography was developed, as an alternative, to produce a reliable absolute quantification method for complex tissue analysis.

4.2. LC mixed-mode chromatography method development

For Mixed-Mode (MM) chromatography, MS detection using single reaction monitoring (SRM) was used on a Waters Quattro micro triple quadrupole MS system coupled with a Waters Acquity UPLC system.

Two different polar C18 stationary phase columns were tested; 1) C18-UPLC ACQUITY-HSST3 and 2) C18-ACE C18-PFP. The following mobile phases were optimised. Mobile phase A; H_2O with 0.2% HCO_2H (v/v) and mobile phase B; MeOH with 0.1% HCO_2H (v/v) (see Chapter 8 for further details). A 1 mM solution of 2-HG standard (50:50 MeOH/ H2O) was used for method development with an injection volume of 2-µL and flow rate of 0.2 mL/min.

Figure 4-1 shows chromatograms for the 2-HG peak using the HSST3 (A), and PFP (B) separately and when combined two columns (C). Peak shape and retention time were significantly improved when the columns were combined the two columns and this was used as an approach for further method development.

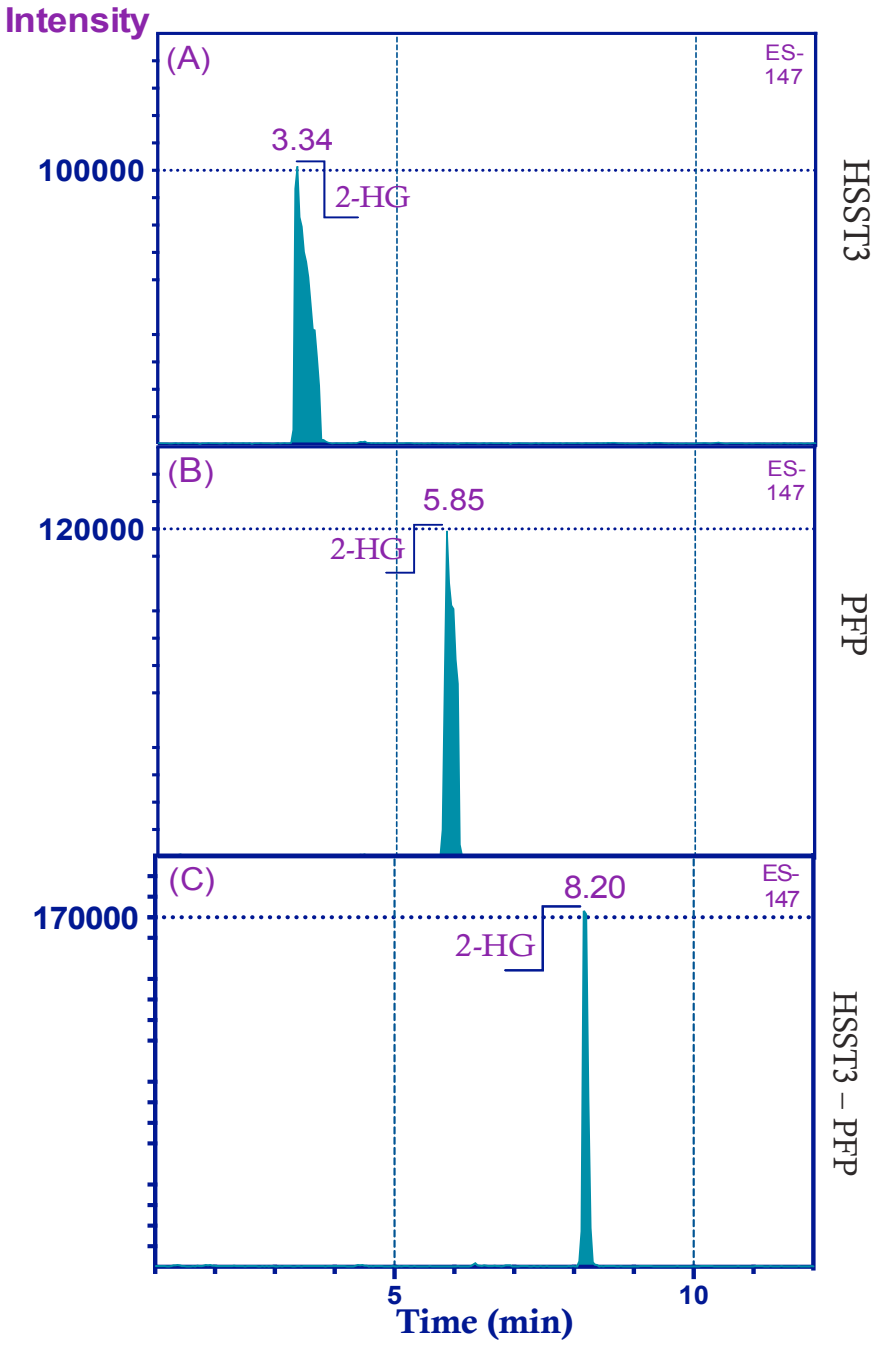

Figure 4-1: Three Liquid chromatography–mass spectrometry (single ion monitoring) chromatograms from the elution test of 2-hydroxyglutarate standard for different stationary phase columns. (A) HSST3, (B) PFP and (C) coupled HSST3 to PFP. Peak shape and retention time were significantly improved when the columns were combined the two columns and this was used as an approach for further method development.

Before analysis, calibration samples were prepared by dilution with water: MeOH (50:50). Calibration samples were prepared at concentrations of 2.5, 5, 25, 50, 250, 500, and 1000 µM. Chromatographic data were collected with Waters MassLynx v4.1

software and analysed using Microsoft Excel. Quantification was achieved for each analyte using linear regression analysis of the peak area (manual integration from the beginning to the end of the peak) of 2-HG standard for versus concentration.

4.3. Metabolite extraction

Metabolite extraction is an important and challenging component of metabolomics and no single method can currently accomplish the extraction of all metabolites from cells, plasmas and tissues. The potentially large dynamic range in terms of compound type and concentrations, contributes to this challenge, as does the relative amenability of various extraction solvents to the electrospray ionization process. In various complex matrices such as brain tissue and cell cultures, the majority of metabolites present are at low concentrations and so an extraction procedure, which ensures minimal sample loss will increase specificity and sensitivity. Common approaches are to use organic solvents for liquid/liquid extraction, acidic solutions such as perchloric acid (PCA) and/or solid phase extraction (SPE) for sample fractionation into simpler components. In this study, a protocol was required which was efficient for the extraction of 2-HG and other metabolites of central metabolism and removed them into an electrospray ionization compatible organic or organic/aqueous solvent.

A number of published protocols indicate that perchloric acid extraction is an appropriate protocol for tissue metabolite extraction but this was not clearly demonstrated using mass spectrometry detection (Kloos el at., 2012). The methanol based solvent extraction method that had been, used previously for cell samples (See Chapter 8), had not been tested on tissue samples. It was therefore decided to compare the performance of both protocols for the extraction of 2-HG from brain tumour tissue. Further details of the two protocols can be found in Chapter 8.

The frozen brain tissue (n = 4) was divided into two halves for extraction by either PCA or MeOH. To assess the efficiency of the extractions, and hence the recovery of 2-HG from the quenched tissue, the tissue extracts were analysed using the mixed-mode LC/MS method described above. Significant differences in 2-HG levels between the extractions from each condition were observed, as shown in Table 4-1. Since the metabolite yields were greater using the MeOH extraction method, this was used subsequently for extraction of metabolites from the human tumour tissues samples.

In order to assess the efficiency of the first extraction, the remaining pellets from the first MeOH and PCA extracts (n=4) were then re-extracted using the MeOH method. This re-extraction was analysed separately from the first extraction to determine the metabolite yield remaining in the pellets. All metabolites of interest were below the limit of detection in the second extract (LoD = 1 µM).

Sample No.	Extraction methods	Mean conc. of 2-HG [µmol/g]	2-HG conc.* PCA extract [µmol/g]	STD	%CV
741	MeOH	1.47	-	0.018	1.25
	PCA	1.07	1.60	0.025	1.24
827	MeOH	0.70	-	0.01	1.11
	PCA	0.50	0.75	0.01	0.79
741	MeOH Re-extracted	Under the LoD	-	-	-
827			-	-	-

*After applying the matrix effect factor (1.5)

Table 4-1: Results of extraction comparison methods from quantitative Liquid chromatography–mass spectrometrya analysis of human glioma tissue samples.

4.4. Matrix effects (MEs)

It has been shown that it is common for the co-eluted matrix to influence signal intensity via competition for available charges and for the access to the droplet surface in electrospray ionisation (Cech and Enke 2000; King et al., 2000). As a consequence, when absolute quantification is being performed, it must be determined

whether MEs play a significant role and measure the extent of their influence on analyte peak areas. Sample clean-up procedures and efficient chromatographic separations can reduce MEs and hence it's very important to quantify the effect on signals of interest when a new method and extraction protocol is being used for the first time.

A standard addition method was used to determine the magnitude of the ME from the tissue samples of interest and calculate a factor to apply to tissue sample analysis to compensate for the matrix effect.

Using sample (1367; 50μL) extracted from glioma tissue the matrix effect was determined using the SA method as follows. 10 μL of sample 1367 was divided between five LC/MS vials, to make a series of five sub-samples with the same volume of unknown concentration of 2-HG in matrix. To these samples a defined amount of (2-HG; 1mM) standard (0,4,6,8 and 10 μL) was added in a variable volume of Milli-Q water (10,8,6,4 and 0 μL) was added to make final volume of 20 μl and final concentrations as indicated in Table 4-2. These standard samples are then analysed and peak areas plotted.

After linear regression and extrapolation, the intercept of the graph with the x-axis was determined (see Figure 4-2). This was used for calculation of the 2-HG concentration and the matrix effect. 2-HG concentration = (x-intercept × total volume)/volume of sample 1367; Table 4-3) (Chingin el at., 2009). Comparison of the 2-HG concentration in the sample, determined using the calibration curve and the standard addition method, allows calculation of the matrix effect factor, which was 1.5 in this case. Multiplication of the 2-HG concentrations in all samples (determined with the calibration curve) with this factor allowed for correction of the matrix

suppression effect in order to obtain a more accurate estimate of the concentration of 2-HG for comparison with MRS measurements.

Vol. of 1367 [µl]	Vol. of added 2-HG [µL]	Vol. of added H_2O [µL]	Final conc. Of added 2-HG [µM]	2-HG Peak Area	Mean of 2-HG Peak Area
10	0	10	0	3202	3239
			0	3240	
			0	3277	
10	4	6	200	3934	3968
			200	4002	
			200	3968	
10	6	4	300	4318	4335
			300	4330	
			300	4357	
10	8	2	400	4739	4748
			400	4748	
			400	4757	
10	10	0	500	5205	5207
			500	5209	
			500	5209	

Table 4-2: Standard addition method using 2-Hydroxyglutarate for determination of the matrix effect in human glioma tissue samples extracted with perchloric acid.

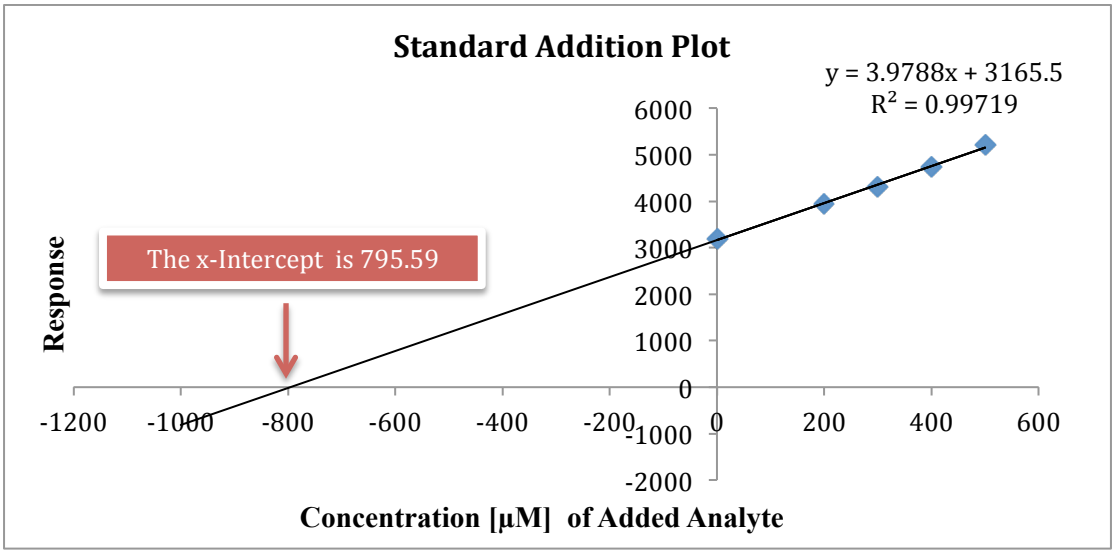

Figure 4-2: Determination of the X-Intercept in human glioma tissue samples extracted with perchloric acid using the standard addition method. Were shown that X-Intercept=795.59

Sample	X- intercept	Vol. of 1367 [µl]	Total Vol. [µl]	2-HG conc. [µM] SA*	2-HG conc. [µM] CC**
1367	795.59	10	20	1591.18	1060.61

* Calibration curve
** Standard addition method

Table 4-3: Results from application of the standard addition method.

4.5. Analysis of 2-HG from tumour tissue samples

Having developed and tested an extraction protocol and determined the matrix effect associated with analysis metabolites extracted from gliomas tissue, using the new MM-LC/MS method for quantification of 2-HG, the protocol was used for the analysis of glioblastomas tissue taken during brain surgery from 13 patients at the John Radcliffe Hospital in Oxford who had already undergone MRS. Recording of tumor size and histological analysis of the tissues prior to MS analysis had been completed to confirm the presence of IDH mutations. (Sarah Larkin and Olaf Ansorge form Department of Neuropathology managed the sampling, cryo-storage and delivery of samples). Details of these sample analyses can be found in Table 4-5.

Calibration curves used for this process were linear up to at least 1000 µM with R2 of 0.998 and detection limits for 2-HG acid of 2 µM signal-to-noise ratio (S/N) of around 3:1. Inter-day (n=3) and intra-day coefficient of variation were better than 11.2 %. The standard deviations (STD) were between (0.15-4.39) and the percentage coefficients of variation (% CV) were lower than 8% for 2-HG.

To investigate the accuracy and precision of the method, spiking experiments were carried out using one of the glioma tissue samples (357). Precision and recovery were determined at low, medium and high concentrations representing physiological and abnormal levels. Intra-day (n = 3) and inter-day (n = 3) coefficients of variation of the 2-HG peak area analysis were assessed at 100, 250 and 500 µM 2-HG. As shown in Table 4-4, the precision is expressed as coefficient of variation (%CV) ranges from

0.29% to level of 2.25%. The accuracy of the method was calculated from these samples and was in the range of 99.98-103.81%. The assay was then applied to control non-glioma (n = 1) and glioma tissue samples (n = 12).

2HG added [µM]	Recovery				Accuracy in %
	Mean* concentration of 2HG [µM]	Mean** concentration of 2HG [µM]	SD	%CV	
100	222.01	103.77	4.99	2.25	103.77
250	481.54	259.53	8.94	1.86	103.81
500	981.45	499.91	2.86	0.29	99.98

Mean 2-HG concentration *before and **after subtracting endogenous 2-HG (118.24 µM) and previously spiked material
[1] %CV = (SD/Mean) × 100
[2]Accuracy (%) = (found concentration /added concentration)×100

Table 4-4: Summary of the recovery and accuracy of 2-hydroxyglutarate determinations in human glioma tissue samples. As shown in Table, the precision is expressed as coefficient of variation (%CV) ranges from 0.29% to level of 2.25%. The accuracy of the method was calculated from these samples and was in the range of 99.98-103.81%. The assay was then applied to control non-glioma (n = 1) and glioma tissue samples (n = 12).

The MM-LC/MS assay was successfully applied to control (n=1) and gliomas tissue samples (n=12); results of the 2-HG quantification are presented in Table 4-5. The results were compared with the MRS analysis of the same samples (See Figure 4-3).

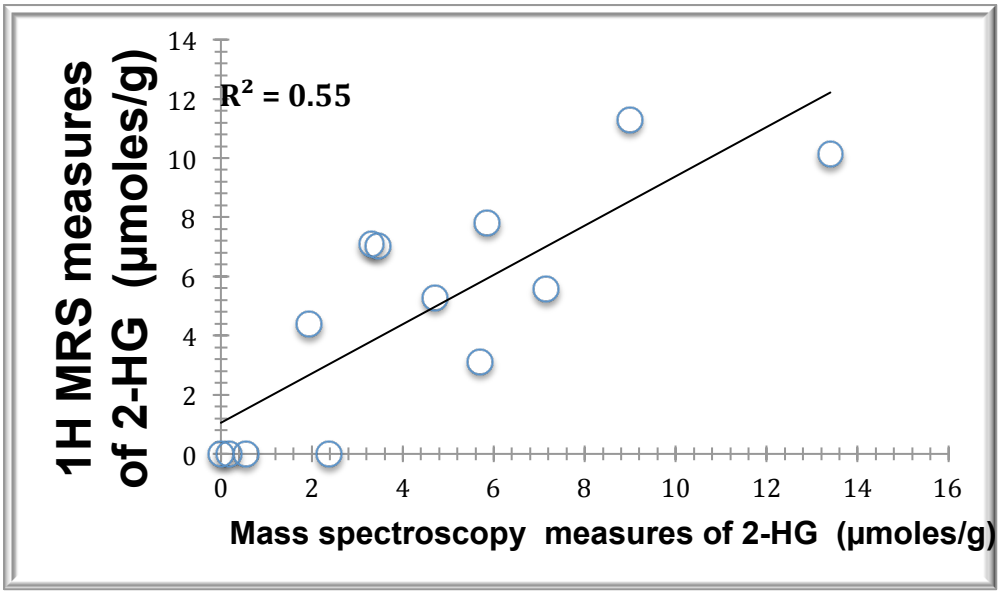

Figure 4-3: Linear regression of 1H magnetic resonance spectroscopy estimates of 2-Hydroxyglutarate concentration vs. mass spectrometry measures of 2- Hydroxyglutarate. The coefficient of determination (R2) was 0.55. The magnetic resonance spectroscopy and mass spectrometry data obtained at different time points.

Case	SH	Diagnosis	2HG (µmoles/g) UPLC-MS	2HG (µmoles/g) MRS	IHC	Sequencing
1	1320/10	pGBM 4	0.11	0.00	W/T	W/T
2	1367/10	sGBM 4	6.00	11.29	R132H	R132H
3	750/10	O 2	3.91	7.81	R132H	R132H
4	948/10	AO 3	2.30	7.02	R132H	R132H
5	784/10	AA 3	5.08	5.28	R132H	R132H
6	357/11	AA 3	3.14	10.12	W/T	R132C
7	262/09	AO 3	1.30	4.39	R132H	R132H
8	291/10	IZ O2	1.59	0.00	R132H	R132H
9	358/11	A 2	2.21	7.10	R132H	R132H
10	439/04	IZ O2	3.80	3.11	R132H	R132H
11	584/05	AO 3	4.77	5.57	R132H	R132H
12	827/10	sGBM 4	0.37	0.00	R132H	R132H
Normal brain	173/11	Front Cx	0.00	0.00	Not done	W/T

Table 4-5: Estimations of 2-Hydroxyglutarate concentration by mass spectrometry and magnetic resonance spectroscopy and IDH mutation status determined by IHC and sequencing for all cases.

The matrix effect factor of 1.5 was used to normalise the quantification results of 2-HG in matrix see Table 4-6. The results were then compared with MRS analysis of the same samples which shown coefficient of determination (R2 = 0.67).

Sample	Mean of final conc. Of 2-HG [µmol/g]	Mean of final conc. Of 2-HG [µmol/g] *	STD*	%CV*
1	0.11	0.17	0.00	-
2	6.00	9.00	0.49	7.65
3	3.91	5.86	0.57	3.15
4	2.30	3.45	3.20	5.92
5	5.08	4.71	0.81	5.51
6	3.14	13.40	0.54	4.02
7	1.30	1.95	1.27	6.35
8	1.59	2.38	0.37	4.51
9	2.21	3.31	3.02	1.39
10	3.80	5.70	0.29	7.63
11	4.77	7.15	4.39	8.57
12	0.37	0.55	0.15	8.33
Normal brain	0.00	0.00	1.43	5.76

*After applying the matrix effect factor (1.5)

Table 4-6: Results from quantitative mass spectrometry analysis of human glioma tissue samples extracted with perchloric acid. The matrix effect factor of 1.5 was used to normalise the quantification results of 2- Hydroxyglutarate in matrix.

4.6. Comparison of MS with MRS data and Conclusions

If we consider a comparison of the data for quantification of 2-HG by MRS and MS analysis, the results show a positive correlation. Where MRS records higher concentrations for 2-HG this is reflected in the LC/MS results. The methods use confirm that the MRS analysis is able to both identify the presence of 2-HG and provide information about the amount present which correlates with an independent methodology (LC/MS). These results therefore pave the way for future MRS studies to investigate its clinical potential as a tool to both diagnose gliomas using 2-HG as a biomarker and to potentially provide clinically relevant information about its concentration.

LC/MS quantification methods developed as part of this thesis work enabled the testing of MRS to identify IDH mutant gliomas through detection of 2-HG spectra. MRS is now being evaluated in the clinic both as an initial diagnostic tool and as a non-invasive method to follow tumour progression during ongoing management of diffuse gliomas John Radcliffe Hospital in Oxford.

Finally, The concentration of 2-HG was determined by the MMC method and found to be 4-60-fold higher in tumours with a mutation in IDH (0.4-6.0 μmoles per gram tumour) compared to wild-type (0-0.1μmoles per gram tumour.

Chapter 5: INHIBITION OF 2-OXOGLUTARATE DEPENDENT OXYGENASES: DISCOVERY OF N-OXALYLGLYCINE IN PLANTS

5.1. Introduction and Aims

2-Oxoglutarate (2-OG) and ferrous iron dependent oxygenases catalyse the two-electron oxidation of a diverse set of substrates in many aerobic life forms (Loenarz et al., 2011). In humans, they play roles in collagen biosynthesis, fatty acid metabolism, hypoxia sensing, nucleic acid repair, and in the regulation of protein biosynthesis at transcriptional, splicing, and translational levels (McDonough et al., 2010; Higashide et al., 1985). The inhibition of selected human 2-OG oxygenases is of interest from the perspective of treating diseases including anaemia and cancer (McDonough et al., 2005; Rose et al., 2011). There are thus considerable ongoing efforts to develop selective inhibitors of human 2-OG oxygenases (Rose et al., 2011; Rabinowitz, 2009). Recently, these efforts have involved rational drug design, in some cases guided by crystal structures (McDonough et al., 2005; Rose et al., 2011; Rabinowitz, 2009; Kruidenier et al., 2012; Aik et al., 2013). However, pioneering studies of 2-OG oxygenase inhibition, principally on the inhibitors of collagen proly-4-hydroxylase(s), led to the identification of natural product inhibitors of 2-OG oxygenases, including compounds such as alahopcin and dealanylalahopcin, and their analogues (Hutton et al., 1966; Hutton et al., 1967; Higashide et al., 1985; Clement et al., 2002; Schlemminger et al., 2003).

The inhibition of 2-OG oxygenases by elevated levels of TCA cycle intermediates and the metabolically related compound 2-hydroxyglutarate is of current medicinal interest, because the concentrations of such compounds are substantially elevated in some tumour cells (Dang et al., 2009). Several TCA cycle intermediates, including 2-hydroxyglutarate, as well as succinate (which is a product of 2-OG oxygenase catalysis, see Figure 5-1) and fumarate are proposed to act as 2-OG oxygenase inhibitors in cells by competition with 2-OG (for some 2-OG oxygenases, 2-OG itself can be inhibitory at sufficiently high levels) and reveal the

potential for biologically relevant inhibition of 2-OG oxygenase by low molecular weight di-acids (Yang et al., 2012; Chowdhury et al., 2011).

N-Oxalylglycine (NOG) is a synthetic broad-spectrum 2-OG oxygenase inhibitor, which is frequently used, in cellular studies of 2-OG oxygenases in its dimethyester form (DMOG) (Hopkinson et al., 2013). NOG was originally developed as an inhibitor of collagen prolyl-4-hydroxylases but it is a competitive inhibitor of many 2-OG oxygenases (Cunliffe et al., 1992). NOG binds to the active site in a similar, but not identical manner to 2-OG; however, it does not act in the catalytic cycle (McDonough et al., 2010; Rabinowitz, 2009; Cunliffe et al., 1992).

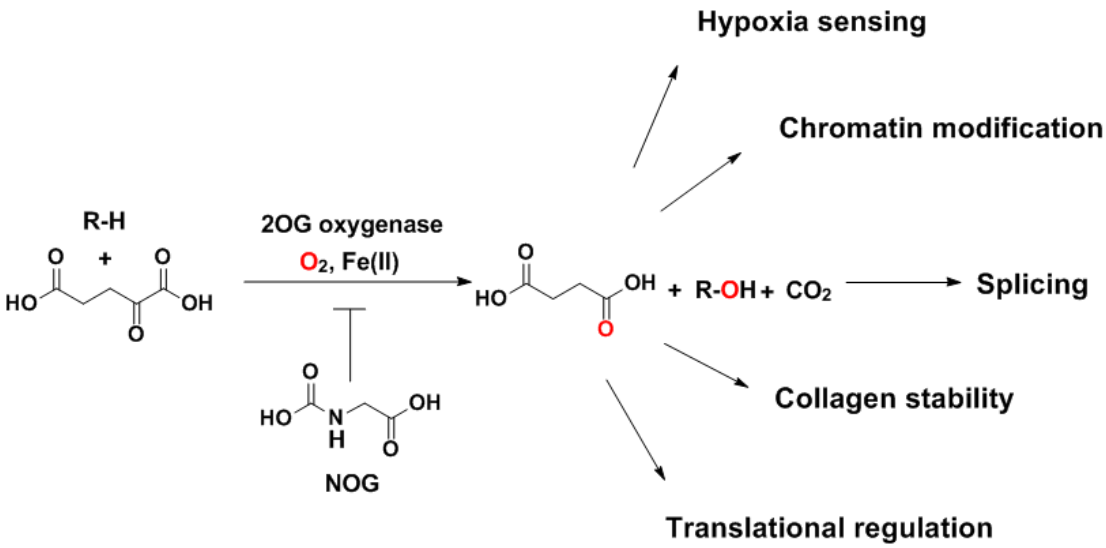

Figure 5-1: **2-oxoglutarate oxygenases catalyse the post-oligomerization hydroxylation, a range of biological processes including, demethylation via hydroxylation of proteins, nucleic acids and fatty acids involved in regulation of hypoxic response, gene expression and translation. The 2-oxoglutarate analogue *N*-Oxalylglycine (NOG) is a simple natural product inhibitor of 2-oxoglutarate oxygenases.**

NOG is chemically synthesised by coupling of activated oxalic acid and glycine, both of which are present in many organisms; it was therefore proposed that NOG might be a natural product present in organisms containing a sufficiently high amount of oxalic acid and it was proposed to investigate this to see whether NOG and related compounds could be found in the commonly available vegetables Spinach (*R. rhabarbarum*), Rhubarb (Rheum rhabarbarum),

Brocoli (*Brassica oleracea*), watercress (*Nasturtium officinale*) and in addition to see whether it occurred naturally in bacterial and mammalian cells (Kasidas and Rose, 1980). We focused on NOG and the closely related compound N-oxalyl-L-glycine (DMOG), dimethyl N-oxalyl-L-phenylalanine (DMNOF) and N-oxalyl-L-alanine (NAA), Figure 5-2), could be found as natural products.

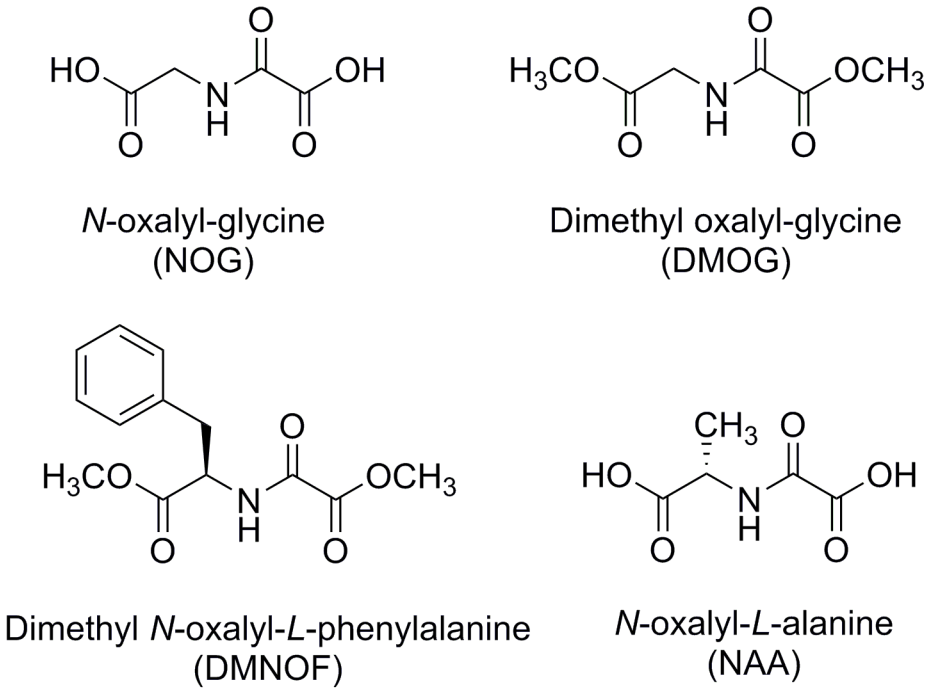

Figure 5-2: **Structures of *N*-oxalyl amino acid derivatives investigated in plant and animal cell extracts. *N*-oxalyl amino acid derivatives: *N*-Oxalylglycine (NOG), N-oxalyl-L-glycine (DMOG), dimethyl N-oxalyl-L-phenylalanine (DMNOF) and N-oxalyl-L-alanine (NAA).**

5.2. Development of a method for the identification and quantification of NOG and other amino acid derivatives

To investigate whether NOG and related derivatives naturally occur in *R. rhabarbarum* leaves, the RP-LC/MS method (development described in chapter 2) was adapted for the analysis of an NOG standard. The detection of NOG (m/z 146, retention time: 10.35 mins) provided a linear response with concentration in the range 10–1000 µM with a correlation coefficient R^2 >0.9980 (see the Appendix A2). The calibration curve constructed was subsequently used for the quantification of NOG, *N*- NAA and the dimethyl ester of DMOG.

The detection limits (LoD) for NOG, NAA and DMOG were 5μM, 6μM and 8μM, respectively, at a signal-to-noise ratio (S/N) of 3:1. The limit of quantification was defined at a (S/N) of 10:1 and were 13μM for NOG, 14μM for NAA and 16μM for DMOG.

5.2.1. LC/MS Analysis Of NOG In R. Rhabarbarum Leaves

Different solvent extraction procedures were applied as shown in Table 5-2 to *R. rhabarbarum* leaves. The extracts were then analysed using the LC/MS method above and retention times and m/z values were compared with standards of the target compounds using appropriate blanks controls either side of samples run. A peak at 10.23 min was observed in the aqueous extracts only, which corresponded to the retention time for the NOG standard at 10.35 mins. When the sample was spiked with NOG standard (50 μM), the magnitude of the peak at 10.23 mins increased, indicating that a species with an equivalent retention time and m/z value to NOG was present in the *R. rhabarbarum* sample (See Figure 5-3).

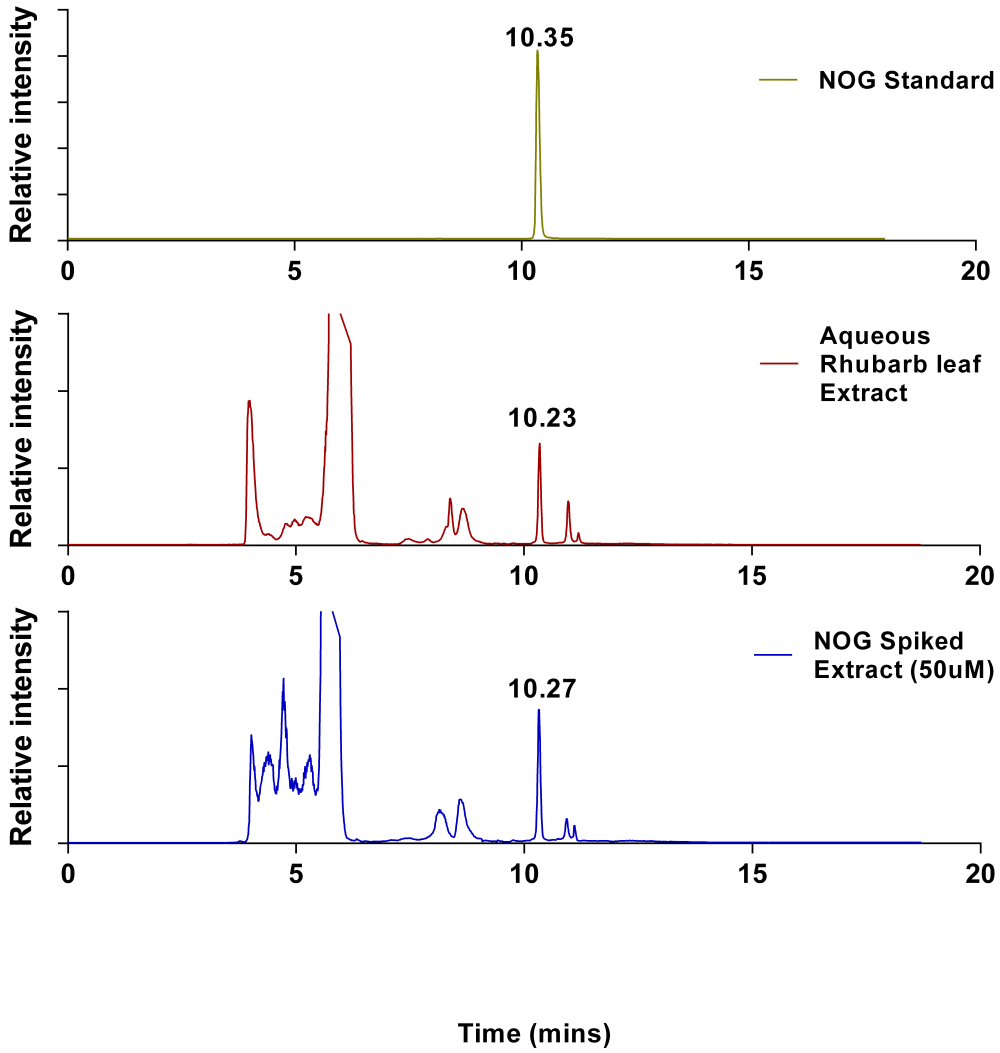

Figure 5-3: Three Liquid chromatography–mass spectrometry (single ion monitoring) chromatograms from the analysis of Rhubarb leaf extracts. In conjunction with m/z accurate mass data (see Figure 5-4c) these chromatograms demonstrate a peak with the same m/z value as *N*-Oxalylglycine is present in the Rhubarb leaf extract at the same retention time (~10.23mins) as the *N*-Oxalylglycine standard. Note the small difference in retention time for the *N*-Oxalylglycine standard compared to the peaks in the leaf extract samples. This is often seen when two very different sample matrices are run, at different times, containing the same compound.

5.2.2. LC-MS/MS Analysis For Identification And Quantification NOG

In order to validate the presence of NOG in the *R. rhabarbarum* extract, further analyses were conducted. Comparative tandem mass spectrometry analysis was performed on the ions corresponding to NOG in the standard and the *R. rhabarbarum* extract separately. The product ion spectrum for underivatized NOG obtained by MS/MS analysis in the negative ion mode showed an M-H ion at m/z 146 and three other significant fragments at m/z 102

corresponding to $[M\text{-}H\text{-}CO_2]^-$, m/z 73 corresponding to $[M\text{-}HN\text{-}CH_2\text{-}CO_2H]^-$ and m/z 59 corresponding to $[M\text{-}HN\text{-}CO\text{-}CO_2H]^-$. The transition from m/z 146-73 was the major fragment used for Multiple Reaction Monitoring (MRM) analysis of the *R. rhabarbarum* extract (Figure 5-4B).

The extracts were then analysed using LC/MS/MS and retention times and m/z values were compared with standards of the target compounds. A peak at 10.33 min was observed in the aqueous extracts, which corresponded to the retention time for the NOG standard at 10.35 mins. When the sample was spiked with authentic NOG standard (50 μM), the magnitude of the peak at 10.27 mins increased, indicating that a species with an equivalent retention time and MRM m/z value to NOG was present in the *R. rhabarbarum* sample (See Figure 5-4A).

Accurate mass analysis on the ions putatively representing NOG from the aqueous extract of *R. rhabarbarum* leaves by high resolution ESI-MS provided an m/z value of 146.0096 (Figure 5-4C), within 0.85 ppm of the theoretical m/z value for the chemical composition of NOG ($C_4H_4O_5N$, calculated as m/z 146.0095).

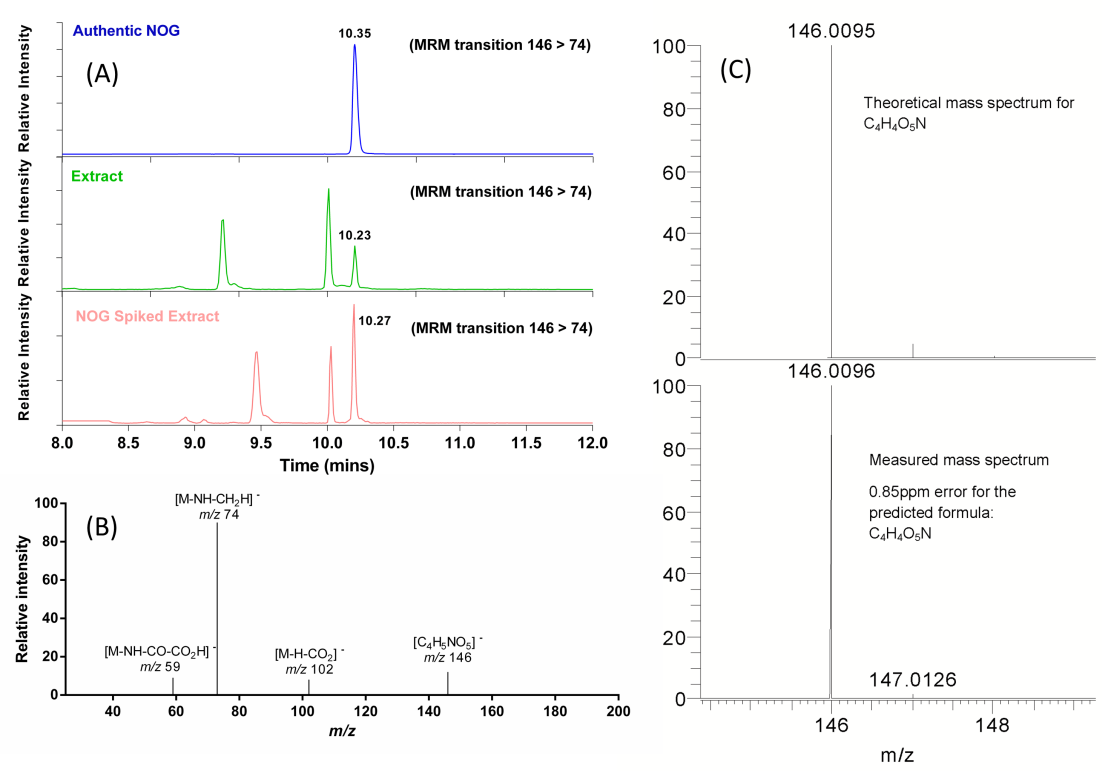

Figure 5-4: LC/MS and LC/MS/MS analysis *R. rhabarbarum* (Rhubarb) leaf extracts to detect *N*-Oxalylglycine. (A) **Three LC/MS/MS chromatograms from 'multiple reaction monitoring' (MRM) analysis showing of: Authentic NOG standard; aqueous Rhubarb leaf extract and the aqueous extract spiked with authentic *N*-Oxalylglycine standard. These demonstrate that a peak at Rt. 10.23 from the plant extract has the same retention time (within experimental error) as the peak from authentic *N*-Oxalylglycine and both provide a transition from m/z 146 to m/z 74 under the same MS/MS conditions at this retention time.** (B) **A CID spectrum from the analysis of *N*-Oxalylglycine standard (m/z 146), demonstrates a transition from 146-73. This was used in in the MRM analysis of *R. rhabarbarum* leaf extract.** (C) **Accurate mass spectra from the analysis of LC-MS purified *R. rhabarbarum* leaf extract by high resolution ESI-MS matches the theoretical mass spectrum (above) within 0.85ppm.**

5.2.3. Isolation And Purification Of NOG From R. Rhabarbarum Leaves For NMR Analysis

The experiments were repeated using a similar extraction method to provide water and acid extracts. Evaporating the solvent on a rotary evaporator collected the crude extract. Characterization of NOG from biological extracts was initially conducted using LC-MS. Eluent from the peak at 10.27 mins was then collected from 45 injections. In order to confirm the presence of NOG in the rhubarb extract, purification of the NOG fraction was performed using 40% CH_3CN in water with isocratic elution using an Atlantis dc18 OBD Prep

Column;100 Å, 5 μm, 19 mm×100 mm (Waters UK Ltd, Elstree, UK). NOG was collected preparatively on this system from a peak eluting at 16.45mins.

The collected LC/MS fraction (rt 16.45 min) of the aqueous extract of *R. rhabarbarum* leaves was then used for ^{1}H NMR (700 MHz) analysis. The ^{1}H NMR spectrum of the collected extract revealed a singlet at δ 3.74 ppm (s), consistent with that of a standard of NOG (Figure 5-5Aa). Spiking the sample with the NOG standard (50 μM) led to an increase in the intensity of the peak at δ 3.74 ppm (Figure 5-5Ab); the ^{1}H NMR spectrum of the NOG standard likewise showed a singlet at δ 3.74 ppm (Figure 5-5Ac). In agreement with the spectrum of the NOG standard, the HSQC spectrum of the LC-MS purified *R. rhabarbarum* leaf extract showed a carbon resonance at δ 43.9 ppm and a proton resonance at δ 3.74, corresponding to the methylene of NOG (Figure 5-5B).

Collectively, the LC-MS, mass fragmentation, NMR, and ESI accurate mass analyses provide compelling evidence for the presence of NOG in *R. rhabarbarum* leaves. The concentration of NOG in *R. rhabarbarum* leaves was determined by LC/MS quantification with the calibration curve constructed using the NOG standard. The amount of NOG at natural abundance in the rhubarb leaf sample was calculated to be 0.197 mg per 3 g dry weight of *R. rhabarbarum* leaves.

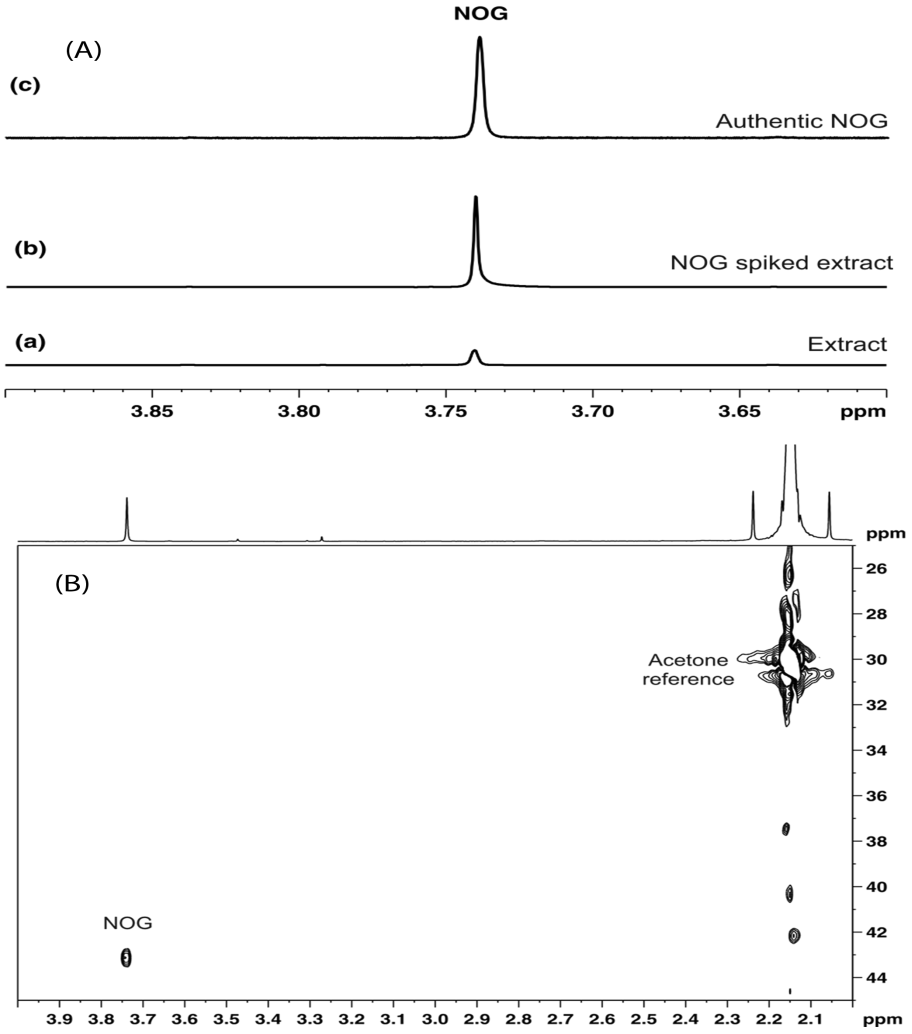

Figure 5-5: (A) **Three ^{1}H NMR spectra: a) ^{1}H NMR spectrum of LC-MS-purified *R. rhabarbarum* leaf extracts. b) ^{1}H NMR spectrum from the *R. rhabarbarum* leaf extract spiked with NOG standard (50 µM). c) ^{1}H NMR spectrum of *N*-Oxalylglycine standard. The ^{1}H NMR spectrum of the plant extract revealed a singlet at δ 3.74 ppm consistent with *N*-Oxalylglycine standard. Spiking the sample with the *N*-Oxalylglycine standard increased the intensity of the peak at δ 3.74 ppm.** (B) **The ^{1}H-^{13}C HSQC NMR spectrum of the LC-MS purified extract. A signal at 3.74/43.9 ppm corresponds to the NOG methylene. The high-intensity crosspeak at 2.15/30, ppm corresponds to acetone.**

5.2.4. LC/MS Identification And Quantification Of N-Oxalyl-L-Alanine In Rhubarb Leaves.

Having demonstrated the presence and quantification of the amount of NOG in *R. rhabarbarum* leaf extracts, the identification of other amino acid derivatives was investigated. The presence of NAA was demonstrated using an *N*-oxalyl-*L*-alanine standard using the same sample preparation and analytical procedures as for NOG. A LC/MS chromatographic peak at 10.29 mins Figure 5-6(b) was observed in the aqueous extract of *R. rhabarbarum* leaves contained a compound with m/z 160; the NAA standard demonstrated an LC/MS peak at *m/z* 160 at a retention time of 10.44 mins Figure 5-6(a). When extract were spiked with a standard solution of NAA (50 μM), the intensity of the peak at elution times 10.34 increased see Figure 5-6(c), providing evidence for NAA in the extracts; for aqueous chromatographic see Figure 5-6. A peak at the retention time for NAA was not present in blanks run either side of the sample.

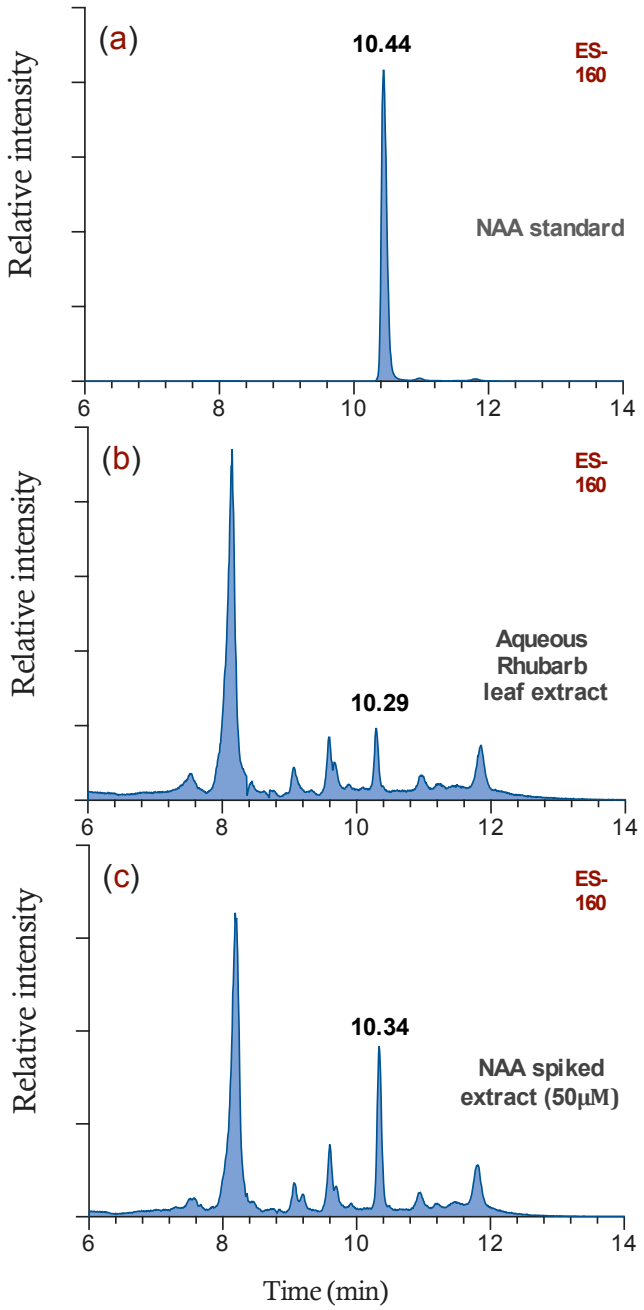

Figure 5-6: Three LC/MS (single ion monitoring) chromatograms from the analysis of Rhubarb leaf aqueous extracts. These chromatograms demonstrate a peak with the same m/z value as an *N*-oxalyl-*L*-alanine is present in the Rhubarb leaf aqueous extract at the same retention time (~10.29mins) as the NAA standard at 10.44 min.

5.2.5. LC/MS Identification And Quantification Of Dimethyl N-Oxalylglycine In Rhibarb Leaves

A similar methodology, but with extraction using acidic methanol, also identified the presence of the DMOG; however, the most likely source for this was acid catalyzed esterification of NOG in the sample as DMOG was not found in the aqueous or MeOH extractions. The most abundant peak in the mass spectrum was the mono-methylated form after loss of CH_3 [$C_5H_7O_5N$, m/z 160]. This was differentiated from NAA (a structural isomer) by retention time on the LC chromatogram and MS fragmentation of the peak at m/z 160>88. Tandem mass spectrometry at this m/z value provided a base peak daughter ion at *m/z* 88 (data shown in figure 5-7) differentiating it from NAA that gave an alternate daughter ion at m/z 84.

A LC-MS/MS chromatographic peak at 10.43 mins Figure 5-7(b) was observed in the acidic extract of *R. rhabarbarum* leaves contained a compound with m/z 160>88; the DMOG standard demonstrated an LC-MS/MS peak at *m/z* 160>88 at a retention time of 10.66 mins Figure 5-7(a). When extract were spiked with a standard solution of DMOG (50 μM), the intensity of the peak at elution times 10.53 increased see Figure 5-7(c), providing evidence for DMOG in the acidic extracts; for chromatographic see Figure 5-7.

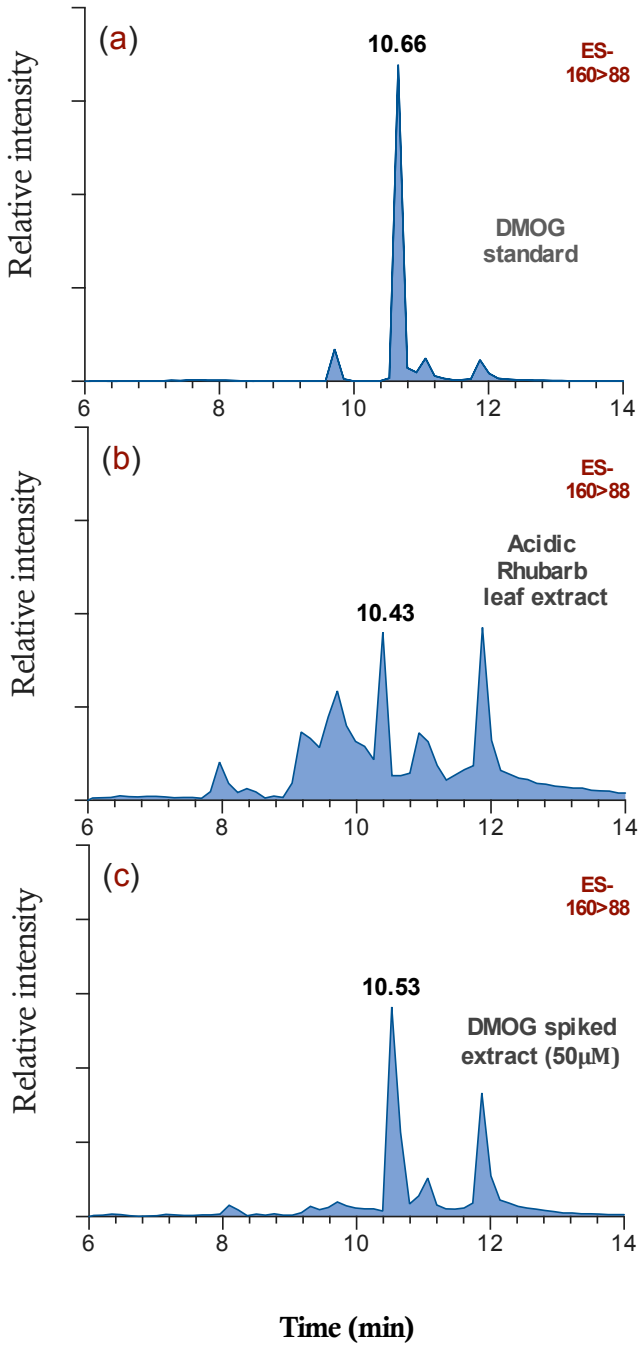

Figure 5-7: Three LC/MS (single ion monitoring) chromatograms from the analysis of Rhubarb leaf Acidic extracts. These chromatograms demonstrate a peak with the same m/z value as N-oxalyl-L-glycine is present in the Rhubarb leaf acidic extract at the same retention time (~10.43mins) as the N-oxalyl-L-glycine standard at 10.66 min. (b) was observed in the acidic extract of *R. rhabarbarum* leaves contained a compound with m/z 160>88; the DMOG standard demonstrated an LC-MS/MS peak at *m/z* 160>88 at a retention time of 10.66 mins Figure (a). When extract were spiked with a standard solution of DMOG (50 µM), the intensity of the peak at elution times 10.53 increased see Figure (c), providing evidence for DMOG in the acidic extracts;

Table 5-1 shows the concentration, amount and peak areas for the LC/MS analysis of NOG, NAA and DMOG. The presence of dimethyl-*N*-oxalyl-*L*-phenylalanine (DMNOF) was investigated but it was not identified in the samples analysed.

	Peak Area		**Conc. (µM)**		**Amount (µg)***	
Analyte:	Water	Acid	Water	Acid	Water	Acid
NOG	16882	2782	65.43	10.78	196	32
NAA	7298	1002	21.15	2.9	63	8
DMOG	-	388	-	8.26	-	24
DMNOF	NF	NF	NF	NF	NF	NF

* In 3 grams of dry leaf. NF: Not found

Table 5-1: Concentrations (in µM) of *N*-oxalyl amino acid derivatives found in *R. rhabarbarum* (Rhubarb) leaf extracts. *N*-Oxalylglycine (NOG), N-oxalyl-L-glycine (DMOG), dimethyl N-oxalyl-L-phenylalanine (DMNOF) and N-oxalyl-L-alanine (NAA).

Investigation of other leaf extracts was conducted to identify whether N-oxalyl amino acid derivatives were present. Broccoli (*Brassica oleracea*) and watercress (*Nasturtium officinale*) leaves showed no evidence for NOG, DMOG or DMNOF; however, NOG, DMOG and NAA were identified in spinach (*Spinacia oleracea)* leaves, based on mass and retention time as for Rhubarb leaves (Table 5-2).

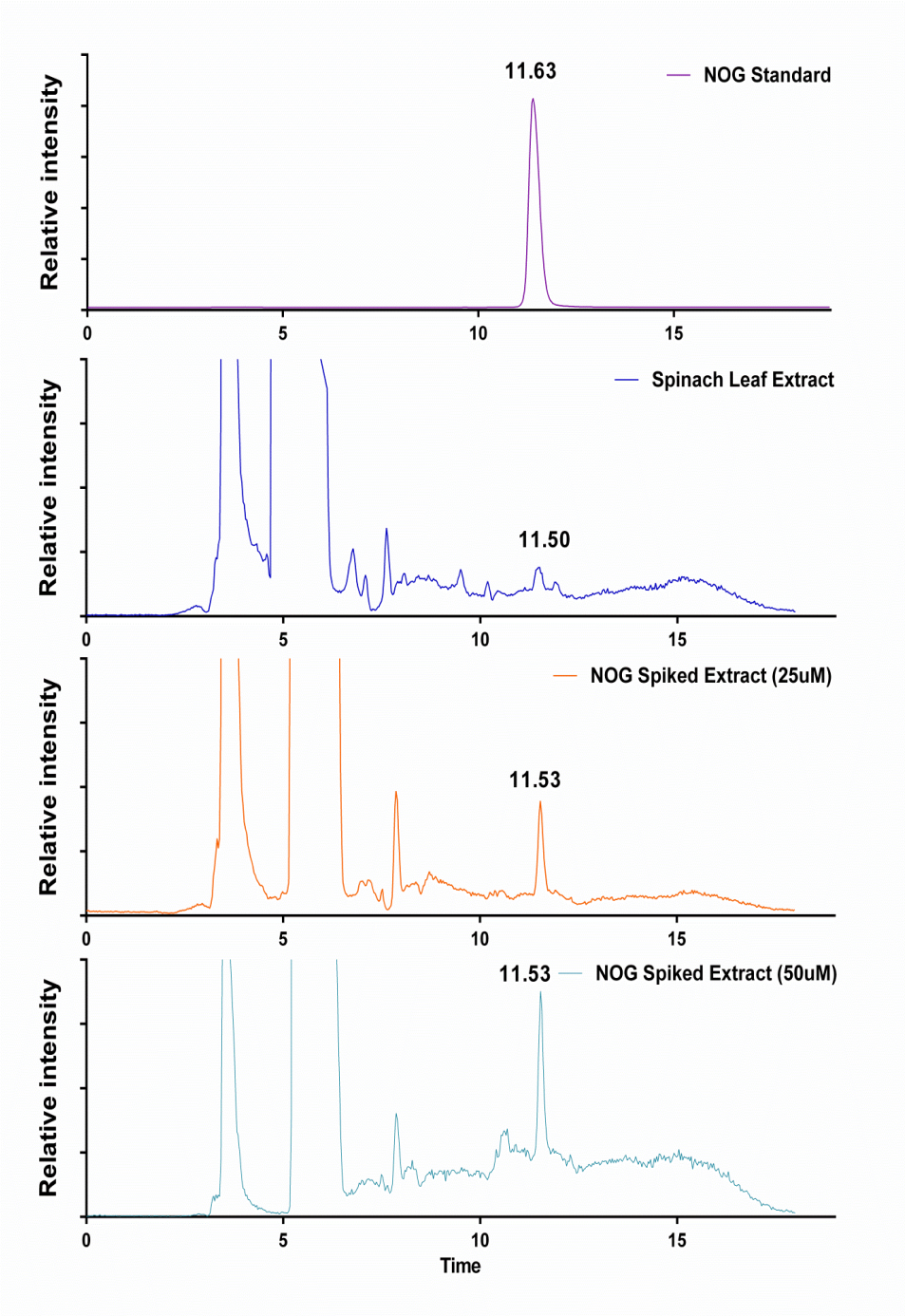

Figure 5-8: Four LC/MS (single ion monitoring) chromatograms from the analysis of NOG standard, aqueous Spinach leaves extract and aqueous spinach leaf extracts spiked with *N*-Oxalylglycine (NOG) standard (25 µM and 50 µM). In conjunction with m/z accurate mass data (see Figure 5-4c) these chromatograms demonstrate a peak with the same m/z value as *N*-Oxalylglycine is present in the spinach leaf extract at the same retention time (11.50 min) as the *N*-Oxalylglycine standard (11.63 min) within analytical error. Note the small differences in retention time for the analyses an NOG standard compared to the peaks in the leaf extract samples. This is often seen when two very different sample matrices are run, at different times, containing the same compound.

5.2.6. Analysis Of Bacterial And Mammalian Cells For The Presence Of The Amino Acid Derivatives Found In Rhibarb And Spinach

It was also investigated whether NOG was present in human and bacterial cells. Human embryonic kidney cells (HEK 293T) and *Escherichia coli* (strain BW25113) cells were subjected to identical analysis and for the plant extracts, but did not provide any evidence for the presence of NOG (Baba et al., 2006). Table 5-2 summarizes the findings.

Natural product	Type	Extraction	NOG	DMOG	NAA	DMNOF
Rhubarb	Leaves	Water	+	-	+	-
Rhubarb	Leaves	Acid	+	+	+	-
Rhubarb	Leaves	MeOH (80%)	-	-	-	-
Rhubarb	Leaves	Ethylacetate	-	-	-	-
Rhubarb	Leaves	Ether	-	-	-	-
Spinach	Leaves	Water	-	-	-	-
Spinach	Leaves	Acid	+	+	-	+
Broccoli	Flower	Water	-	-	-	-
Broccoli	Flower	Acid	-	-	-	-
Watercress	Leaves	Water	-	-	-	-
Watercress	Leaves	Acid	-	-	-	-
Bacterial cells	E. Coli	MeOH (80%)	-	-	-	-
Mammalian cells	HEK 293T	MeOH (80%)	-	-	-	-

Table 5-2: Experimental matrix showing findings of N-oxalyl amino acid derivatives in plants, bacterial and human tissues studied using different extraction methods.

5.3. Conclusions

The novel results demonstrate that NOG, and NAA are present as natural products found in some plant tissues known to contain high levels of oxalic acid, i.e. rhubarb and spinach (Cunliffe et al., 1992). We did not detect NOG in *E. coli*, or human tissue culture cells. Thus, whilst we cannot rule out the possibility that NOG is present in animal cells, there is no evidence for its presence at currently detectable levels. Whether or not the amount of NOG present in rhubarb leaves is bioavailable in sufficient quantity to elicit a physiological effect upon ingestion remains to be determined.

These results are unexpected as NOG in its human cell permeating; dimethyl ester form (DMOG) is widely used in studies on the hypoxic response and chromatin modifications in

animals. In both cases, this is because NOG is a broad-spectrum inhibitor of the biochemically important ferrous iron and 2-OG dependent oxygenases. These enzymes are presently of intense biomedicinal interest because of their roles in hypoxic signaling and epigenetic regulation. The latter extends to plants where 2-OG dependent oxygenases catalyse demethylation of *N*-methylated histone H3 tails.

This work therefore suggests that *N*-oxalyl amino acids have the potential to play a natural role in regulating gene expression by inhibiting 2-OG dependent oxygenases. This is important because of the fact that 2-HG and other TCA cycle intermediate inhibition of 2-OG dependent oxygenases is attracting major interest in the cancer field.

Chapter 6: EXAMINING THE EFFECTS OF KNOCKING DOWN PFKFB3 AND PFKFB4 ON GLYCOLYSIS AND PPP METABOLIC PATHWAYS IN CANCER CELLS

6.1. Introduction and Aims

PFKFB3/4 are overexpressed in human cancers which is regulated by HIF-α levels; they are both required for the survival and growth of multiple cancer types and they regulate the balancing of glucose carbon at a branching point between glycolysis and the pentose phosphate pathway. It would be useful to examine the independent effects of PFKFB3 and PFKFB4 in cancer cellular metabolism in the glycolytic and pentose phosphate pathways. We studied PFKFB3 and PFKFB 4 knocked down cell models using siRNA in normoxic and hypoxic conditions. The aim of these experiments was to identify and quantify key intermediates in both pathways.

A number of glycolytic intermediates are isobaric and therefore have the same m/z value such as glucose-6-phosphate (MW = 260.0297 g/mol) and fructose-6-phosphate (MW = 260.0297 g/mol) (Lei, Huhman et al., 2011). Previous studies have employed the analysis of metabolites by LC-MS to quantify the activity of metabolic pathways, including glycolysis, gluconeogenesis, the PPP and glutaminolysis (Huck, Struys et al., 2003; Hunnewell and Forbes 2010).

6.2. LC-MS Method background

Phosphorylated carbohydrates are key metabolites in various central metabolic pathways including glycolysis and glycogenolysis pathways as well as the pentosephosphate cycle. Therefore, their reliable analytical determination is important, in particular for the monitoring of intracellular metabolites (Oldiges et al., 2007; Dettmer et al., 2007; Theodoridis et al., 2008).

The analysis of monosaccharide phosphates is relatively complicated because of their chemical nature, chromatographic/mass-spectrometric behavior and their low concentration in cells (nmol/g wet tissue) (Jensen et al., 2001). They have isomers that are isobaric; their mass

spectrometric fragmentation patterns are also similar, requiring chromatographic separation prior to mass spectrometry (Sekiguchi et al., 2004; Schaeper et al. 1996 and Meynial et al., 1995). Separation is challenging because of the polar acidic nature of the phosphorylated sugars (Sekiguchi et al., 2004).

Owing to a lack of chromatographic and mass spectrometric differentiation for the analysis of isomeric phosphorylated carbohydrates, many analyses on hexose and pentose phosphates as well as other sugar phosphates are presented as a sum of isomeric forms (Bajad et al., 2006 and Preinerstorfer et al., 2010). Various partially selective chromatographic assays have been proposed to enable separation of isomers. These include HILIC (Antonio et al., 2008), stereoselective HPLC with B-cyclodextrin-bonded stationary phases (Feurle et al., 1998 and Buchholz et al., 2001), HPLC with porous graphitic carbon (Buchholz et al., 2001), anion-exchange chromatography (Swezey 1995 and Sawada et al., 2003), anion-exchange chromatography combined with pulsed amperometric detection (Jeong et al., 2007), and mixed-mode chromatography employing Primesep SB, a mixed-mode column packed with reversed-phase material carrying embedded basic ion pairing groups (Cruz et al., 2008). The latter setup required a high concentration of salt in the eluent (100–500 mM Na acetate) that was not compatible with MS detection or an on-line ion-suppressor or a desalter unit (Preinerstorfer et al., 2010 and Kiefer et al., 2008). B-cyclodextrin-bonded columns may enable separation of sugar-phosphate isomers; however, B-cyclodextrin-bonded columns with internal diameter (i.d.) of 1 mm or less are not commercially available (Antonio et al., 2008; Feurle et al., 1998 and Buchholz et al., 2001).

For the analysis of cellular glycolysis in this chapter the ion pairing RP-IP-LC method developed in chapter 2 was used. This provided satisfactory chromatographic selectivity for the structural isomers of interest including G-6-P and F-6-P (Figure 6-1).

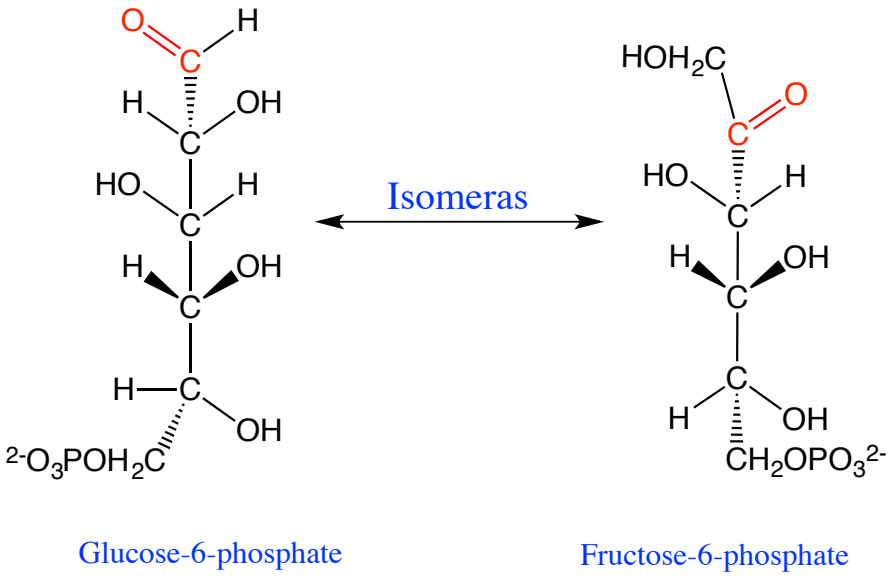

Figure 6-1: Phosphoglucose isomerase changing glucose-6-phosphate and fructose-6-phosphate. These two are isomers of one another, same atoms-different shape.

6.3. Results

6.3.1. Reversed phase liquid chromatography for the analysis of intermediates of glycolysis.

Using method 1 (Chapter Two) for it was investigated whether the isomerases G-6-P and F-6-P could be resolved. Three volatile alkyl-amines, triethylamine (TEA), tributylamine (TBA) and dibutylamine (DBA), adjusted to pH 6.8 by 5 mM acetic acid were tested as aqueous eluent mobile phase (A) coupled to ACE-PFP column. The results for the different amine alkyl-chains showed the systematic increase of retention (TEA < DBA< TBA) see Figure 6-2. It was found that amines with shorter alkyl-chain (TEA) did not provide sufficient resolution for the separation of the isomers (G-6-P/F-6-P) Figure 6-2(A); were the separation and resolution of G-6-P/F-6-P increased with longer alkyl-chain results shown in Figure 6-2 (TEA(A)<DBA(B)<TBA(C)). Higher proportions of organic solvent improved peak shapes and shortened elution time, but coincided with some loss of resolution. As reported (Huck et al., 2003), the co-elution G-6-P/F-6-P could be the result of inappropriate selection of alkyl-

chain length and organic solvent content. Among the investigated amines, TBA provided a reasonable compromise between elution time, resolution and sensitivity, and was therefore used for further investigation.

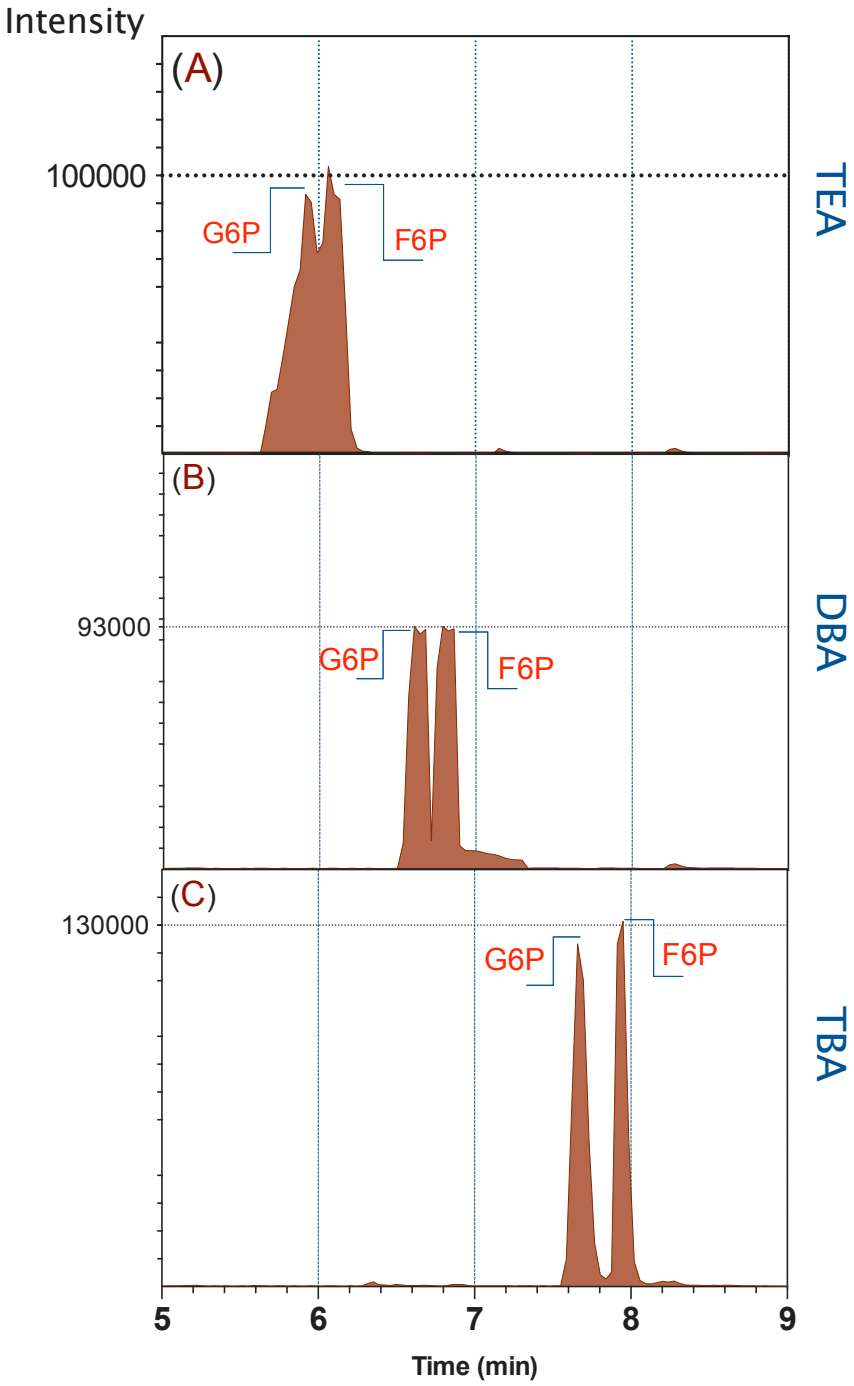

Figure 6-2: Chromatographic separation of glucose-6-phosphate (G-6-P) and fructose-6-phosphate (F-6-P) using ACE-PFP column with different IP alkyl-chains, were triethylamine (TEA), tributylamine (TBA) and dibutylamine (DBA). (A); were the separation and resolution of G-6-P/F-6-P increased with longer alkyl-chain results shown in Figure (TEA(A)<DBA(B)<TBA(C)).

The effect of mobile phase pH on analyte resolution was studied for two aqueous eluents at pH 4.38 and 6.8 (10 mM TBA mixed with 10 mM (pH 6.8) and 15 mM (pH 4.38) acetic acid, respectively) with methanol as the organic eluent and the gradient profile in Table 6-1. The influence of eluent pH on the separation of isomeric sugar phosphates (G-6-P/F-6-P) was not significant. Due to decreasing peak symmetry at pH values lower than 4.38, the pH effect was not further investigated.

Step	Run time (min)	Eluent A (vol.%)	Eluent B (vol.%)
1	0.0	100.0	00.0
2	2.0	80.0	20.0
3	4.0	60.0	40.0
4	10.0	40.0	60.0
5	12.0	100.0	00.0
6	15	100.0	00.0

Table 6-1:Gradient profile applied in the developed LC–MS method; eluent A: 10 mM triethylamine aqueous solution adjusted pH to 4.95 with 15 mM acetic acid, eluent B: methanol.

The effect of TBA concentration was further investigated. Aqueous eluents with various concentrations of tributylamine (TBA) with 15mM of acetic acid (AcOH) were prepared as follows: (A): 5 mM TBA mixed with 15 mM AcOH (pH 4.38); (B): 7.5 mM TBA mixed with 15 mM AcOH (pH 4.68); (C): 10 mM TBA mixed with 15 mM AcOH (pH 4.95). Other LC/MS conditions were kept the same as in Method 1. Figure 6-3 shows the chromatograms While the concentrations of TBA were increased, the sugar phosphate peaks from G-6-P and F-6-P eluted much earlier in Figure 6-3(A) than in Figure 6-3(C). When the AcOH concentration was maintained at 15 mM, an increase in TBA concentration from 5 to 10 mM led to an apparently longer retention for almost all analytes and a slight increase in selectivity (see Figure 6-3A,B and C).

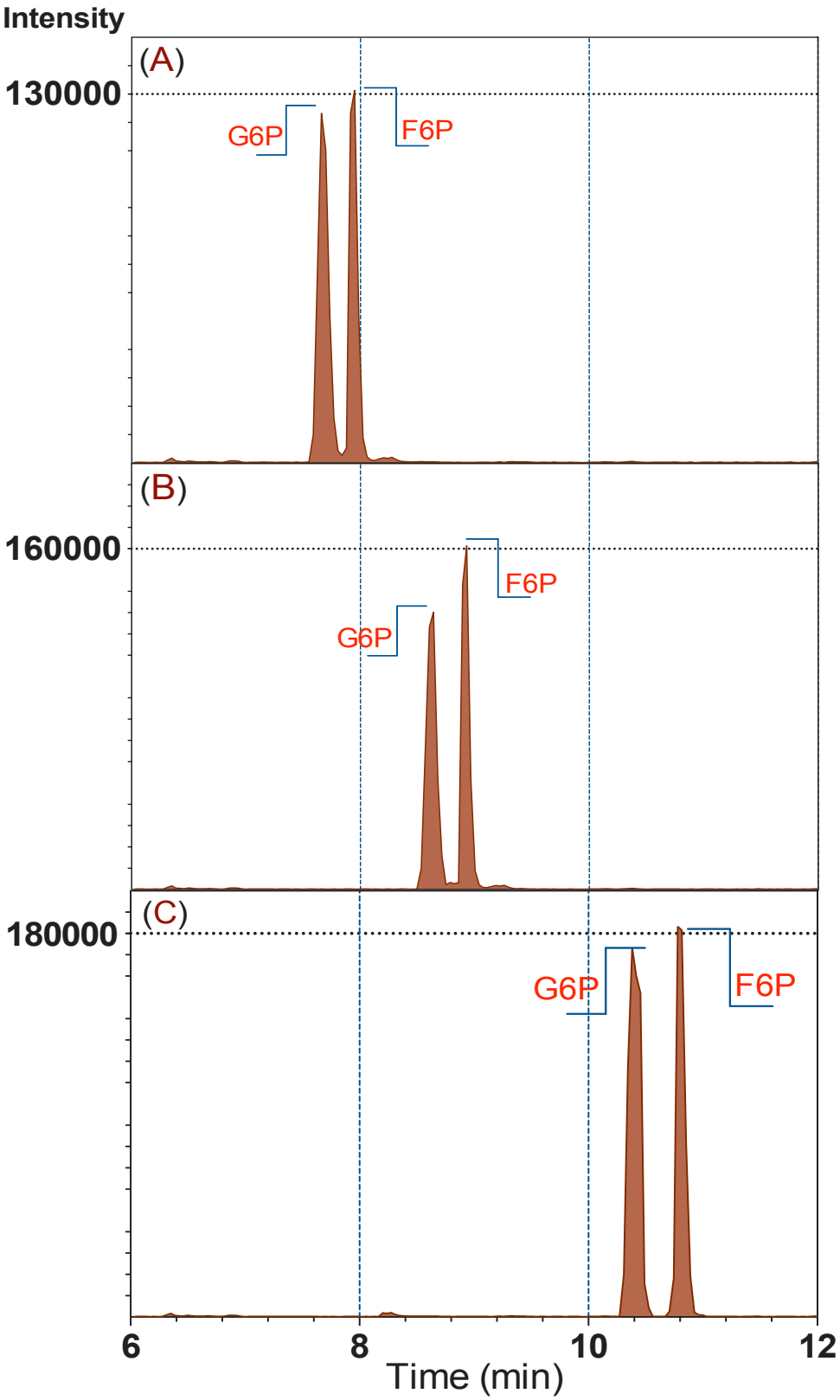

Figure 6-3: Separations Chromatograms for ACE-PFP column of of glucose-6-phosphate (G-6-P) and fructose-6-phosphate (F-6-P) at different triethylamine concentrations. (A) 5 mM, (B) 7.5 mM and (C) 10 mM. When the AcOH concentration was maintained at 15 mM, an increase in TBA concentration from 5 to 10 mM led to an apparently longer retention for almost all analytes and a slight increase in selectivity

Stronger retention with increasing concentration of TBA reagent is well-known in ion-pair chromatography (Huck et al. 2003). When the TBA concentration increased to 10 mM, the selectivity was also slightly improved for separation of G-6-P and F-6-P. On the other hand, a reduction of the MS response by an increased TBA concentration from 5 to 10 mM was not observed. In contrast, the intensity of seven of the targeted sugar phosphates slightly increased.

In practice, the addition of 5 mM TBA in the mobile phase was capable of achieving good peak shape and sufficient resolution for most analytes of interest. Cell extract samples were introduced and it was noted that the peak shape for weakly retained compounds such as G-6-P and F-6-P was poor. This might have been due to the presence of high amounts of endogenous compounds, which competed with analytes in the formation of TBA ion pairs. In order to ensure the amount of TBA was sufficient to form ion pairs with all analytes, increasing the concentration of TBA to 10 mM was necessary. When 10 mM TBA adjusted with 15 mM acetic acid (pH 4.95) was used sufficient resolution, reasonable retention time, better peak shape and high sensitivity Figure 6-4 was seen.

Due to the weaker elution strength of methanol, higher resolution was relatively easily achieved by adjusting methanol content in the gradient. A 5% difference in methanol content (for example, methanol content in the gradient increased from 20 to 25%) was able to finely tune the separation strength of the method. When methanol instead of acetonitrile was applied, it also showed slightly higher resolution for the separation of G-6-P and F-6-P. However, a concession to high resolution with methanol was a prolonged elution time.

Based on these optimisations an LC/MS methods using 10 mM TBA mixed with 15 mM acetic acid was used as mobile phase A and 100% methanol as mobile phase B. This resulted in a run time of 15 min, optimised for resolution and sensitivity.

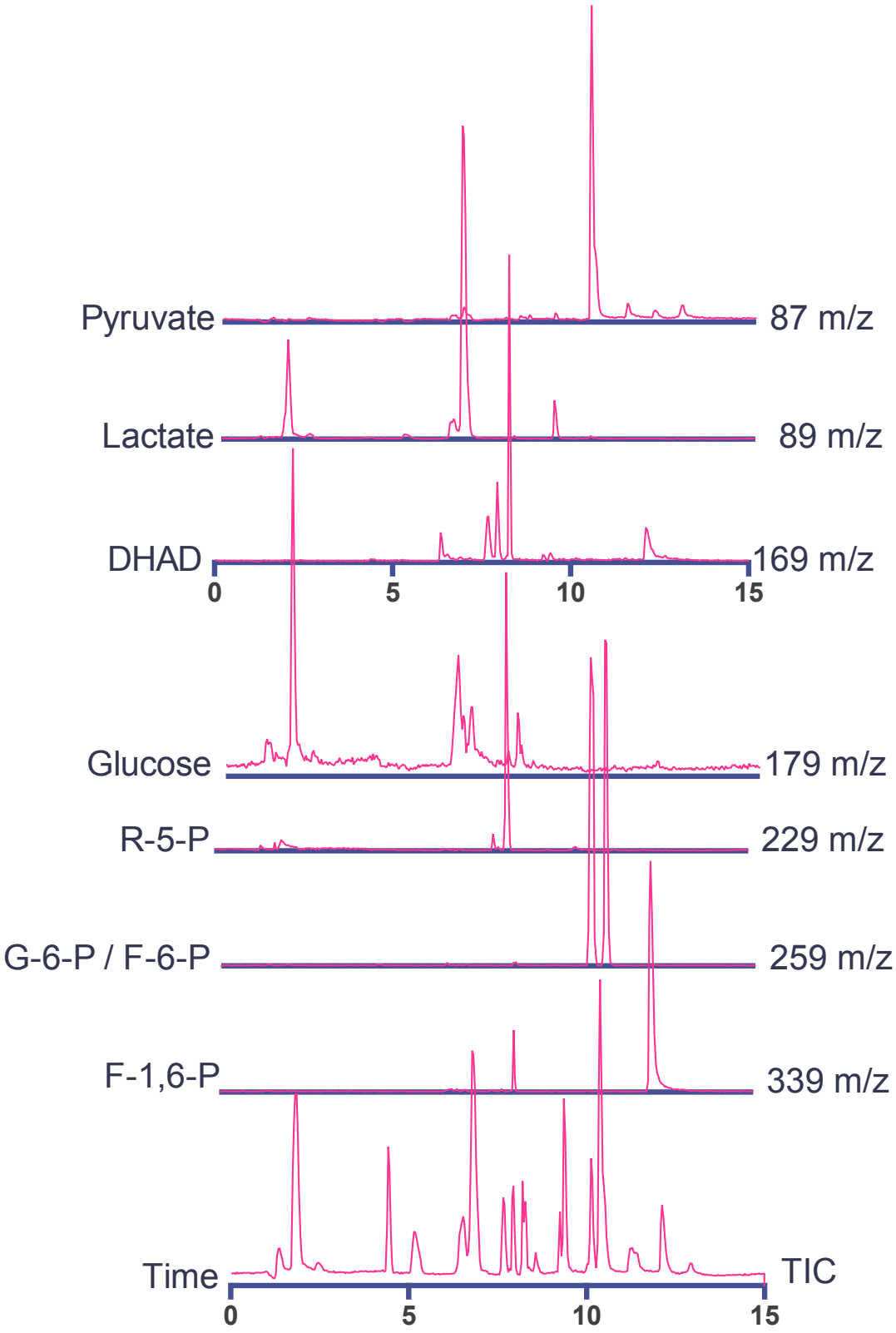

Figure 6-4: **Total ion current chromatogram and extracted ion of targeted metabolites of pentose phosphate pathway and glucoses pathway. Using 10 mM tributylamine with 15 mM acetic acid coupled to ACE-PFP column. Glucose-6-phosphate (G-6-P), Fructose-6- phosphate (F-6-P), Fructose-1, 6-bisphosphate (F-1, 6-BP), Dihydroxyacetone phosphate (DHAP), Ribulose-5-phosphate (R- 5-P).**

6.3.2. Quantitative Method Validation

The results of the validation of the optimized method are summarized in Table 6-2. In general, the calibration graphs show good linearity over three orders of magnitude with correlation coefficients (R^2) 0.9982 or higher (Appendix A3). The LoD and the LoQ were calculated according to DIN 32645 (Kolb et al., 1993). As shown in Table 6-2 the LoDs vary from 1.25 to 5 µM and the LoQs are from 5 µM to 10 µM. Only pyruvate exhibited low sensitivities, which might be attributed to the lower intensity of the product ion (m/z = 87) of PYR. With such low LoDs and LoQs, determination of these metabolites by direct injection of cell extract samples without any previous enrichment step is readily achieved. To check repeatability, three concentration levels of standard mixture were injected three times. The relative standard deviations (RSD) are better than 9% for 50 µM standard and 4% for the 100 µM and 500 µM standards (Table 6-2).

Metabolite	Linearity		Repeatability **(n = 3, CV %)**			LoD	LoQ
	Range	**R^2**	**500µM**	**250µM**	**50µM**	(µM)	(µM)
glucose	5µM-1mM	0.9992	4.89	2.65	2.11	5	10
G-6-P	1.2µM-1mM	0.9994	3.59	2.03	1.86	2	5
F-6-P	1.2µM -1mM	0.9991	4.11	2.56	2.01	2	5
F-1,6-BP	3µM-1mM	0.9995	2.65	2.10	1.86	3	8
DHAP	5 µM -1mM	0.9994	4.37	3.96	1.93	5	10
R- 5-P	3.5µM -1mM	0.9991	3.32	2.65	2.09	3.5	8
Pyruvate	7 µM -1mM	0.9982	7.51	4.66	3.21	7	13

Table 6-2: Linearity of calibration, relative standard deviation of three concentration levels of standards (n = 3), and limits of detection and quantification, determined by the established LC–MS method (2 µL injection), Glucose-6-phosphate (G-6-P), Fructose-6- phosphate (F-6-P), Fructose-1, 6-bisphosphate (F-1, 6-BP), Dihydroxyacetone phosphate (DHAP), Ribulose-5-phosphate (R- 5-P). (LoD) limit of detection, (LoQ) limit of quantitation

6.3.3. Application to the analysis of U87 cells

The validated method was successfully applied to analysis of intracellular metabolites in cell extracts. After sample preparation the cell extract was diluted, 1:3 (v/v) to reduce potassium acetate salts left during cell extraction, which may result in peak shape deterioration. Figure 6-5 shows the comparison of the selective ion chromatograms of G-6-P and F-6-P metabolites

in the cell extract samples of U87 with a standard mixture. It was shown that most of the metabolites in the cell extracts were detected as a single peak, although for a few transitions additional peaks were observed in the selective ion chromatograms. For example, an additional peak was found to elute after F-6-P, which might originate from endogenous galactose-1-phosphate or mannose-6-phosphate, since both standards elute at this retention time and mass. Figure 6-5 shows that the retention times of the metabolites in the cell samples are consistent with those in the standard mixture. Hence, the retention times are not affected by high salt concentration left from the extraction solution (at least 100 mM potassium acetate after 1:3 dilution) or from intracellular salts. The reliability of retention times was additionally confirmed by spiking the standards into the cell extracts. The method was shown to be robust and generally applicable to cellular samples.

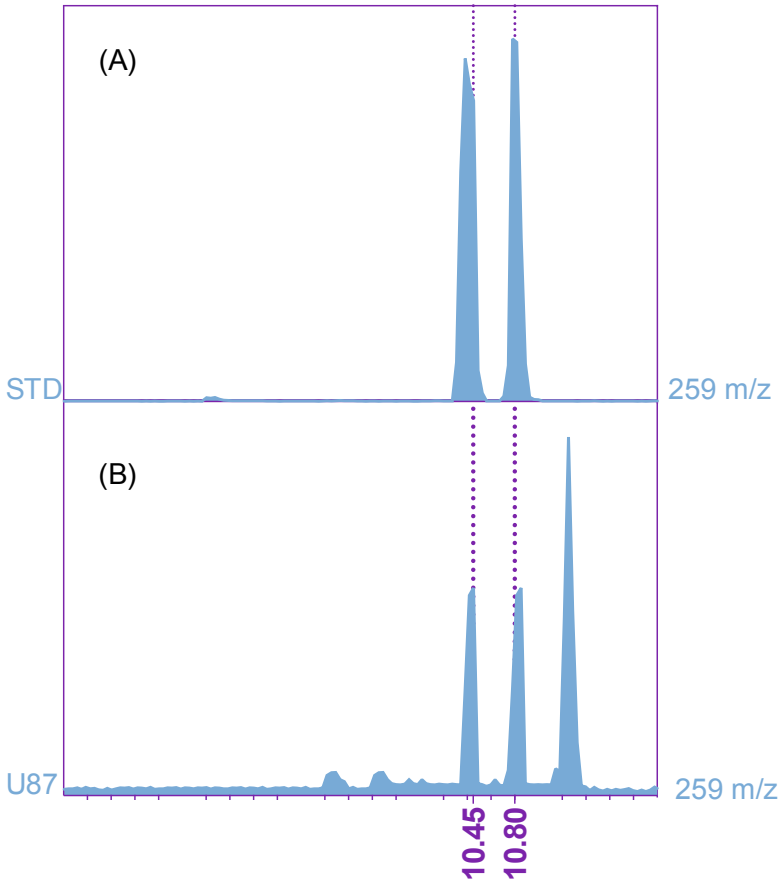

Figure 6-5: Selective ion chromatogram of 259 m/z for Glucose-6-phosphate (G-6-P), , at 10.45 min and Fructose-6- phosphate (F-6-P) at 10.80 min, showing the separation of isomers in standard (A) and extracted U87 samples (B). the X-axis is retention time in minutes.

6.3.4. Results Of Sirna PFKFB3/4 From U87 Cell

It became apparent from the results shown in Figure 6-6 that indirect analysis of the balance between glycolysis and the PPP provided insufficient information to further interpret the involvement of PFKFB3 and PFKFB4 in regulation of these pathways. Therefore, a more direct approach was taken through the use of quantitative mass spectrometry. It is important to note that quantification of individual metabolites does not directly indicate flux through a given pathway. Nevertheless, it can provide an indication of pathway activity. It was not possible to analyse F-2, 6-BP levels by mass spectrometry, due to the metabolite's high acid lability and the difficulty of obtaining a commercial F-2, 6-BP standard of sufficient purity.

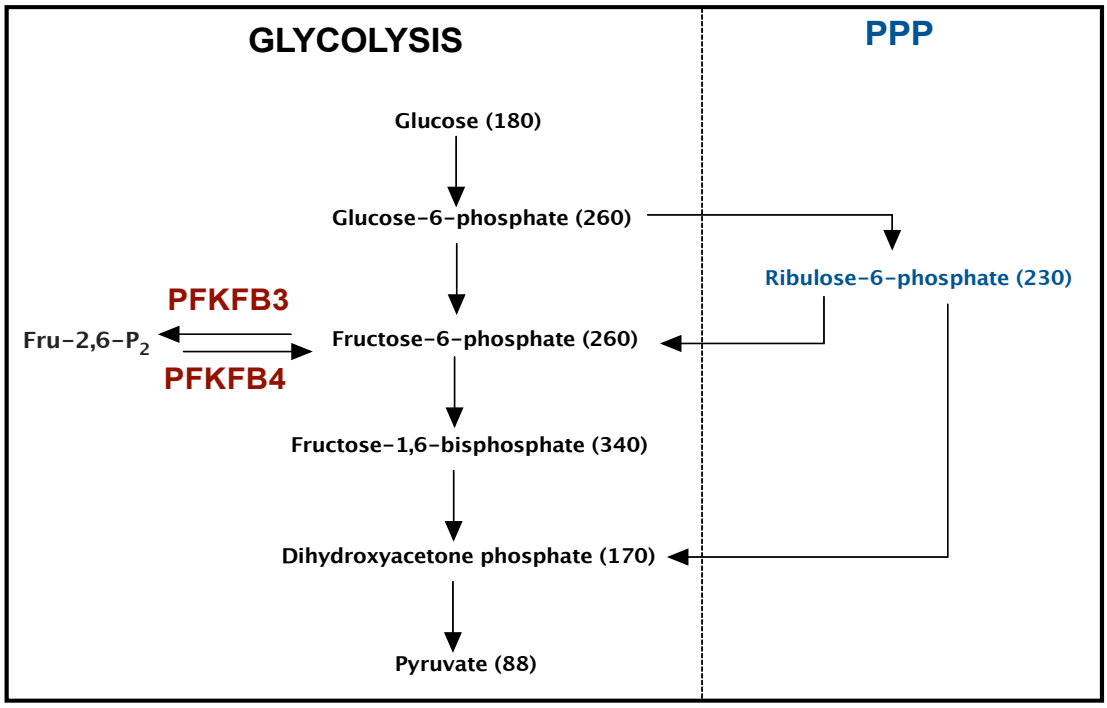

Figure 6-6: Glycolytic and Pentose phosphate pathways metabolites selected for mass spectrometric studies. A series of metabolites involved in glycolysis and the pentose phosphate pathway (PPP) were selected for liquid chromatography-mass spectrometry (LC-MS) analysis. The molecular nominal mass of each metabolite is listed in parentheses and Fructose 2,6-bisphosphate (Fru-2,6-P_2).

All cell-based experiments and cell extractions were performed in collaboration with Jonathan Williams at The Weatherall Institute of Molecular Medicine, University of Oxford. The samples were then prepared and analysed by the author along with interpretation of the data.

As an initial starting point, U87 cells were transfected with control scramble and sequence-specific siRNA to give a single PFKFB3, single PFKFB4 and double (PFKFB3/PFKFB4) siRNA knockdowns (experiment carried out by Jonathan). Three plates for each condition were prepared, one for cell counting and two for analysis, from which an average would be calculated. Half of the plates were incubated under normoxic conditions for 48 hours, and the other half were incubated under hypoxic conditions for the same period of time.

The cells were then extracted by the author, employing 80% aqueous methanol, containing 0.5 mM fumarate acid-2,3-d_2, as an internal standard . The samples were then stored on dry-

ice and lyophilised as quickly as possible, to minimise potential enzymatic degradation of metabolites.

Effective LC/MS separation of each of the metabolites of interest was achieved from the cell extracts, and the peak areas were converted to concentration values using the standard curves, before taking the mean of the two readings (two samples per condition) and normalising for the cell number (Figure 6-7). At first sight, it appeared that suppression of PFKFB3 expression increased the intracellular concentration of all measured metabolites in this initial study, with the exception of the PPP intermediate ribulose-5-phosphate (Figure 6-7F). However, closer inspection of the raw data prior to normalisation revealed that the concentration values for PFKFB3 siRNA knockdown were being artificially enhanced due to the lower cell counts for this condition. It became apparent that for a number of the metabolites being examined, e.g. pyruvate the observed concentration was outside the linear range of the standard curves previously plotted (Figure A3.1, Appendix). This led to the pre-normalised metabolite concentrations being erroneously reported as being similar across the different conditions for a number of metabolites, which led to an over-estimation of the PFKFB3 knockdown values, due to normalisation to a lower cell number. Furthermore, the values calculated for the two experimental sets (identical plates prepared simultaneously) before averaging, demonstrated considerable variation in absolute concentrations, despite correction for metabolite recovery efficiencies. This effect would have been exacerbated in true biological replicates, and so the assay results were unsuitable for further interpretation. The potential increase in R-5-P after PFKFB4 suppression would be interesting to investigate further (Figure 6-7F), to examine if this was a real effect.

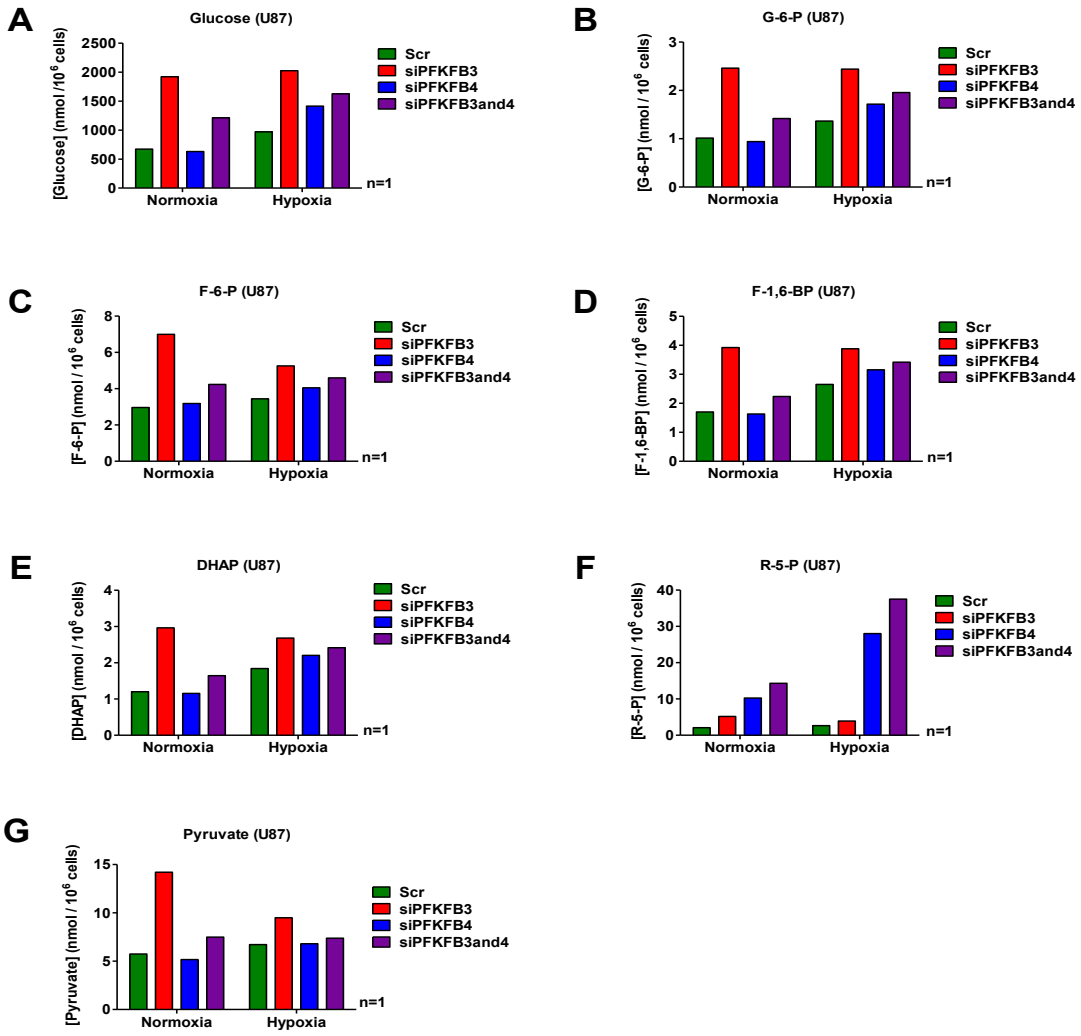

Figure 6-7: Initial quantitative liquid chromatography-mass spectrometry (LC/MS) measuring changes in glycolytic/PPP metabolite concentrations in response to single and double PFKFB3 and PFKFB4 knockdown, under both normoxic and hypoxic conditions in U87 cells. Metabolites (A) glucose, (B) glucose-6-phosphate (G-6-P), (C) fructose-6- phosphate (F-6-P), (D) fructose-1,6-bisphosphate (F-1,6-BP), (E) dihydroxyacetone phosphate, (F) ribulose-5-phosphate (R- 5-P) and (G) pyruvate.

A repeat of the experiment again demonstrated high inter-sample variability between essentially identical samples, prepared simultaneously. It was evident that further optimisation of metabolite extraction was required to reduce inter-sample variability and the potential effects of metabolite-degradation via activity of functional enzymes in the extraction mixture. Initial attempts to reduce the time between extraction and freeze-drying were not met with success. Increasing the amount of sample was not a viable option due to the expense of transfection reagents involved. Re-calibration of the standard curves for higher metabolite concentrations was also required but not pursued.

6.4. Conclusions

In the work described in this chapter, an RP-IPR-–MS method was developed for the identification and quantification of intracellular metabolites involved in glycolysis and the pentose phosphate pathway. This optimized method achieved a compromise between chromatographic resolution (especially for structural isomers) and MS performance. The validation results demonstrated the sensitivity, selectivity and reliability of the method. The method was successfully applied to the analysis of intracellular metabolites in cell extracts.

siRNA, knockdown of PFKFB3 and PFKFB4 produced few changes however. Nevertheless, when we compered the metabolites level changes between the two-difference conditions; the results of hypoxic condition showed high metabolites abundance when compared with metabolites levels in normoxic condition. The potential increase in R-5-P after PFKFB4 suppression would be interesting to investigate further.

Chapter 7: SUMMARY

This chapter summarises the work described in this thesis, the methods developed and tested for the analysis of TCA cycle, glycolysis and other target metabolites, and comments on the potential for future applications of metabolic analysis in the context of cancer studies. It is hoped that the results will aid in facilitating the choice of method suitable for analysis of metabolism in the future.

It is important to characterise the niche which metabolite analysis occupies amongst the many analytical methods available. The approaches involving various forms of metabolite analysis described in this thesis are not suggested as an alternative to the well-established metabolomics techniques, rather as being complementary to them. Compared to global metabolism, targeted metabolite analysis provides information on concentrations changes but also enables investigations into the regio- and stereo- chemistry of metabolites as has been shown here and which can play a very important role un understanding metabolic mechanisms. This is an area currently somewhat neglected but will be increasingly important in the future as metabolomics becomes more comprehensive and routine.

The major aim of the work in this thesis was to develop analytical methods to enable the identification and quantification of metabololitess using targeted metabolite analysis. The methods developed were shown to be useful in a broad range of samples including in vitro cell based experiments, and in vivo tissues samples.

Ongoing research into the function of the IDH1 and IDH2 mutants requires robust and sensitive analytical methods that enable quantification and identification of the products in a wide range of samples, ranging from in vitro assays to in vivo experiments. Such a broad spectrum of samples requires methodologies, which work over a broad range of metabolites, concentrations and a range of different matrices. The chromatographic and extraction methods developed were used to study IDH1 and IDH2 variants and $IDH1^{WT}$ in LN18 cells. These were used to quantify TCA cycle metabolites on a targeted basis; significantly differring

levels of *D*-2-HG and 2-OG were observed in cells with IDH1 and IDH2 variants. Metabolites analysed included those deemed relevant to $IDH1^{R132H}$ biology as indicated by previous reports, including 2-HG enantiomers, amino acids and NAD+/NADH. Metabolite measurements were performed in both time-resolved and TCA cycle metabolite dose response experiments; the methods developed enabled testing of the hypotheses related to IDH variants. For example, simultaneous measurements of 2-HG enantiomers, associated metabolites, amino acids, and NAD+/NADH helped to refine the *D*-2-HG hypothesis. Increases in the NAD+/NADH ratio and increases in *D*-2-HG associated with a decrease in 2-OG for cells with $IDH1^{R132H}$ were observed. This work led to a ^{13}C metabolic flux study using [^{13}C-4]-*L*-aspartic acid in $IDH1^{R132H}$ and $IDH1^{WT}$ LN18 cells which showed that [^{13}C-4]-*L*-aspartic acid carbon could be found in *D*-2-HG as M+3 and M+5 isotopomers only in $IDH1^{R132H}$ cells.The results did not show any isotopmer metabolite labelling patterns which linked aspartic acid with *D*-2-HG via normal TCA cycle conversions. Using untargeted MS, increases in amino acids were detected that may play a role in $IDH1^{R132H}$. An $IDH1^{R132H}$ selective inhibitor was show to decrease levels of *D*-2-HG in cells. A robust mixed mode chromatography method was developed to quantify 2-HG in brain tissues. Sample extraction protocols were compared and the most sensitive determined was found to be the same MeOH extraction protocol used for cells previously described. This method was used in conjunction with the analytical protocol for subsequent patient tissue analyses. Matrix effects were measured using representative tissue samples and a matrix effect compensation factor identified. Concentrations of 2-HG were found to be 4-60-fold higher in tumours with a mutation in IDH (0.4-6.0 μmoles per gram tumour) compared to wild-type (0-0.1μmoles per gram tumour). After applying the matrix effect factor, there was good agreement between the LC/MS and the MRS methods for the quantification of 2-HG in the brain tumour tissue samples (the coefficient of variation (R^2) was 0.67).

The analytical as well as extraction methods developed were shown to be applicable for the analysis of tissues and cell based samples. It is hoped that their continued application will expand the current knowledge on plant metabolism. The method also was applied to the identification and quantification of NOG, DMOG, NAA and DMNOF, as natural products in rhubarb and spinach. The results demonstrate that NOG, and NAA are present as natural products in some plant tissues. No NOG was detected in *E. coli*, or human tissue culture cells. Thus, whilst I cannot rule out the possibility that NOG is present in animal cells, there is no evidence for its presence at currently detectable levels. Whether or not the amount of NOG present in rhubarb leaves (or indeed other plants not yet investigated) is bioavailable in sufficient quantity to elicit physiological effects remains to be investigated. This result suggests the possibility that *N*-oxalyl amino acids may play a natural role in regulating gene expression by inhibiting 2-OG dependent oxygenases. This is important because of the fact that 2-HG and other TCA cycle metabolite intermediate inhibition of 2-OG dependent oxygenases is currently attracting major interest in cancer.

Further development work led to an LC/MS method that could separate metabolites of glycolysis and the PPP pathway and this was used to study changes in both pathways under normoxic and hypoxic conditions. The optimised method achieved a compromise between chromatographic resolution (including structural isomers) and MS sensitivity. Moreover, the possibilities of simultaneous separation of unlabelled and labelled metabolites make this LC/MS method applicable for ^{13}C flux analysis. The LC/MS method developed was also applicable for the study of all metabolites in the glycolysis and PPP pathways.

I developed a rapid sample preparation method for the analysis for human plant cells. Through optimisation extraction solvent, extraction time, and number of extraction cycles, I defined an extraction procedure using methanol/water quenching, and a rapid single extraction step with (80%; 8:2; methanol : water) extraction that yields stable extracts. It was demonstrated that a rapid water wash removed contaminants and substantially improveed the

sensitivity without altering the metabolites. It was also shown that aqueous 80% methanol provides equivalent results to conventional PA organic solvent quenching. It was demonstrated that the method can detect relative changes in metabolism involving TCA cycle, glycolysis, and other target metabolites, with results similar to previous methods, but with overall increases in sensitivity and speed.

Chapter 8:MATERIALS AND METHODS

8.1. Chromatography, Mass Spectrometry and other Equipment.

A Waters ACQUITY^{TM} ultra-performance liquid chromatography (UPLC) system (Waters Corp., Milford, MA, USA) was coupled directly to a Waters Micromass Quattro micro Triple Quadrupole Mass Spectrometer (Waters Corp., Manchester, UK) and used for LC-MS analyses. Chromatographic data were collected using Waters MassLynx v4.1 software and analysed using Microsoft Excel. A Agilent Gas chromatography (GC) system was coupled directly to a Agilent Quadrupole Time-of-Flight (Q-TOF) Mass Spectrometer (Agilent Technologies LDA UK Limited., Stockport, UK). ^{1}H and ^{13}C NMR spectra of the purified rhubarb extract and the NOG standard were collected using a Bruker AVIII 700 spectrometer equipped with a TCI cryoprobe at 298K.

A Sigma 1-14 Microfuge (Sciquip-UK) was used for centrifugation. Scanvac CoolSafe^{TM} freezes dryer (Lebogene UK) for freeze-drying and a SONICS Vibracell VCX750 Ultrasonic Cell Disrupter (Labotal Scintific, USA) for sonication.

8.2. Chemicals and Standards

A list of standards used for the work described in this thesis is provided in Table 8-1. 6 M HCl was from Thermo Fisher Scientific (Northumberland, UK). Water used for all the experiments was purified by Millipore Elix system with 0.22-µm filters at the outlet. The pH was verified by pH-metre Mettler Toledo with the Mettler Toledo InLab 413 pH probe, calibrated to pH 7 and 10 before use. The storage solution was 3 M potassium chloride.

Name	Supplier
TCA cycle intermediate	
Fumarate	Sigma
Succinate	Sigma
d_4-Succinate	Sigma
Malate	Sigma
Aspartate	Sigma
Glutamine	Sigma
2-Oxoglutarate	Sigma
Oxaloacetate	Sigma
Cis-aconatate	Sigma
Glutamate	Sigma
Citrate	Sigma
*Iso*citrate	Sigma
Itaconate	Sigma
D,L-2-hydroxyglutarate	Sigma
N-Acetylaspartate	Sigma
Nucleotide	
NAD^+ / NADH	Sigma
Glycolysis intermediate	
Pyruvate	Sigma
Lactate	Sigma
Glucose	Sigma
Glucose-6-phosphate	Sigma
Fructose-6-phosphate	Sigma
Fructose-1,6-bisphosphate	Sigma
Dihydroxyacetone phosphate	Sigma
Ribulose-5-phosphate	Sigma
NOG derivatives	
N-Oxalyl glycine	Sigma
Dimethyl oxalyl glycine	Sigma
N-Oxalyl alanine	Sigma
Dimethyl N-oxalyl-D-phenylalanine	Sigma
4-Hydroxy-2-oxoglutarate.	Sigma
GC/MS derivatisation	
Methoxyamine	Sigma
Pyridine	Sigma
MTBSTFA + 1% TBDMCS	Sigma
Extractions and UPLC solvents	
Acetonitrile	Sigma
Methanol	Sigma
tri-Butylamine	Sigma
di-Butylamine	Sigma
Formic acid	Sigma
Acetic acid	Thermo Fisher

Table 8-1: Tricarboxylic acid cycle standards used in this work

8.3. Chromatography Methods

Unless stated otherwise chromatography was performed using a Waters Acquity UPLC equipped with a Triple Quadrupole MS detector.

8.3.1. Method 1: IP-RP Chromatographic Separation Developed Of Non-DerivatisedTCA Cycle Intermediate analysis

Dried extracts were dissolved in 60 µL of mobile phase A. Were then analysis using PFP column (ACE, Reading, UK) was used (reversed phase C18-PFP, 2.1×150mm, particles 3µm). The column was operated at flow rate of 1.8 mL/min see Table 8-2.

Phase	Composition (mL)				
	H_2O	TBA	Acetic acid	Acetonitrile	Formic acid
A	996 (v)	2.2 (v)	1.8 (v)	—	—
B	—	—	—	998 (v)	2 (v)

Table 8-2: IP-Reversed phase chromatography of Tricarboxylic acid cycle intermediate mobile phase composition

A linear one-step gradient (Table 8-3) was applied: Phase A 100 to 65 % over 15 min. The column was cleaned for 2 min at a higher acetonitrile concentration (40% Phase A) before reconditioning.

Time (min)	% Phase A	Function
0	100	initial
8	65	separation
10	40	separation
11	40	cleaning
13	100	reconditioning
15	100	reconditioning

Table 8-3: Reversed phase chromatography of Tricarboxylic acid cycle mobile phase gradient

The column temperature was kept at 30°C. The injection volume was 2 µL. MS detection was performed at SIR mode. The flow was split at 1:1 ratio before entering into the mass spectrometer.

8.3.2. Method 2: Chiral IP-RP Chromatographic Separation Of 2-Hydroxyglutarate Enantiomer Using Ion Pairing

Dried extracts were dissolved in 50 µL of mobile phase A. Were then analysis using Chirobiotic column (Astec, Sigma-Aldrich Co, USA) was used (Reversed Phase Chirobiotic, 4.6 × 250 mm, particles 5µm). The column was operated at flow rate of 2.5 mL/min see Table 8-4.

Phase	Composition (mL)				
	H_2O	TBA	Acetic acid	Acetonitrile	Formic acid
A	994 (v)	3.2 (v)	2.8 (v)	—	—
B	—	—	—	998 (v)	1 (v)

Table 8-4: IP-Reversed phase chromatography of 2-Hydroxyglutarate (2-HG) mobile phase composition

A linear one-step gradient (Table 8-5) was applied: Phase A 100 to 75% in 25 min. The column was cleaned for 2 min at a higher acetonitrile concentration (50% Phase A) before reconditioning.

Time (min)	% Phase A	Function
0	100	initial
7	97	separation
12	97	separation
12.1	50	cleaning
14.1	100	reconditioning
15	100	reconditioning

Table 8-5: Reversed phase chromatography of 2-Hydroxyglutrarte (2-HG) mobile phase gradient

The column temperature was kept at 30°C. The injection volume was 2 µL. MS detection was performed at SIR mode. The flow was split at 1:2 ratios before entering into the mass spectrometer. For the samples with complex biological matrices (cell extracts) the cleaning step at higher percentage of acetonitrile was introduced.

The mobile phase used for the enantiomer separation for 2-HG, Glu, Gln and Asp consisted of a mixture of: (A) 10 mM tributylamine adjusted to pH 7.0 with acetic acid 15 mM; and (B) MeCN, 0.1% of formic acid it (v:v). The column used was a Chirobiotic R column of 250 mm

length × 4.6 mm I.D., 5 mm silica gel particles bonded to the macrocyclic glycopeptide ristocetin A (Advanced Separation Technologies, Whippany, NJ, USA). The flow rate was 0.5 mL/min with a split where the effluent from the column was connected to a dead-volume T-connection before it reached the mass spectrometer, allowing only 60 mL/min to flow into the ion source.

8.3.3. LC Mixed-Mode Chromatography

Dried extracts were dissolved in 60 µL of mobile phase A. Were then analysis using C18-UPLC ACQUITY (Waters, UK) column (HSST3 C18, 2.1 × 100 mm, particles 1.8µm) with HPLC-ACE column (ACE, Reading, UK) was used (reversed phase C18-PFP, 2.1×150mm, particles 3µm). The column was operated at flow rate of 1.8 mL/min see Table 8-6.

Phase	Composition (mL)		
	H_2O	Formic acid	Methanol
A	998 (v)	2 (v)	—
B	—	2 (v)	988(v)

Table 8-6: MMC phase chromatography of 2-Hydroxyglutrate (2-HG) mobile phase composition

A linear one-step gradient (Table 8-7): Phase A 100 to 65 % over 15 min. The column was cleaned for 2 min at a higher acetonitrile concentration (40% Phase A) before reconditioning.

Time (min)	% Phase A	Function
0	100	initial
2	95	separation
5	10	separation
7	95	cleaning
8	100	reconditioning
10	100	reconditioning

Table 8-7: MM-chromatography of 2-Hydroxuglutrate mobile phase gradient

The column temperature was kept at 30°C. A constant flow rate at 0.2 ml/min was used. Sample injection was performed using partial-loop with needle overfill (PLNO; loop size 10 µl) mode; the sample injection volume used was 5 µl. A cone voltage of 60 V and a capillary voltage of 3.0 kV were used in negative ionisation mode. The desolvation temperature was set to 190°C and the source temperature to 120°C. MS detection was performed at SIR mode.

8.3.4. LC/MC Method For the Identifcation NOG From Leaves Of R. Rhabarbarum

I used the TCA cycle isomeric method described above, but with changing the precursor and cone voltages for optimizing the signals for NOG, DOMG, NAA and DMNOF; see Table 8-8.

8.3.5. GC/MS Chromatographic Separation Developed Of Derivatives Of TCA Cycle Intermediates

Dried extracts of LN18 cells were dissolved in 10 µL anhydrous pyridine and 50 µL N-methyl-N-(tert-butyldimethylsilyl)trifluoro-acetamide(TBDMS) containing 1% tert butyl di-methyl chlorosilane. The reaction vials were sealed under nitrogen and heated at 80°C for 1 hour. Derivatized metabolite samples (1 µL) were injected in a splitless mode into an HP Agilent 6890 series gas chromatograph machine coupled with an HP Agilent 5973 mass selective detector and separated on DB5-MS 30 m x 250 µm x 0.25 µm column with a 10 m guard column (J&W Scientific, Folsom, CA). The injection, MS transfer, ion source, and quadrupole temperatures were adjusted to 230°C, 250°C, 230°C, and 150°C, respectively. The electron impact mode at 70 eV was used for ionization. Helium was used as the carrier gas at a flow rate of 1.2 mL/min. For polar extracts the intial oven temperature was held at 70°C for 1 min and increased to 120°C at 15°C/min and held for 1 min. Subsequently, the temperature was raised at 10°C/min to a final temperature of 325°C. Full-scan mass spectra were acquired from 50 to 650 m/z at 2.48 scans/sec for both polar and amine extracts.

Metabolites were identified by retention time and mass spectrum comparison with standards; unknowns were putatively identified from their mass spectrum by searching the NIST02 and

Golm Metabolome Database mass spectral libraries using tools available in WsearchPro (www.wsearch.com.au) and confirmed using authentic standards. Absolute peak areas for each metabolite were normalized to the absolute peak area of the internal standard and then further normalized to the total cell number.

8.4. Detection Methods

MS detection in SIR mode was carried out using a Quattro Micro triple quadrupole mass spectrometer (Waters, Milford, USA).

MS detection of the TCA cycle intermediate was performed in negative mode. The capillary voltage was at 3000 V; extractor voltage was at 6 V, and RF lens was at 0.8 V. The desolvation temperature was 2000 C, and the source temperature was 1200 C. The cone gas flow was at 30 L/min and the desolvation gas flow was 450 L/min.

For ion paring chromatography of non-derivatised TCA cycle; the cone voltages and collision energies used for individual intermediate are listed in Table 8-8. Cone voltage and collision energy were identified for the individual intermediate by direct injection of 100 μM solution at 5 μL/min. The conditions for every intermediate are presented in Table 8-8.

8.5. Chromatography-MS Data Processing

Signal processing was performed using the QuanLynx software (Waters, Milford, US) for all LC-MS data.

GC/MS signal processing was performed manually for all data.

8.6. List of Columns Used

Type	Dimensions	Partical Size	Brand Name	Manufacturer
Separation the TCA cycle isomer				
Reversed Phase	2.1 × 100 mm	1,8 µm	Acquity HSST3	Waters
Reversed Phase	2.1 × 100 mm	1,7 µm	C18-PFP	Kinetex
Reversed Phase	2.1 × 150 mm	3 µm	C18-PFP	ACE
Separation the 2-HG enantiomer				
Reversed Phase	4.6 × 250 mm	5 µm	Chirobiotic T	Astec
Reversed Phase	4.6 × 250 mm	5 µm	Chirobiotic V	Astec
Reversed Phase	4.6 × 250 mm	5 µm	Chirobiotic R	Astec

Table 8-8: List of Columns examined for the LC isomeric and enantiomric.

Name	SIR		tR
	Precursor	Cone	
TCA cycle intermediate			
Glu	146.0	14	3.22
Gln	145.0	14	5.81
ASP	133.0	15	6.23
SUC	117.2	13	8.66
MAL	134.1	14	8.92
(D/L)-2-HG	147.2	15	9.34
ICA	191.1	15	9.41
CA	191.1	15	9.83
2-OG	145.1	12	10.21
ACT	173.2	15	10.79
FUM	115.1	12	10.84
NAA	174.2	20	7.56
Nucleotide			
NAD^+	540.1	25	5.98
NADH	664.4	25	8.95
Glycolysis intermediate			
glucose	179.0	15	2.24
Lactate	89.0	13	7.32
R-5-P	229.0	13	8.33
DHAP	169.2	11	8.41
pyruvate	987.1	14	10.19
G-6-P	259.1	15	10.45
F-6-P	259.1	15	10.88
F-1,6-BP	339.2	13	13.21
NOG derivatives			
NOG	146	12	10.35
NOG	146>74	23	10.35
DMOG	160>88	34	10.66
NAA	160	12	10.44
DMNOF	192.2	12	12.11

Table 8-9: Mass spectrometer parameters for SIR mode of detection of the non-derivatised TCA cycle intermediates. Metabolites (Glu) glutamine, (Gln) glutamate, (Asp) aspartate, (SA) succinate, (Mat) malate, (isocit) isocitrate, (2-HG) 2-hydroxyglutate, (2-OG) 2-oxoglutarate, (cit) citrate, (fum) fumarate, Glucose-6-phosphate (G-6-P), Fructose-6- phosphate (F-6-P), Fructose-1, 6-bisphosphate (F-1, 6-BP), Dihydroxyacetone phosphate (DHAP), Ribulose-5-phosphate (R- 5-P).

8.7. Samples Extraction and Purification

8.7.1. Cells Extraction For Quantify TCA Cycle And Associated Intermediate

LN18 cells were grown in liquid culture, 60 µL of extraction solvent (80/% methanol / 20% water; v/v) was added to the collected cell pellet to quench metabolism and initiate the extraction process. The mixture was spun in a Microfuge machine for 10 min at maximum speed and 5 °C to separate extracted pellet from the extracted metabolites. The resulting pellet was then re-extracted twice with 60 µL of solvent at 4 °C. Both of the supernatants were combined to yield 120 µL of final extract. The resulting 120 µL volume was split into two microcentrifuge tubes and spun in a microfuge for 10 min at maximum speed and 5 °C, and freeze-dry at -40 °C were then analyzed separately in three different injections by LC/MS and GCMS.

8.7.2. Tissues Extraction For Quantify 2-HG

A section of tumour sample was cut appropriately (work Carried out be Sarah); the mass was determined and the sample was cooling on ice. Twice the tumour mass (w/v) of ice-cold 0.6 M perchloric acid (PCA) was then added with cooling. Taking care to keep the sample cold, the sample was ground thoroughly using a hand-held homogeniser, transferred to a cold microcentrifuge tube and centrifuged (20,000g, 5 min, 4°C). The supernatant was then transferred to a fresh, cold microcentrifuge tube. Pre-chilled 2 M KHCO3 was added until the pH reached 7. The sample was centrifuged (20,000g, 5 min, 4°C) to remove precipitate; the supernatant was transferred to a fresh microcentrifuge tube and used for LC/MS. For LC-MS measurements, the sample was lyophilised (overnight); the dried residue was then dissolved in 20 µl of mobile phase A, transferred to a recovery vial, and analysed in three different injections.

8.7.3. U87 Cells Extraction For Quantify Glycolysis And Associated Intermediate

U87 cells were were transfected with siRNA in 10 cm dishes (500,000 cells per dish), according to the standard protocol, to provide a scramble Control, PFKFB3 knockdown, PFKFB4 knockdown and a double PFKFB3/PFKFB4 knockdown. 8 identical plates for each condition were set up and incubated overnight at 37 ºC. The media was then aspirated and replaced with 15 mL fresh media (DMEM), before transferring half of the plates to the hypoxic incubator (0.1% O_2). Plates were incubated for a further 48 hours, the media was aspirated and one set of plates counted. The remaining set (3 per condition) was treated with MeOH : H_2O (4:1, 100 µL), containing 0.5 mM fumaric acid-2,3-d2 standard, and then scraped with a cell scraper. The extracts were then combined and transferred to a 2 mL microcentrifuge tube. After centrifuging (Spectrafuge 16M Microcentrifuge, 14000 rpm, 0 ºC, 5 minutes), the supernatant was transferred to a new tube and stored on dry ice, before freeze-drying and dissolving in mobile phase A (60 µL per sample) immediately prior to analysis.

8.7.4. NOG, NAA, DMOG, and DMNOF Extraction From Leaves Of *R. Rhabarbarum*

Leaves of *R. rhabarbarum* (harvested fresh from a garden in Old Boars Hill, Oxford, OX1 5JJ, U.K.) and *S. oleracea* (obtained from a shop, Oxford, UK) were dried in shade at room temperature for three days. Several extraction protocols were utilized as follows: Methanol extraction: 3g of dried leaves were manually crushed and sonicated in MeOH (30 mL, 80% vol/vol) for 15 min at 25°C. The resultant lysed cell debris was separated by centrifugation (15 min, 13,000 rpm); and the plant extracts were then evaporated to dryness using a rotary evaporator. Water extraction: An identical extraction was used except MeOH was replaced by Milli-Q water (30 mL, 15 min, 25°C). Et2O Extraction: An identical extraction processe to the MeOH protocol above was used with diethylether (Et2O) replacing MeOH. For *R. rhabarbarum*, an extraction process using ethylacetate and hydrochloric acid were also used. Ethylacetate replaced MeOH in the MeOH extraction processe described above. For the acid

extraction 30 mL of 6 M HCl in methanol (1% vol/vol) was heated at 80°C for 30 min with the leaves.

E. coli (strain BW25113) cells, grown to OD600 ~0.7 in 2-TY media at 37°C, were lysed in 1 mL MeOH (80% vol/vol) using a bead-beater (Bertin Precellys 24). Glass beads (0.1-0.5 mm) were used with 10 cycles of 5,000 rpm for 20 sec with intermittent cooling on ice). The sample was then centrifuged (30 min, 15,000 rpm); the extract was isolated from the supernatant by vacuum centrifugation. Human kidney cells (HEK 293T) were also extracted in MeOH (80% vol/vol)(1mL) by sonication as before (5 min, 25°C) followed by centrifugation to give a supernatant; the extract was then used for analysis.

8.7.5. Isolation and Purification of NOG from R. Rhabarbarum Leaves

The experiments were repeated using similar an extraction method to provide water and acid extracts. The crude extract was collected by evaporating the solvent on a rotary evaporator. Characterization of NOG from biological extracts was initially conducted using LC-MS. Eluent from the peak at 10.27 mins was collected from 45 injections. In order to investigate the presence of NOG in the rhubarb extract, purification of the NOG fraction was performed using 40% CH_3CN in water with isocratic elution using an Atlantis dc18 OBD Prep Column;100 Å, 5 µm, 19 mm×100 mm (Waters UK Ltd, Elstree, UK). NOG was collected preparatively on this system from a peak eluting at 16.45mins.

8.8. Cell Culture and In Vitro Techniques

8.8.1. Cell Lines and Media

The U87 cell line was from (Clare Hall laboratories, UK. Roswell Park Memorial Institute-1640); LN18 cell line mutants and non mutants from Dr Chiara Bardella and Prof. Ian Tomlinson lab glioblastoma (Wellcome Trust Centre for Human Genetics, University of Oxford); media and foetal bovine serum (FBS) Gold were both from PAA Laboratories,

Dulbecco's Modified Eagle Medium (DMEM) was from Gibco (Invitrogen, Glasgow, UK). All cell lines were cultured in DMEM media containing 10% FBS and 1% Penicillin-Streptomycin. All plastic ware was purchased from Corning.

8.8.2. Culturing and Passaging Cells

Cells were grown in T175 cell culture flasks and passaged by first aspirating the media, washing with phosphate buffered saline solution (PBS) (10 mL) and incubating with 1x trypsin/ethylenediaminetetraacetic acid (EDTA) solution (3 mL) for 3 minutes. Media (10 mL) was added and the cell suspension transferred to a 50 mL Falcon tube, before being centrifuged (Heraeus Biofuge primo, 1000 rpm, 4 minutes). The supernatant was aspirated and the cell pellet re-suspended in media (1 mL). The suspension was then typically split 1:10 and reseeded in T175 flasks with fresh media (30 mL).

8.8.3. Long-term Cell Storage and Recovery

Cell pellets were prepared as described above and re-suspended in FBS containing 10% DMSO at an approximate density of 2 million cells/mL. The cell suspension was aliquoted in individual cryo-vials (1 mL/vial). The vials were then transferred to a Mr Frosty (Nalgene, Nalge Nunc International Corporation, Rochester, USA) container, insulated with isopropanol, and placed in a -80 ºC freezer, which permitted freezing of the vials at a rate of 1 ºC per minute. Once frozen, cell vials were transferred to liquid nitrogen for long-term storage. To recover the cells, the vials were thawed rapidly using a water bath (37 ºC), before re-suspending in media (10 mL) and centrifuging (Heraeus Biofuge primo, 1000 rpm, 4 minutes). Cell pellets were re-suspended in media and transferred to a T75 cell culture flask with fresh media (20 mL) and incubated overnight. The media was replaced the following day and the cells incubated until reaching confluency. Cells were passaged twice before use in any experiments.

8.8.4. Cell Counting

A Coulter Particle counter Z2 (Beckman Coulter, High Wycombe, UK) was used to count cells. A 400 µL cell suspension was diluted in 19.6 mL isotonic buffered saline solution, and a cell count performed according to the manufacturer's instructions, between the particle size range 9-22 µm.

8.8.5. Hypoxic Exposure

Hypoxic incubations were performed using an INVIVO2 400 hypoxic work station (Pro-Lab Diagnostics, Bromborough, wirral, UK), at 0.1% O_2 / 5% CO_2 / 37 ºC. Cells were allowed to adhere to plates for at least 4 hours after re-seeding, prior to hypoxic exposure. Media changes under hypoxic conditions were performed in the hypoxic chamber, with media that had been equilibrated under hypoxic conditions overnight.

8.9. Cell Treatments

8.9.1. Cells cultured with Inhibitors (AGI-5198) of Mutant IDH1

The LN18 glioblastoma cell line was from Clare Hall laboratories, UK. Roswell Park Memorial Institute-1640, (RPMI) media and foetal bovine serum (FBS) Gold were both from (Invitrogen, Glasgow, UK). Dulbecco's Modified Eagle Medium (DMEM) was from Gibco (Invitrogen, Glasgow, UK). All cell lines were cultured in DMEM media containing 10% FBS and 1% Penicillin-Streptomycin. After 24h of cultured, the cell were then allowed to incubate another 24 hours in fresh media treated with 50 µM of AGI-5198 (Xcess Biosciences Inc., San Diego, US).

8.9.2. Transient siRNA Suppression of Gene Expression

Cells were passaged and counted as described above, using media without penicillin an streptomycin inhibition, then re-suspended at a concentration of 104,167 cells/mL. Oligofectamine™ transfection reagent (Invitrogen, 18 µL/reaction) was diluted in Optimem™ (Invitrogen, Glasgow, UK) (72 µL/reaction), and incubated for 5 minutes at room temperature (RT). Meanwhile, siRNA stock solutions (20 µM, 6 µL/reaction) were diluted in Optimem™ (1.10 mL/reaction), to which the diluted Oligofectamine™ (90 µL/reaction) was added. After incubation for 20 minutes at RT, the solution (1.2 mL) was added to the cell suspension (4.8 mL) in a 10 cm cell culture dish and incubated overnight at 37 ºC (final siRNA concentration 20 nM). The media was then aspirated and replaced with media (15 mL) containing Penicillin-Streptomycin (1%) and the plates treated in accordance with individual experiments. The volumes above are given for 10 cm culture dishes, and were scaled down by 50% for 6 cm dishes.

8.9.3. Transient PFKFB3 and PFKFB4 Over-expression

The U87 cells were plated in 10 cm dishes and incubated until reaching approximately 80% confluency. Prior to transfection, the media was removed and replaced with DMEM media, without penicillin-streptomycin inhibition (5.8 mL). To 3 sterile Eppendorf tubes were added OptimemTM (176 µL) and one of either (1) PFKFB3 human cDNA clone (Origene, SC117283, 8 µL, 0.5 µg/µL), (2) PFKFB4 human cDNA clone (Origene, SC110972, 8 µL, 0.5 µg/µL), or (3) DEPC-treated water (8 µL, Mock). After equilibrating to room temperature, the FuGENE® transfection reagent (16 µL) was added to each eppendorf tube and mixed immediately, taking care not to allow the transfection reagent to touch the sides of the tube. This was incubated at RT for 15 minutes, before adding the entire volume to the 10 cm dishes. Plates were incubated for 24 hours at 37 ºC, before lysing according to the standard protocol.

Appendices

A1: Successful quantification and identification of the TCA-cycle metabolites by LC-MS of LN18 cancer cells.

	Mean concentration (μM)											
LN18 cells	Fumarate	Succinate	Itconitate	Aspartate	Malate	Glutamine	2-OG	Glutamate	2-HG	Cis-Aconitate	Iso-Citrate	Citrate
Untransduced	82	147	23	198	766	581	200	946	1797	11	20	904
IDH1-WT	143	118	21	191	751	613	221	1246	2284	7	16	520
IDH1-R132H	88	92	15	241	436	666	54	1318	16606	5	19	472
IDH1-R132C	123	93	16	233	441	458	42	945	16559	4	16	445
IDH2-WT	138	136	22	192	785	694	231	1335	2657	7	18	524
GFP	123	121	22	200	808	646	210	1322	1637	8	12	725
IDH2-R172K	62	137	24	207	845	654	85	1038	19624	8	17	760
IDH2-R172M	138	114	19	222	612	616	83	1132	15499	6	15	542

A2: Calibration curve constructed from the triplicate LC/MS analysis of NOG. The calibration curve was used to determine the absolute amount of NOG in Spinach and Rhubarb leaves. The straight line provided an R^2 value of 0.998 over the range 10-1000 µM.

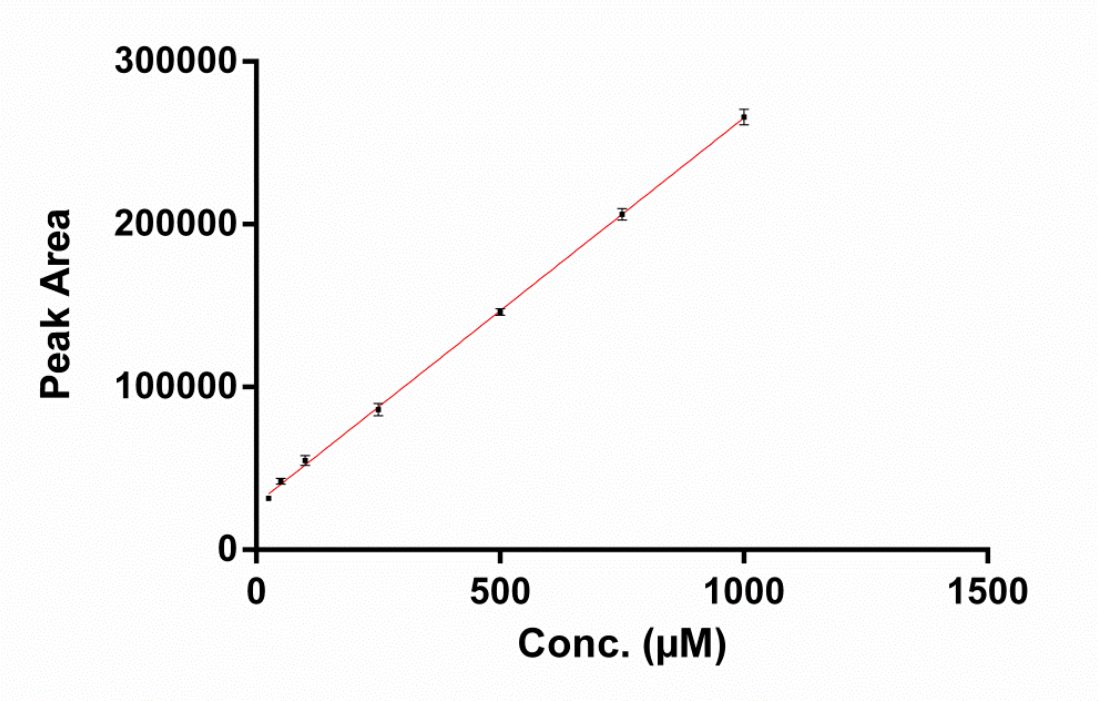

A3: Standard curves showing a linear relationship between metabolite concentration and relative area units in LC-MS assays.

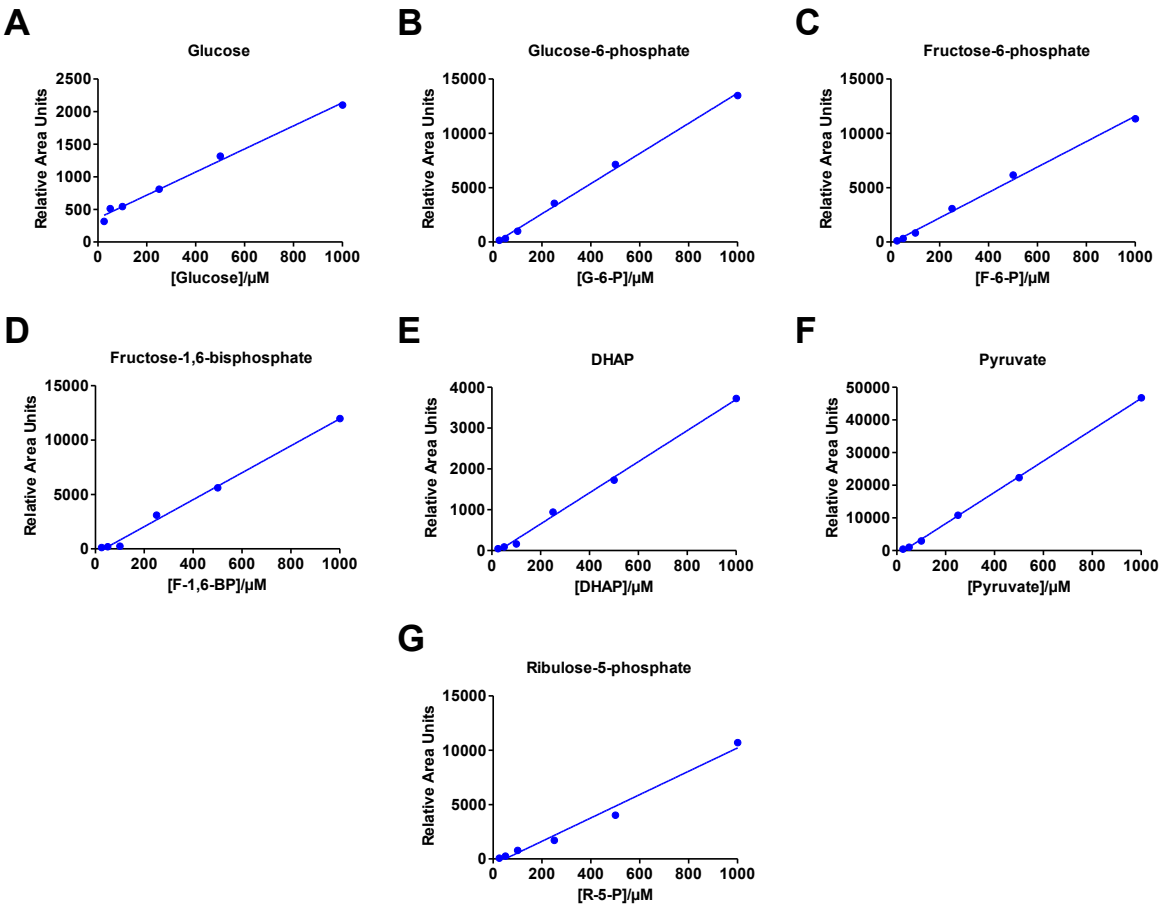

References

Aba et al., (2006). “Oxidative metabolism in cultured rat astroglia: effects of reducing the glucose concentration in the culture medium and of D-aspartate or potassium stimulation.” J Cereb Blood Flow Metab. **26**(2):153-160.

Aik et al., (2013). "Structural basis for inhibition of the fat mass and obesity associated protein (FTO)." J Med Chem **56**(9):3680-8.

Albers et al., (1998). "Distribution of 14C-labelled carbon from glucose and glutamate during anaerobic growth of Saccharomyces cerevisiae." Microbiology. 144(Pt 6):1683–1690.

Antignac et al., (2005). “The ion suppression phenomenon in liquid chromatography mass spectrometry and its consequences in the field of residue analysis.” Anal Chim Acta **529**(1):129 – 136.

Antonelli, M., Buttarelli, F.R., et al. (2010). "Prognostic significance of histological grading, p53 status, YKL-40 expression, and IDH1 mutations in pediatric high-grade gliomas." J Neurooncol **99**(2): 209-215

Antonio et al., (2008). “Hydrophilic interaction chromatography/electrospray mass spectrometry analysis of carbohydrate-related metabolites from Arabidopsis thaliana leaf tissue.” Rapid Commun Mass Spectrom. **22**(9):1399-407.

Araujo et al., (2010). "Identification of the 2-hydroxyglutarate and isovaleryl-CoA dehydrogenases as alternative electron donors linking lysine catabolism to the electron transport chain of Arabidopsis mitochondria." Plant Cell. 22(5):1549–1563.

Atsumi, T., J. Chesney, et al. (2002). "High expression of inducible 6-phosphofructo-2-kinase/fructose-2,6-bisphosphatase (iPFK-2; PFKFB3) in human cancers." Cancer Research **62**(20): 5881-5887.

Baba et al., (2006). "Construction of Escherichia coli K-12 in-frame, single-gene knockout mutants: the Keio collection." Molecular Systems Biology 2006. 2. 2006.0008.

Bailey, J.M., & Colman, R.F. (1985). "Affinity labeling of NADP+-specific isocitrate dehydrogenase by a new fluorescent nucleotide analogue, 2-[(4-bromo-2,3-dioxobutyl)thio]-1,N6-ethenoadenosine 2',5'-bisphosphate." Biochemistry **24** (20):5367-77.

Bajad et al., (2006). “Separation and quantitation of water soluble cellular metabolites by hydrophilic interaction chromatography-tandem mass spectrometry.” J Chromatogr A. **1125**(1):76-88.

Balss, J., Meyer, J., et al. (2008). "Analysis of the IDH1 codon 132 mutation in brain tumors." Acta Neuropathol **116**(6):597-602

Bando, H., T. Atsumi, et al. (2005). "Phosphorylation of the 6-phosphofructo-2-kinase/fructose 2,6-bisphosphatase/PFKFB3 family of glycolytic regulators in human cancer." Clin Cancer Res **11**(16): 5784-5792.

Bartha and G. Vigh. (1983). "Studies in reversed-phase ion-pair chro-matography: I. Adsorption isotherms of tetraalkylammonium ion- pair reagents on Lichrosorb RP-18 in methanol-water eluents." J. Chromatogr 260(2):337–345.

Bartha et al., (1984). "Studies in reversed- phase ion-pair chromatography: IV. The role of the chain length of the pairing ion." J. Chromatogr. 291:91–102.

Bartha, et al., (1990). "Extension of the electrostatic retention model of reversed-phase ion-pair chromatography to include the simultaneous effects of the organic modifier and the pairing ion." J. Chromatogr 506:85–96.

Bartrons, R. and J. Caro. (2007). "Hypoxia, glucose metabolism and the Warburg's effect." J Bioenerg Biomembr **39**(3): 223-229.

Becker et al., (2012). “LC-MS-based metabolomics in the clinical laboratory.” J Chromatogr B Analyt Technol Biomed Life Sci. **1**(883-884): 68-75.

Begley, P., et al., (2009). "Development and Performance of a Gas Chromatography−Time-of-Flight Mass Spectrometry Analysis for Large-Scale Nontargeted Metabolomic Studies of Human Serum." Anal. Chem. 81(16):7038-7046.

Bertout, J. A., S. A. Patel, et al. (2008). "The impact of O2 availability on human cancer." Nat Rev Cancer **8**(12): 967-975.

Bhujwalla, Z. M., D. Artemov, et al. (2002). "Combined vascular and extracellular pH imaging of solid tumors." NMR Biomed **15**(2): 114-119.

Birkler et al., (2010). " A UPLC-MS/MS application for profiling of intermediary energy metabolites in microdialysis samples--a method for high-throughput." J Pharm Biomed Anal. 53(4):983-90.

Bleeker, F.E., Lamba, S., et al. (2009). "IDH1 mutations at residue p.R132 (IDH1(R132)) occur frequently in high-grade gliomas but not in other solid tumors." Hum Mutat **30**(1):7-11.

Bobarykina, A. Y., D. O. Minchenko, et al. (2006). "Hypoxic regulation of PFKFB-3 and PFKFB-4 gene expression in gastric and pancreatic cancer cell lines and expression of PFKFB genes in gastric cancers." Acta Biochim Pol **53**(4): 789-799.

Brizel, D. M., S. P. Scully, et al. (1996). "Tumor oxygenation predicts for the likelihood of distant metastases in human soft tissue sarcoma." Cancer Research **56**(5): 941-943.

Brown, J. M. and A. J. Giaccia (1998). "The unique physiology of solid tumors: Opportunities (and problems) for cancer therapy." Cancer Research **58**(7): 1408-1416.

Brown, J. M. and W. R. William (2004). "Exploiting tumour hypoxia in cancer treatment." Nature Reviews Cancer **4**(6): 437-447.

Buchholz et al., (1995). “Quantification of intracellular metabolites in Escherichia coli K12 using liquid chromatographic-electrospray ionization tandem mass spectrometric techniques.” Anal Biochem. **295**(2):129-37.

Buscher et al., (2009). "Cross-Platform Comparison of Methods for Quantitative Metabolomics of Primary Metabolism." Anal. Chem. 81(61):2135-2143.

Buzzai, M., R. G. Jones, et al. (2007). "Systemic treatment with the antidiabetic drug metformin selectively impairs p53-deficient tumor cell growth." Cancer Res **67**(14): 6745-6752.

Bylund et al., (2007). " Analysis of low molecular mass organic acids in natural waters by ion exclusion chromatography tandem mass spectrometry." J Chromatogr A. 1176(1-2):89-93.

Capper, D., Zentgraf, H., et al. (2009). "Monoclonal antibody specific for IDH1 R132H mutation." Acta Neuropathol **118**(5):599-601.

Ceccarelli, C., Grodsky, N.B., et al. (2002). "Crystal structure of porcine mitochondrial NADP+-dependent isocitrate dehydrogenase complexed with Mn2+ and isocitrate. Insights into the enzyme mechanism." J Biol Chem **277**(45):43454-62.

Cech and Enke. (2000). “Relating electrospray ionization response to nonpolar character of small peptides.” Anal. Chem. **72**(13):2717–2723.
Cell Research **23**:975-977.

Chabner, B. A. and T. G. Roberts, Jr. (2005). "Timeline: Chemotherapy and the war on cancer." Nat Rev Cancer **5**(1): 65-72.

Chen, C. Y. and A. B. Shyu (1995). "AU-rich elements: characterization and importance in mRNA degradation." Trends Biochem Sci **20**(11): 465-470.

Chesney, J., R. Mitchell, et al. (1999). "An inducible gene product for 6-phosphofructo-2-kinase with an AU-rich instability element: Role in tumor cell glycolysis and the Warburg effect." Proceedings of the National Academy of Sciences of the United States of America **96**(6): 3047-3052.

Chingin et al., (2009). “Detection of Diethyl Phthalate in Perfumes by Extractive Electrospray Ionization Mass Spectrometry.” Anal. Chem. **81**(1):123-129.
Choi et al., (2012). Measuring Complete Isotopomer Distribution of Aspartate Using Gas Chromatography/Tandem Mass Spectrometry." Anal. Chem. 84 (10):4628–4632.
Chowdhury et al., (2011). “The oncometabolite 2-hydroxyglutarate inhibits histone lysine demethylases. EMBO Rep. **12**(5):463-9.
Christensen, B.C., Smith, A.A., et al. (2011). "DNA methylation, isocitrate dehydrogenase mutation, and survival in glioma." J Natl Cancer Inst **103**(2):143-53.
Clement et al., (2002). “The antifungal drug ciclopirox inhibits deoxyhypusine and proline hydroxylation, endothelial cell growth and angiogenesis in vitro.” International Journal of Cancer **100**(4):491-498.
Cockman, M. E., N. Masson, et al. (2000). "Hypoxia inducible factor-alpha binding and ubiquitylation by the von Hippel-Lindau tumor suppressor protein." Journal of Biological Chemistry **275**(33): 25733-25741.
Comte et al., (1997). "A 13C mass isotopomer study of anaplerotic pyruvate carboxylation in perfused rat hearts." J. Biol. Chem. 272 (42):26125– 26131.
Coote and Kirsop. (1974). "The content of some organic acids in beer and other fermented media." J. Inst. Brew. 80(5):474–483.
Craig et al., (2005). “Three-tesla imaging of the knee: initial experience.” Skeletal Radiol. **34**(8):453-461.
Cruz et al., (2008). “Metabolite profiling of Calvin cycle intermediates by HPLC-MS using mixed-mode stationary phases.” Plant J. **55**(6):1047-60.
Cunliffe et al., (1992). “Novel inhibitors of prolyl 4-hydroxylase. 3. Inhibition by the substrate analogue N-oxaloglycine and its derivatives.” J Med Chem. **35**(14): 2652-2658.
Cunningham, J. T., J. T. Rodgers, et al. (2007). "mTOR controls mitochondrial oxidative function through a YY1-PGC-1alpha transcriptional complex." Nature **450**(7170): 736-740.
Currie, C. J., C. D. Poole, et al. (2012). "Mortality after incident cancer in people with and without type 2 diabetes: impact of metformin on survival." Diabetes Care **35**(2): 299-304.
Cuzick, J., I. Sestak, et al. (2013). "Selective oestrogen receptor modulators in prevention of breast cancer: an updated meta-analysis of individual participant data." Lancet **381**(9880): 1827-1834.
Dang, L., White, D.W., et al. (2010). "Cancer-associated IDH1 mutations produce 2-hydroxyglutarate." Nature **465**(7300):966.
dasNeves et al., (1996). "New method for the chiral HRGC assay of L-2-hydroxyglutaric aciduria in urine." J High Res Chromatogr 19(3):161– 164.
DeBerardinis, R. J., A. Mancuso, et al. (2007). "Beyond aerobic glycolysis: transformed cells can engage in glutamine metabolism that exceeds the requirement for protein and nucleotide synthesis." Proc Natl Acad Sci U S A **104**(49): 19345-19350.
Derrmer et al., (2007). “Mass spectrometry-based metabolomics.” Mass Spectrom Rev. **26**(1): 51-78.
Dewhirst, M. W. (1998). "Concepts of oxygen transport at the microcirculatory level." Seminars in Radiation Oncology **8**(3): 143-150.
Dowling, R. J., P. J. Goodwin, et al. (2011). "Understanding the benefit of metformin use in cancer treatment." BMC Med **9**: 33.
Downward, J. (2003). "Targeting RAS signalling pathways in cancer therapy." Nat Rev Cancer **3**(1): 11-22.
Druker, B. J., C. L. Sawyers, et al. (2001). "Activity of a specific inhibitor of the BCR-ABL tyrosine kinase in the blast crisis of chronic myeloid leukemia and acute

lymphoblastic leukemia with the Philadelphia chromosome." N Engl J Med **344**(14): 1038-1042.
Druker, B. J., S. Tamura, et al. (1996). "Effects of a selective inhibitor of the Abl tyrosine kinase on the growth of Bcr-Abl positive cells." Nat Med **2**(5): 561-566.
Druker, B. J., S. Tamura, et al. (1996). "Effects of a selective inhibitor of the Abl tyrosine kinase on the growth of Bcr-Abl positive cells." Nat Med **2**(5): 561-566.
Dubbink, H.J., Taal, W., et al. (2009). "IDH1 mutations in low-grade astrocytomas predict survival but not response to temozolomide." Neurology **73**(21):1792-5.
Dummer, R. and K. T. Flaherty (2012). "Resistance patterns with tyrosine kinase inhibitors in melanoma: new insights." Curr Opin Oncol **24**(2): 150-154.
Dunn, W.B., et al., (2006). "Closed-Loop, Multiobjective Optimization of Two-Dimensional Gas Chromatography/Mass Spectrometry for Serum Metabolomics." Anal Chem. 79(2):464-476.
Edwards et al., (2007). "Effect of decreasing column inner diameter and use of off-line two-dimensional chromatography on metabolite detection in complex mixtures." J Chromatogr A. 1172(2):127-134.
Ekborg-ott et al., (1998). " Highly enantioselective HPLC separations using the covalently bonded macrocyclic antibiotic, ristocetin A, chiral stationary phase." Chirality. 10(5):434-83.
Eksborg, S. and Schill, G. (1973). "Ion Pair Partition Chromatography of Organic Ammonium Compounds." Anal. Chem. 45(12):2092-2100.
Elstrom, R. L., D. E. Bauer, et al. (2004). "Akt stimulates aerobic glycolysis in cancer cells." Cancer Res **64**(11): 3892-3899.
Ema, M., S. Taya, et al. (1997). "A novel bHLH-PAS factor with close sequence similarity to hypoxia-inducible factor 1alpha regulates the VEGF expression and is potentially involved in lung and vascular development." Proc Natl Acad Sci U S A **94**(9): 4273-4278.
Engqvist et al., (2011). "Plant D-2-hydroxyglutarate dehydrogenase participates in the ca- tabolism of lysine especially during senescence. J. Biol. Chem. **286**(13):11382–11390.
Fairchild et al., (2010). "Two-dimensional liquid chromatography/mass spectrometry/mass spectrometry separation of water-soluble metabolites." J Chromatogr A. **1217**(52):8161-8166.
Farber, S. and L. K. Diamond (1948). "Temporary remissions in acute leukemia in children produced by folic acid antagonist, 4-aminopteroyl-glutamic acid." N Engl J Med **238**(23): 787-793.
Farber, S., E. C. Cutler, et al. (1947). "The Action of Pteroylglutamic Conjugates on Man." Science **106**(2764): 619-621.
Farré et al., (2007). "Recently developed GC/MS and LC/MS methods for determining NSAIDs in water samples." Anal. Bioanal. Chem. **387**(4):1203–1214.
Feurle et al., (1998). “Analysis of phosphorylated carbohydrates by high-performance liquid chromatography–electrospray ionization tandem mass spectrometry utilising a β-cyclodextrin bonded stationary phase.” Journal of Chromatography A **803**(1): 111-119.
Fiehn, O. (2002). "Metabolomics – the link between genotypes and phenotypes." Plant Molecular Biology. **48**(1-2):155-171.
Figueroa, M.E., Abdel-Wahab, O., et al. (2010a). "Leukemic IDH1 and IDH2 mutations result in a hypermethylation phenotype, disrupt TET2 function, and impair hematopoietic differentiation." Cancer Cell **18**(6):553-67.
Figueroa, M.E., Lugthart, S., et al. (2010b). "DNA methylation signatures identify biologically distinct subtypes in acute myeloid leukemia." Cancer Cell **17**(1):13-27.
Fischer, K., P. Hoffmann, et al. (2007). "Inhibitory effect of tumor cell-derived lactic acid on human T cells." Blood **109**(9): 3812-3819.

Fleischer, M., R. Kessler, et al. (2011). "LOH on 10p14-p15 targets the PFKFB3 gene locus in human glioblastomas." Genes Chromosomes Cancer **50**(12): 1010-1020.
Frame, F. M. and N. J. Maitland (2011). "Cancer stem cells, models of study and implications of therapy resistance mechanisms." Adv Exp Med Biol **720**: 105-118.
Francine et al., (2013). "Differentiation therapy for IDH1/2 mutant malignancies." Cell Research **23**:975–977
Frank, N. Y., T. Schatton, et al. (2010). "The therapeutic promise of the cancer stem cell concept." J Clin Invest **120**(1): 41-50.
Fukunaga et al., (1978). "The differential effects of TCA-cycle acids on the growth of plant cells cultured in liquid media containing various nitrogen sources." Planta.**139**(3):199-202.
Garcia-Cao, I., M. S. Song, et al. (2012). "Systemic elevation of PTEN induces a tumor-suppressive metabolic state." Cell **149**(1): 49-62.
Garrett, C. R., H. M. Hassabo, et al. (2012). "Survival advantage observed with the use of metformin in patients with type II diabetes and colorectal cancer." Br J Cancer **106**(8): 1374-1378.
Garrett, C. R., H. M. Hassabo, et al. (2012). "Survival advantage observed with the use of metformin in patients with type II diabetes and colorectal cancer." Br J Cancer **106**(8): 1374-1378.
Gatenby, R. A. and R. J. Gillies (2004). "Why do cancers have high aerobic glycolysis?" Nature Reviews Cancer **4**(11): 891-899.
Gerlinger, M., A. J. Rowan, et al. (2012). "Intratumor heterogeneity and branched evolution revealed by multiregion sequencing." N Engl J Med **366**(10): 883-892.
Ghassempour et al., (2004). "Monitoring of the fermentation media of citric acid by the trimethylsilyl derivatives of the organic acids formed." J. Agric. Food Chem. **52**(21):6384–6388.
Gibney, M.J., et al., (2005). "Metabolomics in human nutrition: opportunities and challenges." Am J Clin Nutr. **82**(3):497-503.
Gibson et al., (1993). "Stable-isotope dilution analysis of D- and L-2-hydroxyglutaric acid: application to the detection and prenatal diagnosis of D- and L-2-hydroxyglutaric acidemias." Pediatr Res. **34**(3):277– 80.
Gillies, R. J. and R. A. Gatenby (2007). "Adaptive landscapes and emergent phenotypes: why do cancers have high glycolysis?" J Bioenerg Biomembr **39**(3): 251-257.
Gillies, R. J., D. Verduzco, et al. (2012). "Evolutionary dynamics of carcinogenesis and why targeted therapy does not work." Nat Rev Cancer **12**(7): 487-493.
Gilman, A. and F. S. Philips (1946). "The Biological Actions and Therapeutic Applications of the B-Chloroethyl Amines and Sulfides." Science **103**(2675): 409-436.
Giroux, S. (2013). "Overcoming acquired resistance to kinase inhibition: the cases of EGFR, ALK and BRAF." Bioorg Med Chem Lett **23**(2): 394-401.
Goidts, V., J. Bageritz, et al. (2012). "RNAi screening in glioma stem-like cells identifies PFKFB4 as a key molecule important for cancer cell survival." Oncogene **31**(27): 3235-3243.
Gold et al., (2004). "Musculoskeletal MRI at 3.0 T: Relaxation Times and Image Contrast." AJR Am J Roentgenol. **183**(2):343-51.
Gomez, M., A. Manzano, et al. (2012). "Sertoli-secreted FGF-2 induces PFKFB4 isozyme expression in mouse spermatogenic cells by activation of the MEK/ERK/CREB pathway." Am J Physiol Endocrinol Metab **303**(6): E695-707.
Goodman, L. S., M. M. Wintrobe, et al. (1946). "Nitrogen mustard therapy; use of methyl-bis (beta-chloroethyl) amine hydrochloride and tris (beta-chloroethyl) amine hydrochloride for Hodgkin's disease, lymphosarcoma, leukemia and certain allied and miscellaneous disorders." J Am Med Assoc **132**: 126-132.

Goren, N., A. Manzano, et al. (2000). "6-Phosphofructo-2-kinase/fructose-2,6-bisphosphatase expression in rat brain during development." Brain Res Mol Brain Res **75**(1): 138-142.
Graeber, T. G., C. Osmanian, et al. (1996). "Hypoxia-mediated selection of cells with diminished apoptotic potential in solid tumours." Nature **379**(6560): 88-91.
Grassian et al., (2014). "IDH1 mutations alter citric acid cycle metabolism and increase dependence on oxidative mitochondrial metabolism." Cancer Res. **74**(12):3317-3331.
Gray, L. H., A. D. Conger, et al. (1953). "The concentration of oxygen dissolved in tissues at the time of irradiation as a factor in radiotherapy." British Journal of Radiology **26**(312): 638-648.
Gregersen et al., (1977). "Low molecular weight organic acids in the urine of the newborn." Acta Paediatr Scand. **66**(1): 85–89.
Griffin, J. L. and R. A. Kauppinen (2007). "Tumour metabolomics in animal models of human cancer." J Proteome Res **6**(2): 498-505.
Gross et al., (2010). "Cancer-associated metabolite 2-hydroxyglutarate accumulates in acute myelogenous leukemia with isocitrate dehydrogenase 1 and 2 mutations." J Exp Med. **207**(2):339–344.
Gu, Y. Z., S. M. Moran, et al. (1998). "Molecular characterization and chromosomal localization of a third alpha-class hypoxia inducible factor subunit, HIF3alpha." Gene Expr **7**(3): 205-213.
Guppy, M., P. Leedman, et al. (2002). "Contribution by different fuels and metabolic pathways to the total ATP turnover of proliferating MCF-7 breast cancer cells." Biochem J **364**(Pt 1): 309-315.
Haliloglu, G., Jobard, F., et al. (2008). "L-2- hydroxyglutaric aciduria and brain tumors in children with mutations in the L2HGDH gene: neuroimaging findings." Neuropediatrics **39**(2):119-22.
Hamilton, J. A., M. J. Callaghan, et al. (1997). "Identification of PRG1, a novel progestin-responsive gene with sequence homology to 6-phosphofructo-2-kinase/fructose-2,6-bisphosphatase." Mol Endocrinol **11**(4): 490-502.
Han et al., (2013). " Metabolomic analysis of key central carbon metabolism carboxylic acids as their 3-nitrophenylhydrazones by UPLC/ESI-MS." Electrophoresis. 34(19):2891-900.
Hanahan, D. and R. A. Weinberg (2000). "The hallmarks of cancer." Cell **100**(1): 57-70.
Hanahan, D. and R. A. Weinberg (2011). "Hallmarks of cancer: the next generation." Cell **144**(5): 646-674.
Hara, S., J. Hamada, et al. (2001). "Expression and characterization of hypoxia-inducible factor (HIF)-3alpha in human kidney: suppression of HIF-mediated gene expression by HIF-3alpha." Biochem Biophys Res Commun **287**(4): 808-813.
Harris, A. L. (2002). "Hypoxia - A key regulatory factor in tumour growth." Nature Reviews Cancer **2**(1): 38-47.
Hartmann et al., (2009). "Type and frequency of IDH1 and IDH2 mutations are related to astrocytic and oligodendroglial differentiation and age: A study of 1,010 diffuse gliomas." Acta Neuropathol **118**(4):469–474.
Hartong et al., (2008). "Insights from retinitis pigmentosa into the roles of isocitrate dehydrogenases in the Krebs cycle." Nat Genet. **40**(10):1230-1234.
Haselbeck & McAlister-Henn., (1993). "Function and expression of yeast mitochondrial NAD- and NADP-specific isocitrate dehydrogenases." J Biol Chem. **268**(16) :12116-12122.
Haselbeck et al., (1992). "Isolation and sequence of a cDNA encoding porcine mitochondrial NADP-specific isocitrate dehydrogenase." Biochemistry. **31** (27):6219-6223.
Hegi et al., (2005). "MGMT gene silencing and benefit from temozolomide in glioblastoma." N Engl J Med. **352**(10):997-1003.

Helmlinger, G., F. Yuan, et al. (1997). "Interstitial pH and pO2 gradients in solid tumors in vivo: high-resolution measurements reveal a lack of correlation." Nat Med **3**(2): 177-182.
Henke et al., (1998). "IDP3 encodes a peroxisomal NADP-dependent isocitrate dehydrogenase required for the beta- oxidation of unsaturated fatty acids." J Biol Chem. **273**(6):3702-3711.
Higashide et al., (1985). "Alahopcin, a new dipeptide antibiotic produced by Streptomyces albulus subsp. ochragerus subsp. nov." J Antibiot (Tokyo) **38**(3): 285-95.
Hirata, T., M. Kato, et al. (1998). "Expression of human placental-type 6-phosphofructo-2-kinase/fructose 2,6-bisphosphatase in various cells and cell lines." Biochem Biophys Res Commun **242**(3): 680-684.
Hopkinson et al., (2013). "5-Carboxy-8-hydroxyquinoline is a broad spectrum 2-oxoglutarate oxygenase inhibitor which causes iron translocation." Chemical Science **4**(8):3110-3117.
Howell, A. and D. G. Evans (2013). "Breast cancer prevention: SERMs come of age." Lancet **381**(9880): 1795-1797.
Hu, C. J., L. Y. Wang, et al. (2003). "Differential roles of hypoxia-inducible factor 1alpha (HIF-1alpha) and HIF-2alpha in hypoxic gene regulation." Mol Cell Biol **23**(24): 9361-9374.
Huang, L. E., J. Gu, et al. (1998). "Regulation of hypoxia-inducible factor 1 alpha is mediated by an O-2-dependent degradation domain via the ubiquitin-proteasome pathway." Proceedings of the National Academy of Sciences of the United States of America **95**(14): 7987-7992.
Huang, L. E., Z. Arany, et al. (1996). "Activation of hypoxia-inducible transcription factor depends primarily upon redox-sensitive stabilization of its alpha subunit." J Biol Chem **271**(50): 32253-32259.
Huang, X., and Regnier, F.E. (2007). "Differential Metabolomics Using Stable Isotope Labeling and Two-Dimensional Gas Chromatography with Time-of-Flight Mass Spectrometry." Anal. Chem. 80(1):107-114.
Huck, J. H., E. A. Struys, et al. (2003). "Profiling of pentose phosphate pathway intermediates in blood spots by tandem mass spectrometry: application to transaldolase deficiency." Clin Chem **49**(8): 1375-1380.
Hung and Taylor (1981). "Ion-exchange-desolvation mechanism on octadecyl silica using anionic hydrophobic pairing ions." J. Chromatogr 209:175–190.
Hunnewell and Forbes. (2010). "Active and Inactive Metabolic Pathways in Tumor Spheroids: Determination by GC-MS." Biotechnology Progress **26**(3): 789-796.
Hutton et al., (1966). "Requirements for α-ketoglutarate, ferrous ion and ascorbate by collagen proline hydroxylase." Biochemical and Biophysical Res Communications **24**(2):179-184.
Hutton et al., (1967). "Conversion of the amino acid sequence Gly-Pro-Pro in protein to Gly-Pro-Hyp by collagen proline hydroxylase." Archives of Biochemistry and Biophysics **121**(2):384-391.
Ichimura et al., (2009). "IDH1 mutations are present in the majority of common adult gliomas but rare in primary glioblastomas." Neuro Oncol. **11**(4):341-347.
Israelsen, W. J. and M. G. Vander Heiden (2010). "ATP consumption promotes cancer metabolism." Cell **143**(5): 669-671.
Ivan, M., K. Kondo, et al. (2001). "HIFalpha targeted for VHL-mediated destruction by proline hydroxylation: implications for O2 sensing." Science **292**(5516): 464-468.
Iwai, K., K. Yamanaka, et al. (1999). "Identification of the von Hippel-lindau tumor-suppressor protein as part of an active E3 ubiquitin ligase complex." Proc Natl Acad Sci U S A **96**(22): 12436-12441.

Jaakkola, P., D. R. Mole, et al. (2001). "Targeting of HIF-alpha to the von Hippel-Lindau ubiquitylation complex by O2-regulated prolyl hydroxylation." Science **292**(5516): 468-472.
Jaffe, N., E. Frei, 3rd, et al. (1974). "Adjuvant methotrexate and citrovorum-factor treatment of osteogenic sarcoma." N Engl J Med **291**(19): 994-997.
Jain et al., (2012). "Metabolite Profiling Identifies a Key Role for Glycine in Rapid Cancer Cell Proliferation." Science. **336**(6084):1040-1044.
Jain, R. K. (2005). "Normalization of tumor vasculature: an emerging concept in antiangiogenic therapy." Science **307**(5706): 58-62.
Jansen and Louis., (2010). "Molecular pathology in adult gliomas: Diagnostic, prognostic, and predictive markers." Lancet Neurol. **9**(7):717-26.
Jennings et al., (1994). "Cytosolic NADP(+)-dependent isocitrate dehydrogenase. Isolation of rat cDNA and study of tissue-specific and developmental expression of mRNA." J Biol Chem. **269**(37): 23128-23134.
Jennings et al., (1997). "Expression and mutagenesis of mammalian cytosolic NADP+-specific isocitrate dehydrogenase." Biochemistry. **36**(44):13743-13747.
Jensen et al., (2001). "Neonatal screening for galactosemia by quantitative analysis of hexose monophosphates using tandem mass spectrometry: a retrospective study." Clin Chem. **47**(8):1364-72.
Jeong et al., (2007). "Determination of sugar phosphates by high-performance anion-exchange chromatography coupled with pulsed amperometric detection." J Chromatogr A. **1164**(1-2):167-73.
Jin et al., (2011). "2-hydroxyglutarate production, but not dominant negative function, is conferred by glioma-derived NADP-dependent isocitrate dehydrogenase mutations." PLoS One **6**(4): e16812.
Jo et al., (2001). "Control of mitochondrial redox balance and cellular defense against oxidative damage by mitochondrial NADP+-dependent isocitrate dehydrogenase." J Biol Chem. **276**(19): 16168-16176.
Jo et al., (2002). "Cellular defense against UVB-induced phototoxicity by cytosolic NADP(+)-dependent isocitrate dehydrogenase." Biochem Biophys Res Commun. **292**(2): 542-549.
John C. et al., (2007). "The Handbook of Metabonomics and Metabolomics. J.K.N. John C. Lindon, and Elaine Holmes, editor. Netherlands: Elsevier 1-33.
Jones, D. T. and A. L. Harris (2006). "Identification of novel small-molecule inhibitors of hypoxia-inducible factor-1 transactivation and DNA binding." Molecular Cancer Therapeutics **5**(9): 2193-2202.
Jordan, V. C. (2007). "Chemoprevention of breast cancer with selective oestrogen-receptor modulators." Nat Rev Cancer **7**(1): 46-53.
Kaadige, M. R., M. G. Elgort, et al. (2010). "Coordination of glucose and glutamine utilization by an expanded Myc network." Transcription **1**(1): 36-40.
Kang et al., (2009). "Mutational analysis of IDH1 codon 132 in glioblastomas and other common cancers." Int J Cancer. **125**(2): 353-355.
Kasidas and Rose. (1980). "Oxalate Content of Some Common Foods: Determination by an Enzymatic Method." J Hum Nutr. **34**(4):255-66.
Kaunzinger et al., (1996). "Chiral compounds as indicators of inherited metabolic disease. Simultaneous stereodifferentiation of lactic-, 2-hydroxyglutaric- and glyceric acid by enantioselective cGC." Enantiomer. **1**(3):177– 82.
Ke, Q. and M. Costa (2006). "Hypoxia-inducible factor-1 (HIF-1)." Mol Pharmacol **70**(5): 1469-1480.
Kehrer and Lund. (1994). "Cellular reducing equivalents and oxidative stress." Free Radic Biol Med **17**(1): 65-75.
Kelly and Plaut. (1981). "Physical evidence for the dimerization of the triphosphopyridine-specific isocitrate dehydrogenase from pig heart." J Biol Chem. **25**: 6330-334.

Kessler, R. and K. Eschrich (2001). "Splice isoforms of ubiquitous 6-phosphofructo-2-kinase/fructose-2,6-bisphosphatase in human brain." Brain Res Mol Brain Res **87**(2): 190-195.
Kessler, R., F. Bleichert, et al. (2008). "6-Phosphofructo-2-kinase/fructose-2,6-bisphosphatase (PFKFB3) is up-regulated in high-grade astrocytomas." J Neurooncol **86**(3): 257-264.
Kiefer et al., (2008). "Quantitative metabolome analysis using liquid chromatography-high-resolution mass spectrometry." Anal Biochem. **382**(2):94-100.
Kim et al., (2007). "Regulation of singlet oxygen-induced apoptosis by cytosolic NADP+-dependent isocitrate dehydrogenase." Mol Cell Biochem. **302**(1-2): 27-34.
Kim KR, et al., (2000). "Enantiomeric separation and discrimination of 2-hydroxy acids as O-trifluoro- acetylated (S)-(+)-3-methyl-2-butyl esters by achiral dual-capillary column gas chromatography." J Chromatogr A. **874**:91–100.
Kim, J. W., I. Tchernyshyov, et al. (2006). "HIF-1-mediated expression of pyruvate dehydrogenase kinase: a metabolic switch required for cellular adaptation to hypoxia." Cell Metab **3**(3): 177-185.
Kim, S. G., N. P. Manes, et al. (2006). "Crystal structure of the hypoxia-inducible form of 6-phosphofructo-2-kinase/fructose-2,6-bisphosphatase (PFKFB3) - A possible new target for cancer therapy." Journal of Biological Chemistry **281**(5): 2939-2944.
King et al., (2000). "Mechanistic investigation of ionization suppression in electrospray ionization." J Am Soc Mass Spectrom **11**(11):942-950.
Kloosa el at., (2012). "Derivatization of the tricarboxylic acid cycle intermediates and analysis by online solid-phase extraction-liquid chromatography–mass spectrometry with positive-ion electrospray ionization." J Chromatogr A. **1232**:19–26.
Knox and Hartwick. (1981). "Mechanism of ion-pair liquid chro- matography of amines, neutrals, zwitterions and acids using anionic hetaerons." J. Chromatogr. 204:3–21.
Koh et al., (2004). "Cytosolic NADP+-dependent isocitrate dehydrogenase plays a key role in lipid metabolism." J Biol Chem. **279**(38): 39968-39974.
Kolb M, et al., (1993). "Calculation of detection limit, identification limit and determination limit according to DIN 32645 with the aid of a computer program." Acta Hydrochim Hydrobiol. **21**(6):308–311.
Kombu, et al., (2011). "Analysis of the citric acid cycle intermediates using gas chromatography–mass spectrometry." Methods Mol Biol. **708**:147-57.
Kopchick and Hartline. (1979). "Alpha-hydroxyglutarate as an intermediate in the catabolism of alpha-aminoadipate by Pseudomonas putida." J. Biol. Chem. **254**(9):3259–3263.
Koubaa M, et al., (2013). "Highlighting the tricarboxilic acid cycle: liquid and gas chromatography–mass spectrometry analyses of 13C-labeled organic acids." Anal Biochem. **436**(2):151–159.
Kranendijk et al., (2010). "IDH2 mutations in patients with D-2-hydroxyglutaric aciduria." Science. **330**(6002):336.
Krishna, R. and L. D. Mayer (2000). "Multidrug resistance (MDR) in cancer. Mechanisms, reversal using modulators of MDR and the role of MDR modulators in influencing the pharmacokinetics of anticancer drugs." Eur J Pharm Sci **11**(4): 265-283.
Kroemer, G. and J. Pouyssegur (2008). "Tumor cell metabolism: cancer's Achilles' heel." Cancer Cell **13**(6): 472-482.
Kruidenier et al., (2012). "A selective jumonji H3K27 demethylase inhibitor modulates the proinflammatory macrophage response." Nature **488**(7411):404-8.

Kubota et al., (2005). " Development of an HPLC-fluorescence determination method for carboxylic acids related to the tricarboxylic acid cycle as a metabolome tool." Biomed Chromatogr. **19**(10):788-95.
Kuwai, T., Y. Kitadai, et al. (2003). "Expression of hypoxia-inducible factor-l alpha is associated with tumor vascularization in human colorectal carcinoma." International Journal of Cancer **105**(2): 176-181.
Laffaire et al., (2010). "Methylation profiling identifies 2 groups of gliomas according to their tumorigenesis." Neuro Oncol. **13**(1): 84-98.
Lee et al., (2002). "Cytosolic NADP(+)-dependent isocitrate dehydrogenase status modulates oxidative damage to cells." Free Radic Biol Med. **32**(11): 1185-1196.
Lee et al., (2004). "Role of NADP+- dependent isocitrate dehydrogenase (NADP+-ICDH) on cellular defence against oxidative injury by gamma-rays." Int J Radiat Biol. **80**(9): 635-642.
Lei et al., (2011). "Mass spectrometry strategies in metabolomics." J Biol Chem **286**(29): 25435-25442.
Lei, Z., D. V. Huhman, et al. (2011). "Mass spectrometry strategies in metabolomics." J Biol Chem **286**(29): 25435-25442.
Lewis, L. D. (2006). "Cancer pharmacotherapy: 21st century 'magic bullets' and changing paradigms." Br J Clin Pharmacol **62**(1): 1-4.
Li, B., K. Takeda, et al. (2012). "Coordinated expression of 6-phosphofructo-2-kinase/fructose-2,6-bisphosphatase 4 and heme oxygenase 2: evidence for a regulatory link between glycolysis and heme catabolism." Tohoku J Exp Med **228**(1): 27-41.
Li, F., Y. Wang, et al. (2005). "Myc stimulates nuclearly encoded mitochondrial genes and mitochondrial biogenesis." Mol Cell Biol **25**(14): 6225-6234.
Li, T., N. Kon, et al. (2012). "Tumor suppression in the absence of p53-mediated cell-cycle arrest, apoptosis, and senescence." Cell **149**(6): 1269-1283.
Liu, N. and Z. X. Wang (2011). "Kumada Coupling of Aryl, Heteroaryl, and Vinyl Chlorides Catalyzed by Amido Pincer Nickel Complexes." Journal of Organic Chemistry **76**(24): 10031-10038.
Loenarz and Schofield. (2011). “Physiological and biochemical aspects of hydroxylations and demethylations catalyzed by human 2-oxoglutarate oxygenases.” Trends Biochem Sci. **36**(1):7-18.
Lopez et al., (2010). "IDH1(R132) mutation identified in one human melanoma metastasis, but not correlated with metastases to the brain." Biochem Biophys Res Commun. **398**(3): 585-587.
Louis et al., (2007). “The 2007 WHO classification of tumors of the central nervous system.” Acta Neuropathol. **114**(2):97–109.
Lu, W., et al., (2010). "Metabolomic Analysis via Reversed-Phase Ion-Pairing Liquid Chromatography Coupled to a Stand Alone Orbitrap Mass Spectrometer." Anal. Chem. **82**(8):3212- 3221.
Lunt, S. Y. and M. G. Vander Heiden (2011). "Aerobic glycolysis: meeting the metabolic requirements of cell proliferation." Annu Rev Cell Dev Biol **27**: 441-464.
Luo et al., (2007). "Simultaneous determination of multiple intracellular metabolites in glycolysis, pentose phosphate pathway and tricarboxylic acid cycle by liquid chromatography-mass spectrometry." J Chromatogr A. **1147**(2):153-64.
Ma et al., (2009). “A Single Nutrient Feed Supports Both Chemically Defined NS0 and CHO Fed-Batch Processes: Improved Productivity and Lactate Metabolism.” Biotechnol Prog. **25**(5):1353-1363.
Mailloux et al., (2007). "The tricarboxylic acid cycle, an ancient metabolic network with a novel twist." PLoS One. **2**(8): e690.
Mamas et al., (2011). "The role of metabolites and metabolomics in clinically applicable biomarkers of disease." Archives of Toxicology **85**(1):5- 17.

Mantri et al., (2012). “Self-hydroxylation of the splicing factor lysyl hydroxylase, JMJD6.” Med. Chem. Comm **3**:80-85.
Manzano, A., J. L. Rosa, et al. (1998). "Molecular cloning, expression, and chromosomal localization of a ubiquitously expressed human 6-phosphofructo-2-kinase/fructose-2,6-bisphosphatase gene (PFKFB3)." Cytogenetics and Cell Genetics **83**(3-4): 214-217.
Manzano, A., J. X. Perez, et al. (1999). "Cloning, expression and chromosomal localization of a human testis 6-phosphofructo-2-kinase/fructose-2,6-bisphosphatase gene." Gene **229**(1-2): 83-89.
Marcucci et al., (2010). "IDH1 and IDH2 gene mutations identify novel molecular subsets within de novo cytogenetically normal acute myeloid leukemia: a Cancer and Leukemia Group B study." J Clin Oncol. **28**(14): 2348-2355.
Mardis et al., (2009). "Recurring mutations found by sequencing an acute myeloid leukemia genome." N Engl J Med. **361**(11): 1058-1066.
Mardis, E. R., L. Ding, et al. (2009). "Recurring mutations found by sequencing an acute myeloid leukemia genome." N Engl J Med **361**(11): 1058-1066.
Marsin, A. S., C. Bouzin, et al. (2002). "The stimulation of glycolysis by hypoxia in activated monocytes is mediated by AMP-activated protein kinase and inducible 6-phosphofructo-2-kinase." J Biol Chem **277**(34): 30778-30783.
Maschek, G., N. Savaraj, et al. (2004). "2-deoxy-D-glucose increases the efficacy of adriamycin and paclitaxel in human osteosarcoma and non-small cell lung cancers in vivo." Cancer Res **64**(1): 31-34.
Masson, N., C. Willam, et al. (2001). "Independent function of two destruction domains in hypoxia-inducible factor-alpha chains activated by prolyl hydroxylation." EMBO J **20**(18): 5197-5206.
Masui, K., B. Gini, et al. (2013). "A tale of two approaches: complementary mechanisms of cytotoxic and targeted therapy resistance may inform next-generation cancer treatments." Carcinogenesis **34**(4): 725-738.
Matoba, S., J. G. Kang, et al. (2006). "p53 regulates mitochondrial respiration." Science **312**(5780): 1650-1653.
Mattes, W. B., J. A. Hartley, et al. (1986). "DNA sequence selectivity of guanine-N7 alkylation by nitrogen mustards." Nucleic Acids Res **14**(7): 2971-2987.
Matuszewsky et al., (2003). “Strategies for the assessment of matrix effect in quantitative bioanalytical methods based on HPLC–MS/MS.” Anal. Chem. **75** (13):3019–3030.
Maxwell, P. H., M. S. Wiesener, et al. (1999). "The tumour suppressor protein VHL targets hypoxia-inducible factors for oxygen-dependent proteolysis." Nature **399**(6733): 271-275.
McDonough et al., (2005). “Selective Inhibition of Factor Inhibiting Hypoxia-Inducible Factor.” Journal of the American Chemical Society **127**(21):7680-7681.
McDonough et al., (2010). “Structural studies on human 2-oxoglutarate dependent oxygenases.” Current Opinion in Structural Biology **20**(6):659-672.
Melin et al., (1979). "Reversed-phase ion-pair chromatography with an adsorbing stationary phase and a hydrophobic quaternary ammonium ion in the mobile phase: I. Retention studies with tetrabutylammonium as cationic component." J Chromatogr. **185**:225–239.
Mendoza, E. E., M. G. Pocceschi, et al. (2012). "Control of Glycolytic Flux by AMP-Activated Protein Kinase in Tumor Cells Adapted to Low pH." Transl Oncol **5**(3): 208-216.
Meynial et al., (1995). “Simultaneous Separation of Nucleotides and Nucleotide Sugars Using an Ion-Pair Reversed-Phase HPLC: Application for Assaying Glycosyltransferase Activity.” Anal. Chem.**67**(9):1627–1631.
Michelakis, E. D., L. Webster, et al. (2008). "Dichloroacetate (DCA) as a potential metabolic-targeting therapy for cancer." Br J Cancer **99**(7): 989-994.

Minard & McAlister-Henn. (1999). "Dependence of peroxisomal beta-oxidation on cytosolic sources of NADPH." J Biol Chem. **274**(6): 3402-3406.
Minchenko, O. H., A. Ochiai, et al. (2005). "Overexpression of 6-phosphofructo-2-kinase/fructose-2,6-bisphosphatase-4 in the human breast and colon malignant tumors." Biochimie **87**(11): 1005-1010.
Minchenko, O. H., I. L. Opentanova, et al. (2005). "Expression and hypoxia-responsiveness of 6-phosphofructo-2-kinase/fructose-2,6-bisphosphatase 4 in mammary gland malignant cell lines." Acta Biochim Pol **52**(4): 881-888.
Minchenko, O. H., T. Ogura, et al. (2005). "6-Phosphofructo-2-kinase/fructose-2,6-bisphosphatase gene family overexpression in human lung tumor." Ukr Biokhim Zh **77**(6): 46-50.
Minchenko, O. H., T. Ogura, et al. (2005). "Splice isoform of 6-phosphofructo-2-kinase/fructose-2,6-bisphosphatase-4: expression and hypoxic regulation." Mol Cell Biochem **280**(1-2): 227-234.
Minchenko, O., I. Opentanova, et al. (2003). "Hypoxic regulation of the 6-phosphofructo-2-kinase/fructose-2,6-bisphosphatase gene family (PFKFB-1-4) expression in vivo." FEBS Lett **554**(3): 264-270.
Minchenko, O., I. Opentanova, et al. (2004). "Hypoxia induces transcription of 6-phosphofructo-2-kinase/fructose-2,6-biphosphatase-4 gene via hypoxia-inducible factor-1alpha activation." FEBS Lett **576**(1-2): 14-20.
Monton, M.R.N., and Soga, T. (2007). "Metabolome analysis by capillary electrophoresis-mass spectrometry." J Chromatogr A. 1168(1-2):237-46;
Morrison, W. B. (2010). "Cancer chemotherapy: an annotated history." J Vet Intern Med **24**(6): 1249-1262.
Muth A, et al., (2003). "Stereoselective analysis of 2-hydroxysebacic acid in urine of patients with Zellweger syndrome and of premature infants fed with medium-chain triglycerides." J Inherit Metab Dis. **26**(6):583–92.
Nekrutenko et al., (1998). "Cytosolic isocitrate dehydrogenase in humans, mice, and voles and phylogenetic analysis of the enzyme family." Mol Biol Evol. **15**(12): 1674-1684.
Nichols et al., (1993). "Molecular cloning and deduced amino acid sequences of the gamma-subunits of rat and monkey NAD(+)-isocitrate dehydrogenases." Biochem J. **295**(Pt 2): 347-350.
Nichols et al., (1995). "Molecular cloning and deduced amino acid sequences of the alpha- and beta- subunits of mammalian NAD(+)- isocitrate dehydrogenase." Biochem J. **310**(Pt 3): 917-922.
Nicholson et al., (1999). "'Metabonomics': understanding the metabolic responses of living systems to pathophysiological stimuli via multivariate statistical analysis of biological NMR spectroscopic data." Xenobiotica **29**(11):1181-1189.
Niessen et al., (2006). "Matrix effects in quantitative pesticide analysis using liquid chromatography mass spectrometry. Mass Spectrom Rev **25**(6):881–899.
Noushmehr et al., (2010). "Identification of a CpG island methylator phenotype that defines a distinct subgroup of glioma." Cancer Cell. **17**(5): 510-522.
Novellasdemunt, L., L. Bultot, et al. (2013). "PFKFB3 activation in cancer cells by the p38/MK2 pathway in response to stress stimuli." Biochem J **452**(3): 531-543.
Novellasdemunt, L., M. Obach, et al. (2012). "Progestins activate 6-phosphofructo-2-kinase/fructose-2,6-bisphosphatase 3 (PFKFB3) in breast cancer cells." Biochem J **442**(2): 345-356.
Nyhan et al., (1995). "D-2- hydroxyglutaric aciduria." J Child Neurol. 10(2):137-142.
Obach, M., A. Navarro-Sabate, et al. (2004). "6-Phosphofructo-2-kinase (pfkfb3) gene promoter contains hypoxia-inducible factor-1 binding sites necessary for transactivation in response to hypoxia." J Biol Chem **279**(51): 53562-53570.

Oda, T., C. Heaney, et al. (1994). "Crkl is the major tyrosine-phosphorylated protein in neutrophils from patients with chronic myelogenous leukemia." J Biol Chem **269**(37): 22925-22928.
Ohh, M., C. W. Park, et al. (2000). "Ubiquitination of hypoxia-inducible factor requires direct binding to the beta-domain of the von Hippel-Lindau protein." Nat Cell Biol **2**(7): 423-427.
Okamura, N. and R. Sakakibara (1998). "A common phosphorylation site for cyclic AMP-dependent protein kinase and protein kinase C in human placental 6-phosphofructo-2-kinase/fructose-2,6-bisphosphatase." Biosci Biotechnol Biochem **62**(10): 2039-2042.
Okar, D. O., A. Manzano, et al. (2001). "PFK-2/FBPase-2: maker and breaker of the essential biofactor fructose-2, 6-bisphosphate." Trends in Biochemical Sciences **26**(1): 30-35.
Oldiges et al., (2007). "Metabolomics: current state and evolving methodologies and tools." Appl Microbiol Biotechnol. **76**(3): 495-511.
Osborn, M. J., M. Freeman, et al. (1958). "Inhibition of dihydrofolic reductase by aminopterin and amethopterin." Proc Soc Exp Biol Med **97**(2): 429-431.
Overgaard, J. and M. R. Horsman (1996). "Modification of hypoxia-induced radioresistance in tumors by the use of oxygen and sensitizers." Seminars in Radiation Oncology **6**(1): 10-21.
Paavilainen and Korpela. (1993). "Comparison of high-performance liquid and gas-chromatography in the determination of organic-acids in culture media of alkaliphilic bacteria." J. Chromatogr. **634**(2):273–280.
Paradise, R. K., D. A. Lauffenburger, et al. (2011). "Acidic extracellular pH promotes activation of integrin alpha(v)beta(3)." PLoS One **6**(1): e15746.
Park, K. H., S. E. Choi, et al. (2005). "Downregulation of the anaphase-promoting complex (APC)7 in invasive ductal carcinomas of the breast and its clinicopathologic relationships." Breast Cancer Res **7**(2): R238-247.
Parsons et al., (2008). "An integrated genomic analysis of human glioblastoma multiforme." Science. **321**(5897):1807–1812.
Paschka et al., (2010). "IDH1 and IDH2 mutations are frequent genetic alterations in acute myeloid leukemia and confer adverse prognosis in cytogenetically normal acute myeloid leukemia with NPM1 mutation without FLT3 internal tandem duplication." J Clin Oncol. **28**(22): 3636-3643.
Patiar, S. and A. L. Harris (2006). "Role of hypoxia-inducible factor-1 alpha as a cancer therapy target." Endocrine-Related Cancer **13**: S61-S75.
Paugh et al., (2010). "Integrated molecular genetic profiling of pediatric high-grade gliomas reveals key differences with the adult disease." J Clin Oncol. **28**(18): 3061-3068.
Pelicano, H., D. S. Martin, et al. (2006). "Glycolysis inhibition for anticancer treatment." Oncogene **25**(34): 4633-4646.
Peng et al., (2001). "Effects of L- glutamate, D-aspartate, and monensin on glycolytic and oxidative glucose metabolism in mouse astrocyte cultures: further evidence that glutamate uptake is metabolically driven by oxidative metabolism." Neurochem Int. **38**(5):437–43.
Peuhkurinen et al., (1983). " Tricarboxylic acid cycle metabolites during ischemia in isolated perfused rat heart." Am J Physiol. 244(2):H281-8.
Phillips et al., (2006). "Molecular subclasses of high-grade glioma predict prognosis, delineate a pattern of disease progression, and resemble stages in neurogenesis." Cancer Cell. **9**(3): 157-173.
Pierce et al., (2008). "Recent advancements in comprehensive two-dimensional separations with chemometrics." J Chromatogr A. **1184**(1-2):341-352.

Pierotti, M. A., F. Berrino, et al. (2013). "Targeting metabolism for cancer treatment and prevention: metformin, an old drug with multi-faceted effects." Oncogene **32**(12): 1475-1487.
Pollack et al., (2011). "IDH1 mutations are common in malignant gliomas arising in adolescents: a report from the Children's Oncology Group." Childs Nerv Syst. **27**(1): 87-94.
Porporato, P. E., S. Dhup, et al. (2011). "Anticancer targets in the glycolytic metabolism of tumors: a comprehensive review." Front Pharmacol **2**: 49.
Preinerstorfer et al., (2010). "Metabolic profiling of intracellular metabolites in fermentation broths from beta-lactam antibiotics production by liquid chromatography-tandem mass spectrometry methods." J Chromatogr A. Jan **1217**(3):312-28.
Pusch et al. (2014). "D-2-Hydroxyglutarate producing neo-enzymatic activity inversely correlates with frequency of the type of isocitrate dehydrogenase 1 mutations found in glioma." Acta Neuropathol Commun. **2**:19.
Rabinowitz. (2009). "Inhibition of Hypoxia-Inducible Factor Prolyl Hydroxylase Domain Oxygen Sensors: Tricking the Body into Mounting Orchestrated Survival and Repair Responses." J. Med. Chem. **56**(23):9369–9402.
Ramachandran and Colman. (1980). "Chemical characterization of distinct subunits of pig heart DPN-specific isocitrate dehydrogenase." J Biol Chem. **255**(15): 8859-8864.
Rashed et al., (2000). "Chiral liquid chromatography tandem mass spectrometry in the determination of the configuration of 2-hydroxyglutaric acid in urine." Biomed Chromatogr.**14**(5):317-20.
Rasmusson et al., (1990). "NADP-utilizing enzymes in the matrix of plant mito- chondria 1." Plant Physiol. **94**(3): 1012–1018.
Reaves and Rabinowitz, J.D. 2011. "Metabolomics in systems microbiology." Current Opin Biotechnol. **22**(1):17-25.
Reitman and Yan. (2010). "Isocitrate dehydrogenase 1 and 2 mutations in cancer: Alterations at a crossroads of cellular metabolism." J Natl Cancer Inst. **102**(13):932-41.
Reitman et al., (2011). "Profiling the effects of isocitrate dehydrogenase 1 and 2 mutations on the cellular metabolome." Proc Natl Acad Sci U S A. **108**(8): 3270-3275.
Reynolds, T. Y., S. Rockwell, et al. (1996). "Genetic instability induced by the tumor microenvironment." Cancer Research **56**(24): 5754-5757.
Riera, L., A. Manzano, et al. (2002). "Insulin induces PFKFB3 gene expression in HT29 human colon adenocarcinoma cells." Biochim Biophys Acta **1589**(2): 89-92.
Robertson, D.G. (2005). "Metabonomics in Toxicology: A Review." Toxicological Sciences **85**(2):809-822.
Robey, R. B. and N. Hay (2009). "Is Akt the "Warburg kinase"?-Akt-energy metabolism interactions and oncogenesis." Semin Cancer Biol **19**(1): 25-31.
Roessner, U., C. Wagner, et al. (2000). "Technical advance: simultaneous analysis of metabolites in potato tuber by gas chromatography-mass spectrometry." Plant J **23**(1): 131-142.
Rofstad, E. K., B. Mathiesen, et al. (2006). "Acidic extracellular pH promotes experimental metastasis of human melanoma cells in athymic nude mice." Cancer Res **66**(13): 6699-6707.
Rohle et al., (2013). "An Inhibitor of Mutant IDH1 Delays Growth and Promotes Differentiation of Glioma Cells." Science. **340**(6132):626-30.
Ronnebaum et al., (2006). "A pyruvate cycling pathway involving cytosolic NADP-dependent isocitrate dehydrogenase regulates glucose-stimulated insulin secretion." J Biol Chem. **281**(41): 30593-30602.

Ros, S. and A. Schulze (2013). "Balancing glycolytic flux: the role of 6-phosphofructo-2-kinase/fructose 2,6-bisphosphatases in cancer metabolism." Cancer & Metabolism **1**(8): 1-10.
Ros, S. and A. Schulze (2013). "Balancing glycolytic flux: the role of 6-phosphofructo-2-kinase/fructose 2,6-bisphosphatases in cancer metabolism." Cancer & Metabolism **1**(8): 1-10.
Rose et al., (2011). “Inhibition of 2-oxoglutarate dependent oxygenases.” Chem Soc Rev **40**(8):4364-97.
Rosenqvi et al., (1972). "Gas-chromatographicanalysisofcitric-acid cycle and related compounds from Escherichia coli as their trimethylsilyl derivatives." Anal. Biochem. 46(1):224–231.
Saed, G. M., N. M. Fletcher, et al. (2011). "Dichloroacetate induces apoptosis of epithelial ovarian cancer cells through a mechanism involving modulation of oxidative stress." Reprod Sci **18**(12): 1253-1261.
Saghatelian et al., (2004). "Assignment of Endogenous Substrates to Enzymes by Global Metabolite Profiling†." Biochemistry **43**(45):14332-14339.
Saguir et al., (2002). “Effect of L-malic and citric acids metabolism on the essentialamino acid requirements for Oenococcus oeni growth.” Journal of Applied Microbiology **93**(2):295–301.
Sakai, A., M. Kato, et al. (1996). "Cloning of cDNA encoding for a novel isozyme of fructose 6-phosphate, 2-kinase/fructose 2,6-bisphosphatase from human placenta." J Biochem **119**(3): 506-511.
Sakakibara, R., M. Kato, et al. (1997). "Characterization of a human placental fructose-6-phosphate 2-kinase fructose-2,6-bisphosphatase." Journal of Biochemistry **122**(1): 122-128.
Sakata, J., Y. Abe, et al. (1991). "Molecular cloning of the DNA and expression and characterization of rat testes fructose-6-phosphate,2-kinase:fructose-2,6-bisphosphatase." J Biol Chem **266**(24): 15764-15770.
Sanchez, W. Y., S. L. McGee, et al. (2013). "Dichloroacetate inhibits aerobic glycolysis in multiple myeloma cells and increases sensitivity to bortezomib." Br J Cancer **108**(8): 1624-1633.
Sanson et al., (2009). "Isocitrate dehydrogenase 1 codon 132 mutation is an important prognostic biomarker in gliomas." J Clin Oncol. **27**(25): 4150-4154.
Sasieni, P. D., J. Shelton, et al. (2011). "What is the lifetime risk of developing cancer?: the effect of adjusting for multiple primaries." Br J Cancer **105**(3): 460-465.
Sawada et al., (2003). “Determination of sugar phosphates and nucleotides related to photosynthetic metabolism by high-performance anion-exchange liquid chromatography with fluorometric and ultraviolet detection.” Anal Biochem. **314**(1):63-9.
Sawyers, C. (2004). "Targeted cancer therapy." Nature **432**(7015): 294-297.
Sazanov and Jackson. (1994). "Proton-translocating transhydrogenase and NAD- and NADP-linked isocitrate dehydrogenases operate in a substrate cycle which contributes to fine regulation of the tricarboxylic acid cycle activity in mitochondria." FEBS Lett. **344**(2-3): 109-116.
Schaeper et al., (1996). “Separation of phosphorylated sugars using capillary electrophoresis with indirect photometric detection.” J Capillary Electrophor. **3**(4):215-21.
Schlemminger et al., (2003). “Analogues of dealanylalahopcin are inhibitors of human HIF prolyl hydroxylases.” Bioorganic & Medicinal Chemistry Letters **13**(8): 1451-1454.
Scholnick, P., D. Lang, et al. (1973). "Regulatory mechanisms in carbohydrate metabolism. IX. Stimulation of aerobic glycolysis by energy-linked ion transport and inhibition by dextran sulfate." J Biol Chem **248**(14): 5175.

Schulze, A. and A. L. Harris (2012). "How cancer metabolism is tuned for proliferation and vulnerable to disruption." Nature **491**(7424): 364-373.
Sekiguchi et al., (2004). “Analysis of sugar phosphates in plants by ion chromatography on a titanium dioxide column with pulsed amperometric detection.” J Chromatogr A. **1039**(1):71–76.
Semenza, G. L. (2007). "Evaluation of HIF-1 inhibitors as anticancer agents." Drug Discovery Today **12**: 853-859.
Semenza, G. L. and G. L. Wang (1992). "A nuclear factor induced by hypoxia via de novo protein synthesis binds to the human erythropoietin gene enhancer at a site required for transcriptional activation." Mol Cell Biol **12**(12): 5447-5454.
Serkova, N.J., et al., (2007). "Early detection of graft failure using the blood metabolic profile of a liver recipient." Transplantation. 83(4):517-521.
Shannon, A. M., D. J. Bouchier-Hayes, et al. (2003). "Tumour hypoxia, chemotherapeutic resistance and hypoxia-related therapies." Cancer Treatment Reviews **29**(4): 297-307.
Shechter et al., (2003). "IDH1 gene transcription is sterol regulated and activated by SREBP-1a and SREBP-2 in human hepatoma HepG2 cells: evidence that IDH1 may regulate lipogenesis in hepatic cells." J Lipid Res. **44**(11): 2169-2180.
Shin et al., (2004). "Regulation of high glucose-induced apoptosis by mitochondrial NADP+-dependent isocitrate dehydrogenase." Biochem Biophys Res Commun. **325**(1): 32-38.
Smallbone, K., D. J. Gavaghan, et al. (2005). "The role of acidity in solid tumour growth and invasion." J Theor Biol **235**(4): 476-484.
Soga et al., (2002). "Simultaneous determination of anionic intermediates for Bacillus subtilis metabolic pathways by capillary electrophoresis electrospray ionization mass spectrometry." Anal. Chem. **74**(10):2233–2239.
Soga et al., (2003). "Quantitative metabolome analysis using capillary electrophoresis mass spectrometry." Journal of Proteome Research, 2(5):488–494.
Sonoda et al., (2009). "Analysis of IDH1 and IDH2 mutations in Japanese glioma patients." Cancer Sci. **100**(10): 1996-1998.
Soundar et al., (2000). "Identification by mutagenesis of arginines in the substrate binding site of the porcine NADP-dependent isocitrate dehydrogenase." J Biol Chem. **275**(8): 5606-5612.
Stancheva et al., (2014). “IDH1/IDH2 but not TP53 mutations predict prognosis in Bulgarian glioblastoma patients.” Biomed Res Int. **2014**:654727.
Struys et al., (2004). "Measurement of Urinary D- and L-2- Hydroxyglutarate Enantiomers by Stable-Isotope- Dilution Liquid Chromatography–Tandem Mass Spectrometry after Derivatization with Diacetyl-L-Tartaric Anhydride. Clin Chem. **50**(8):1391-5.
Stubbs et al., (2009). “Application of a Proteolysis/Mass Spectrometry Method for Investigating the Effects of Inhibitors on Hydroxylase Structure.” Journal of Medicinal Chemistry **52**(9):2799-2805.
Stubbs, M. and J. R. Griffiths (2010). "The altered metabolism of tumors: HIF-1 and its role in the Warburg effect." Adv Enzyme Regul **50**(1): 44-55.
Stupp et al., (2005). "Radiotherapy plus concomitant and adjuvant temozolomide for glioblastoma." N Engl J Med. **352**(10): 987-996.
Stupp et al., (2009). "Effects of radiotherapy with concomitant and adjuvant temozolomide versus radiotherapy alone on survival in glioblastoma in a randomised phase III study: 5-year analysis of the EORTC-NCIC trial." Lancet Oncol. **10**(5): 459-466.
Subarsky, P. and R. P. Hill (2003). "The hypoxic tumour microenvironment and metastatic progression." Clinical & Experimental Metastasis **20**(3): 237-250.
Sullivan, R. J. and K. T. Flaherty (2013). "Resistance to BRAF-targeted therapy in melanoma." Eur J Cancer **49**(6): 1297-1304.

Swanton, C. (2012). "Intratumor heterogeneity: evolution through space and time." Cancer Res **72**(19): 4875-4882.
Swietach, P., R. D. Vaughan-Jones, et al. (2007). "Regulation of tumor pH and the role of carbonic anhydrase 9." Cancer Metastasis Rev **26**(2): 299-310.
Tahiliani et al., (2009). "Conversion of 5-methylcytosine to 5-hydroxymethylcytosine in mammalian DNA by MLL partner TET1." Science. **324**(5929): 930-935.
Tanenbaum. (2006). "Clinical 3T MR imaging: mastering the challenges." Magn Reson Imaging Clin N Am. **14**(1):1-15.
Tanimoto, K., Y. Makino, et al. (2000). "Mechanism of regulation of the hypoxia-inducible factor-1 alpha by the von Hippel-Lindau tumor suppressor protein." EMBO J **19**(16): 4298-4309.
Taylor. (2005). "Matrix effects: The Achilles heel of quantitative high performance liquid chromatography electrospray-tandem mass spectrometry." Clin Biochem. **38**(4):328-34.
Telang, S., A. Yalcin, et al. (2006). "Ras transformation requires metabolic control by 6-phosphofructo-2-kinase." Oncogene **25**(55): 7225-7234.
Tennant, D. A., R. V. Duran, et al. (2010). "Targeting metabolic transformation for cancer therapy." Nat Rev Cancer **10**(4): 267-277.
Theodoridis et al., (2008). "LC-MS-based methodology for global metabolite profiling in metabonomics/metabolomics." TrAC - Trends in Analytical Chemistry. **27**(3): 251-260.
Thompson, C. B. (2009). "Attacking cancer at its root." Cell **138**(6): 1051-1054.
Trygg et al., (2005). "Extraction and GC/MS analysis of the human blood plasma metabolome." Anal. Chem. **77**(24):8086–8094.
Udagawa, T. and M. Wood (2010). "Tumor-stromal cell interactions and opportunities for therapeutic intervention." Curr Opin Pharmacol **10**(4): 369-374.
van Roermund et al., (1998). "Peroxisomal beta-oxidation of polyunsaturated fatty acids in Saccharomyces cerevisiae: isocitrate dehydrogenase provides NADPH for reduction of double bonds at even positions." Embo J. **17**(3): 677-687.
Vander et al., (2009). "Understanding the Warburg effect: the metabolic requirements of cell proliferation." Science. **324**(5930): 1029- 1033.
Vander Heiden, M. G. (2011). "Targeting cancer metabolism: a therapeutic window opens." Nat Rev Drug Discov **10**(9): 671-684.
Vander Heiden, M. G., L. C. Cantley, et al. (2009). "Understanding the Warburg effect: the metabolic requirements of cell proliferation." Science **324**(5930): 1029-1033.
Ventura, F., S. Ambrosio, et al. (1995). "Cloning and expression of a catalytic core bovine brain 6-phosphofructo-2-kinase/fructose-2,6-bisphosphatase." Biochem Biophys Res Commun **209**(3): 1140-1148.
Verhaak et al., (2010). "Integrated genomic analysis identifies clinically relevant subtypes of glioblastoma characterized by abnormalities in PDGFRA, IDH1, EGFR, and NF1." Cancer Cell. **17**(1): 98-110.
Vincent et al., (2000). Citrate release by perfused rat hearts: a window on mitochondrial cataplerosis." Am J Physiol Endocrinol Metab. 278(5):E846-56.
Vivanco, I. and C. L. Sawyers (2002). "The phosphatidylinositol 3-Kinase AKT pathway in human cancer." Nat Rev Cancer **2**(7): 489-501.
Wagner et al., (2010). "Simultaneous quantitative determination of alpha-ketoglutaric acid and 5-hydroxymethylfurfural in human plasma by gas chromatography–mass spectrometry." Anal. Bioanal. Chem. 396(7):2629–2637.
Wang, G. L., B. H. Jiang, et al. (1995). "Hypoxia-inducible factor-1 is a basic-helix-loop-helix-PAS heterodimer regulated by cellular O-2 tension." Proceedings of the National Academy of Sciences of the United States of America **92**(12): 5510-5514.
Wang, Q., C. Moyret-Lalle, et al. (2003). "Alterations of anaphase-promoting complex genes in human colon cancer cells." Oncogene **22**(10): 1486-1490.

Wang, T., C. Marquardt, et al. (1976). "Aerobic glycolysis during lymphocyte proliferation." Nature **261**(5562): 702-705.
Warburg, O. (1956). "Origin of Cancer Cells." Science **123**(3191): 309-314.
Ward et al., (2010). "The common feature of leukemia-associated IDH1 and IDH2 mutations is a neomorphic enzyme activity converting alpha-ketoglutarate to 2-hydroxyglutarate." Cancer Cell. **17**(3): 225-234.
Ward, P. S. and C. B. Thompson (2012). "Metabolic reprogramming: a cancer hallmark even warburg did not anticipate." Cancer Cell **21**(3): 297-308.
Wartenberg, M., F. C. Ling, et al. (2003). "Regulation of the multidrug resistance transporter P-glycoprotein in multicellular tumor spheroids by hypoxiainducible factor-1 and reactive oxygen species." Faseb Journal **17**(1): 503-505.
Watanabe et al., (2009). "IDH1 mutations are early events in the development of astrocytomas and oligodendrogliomas." Am J Pathol. **174**(4): 1149-1153.
Wegener et al., (1968). "Propionate metabolism. 3. Studies on the signif- icance of the alpha-hydroxyglutarate pathway." Arch. Biochem. Biophys. **123**(1)62–65.
Wei, R., Li, G., and Seymour, A.B. (2010). "High-Throughput and Multiplexed LC/MS/MRM Method for Targeted Metabolomics." Anal. Chem. 82(13):5527-5533.
Weinhouse, S. (1976). "The Warburg hypothesis fifty years later." Z Krebsforsch Klin Onkol Cancer Res Clin Oncol **87**(2): 115-126.
Wick, A. N., D. R. Drury, et al. (1957). "Localization of the primary metabolic block produced by 2-deoxyglucose." J Biol Chem **224**(2): 963-969.
Williams, A. C., T. J. Collard, et al. (1999). "An acidic environment leads to p53 dependent induction of apoptosis in human adenoma and carcinoma cell lines: implications for clonal selection during colorectal carcinogenesis." Oncogene **18**(21): 3199-3204.
Williams, K. J., B. A. Telfer, et al. (2005). "Enhanced response to radiotherapy in tumours deficient in the function of hypoxia-inducible factor-1." Radiotherapy and Oncology **75**(1): 89-98.
Winkler et al., (1986). "Multiple NADPH-producing pathways control glutathione (GSH) content in retina." Exp Eye Res. **43**(5): 829-847.
Wishart DS, et al., (2013). HMDB 3.0--The Human Metabolome Database in 2013. Nucleic acids Res. **41**:D801-807.
Wishart, D.S., et al., (2001). "Magnetic Resonance Diagnostics: A New Technology for High-Throughput Clinical Diagnostics." Clin Chem. **47**(10):1918-1921.
Wouters, A., B. Pauwels, et al. (2007). "Review: Implications of in vitro research on the effect of radiotherapy and chemotherapy under hypoxic conditions." Oncologist **12**(6): 690-712.
Xu et al., (2004). "Structures of human cytosolic NADP-dependent isocitrate dehydrogenase reveal a novel self-regulatory mechanism of activity." J Biol Chem. **279**(32): 33946-33957.
Xu et al., (2011). "Oncometabolite 2- hydroxyglutarate is a competitive inhibitor of alpha-ketoglutarate-dependent dioxygenases." Cancer Cell. **19**(1): 17-30.
Yan et al., (2009). "IDH1 and IDH2 mutations in gliomas." N Engl J Med **360**:765–773.
Yang et al., (2006). "Brunengraber, Metabolomic assays of the concentration and mass isotopomer distribution of gluconeogenic and citric acid cycle intermediates." Metabolomics 2(2):85–94.
Yang et al., (2010). " Streamlined pentafluorophenylpropyl column liquid chromatography-tandem quadrupole mass spectrometry and global 13C-labeled internal standards improve performance for quantitative metabolomics in bacteria." J Chromatogr A. 1217(47):7401-10.

Yang et al., (2010). "Urinary metabonomic study of lung cancer by a fully automatic hyphenated hydrophilic interaction/RPLC-MS system." J Sep Sci. 33(10):1495-1503.
Yang et al., (2012). “The emerging role of fumarate as an oncometabolite.” Frontiers in Oncology **2**(85):1-7.
Yang, Q., et al., (2010). "Urinary metabonomic study of lung cancer by a fully automatic hyphenated hydrophilic interaction/RPLC-MS system." J Sep Sci. 33(10):1495-1503.
Yang, S., et al., (2009). "Liquid chromatography- tandem quadrupole mass spectrometry and comprehensive two-dimensional gas chromatography-time-of-flight mass spectrometry measurement of targeted metabolites of Methylobacterium extorquens AM1 grown on two different carbon sources." J Chromatogr A. 1216(15):3280-3289.
Yap, T. A., M. Gerlinger, et al. (2012). "Intratumor heterogeneity: seeing the wood for the trees." Sci Transl Med **4**(127): 127ps110.
Yu, F., S. B. White, et al. (2001). "HIF-1alpha binding to VHL is regulated by stimulus-sensitive proline hydroxylation." Proc Natl Acad Sci U S A **98**(17): 9630-9635.
Yun, S. J., S. W. Jo, et al. (2011). "PFKFB4 as a prognostic marker in non-muscle-invasive bladder cancer." Urol Oncol **30**(6): 893-899.
Zhao and Winkler. (1996). "A novel alpha-ketoglutarate reductase activity of the serA-encoded 3-phosphoglycerate dehydrogenase of Escherichia coli K-12 and its possible implications for human 2 hydroxyglutaric aciduria." J. Bacteriol. **178**(1):232–239.
Zhao et al., (2009). “Glioma-derived mutations in IDH1 dominantly inhibit IDH1 catalytic activity and induce HIF-1alpha.” Science. **324**(5924):261–265.
Zhao S, et al., (2009). “Glioma-derived mutations in IDH1 dominantly inhibit IDH1 catalytic activity and induce HIF-1alpha.” Science 324(5924):261–265.
Zu, X. L. and M. Guppy (2004). "Cancer metabolism: facts, fantasy, and fiction." Biochem Biophys Res Commun **313**(3): 459-465.